8-19-2016 12:00 AM

Study on Developments of Processes for Powder Coatings

Shan Gao
The University of Western Ontario

Supervisor
Jesse Zhu
The University of Western Ontario Joint Supervisor
Hui Zhang
The University of Western Ontario

Graduate Program in Chemical and Biochemical Engineering
A thesis submitted in partial fulfillment of the requirements for the degree in Doctor of Philosophy

Abstract

Powder coating, which utilizes polymer resin based powder, is a relatively young technology for decorative and protective purposes. It was first developed in the early 1950s and gradually grew into automotive finishes. Compared to conventional liquid coating, powder coating is an environmentally friendly technology, given that there is no emission of harmful solvent throughout the entire operating process. It is also much more efficient, economical and energy saving as a result of the capability to reuse all the powder. However, there are still some problems in the powder coating process limiting its application. This thesis focused on studying some key aspects of the manufacturing and application processes of both coarse powder and fine powder. Several new techniques were developed during the process.

The study started with an investigation of powder coating manufacturing processes. Most of the research was aiming at maximizing the productivity, while the produced powder has a wide particle size distribution, leading to a poor surface condition. In order to narrow the particle size distribution, a new design of classifying cyclone for an air classifying mill (ACM) with a reversed air inlet was studied. Experimental results indicated that this novel cyclone design could effectively reduce the span of the particle size distribution, without deteriorating the collection efficiency compared to conventional cyclones.

In addition, the spraying properties of powder coatings were investigated during electrostatic spraying. In order to overcome the Faraday Cage effect, a modified corona spray gun with a multi-electrode design supplied by an alternating charging pattern was invented. Experimental results demonstrated that the Faraday Cage effect could be significantly mitigated by using the new spray gun at various gun voltages. Besides, the new design of spray gun could provide higher transfer efficiency compared to its conventional counterpart.

Moreover, this study also improved the powder coating processing technique involving metallic pigments. To achieve better bonding between metallic pigments and powder

coating particles, a liquid bonding agent (bonder) was introduced into the blending process. It was found that the concentration of metallic pigments changed minutely from the pre-sprayed and post-sprayed powder, indicating that the recycled powder could be reused. Therefore, this new bonding method of utilizing liquid bonder could provide a strong affinity between the powder coating and metallic pigments so as to prevent separation of the two materials during spraying.

At the end, a pre-heating method of applying powder coating onto thermoplastic substrates, which helps powder deposition and adhesion onto plastic substrates, was studied. Three widely used powder coatings have been tested for this method. The coating films were evaluated by both visual inspection and instrumental measurements. It was found that this new processing method could provide a smooth surface as well as a strong adhesion to the difficult substrate. Furthermore, for the purpose of protecting the thermoplastic substrate from deformation during the curing process, a UWO low-cure method was applied to these three powder coatings. Compared with commercial low-cure powder, the UWO low-cure coatings perform better in a few aspects.

The discoveries and analyses in this thesis work are contributing to powder coating development. Several original techniques have been invented in this study and they could provide a good guideline for future work of modern powder coating technology.

Keywords: powder coating, cyclone, corona charge spraying, Faraday Cage effect, transfer efficiency, insulating substrate

Co-Authorship Statement

Dr. Jesse Zhu and Dr. Hui Zhang provided full supervision to this PhD thesis study.

Related publications：

1.

Title: Powder coating of plastic components

Authors: Shan Gao, Xinping Zhu, Hui Zhang and Jesse Zhu. All the researches were conducted by Shan Gao with the help of Xinping Zhu, under the supervision of Dr. Jesse Zhu and Dr. Hui Zhang. The authors would like to thank Fraunhofer Project Center in providing materials for this study. Helpful discussions with Dr. Jeff Wood and Ying Fan from Western Engineering are highly appreciated. The final version of this manuscript will be published in ***Automotive Composites Conference & Exhibition (ACCE),*** Novi, MI, September 9-11, 2016.

I dedicate this book to my beloved father, mother and my husband, who always supported and encouraged me to go on every adventure, especially this one.

Acknowledgments

This thesis is the account of my three-year PhD research in the field of powder coating technology at Western University, Canada.

In the beginning, I would like to express my deep gratitude to my supervisor, Dr. Jesse Zhu, professor in the Department of Chemical & Biochemical Engineering (CBE), fellow of Royal Society of Canada and Canadian Academy of Engineering. Dr. Zhu supervised me with his expertise and encouraged me throughout my entire research. He also guided me in consideration of my capability and research interests. I am also grateful to my co-supervisor, Dr. Hui Zhang, a research professor in CBE. Dr. Zhang provided a great help on my research and thesis writing. Working and discussing with him in the laboratory, I was inspired by his research enthusiasm, which also encouraged me to work on this thesis.

I am grateful to Dr. Boxin Zhao, associate professor in the Department of Chemical Engineering at University of Waterloo. Dr. Jeff Wood, associate professor in the Department of Mechanical and Material Engineering at Western University. Dr. Ajay Ray and Dr. Charles Xu, professors of CBE at Western University. As the examiners of my thesis defense, they contribute so much to provide their thoughtful comments and suggestions for the revision and improvement of the thesis.

I want to extend my appreciation to my advisory committee members: Dr. Shahzard Barghi, Assistant Professor & Director of Master of Engineering program in CBE at Western University and Dr. Dominic Pjontek, Assistant Professor in CBE at Western University for their advice and help on my research during the past 3 years.

In addition, I am also grateful to Dr. Wood and Dr. Fan in in the Department of Mechanical and Material Engineering at Western University. They provided useful knowledge and valuable comments to this thesis study.

Moreover, I am also grateful to Dr. Chaoyu Yan, professor at China University of Petroleum for his great help in this research; Mr. Michael Zhu and Mr. Jianzhang Wen for their assistances on the experiment setups; to Mrs. Ying Ma for sharing her laboratory

equipment; to Dr. Yong Liu for his help on conducting analysis on experimental samples; to Chengxiu Wang for her valuable help and sharing her research experience with me; to Shuai Yang and Michael Nelson for their great help in the thesis writing; to Danni Bao and Xinping Zhu for their great assistances on designing and conducting a part of the experiment work of my research; to my friends Zeneng Sun and Mengqi Han for binging my studies so much joys; to my friends Xiao Zhao, Yin Liu, Xu Han and Shuling Yan for their help and kindness all the time; to my colleagues who helped me throughout the entire study, Yandy Zhou, Mohammad Bhuiyan, Rezwana Yeasmin, Tang Li, Qingliang Yang, Jiangshan Liu for sharing experiences and enjoyment of working with them.

Specially, I want to deliver the deepest thankfulness to my parents, Jinsen Gao and Li Zhou for their understanding and support all the time; to my dear husband, Xiutian Cui, for his years' encouragement and endless love. Without his technical support on this research and dedication to the family, this thesis could not have been possible to be accomplished.

Table of Contents

List of Figures

List of Tables

List of Abbreviations and symbols

Abbreviations:

EPA	Environmental Protection Agency
VOCs	Volatile Organic Compounds
ACM	Air classifying mill
IC	Internal Corona
SEM	Scanning electron microscope
PA	Polyacrylate
PVA	Polyvinyl alcohol
BHP	Bag house powder
$D_{10\ 50\ 90}$	Particle diameter, where 10,50 and 90 represents the volume percentage of the powder smaller than the diameter (μm)
DOI	Distinctiveness of image
MEK	Methyl ethyl ketone
IR	Infrared
SAG	Secondary air guider

Symbols:

V_t	Particle tangential velocity component (m/s)
R	Device radial position (m)
K	Cyclone geometry constants
V_p	Rotational velocity of the particle (m/s)
V_c	Rotational velocity of the classifier blade (m/s)
R	Distance from the center of the blade to the particle (m)
F_d	Drag force (N)
F_c	Centrifugal force (N)
Q_{max}	Saturation charge (c)
ε_r	Particle relative permittivity (F/m)
τ	Time for particle to reach half saturation charge (s)
J	Current density (A/m^2)
Q/M	Charge to mass ratio
FPTE	First-pass Transfer Efficiency (%)
FCR	Faraday Cage Resistance (%)

1 Chapter 1: General Introduction

1.1 Introduction

1.1.1 Powders

Powders are dry solid materials composed of very fine and loose particles which could be obtained by pulverizing bulk materials [1]. Powders also refer to the granular materials with finer sizes which could have the greatest tendency to form clumps. Powder technology could be described as study of the particle dispersion properties [2]. Powders have a great importance to industries due to the fact that they have greater specific areas compared with the coarse granular material and so they have been studied in detail in the fields of chemical reactions, powder coating industry and pharmaceutical applications. However, finer particles tend to have more difficulties in fluidization, pneumatic transport and spraying, resulting from the inter-particle cohesion and the low flowability. Generally, powders may be classified into four groups according to Geldart's classification in terms of particle sizes and densities [3]. This famous classification depicts the flow characteristics of the powder during handling and processing. Also the theory has been widely used today in guiding many powder studies.

1.1.1 Powder coating technology

Powder coating is a technology of decorative and protective coatings which was first developed in the early 1950s. The biggest advantage of powder coating is environmental friendliness due to having zero volatile compound emissions. In response to the announced federal EPA (Environmental Protection Agency) guideline (Clean Air Act of 1970) with the restriction of quantity and type of solvents, powder coating is applied by spraying the charged particles onto grounded substrates [4]. In North America, almost five thousand companies are using powder coatings in their final products for better corrosion, chemical and abrasion resistance. Powder coating is a young and fast growing technology in industrial finishing and takes up over fifteen percent of coating market in North America.

In the modern manufacturing powder coating process, paint ingredients including resin, curing agent, filler and various additives such as degassing agent are mixed and extruded into solid composite pieces. After grinding and classifying, the powder particles are electrostatically sprayed to the substrate. The resin-based coating melts quickly when being heated in a baking oven, and is then transformed to a continuous film on the substrate. Compared with the conventional coating process, powder coating does not involve any solvent so it eliminates the Volatile Organic Compounds (VOCs) emission.

Although the market share of the powder coating is still limited currently, taking up only 8%-9% of industrial finishing by volume, due to its multiple advantages, almost all the metal finishing market has chosen powder coating in the recent two decades. The powder coating materials have been produced at a value of nearly 4 million USD each year in industrial operations [5]. Besides metal substrate, powder coating also began to be developed on plastics, wood and other non-conductive materials. Furthermore, the other advantages of powder coating compared with the traditional liquid coating is that powder coating has the potential to recover all the recycled powders, making it much more efficient, economical and energy saving, and it also has greater surface resistance to chemicals and UV radiation.

1.2 Challenges and opportunities of powder coating application

In the coating industry, the film appearance of the final product is the most significant factor. The most commonly used powder in current technology is median particle sizes (also known as coarse powder), with diameters between 30 to 60 μm. Compared with the conventional liquid coating, the current limitations of the powder coating surface film are mainly thick film thickness (25-50 μm) and poor surface quality which highly affects the aesthetic appearance. As a result, the powder coating coated components are used as underbody, car wheel or other interior part in most of the automotive applications [6]. Other powder coating applications has been limited to those which do not have high requirements of aesthetic purpose such as office furniture and hand tools.

The potential solution for improving the film quality is by utilizing finer powders of smaller particle sizes. The smoothness of the film could be significantly improved by replacing coarse powder with fine or ultrafine powder [7]. Moreover, the film thickness obtained by using ultrafine powder (median particle size below 30 μm) is comparable with the liquid coating, also it has been realized for the application of the clear top coating for automotive industry [3,6,8,9]. For the automotive industry, there are thirteen plants of General Motors using powder primers in production lines. In BMW Germany plants, several applications of the car body have been successfully applied with powder clear coats and put on the market [10,11]. In 2005, Zhu and Zhang developed a new technique of better improving the coating qualities by using ultrafine powder coatings with particle size smaller than 20 μm [9].

However, there are still many fundamental problems and challenges for the ultrafine powder application due to their smaller sizes, so it is hard to produce. The dispersion and handling problem is more severe than the regular coarse powder. The large amount of the small particles generated during the grinding process agglomerate easily and results in the low particle flowability. One effective way to enhance the powder flowability is to add flow additives such as nanoparticles. However, it may deteriorate the appearance of the final coating film by adding any extra additives as it may result in poor blending and agglomeration.

Besides the powder properties, the production of fine powder coating in every manufacturing step is more challenging than before. In the extrusion and grinding process, very fine particles are hard to be classified and can cause wide particle size distribution. During the spraying, more defects occur on the final coating surface as a result of the uneven distribution. Furthermore, it has been disclosed by many researchers that the transfer efficiency of fine powder is lower than that of coarse powder as they carry less electric charge. In addition, fine particles are easy to be influenced and to drift away by the air turbulences during spraying, and also by stronger back ionization in using fine particles during the spraying [12]. Additionally, the corona charging process of the powder coating is facing a problem in coating application on irregular shaped targets that have recessed areas. Powder coatings have less tendency to cover those cavities or holes

due to the Faraday Cage effect. So the traditional corona spraying has a poor performance to provide sufficient coverage for recessed areas of those coating targets with complex geometries.

1.3 Research objectives

With the increasing demand of the fine powder coating product with satisfactory finishes in the industry, the research on the manufacturing and handling of the fine powders is worth conducting. The challenges and problems encountered in developing powder coating technology have a great need to be solved. The research objectives of this study were to expand powder coating's manufacturing and handling process to non-conductive parts, meanwhile solving the problems of the powder processing and spraying. Several modifications on the equipment of the grinding and classifying systems and the corona spraying gun have been finished to improve the powder properties and spraying performance. Furthermore, the manufacturing process of the functional powder coatings has been invented and evaluated in this study.

This study has fulfilled several industrial ideas and demands, at the same time with great support of the industrial devices, materials and practices. A series of studies in collaboration with Nordson (Ohio, USA) in researching the corona spraying gun, Langfabo (Shandong, China) in developing the functional powder technology, and Fraunhofer Project Centre for Composites Research @ Western (Ontario, Canada) in applying powder coating on thermoplastics has been conducted. Problems and difficulties in the operating process have been solved and overcome during the comprehensive study.

The experimental studies of this research could be classified into four sections:

I. The powder product obtained from current manufacturing process has large particle size distributions, which brings a lot of side effects in the future operating processes. The first section of this study was aiming at modifying the current classifying and collection process in order to get the final powder product with a narrower particle size distribution, so as to improve the powder properties. A

secondary air-guider was developed and added to the conventional collecting cyclone, and was validated by a series of experiments.

II. Functional powder coating with for aesthetic use has gained increasing popularity in recent years. However, due to the different charging performance of the regular powder coating and the functional powders, it has been difficult to spray the powder blend onto the target at a fixed mixing ratio. In this part of the research, a new processing technique of pre-mixing the metallic pigments with regular powder coatings to achieve a uniform charging performance during the spraying was invented, and it also improved the recyclability of the powder material.

III. The third section is the study of modifying the corona spraying gun. The operating conditions and optimization of a commercial corona spraying gun has been studied in this section. One common problem in using the corona spray gun is with the insufficient powder coverage in the recessed area of the target with complex configuration, also known as the Faraday Cage effect. In addition, several modifications were conducted on the spraying gun in solving the effect, followed by a series of experiments.

IV. The final section was to develop a method of applying powder coating on the non-conductive substrate. Powder coating is realized by electrostatic spraying onto a grounded metal target for maintaining the powder deposition, however, the non-conductive substrate could not be applied using electrostatic spraying process. A new method has been investigated by heating the substrate to certain temperature, followed by spraying. The first pass powder gets melted and cured due to the high temperature so as to improve the powder transfer efficiency. Extensive experiments were conducted to evaluate the new method.

1.4 Thesis structure

This thesis is written in the “Integrated-Article” form and fulfills the format requirements outlined in the Thesis Regulation Guide of the School of Graduate and Postdoctoral Studies (SGPS) of Western University. The thesis consists of eight chapters and is arranged as follows:

Chapter 1 generally introduces the background of powder coating technology and applications. It starts with the research objectives of this PhD thesis. The thesis structure and research contributions are also stated in this chapter.

Chapter 2 presents the comprehensive review from the previous literatures related to this research. It mainly provides the detailed knowledge of powder coating processes to explain the background of this study better. The main apparatus and materials are outlined in this chapter.

Chapter 3 discusses a modified cyclone design of the classic grinding system, mainly for improving the particle size distribution. A secondary air-guider was utilized and installed at the bottom of the cyclone, and then examined by experimental evaluations.

Chapter 4 contains a new technique in processing metallic power in powder coatings. A new bonding method between metallic pigments and powder coating is developed in order to reach a uniform charging performance during the spraying. The optimization experiment of the liquid bonder and spacer is also explained in this chapter.

Chapter 5 describes a modified design of spray gun. It reviews the finding of the baseline operating condition of a corona spray gun. Then the modified design, by adding additional electrodes, is evaluated by Faraday Cage resistance and transfer efficiency. It also includes the optimization experiments for electrode adjustments.

Chapter 6 discusses a new processing technique in spraying non-conductive substrates using a pre-heating method before spraying. Three commonly used powder coatings are tested on thermoplastic substrate. The sprayed articles are evaluated by both visual inspection and instrumental measurements.

Chapter 7 contains the general discussion on the results of this study.

Chapter 8 is the overall summarization of the experimental results contained in this study. It also provides suggestions for future work.

1.5 Major contributions

Four major contributions of this study can be summarized as below:

- A modified cyclone design of the current grinding process has been invented to achieve a narrower particle size distribution. A secondary air inlet was added at the cyclone bottom which provides the reverse air inlet so that the smaller particles could be effectively removed during the collection process. In this way, the novel design was able to narrow down the particle size distribution. In addition, a secondary air guider was utilized so as to retain the comparable collection efficiency compared with the conventional cyclone. Also the different configuration of the secondary air guider was comprehensively investigated. It was found that the convex shaped air guider could narrow the particle size distribution as well as retain the cyclone efficiency.
- A new technique in processing metallic powder and powder coating was invented. Those two materials are strongly bonded with liquid bonder so as to reach a uniform charging performance during the spraying. As a result, the recycled powder has more possibility to be reused, as the concentration of metallic pigments remains unchanged before and after spraying. A spacer was also utilized in the bonding process to avoid the agglomeration of metallic pigments, as that helps to give the good dispersion of these two materials during the manufacturing process.
- The modifications developed on the corona spray gun could significantly improve the Faraday Cage resistance during the spraying by adding alternating charging electrodes. With the specially designed configuration, the spray gun with multi-electrode could effectively solve the Faraday Cage effect. The improvement of visual appearance is also significant. Meanwhile, the obtained transfer efficiency was comparable with the normal corona spray gun by adjusting the charging performance of the additional electrodes.
- A modified technique in applying powder coating on non-conductive substrates using pre-heating method was proven to be able to obtain a stable adhesion and

smooth coating film. Unlike the conventional pretreatment which makes the manufacturing process complex, only by pre-heating the thermoplastic substrate to a certain temperature and then by spraying could achieve the acceptable coating finishes. Furthermore, the invention of a UWO low-cure powder coating formulation provided the opportunity of further reducing the curing temperature, which could protect the substrate better from deformation.

References

[1] Cao, Guozhong. Synthesis, properties and applications. Imperial college press, London, 2004

[2] Holdich, Richard G. Fundamentals of particle technology. Midland Information Technology and Publishing, 2002.

[3] Geldart, Derek. "Types of gas fluidization." Powder technology 7.5 (1973): 285-292.

[4] Craine, K. "Energy Savings in Powder Coatings." Product Finishing(London) 34.8 (1981): 17-18.

[5] Kiefer, Steven L. "Powder coating material developments promise new opportunities for finishers." Metal finishing 102.1 (2004): 35-37.

[6] Biris, A. S., et al. "Gloss and texture control of powder coated films. "Particulate science and technology 19.3 (2001): 199-217.

[7] Wu, Souheng. "Electrostatic charging and deposition of powder coatings. "Polymer-Plastics Technology and Engineering 7.2 (1976): 119-220.

[8] Bocchi, Greg. "Powder coating technology." Advanced materials & processes 155.4 (1999): 23-26.

[9] Zhu, Jing-xu, and Hui Zhang. "Ultrafine powder coatings: an innovation". Powder Coat 16 (2005): 39-47.

[10] Gribble P., Development Status of Powder Coatings for OEM Automotive Applications, Finishing Today, 2003.

[11] Biller, Kevin. "OEM Automotive Powder Coatings." Industrial Paint & Powder82.7 (2006): 15-18.

[12] Sharma, Rajesh, et al. "Effect of ambient relative humidity and surface modification on the charge decay properties of polymer powders in powder coating." IEEE Transactions on Industry Applications 39.1 (2003): 87-95.

2 Chapter 2: Literature Review

2.1 Powder

Powders are defined as granular materials that have finer grain sizes (less than 100 μm) [1]. Powder may become suspended in the atmosphere for a long time if the particle size is sufficiently small. The interactions between the powder phase and the air could create an expansion of the powder. However, powders tend to return to the packed status due to the force of gravity. This aerodynamic property of powder is widely used in industrial applications, such as powder fluidization and pneumatic conveying.

Powders have great importance in industry and medicine, and they have been studied in detail in the field of chemical reactions, powder coating industry and pharmaceutical applications [2]. It has been a challenge in handling and processing fine powders (medium size less than 30 μm) due to its strong inter-particle forces, mainly Van der Walls attraction [3]. The ability of a powder to flow is defined as powder flowability. A poor powder flowability is mainly due to strong cohesion between particles, which brings many difficulties such as agglomeration, de-agglomeration and de-fluidization problems in most of the industrial applications. To solve these problems, research has been conducted many ways in improving the powder flowability including mechanical vibration or adding flow agents, so as to modify the powder performance during handling and processing [68-71].

The measurement of powder flowability is for characterizing flow properties, as well as designing equipment for handling of powders [4]. The most famous classification based on powder sizes and densities was proposed by Geldart in 1973, which classified powders into four groups according to their flow behaviors [5]. As shown in Figure 2.1, four powder groups (A, B C and D) which were denoted “aeratable”, “bubbling”, “cohesive” and “spoutable” in Geldart’s chart, indicating different powder fluidization behaviors. Geldart’s chart had been greatly helpful on powder involved fields in that it could provide a clear criterion for researchers to quickly predict the powder flowability without using complex testing processes.

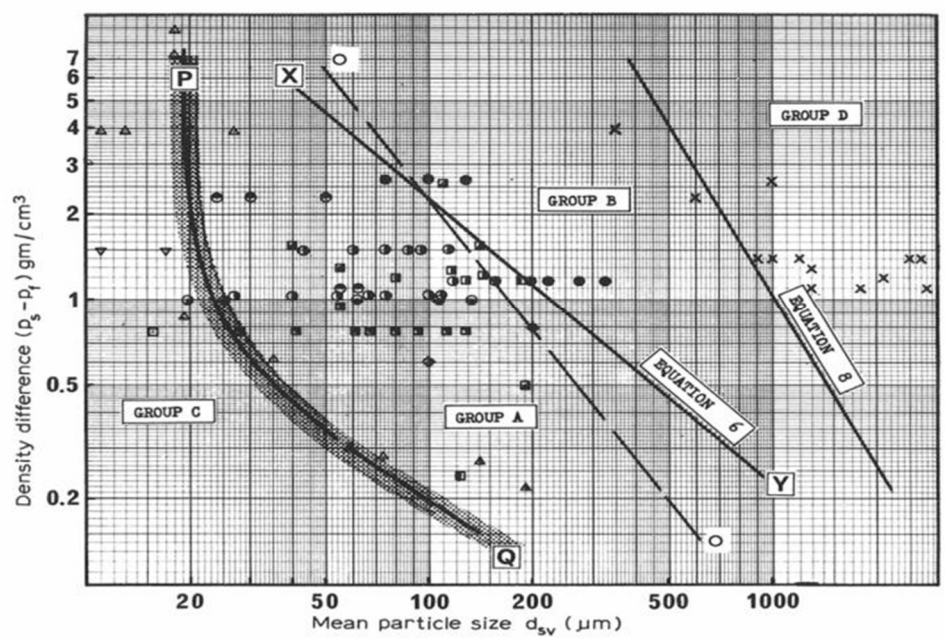

Figure 2.1 Geldart's chart for powder classifications [5]

Many other researchers also have proposed powder classification criteria. It has always been challenging for researchers to test the flowability of a large scale of powder varieties. A series of preliminary works of Carr claimed a grade for powder flowability and ranked them based on angle of repose, angle of spatula, angle of fall, uniformity and Carr's dispersitility and cohesion [7]. In a classification method proposed by Jenike, powders were categorized into five groups with different flowability from "free flowing" to "non-flowing", based on analyzing the flow function [8]. In addition, Taylor et al. demonstrated a composite index using a flow measurement technique to qualify the flow properties of tablet and capsule formulations [6]. In further discussing powder flowability in various production processes, a combination of particle physical properties and the equipment used for handling and/or processing has been investigated to address this multidimensional problem [10]. However, the accuracy could not be assured due to variations between characterization methods, which has been a confusion for a long time [6, 9]. This concept was proven by the recent work of Huang, which found that inconsistency exists among varieties of characterization techniques. The study also resolved the confusion problem by characterizing the powder under different states from dynamic to static [11]. In similarity, Krantz conducted a characterization experiment in

testing different powder material under stress states from static to dynamic [12]. These two researches also claimed that there is no single technique that could fully characterize a powder, as powder flow properties are dependent upon stress state. It was also suggested that characterization techniques under both static and dynamic states are needed in order to completely understand and describe the flow properties, as well as to predict powder behavior under different processing conditions.

2.2 Powder Coating Technology

Powder coating technology is one of the powder applications, and it was first developed in the USA in 1950s [13]. It was fast developed in powder formulation on metal substrates in the finishing industry for decorative as well as durability considerations [14]. Benefiting from its advantages of being environmentally friendly with no Volatile Organic Compounds (VOCs) releasing over conventional liquid coating, at the same time resisting corrosion and chip with less energy cost, powder coating rapidly gained popularity in many industries [15].

Powder coating materials are either thermoplastic or thermosetting. The main types of thermoplastic are polymers with high molecular weight, such as polyethylene, polypropylene, nylon, polyamides, polyvinyl chloride and polyesters [15,16]. A thermoplastic coating melts when its melting temperature is reached, and it returns to solid to form as a coating film after it cools down and retains the same chemical composition. The same transformation starts again when reheating the thermoplastic material. However, thermosetting coatings are lower molecular weight solid resins which melt when heat is applied. Being different from thermoplastic materials, the molecules of thermosetting coatings are chemically cross-linked with each other or with reactive agents to form a polymer with higher molecular weight. Thus, the final coating layer of melted thermosetting material has different chemical structures from the original resin, and could not be re-melted by applying the same heating process when the reactions are completed. This cross-linking process is also known as the coating curing process. Final coating film is strongly bonded with coating substrate after curing, also the mechanical properties of the coating itself could be enhanced during the cross-linking reaction.

The major portion of powder coating market is using thermosetting coatings with more than 90% of the market share. Thermosetting coating consists of resin, filler, curing agent, color pigments and other additives such as flow agent. Resins as the basic composition of thermosetting material and they also control the melting point, flow and leveling properties of coating film. There are several main types of resins in the market: epoxy, polyester, polyurethane and acrylic [15]. Detailed properties of thermosetting coating materials are discussed as follows.

Polyester powder coatings

Polyester coatings are often applied on exterior products due to its good weathering characteristics. The coating film is tough and resists cracking because of the contained polar groups. It could also provide a better finish with higher gloss and less yellowing when applied over the appropriate pre-treatment [17]. The typical uses of polyester powder coatings are outdoor applications like automotive components, garden furniture and outdoor use electrical equipment.

Epoxy powder coatings

Epoxy powder coatings are recommended for internal products with good flow and toughness. The adhesion between epoxy coatings and metal surface is excellent so generally primer is not required in coating process. It could also provide smooth finishes with resistance to corrosion, scratching and chemicals. However, epoxy coatings chalk when subjected to UV radiation. For this reason, they are used mainly for indoor applications such as furniture decorations.

Epoxy and Polyester coatings

This coating type combines epoxy resin and polyester resin to form a product which is very close to its epoxy counterpart. It is also known as hybrid powder coatings in combining both characteristics of epoxy and polyester, also it has a competitively lower price. Hybrid coatings are usually for use where tough, flexible and excellent decorative appearances are required, but it begins to chalk when exposed to UV radiation. Hybrids

are likely to be used in many of the same applications as epoxies. The mixing ratio of the two resins is always adjusted to provide desired coating properties.

Polyurethane powder coatings

Polyurethane coatings are suitable for both indoor and outdoor applications. Due to its low viscosity during curing, it could provide a high level of smoothness and gloss coating film. Polyurethane coatings are considered a high end version of polyesters with even stronger bonding to the coating target as well as a better overall appearance in color, gloss and smoothness. Of course the cost of polyurethane is higher as compared to a polyester powder.

Acrylic powder coatings

Acrylic powder offers excellent thin film appearance with good exterior durability and chemical resistance. Because of their perfect electrostatic application characteristic, acrylic powder coatings are often used for top coats on automotive bodies. However, flexibility and impact resistance of acrylic powder coatings are very poor. The overall compatibility with other commonly used powder coating types is relatively weak, which limits acrylic's application [18].

2.3 Powder Coating Manufacturing Processes

Powder coating manufacturing processes include two main stages: (1) hot extrusion: different ingredients are mixed in microscopic scale into a paste, then they form a homogeneous product in the form of chips; (2) Chip product is then ground, classified and collected into powder with a mean particle size of 30-40 μm by using grinding system. The most commonly used one is the air classifying mill (ACM). Each of the processes is discussed as follows.

2.3.1 Hot extrusion

The first step of production of powder coating starts with the hot melt compounding process. It is a classic mixing technique and has been widely used for over 70 years by the industry [19]. During this operation, binder and cross-linker are melted and mixed on

a microscopic scale. The mixture agglomerates are broken into particles due to the high shear mixing characteristic, and are wetted by the melted binder, and then homogeneously dispersed together with additives uniformly [20-22].

Figure 2.2 illustrates a typical hot extrusion process. A common extrusion system includes the screws, barrel and heating/cooling system.

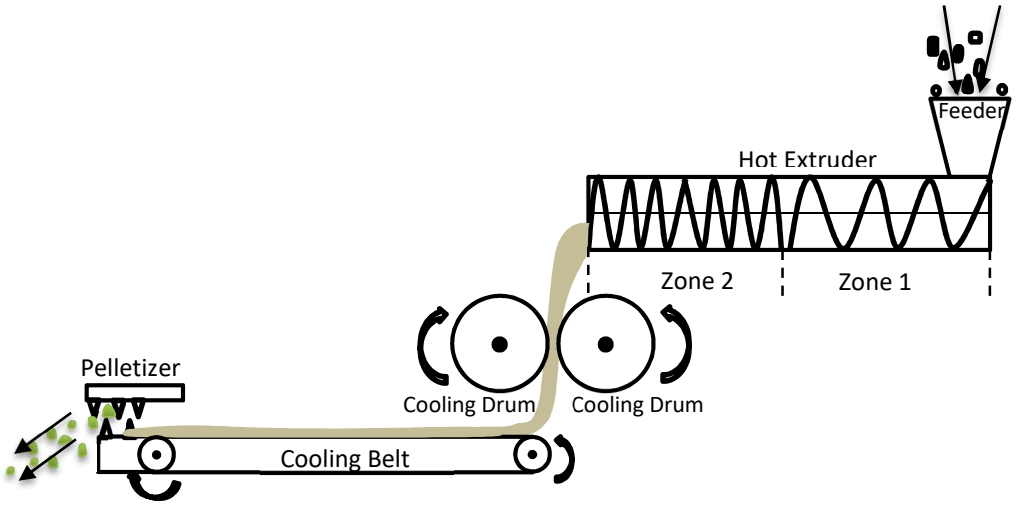

(a) Hot extruder

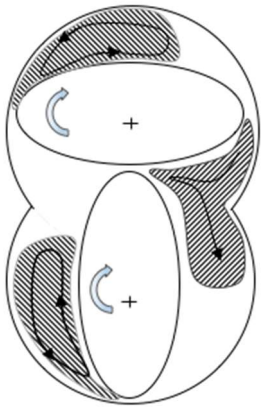

(b) kneading disks in zone 2

Figure 2.2 Hot extrusion process

For powder coating manufacturing, a co-rotating twin screw system is widely accepted to realize a continuous production. In the beginning of hot extrusion process, raw materials including resin, pigment, filler, curing agent, degassing and flow agent etc. are pre-mixed

and fed into the feeder. There are two zones with different temperatures of extruder barrel. As shown in Figure 2.2 (a), zone 1 contains a pair of one-piece screws with large helical threads pushing materials forward. This zone is also where the raw materials start to soften at 40-60 °C. When moving into zone 2, the actual mixing begins at an increasing temperature from 100 to 130 °C. The cross-cut operational scheme shown in Figure 2.2 (b) demonstrates a twin screws with lens-shaped kneading elements arranged in zone 2 of extruder. It could provide an efficient conveying and pressure build up action. Driven by strong agitating force, the softened material is continuously transferred from the district between the wall and kneading disks. The inter-meshing and high shear motion of the screws also help mixing and dispersing to take place. During this homogenizing process, pre-curing of the material could occur if the temperature is not well controlled in the two zones. Larger size of cured material can jam the screws, and may cause operating hazards. Any pre-cured pieces after spraying cause defects on coating finishes.

The homogenous product obtained from the hot extruder is followed by cooling procedure. Two cooling drums roll the hot mixed material into a solid thin sheet and guide it to a long cooling belt with a pelletizer at the end. The cooled sheet is finally crushed into pieces, which are known as powder coating chips and are ready for grinding.

2.3.2 Grinding, classifying and collecting

Grinding

Fine grinding process follows the hot extrusion in powder coating industry after the collected material is completely cooled down. Different types of grinding mills are utilized for the process to achieve size reduction of solid granules. Most of the contemporary grinding systems combine the function of size classification and de-dusting devices together. Figure 2.3 shows the key grinding component of a common impact pulverizer. A chamber with a main rotor with grinding elements evenly distributed at the

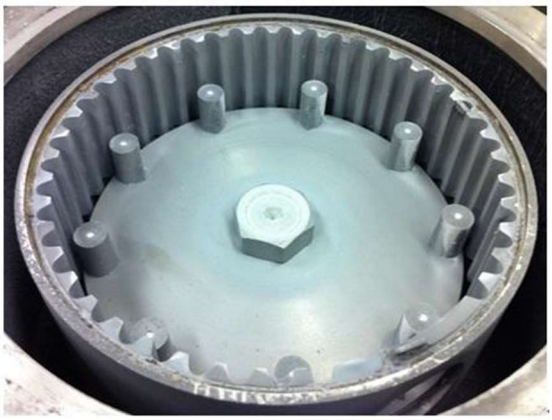

Figure 2.3 A grinder mill of grinding system

edge, and a stationary annular wall with vertical grooves are fitted at the outer part of the rotor with a certain gap size. When the main rotor is operating at a high linear speed (110 m/s), the fed powder coating chips in this grinding chamber are ground fast and broken into powders due to the high shear and impacts between rotating pins and grooves.

Classifying

The contemporary powder coating technique requires an effective classifying process for adjusting the particle size. In particular, fine powder handling is even more challenging because of the agglomeration due to cohesion between particles. These clusters can be broken up by collisions driven by air force. Screen mesh is the best known type of classifier used in separating powders by industries. However, for dry classification of those particle less than 70 μm, the capability of screen classifier decreases rapidly, so that other types of classifiers are recommended. For example, centrifugal classifier of cross-flow or counter-flow, rotor classifiers, cascade classifiers and circulating air classifiers are recommended [23]. Centrifugal classifier with counter-flow is the most widely used one in powder coating industry. The work of the centrifugal classifier is based on vertical air flow action of rotary and cyclonic devices. The effect of the classifier in a cyclone is normally obtained by the tangential air inlet in the case of cyclones shows in Figure 2.4.

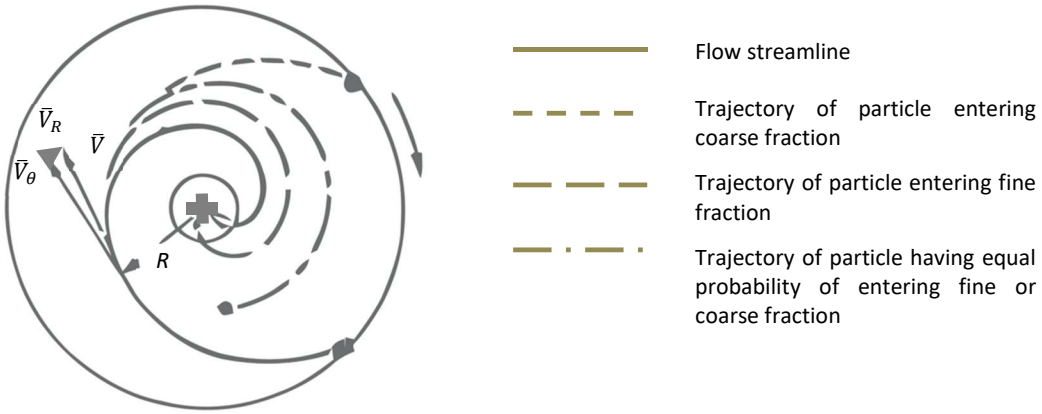

Figure 2.4 Principles of air classifiers [72]

The air vortex causes an inward spiral movement from the tangential inlet to the central outlet. The tangential velocity component (V_t) of one particle in separating device at radial position (R) is given by [24]:

$$V_t = K \cdot R^n \qquad \text{Eq. 2.1}$$

where K and n are geometry constants. The exponent n has the value of 1 for the ideal case for rotary classifiers and -1 for cyclonic classifiers.

However, there is a difference between the tangential velocity component with an actual condition, resulting from the existence of a forced vortex in rotary centrifugal air classifiers that is in the middle of the above two extreme cases. As illustrated in Figure 2.5, a classifier that has a high speed classifying rotor with guider vanes set up on the top of cyclone. When the upward particles encounter the rotating rotor, only small particles could pass through to the top of cyclone while larger particles are rejected. Those larger particles are driven down stream to the cyclone bottom and collected for the further processing.

Figure 2.6 demonstrates the top view of a simplified classifier. A particle in the space between classifier vanes is driven by two forces: drag force (F_d) generated by the driving air and centrifugal force (F_c) caused by spin of the particle. The particle remains in equilibrium if the two forces are equal, and the size of this particle is called the cut-size of this classifier. Bigger particles over the cut-size has larger centrifugal forces and vice

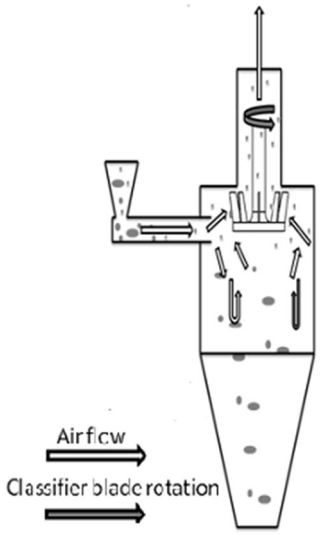

Figure 2.5 A classifier for powder coating

versa. In this way, the cut-size can be varied by decreasing the rotating speed of the classifier by controlling centrifugal force on the particle. The cut-size can also be

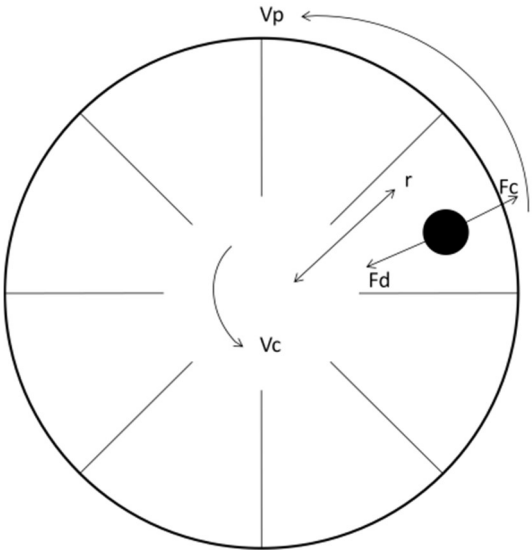

Vp: rotational velocity of the particle; Vc: rotational velocity of the classifier blade;

Figure 2.6 Forces acting on particle within a rotating classifier (Top view)

controlled by changing the drag force of the particle by adjusting the air velocity. In reality, the forces on a particle in classifying process are much more complex than in theory. Due to the influence of air velocity and existence of turbulences and eddies, the

particle can not be successfully classified as predicted. It is because small particles could not pass through the vanes due to outward drag caused by turbulences. Those larger particles could also be driven deeper to the vanes as a result of the centrifugal force decrease. Hence, larger particles could possibly be carried out by the escaping air flow. These above influences directly affect the efficiency and cut-size of the classifier, and further cause the wider particle size distribution of the collected powder product.

Collecting

The collection process of fine powders is usually accomplished by a cyclone in order to separate powder coatings from the air after pneumatic transport. A cyclone is a classic separator which was first invented in 1800's and became the essential component in the modern powder coating grinding systems [20, 25]. They have the advantages of low maintenance and low capital cost, as well as that it could considerably reduce the cleaning expense compared with filters. A typical cyclone consists of a tangential inlet on the top, a vortex finder, a cylindrical barrel and a solid outlet, as shown in Figure 2.7.

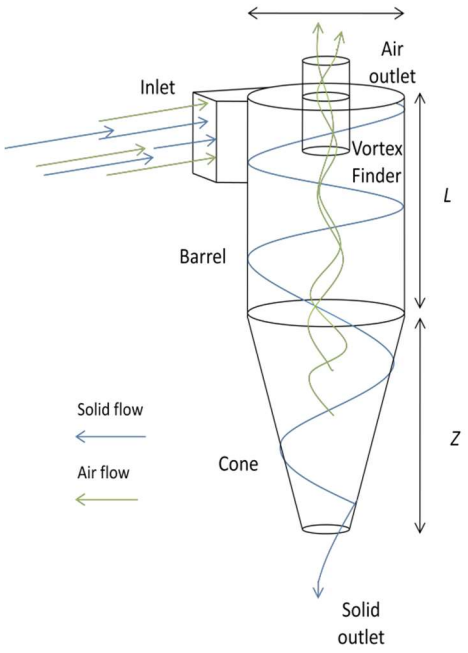

Figure 2.7 A cyclone design

Particles entering from the cyclone inlet are driven by the combination of centrifugal

force and gravity so that they flow spirally along the cyclone inner wall towards the solid outlet. At the same time, majority of air escapes from the air outlet at top of the vortex finder due to the negative pressure while a certain amount of air is flowing downward and creating an “outer vertex” along the cyclone wall [26,27]. This downward velocity diminishes when the air moves close to cyclone bottom, and it eventually turns upward due to the strong suction at the air outlet. This spiral air flow from the cyclone bottom and along the center axis forms an “inner vortex”. Meanwhile, the horizontal inward drift occurs due to the fact that some of the air from the outer vortex is carried away by this inner vortex [27].

The mechanism of cyclones has been widely studied by previous researchers. Leith claimed in 1979 that spinning gas streams due to the centrifugal effect is the key factor to separate particles from the air [35]. Particles are thrown from the cyclone wall to center and they tend to orbit around the cyclone axis according to numerical studies. It is also found that the upward inner vortex flow could create inward drag on the spinning particles near cyclone wall [25,27]. On the other hand, many researchers focused on collection efficiency, and found that the main reason causing great reduction of cyclone efficiency is the particle loss [29-41].

The theoretical cut-size figure is shown in Figure 2.8 with a solid line. Ideally, the situation for particle collection efficiency is either 0% if all the particles are smaller than cut-size, or 100% for particles larger than cut-size that are all collected due to gravity and centrifugal forces. However, the actual efficiency curve follows the dotted S-shaped line. The difference between theoretical and actual grade efficiency curve is due to the following two reasons: Stairmand pointed out that smaller particles could easily agglomerate into clusters which could have been retained inside the cyclone and behaved like larger particles [28].

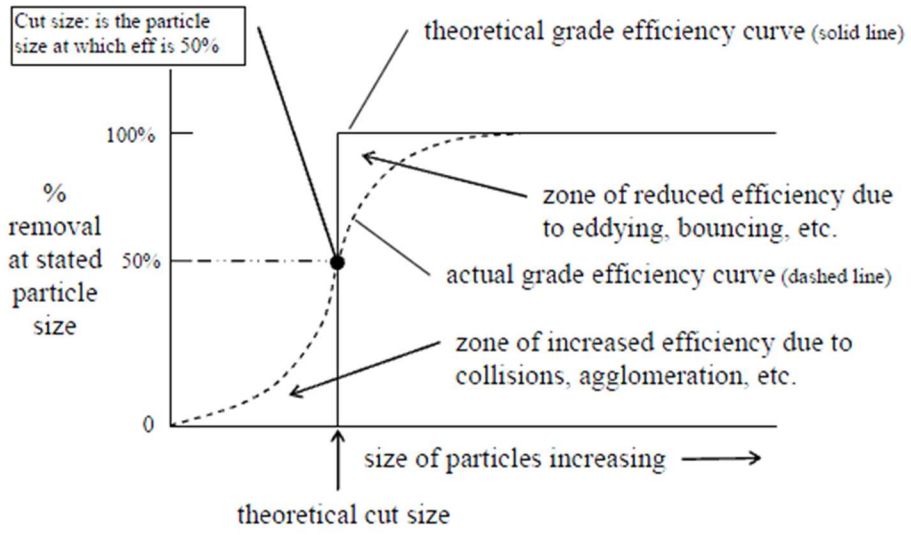

Figure 2.8 Diagram of grade efficiency curve [29]

Moreover, smaller particles could also attach onto larger particle surface by inter-particle forces. In this case, the particles below cut-size are collected so that those particles have a collection efficiency higher than 0%. On the other hand, the collection efficiency for those particles larger than cut-size could not reach 100%, because larger particles could also be guided out through the air outlet by the inner vortex due to the air turbulences and bounces.

In the process of collecting powder coatings, it is crucial to remove small particles as well as retain large particles. However, there is no successful design that has selectivity on particle size currently. Larger particles escape from the cyclone top directly causing reduction of collection efficiency. Therefore, a cyclone with the design of selection on particle size will solve the urgent problem in producing powder coatings.

Air classifying mill

In 1962, the first Mikro ACM (air classifying mill) invented by Hosokawa came on the market. It works as a size reduction mill for various products including powder coatings. The combination of grinding, classifying and integral dynamic collecting could be achieved in one stage operation using ACM, and then it has been fast developed and adapted to many industries especially fine and ultrafine powder coating applications.

Compared with each single stage operations, ACM is less time consuming and less operation complexity. Figure 2.9 demonstrated a typical ACM operating process. The

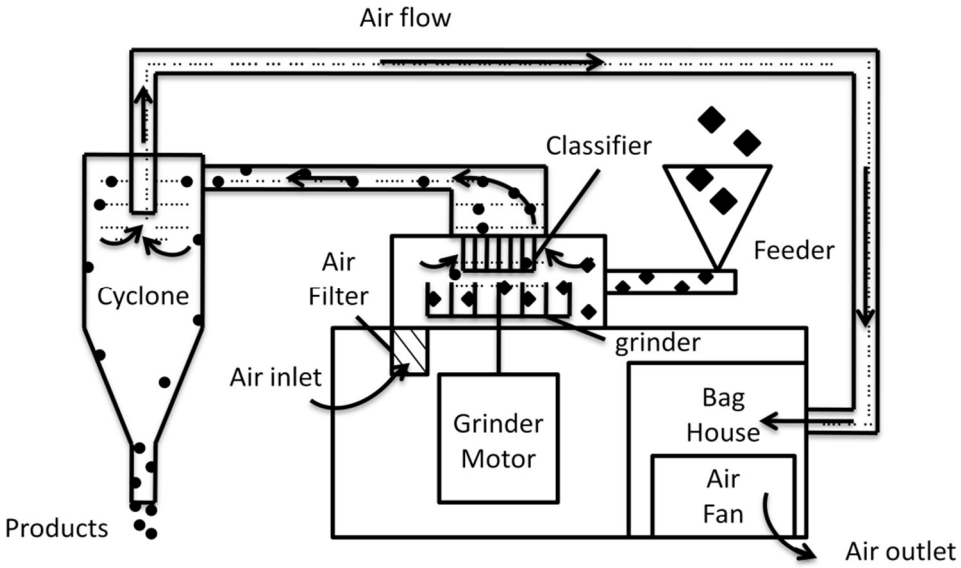

Figure 2.9 A typical air classifying mill (ACM) operation [73]

product is fed from the feeder and pneumatically transferred to the mill chamber, where size reduction takes place. Due to the high speed of rotating grinding rotor, particles are crushed into smaller pieces by the impact on grinding pins and grinder wall with grooves. The striking edge velocity of particles could reach 140 m/s so that d_{10} less than 10 μm is achieved during grinding process. Fine product and air mixtures are distributed by the classifier blades uniformly. At the same time the separation of coarse powder and fine powder takes place due to mass difference. Fine particles which pass through the classifier are guided to an outlet connection followed by a collecting cyclone, while larger particles are rejected and return to mill chamber to repeat the grinding process till they reach the ideal size. There are four essential operating parameters during operating ACM, namely air velocity, feeder speed, grinder speed and classifier speed [42]. Higher total air velocity benefits the classifying efficiency in that it could directly increase the centrifugal force on the particles. Above all, higher air flow could reduce the system temperature so as to help protect the entire system with many moving components. So in order to obtain finer powder coating products, the increase of grinding speed and/or classifier speed is needed. A proper reduction of feeder speed and air velocity is also

helpful to get finer products. In summary, ACM is a grinding system controlled by adjusting overall parameters according to the desired particles sizes. Hence, trials are always needed prior to the production due to the complex determinants.

2.4 Powder Coating Applications

Generally, it is thought that application of powder coating has more difficulties than conventional liquid coating. Unlike those wet paints, powder coating could not dissolve or suspend into solvents. Difficulties of powder coating application are with how to apply it evenly and let the coating melt to form a smooth and continuous film on coating substrate. Also challenges arise in objects with complex geometry. However, it could not draw the conclusion that powder coating is always problematic [20]. Compared to conventional liquid coating, powder coating presents some advantages such as eliminating volatile solvents and have potential 100% utilization of over-sprayed powders. Many different coating techniques have been developed for powder coating application in the past decades, including thermal spraying, electrostatic spraying, fluidized bed, electrostatic fluidized bed and flame spray. The flame spray was invented in 1985 but not yet widely used [43]. These techniques have been proven effective in powder coating application and more advanced than liquid coating. They offer the advantages such as good edge covering, uniform film thickness, absence of sagging problem, low overall costs and more importantly, the recyclability of waste coating materials which meets the most stringent environmental regulations [44]. Some spraying techniques are typical and most widely used currently and they are described in the following sections.

Thermal spraying

Powder coatings become soft and melted at certain temperature. Inspired by this characteristic of powder coatings, thermal spraying was firstly invented for applying powder coatings in the late 1940s [45]. A thermal spray gun is demonstrated in Figure 2.10. At the beginning of the thermal spraying process, the cold air is first heated up and prepared for melting the powder coatings. The fed particles quickly get softened in contact with the heated air and are then transported through the gun to coating target. Then the melted particles build up and form coating film after cooling down. Thermal

spraying is still being used nowadays in powder coating industry. However, the limit of this technique is due to that it is very difficult to control the heating of powder so that it is only suitable for thermal plastic coating application.

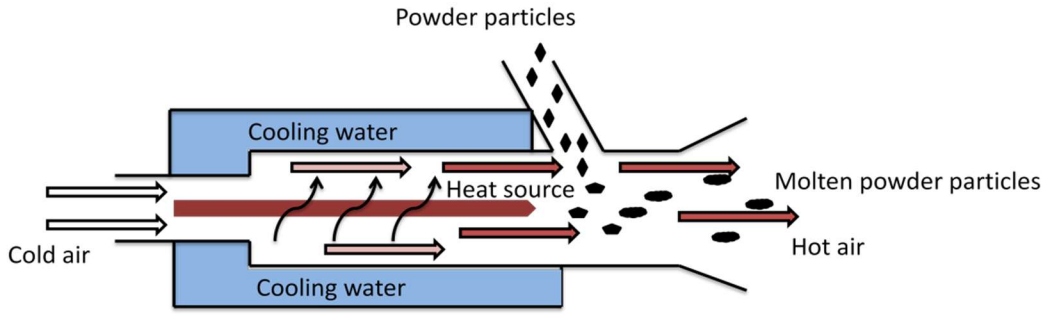

Figure 2.10 Thermal spraying gun

Furthermore, the obtained film thickness after thermal spraying is up to few millimeters in scale, resulting in a rough coating finishes. Also the bonding between substrate and powder coating is weak. Other new techniques were required to overcome those difficulties.

Fluidized bed coating

Powder coatings were firstly applied by fluidized beds, as was patented by Gemmer in 1963 [46]. In this process, the workpiece is pre-heated before conveying into fluidized

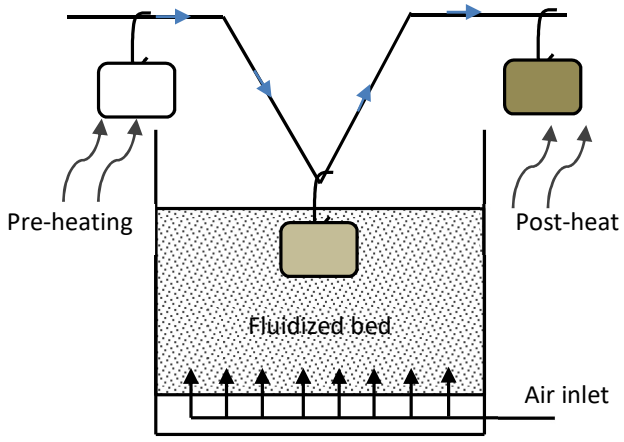

Figure 2.11 Fluidized bed powder coating process

bed, where powder coatings stay at room temperature and are kept fluidized by means of the air stream. Figure 2.11 illustrates a fluidized bed powder coating application. When the pre-heated coating part is moving and dipped into fluidized bed, powder particles soften and adhere to the substrate. The final coating film thickness is determined by heat capacity and temperature of workpiece and its residence time. Then the coated part is cured to form the final coating in a baking oven. The particle deposition rate depends on the particle size very much. In fluidized beds, fine particles are always consumed faster than coarse particles, resulting in size distribution changes with time. However, it could be mitigated by supplying fresh powder continuously. In this way, a constant operating sequence between two dipping operations and residence time of one workpiece could be controlled so as to obtain a final coating product with high quality.

Fluidized bed application could provide an improved overall coating finish compared with thermal spraying due to the better control of heating. The thickness after fluidized bed coatings arrange from 50 to 150 μm which is suitable for both thermosetting and thermoplastic applications [45].

Electrostatic spraying

Electrostatic spraying is one of the most popular techniques for applications of powder coating. It was developed by Pieter and first introduced to industry in the 1960s [47]. The basic principle of electrostatic coating is that the powder is quickly charged in a spray gun chamber and deposited onto coating target by propulsion of compressed air. Charged powder particles can deposit on the grounded target surface firmly due to strong electrostatic force. Some researchers have discovered that particles are still held to coating surface when removing the electric field derived from the gun, as is due to the image charges in the substrate. The negative ions flow from the grounded wire to neutralize the charged particle, meanwhile this image charges can be considered as a capacitor [48]. In this way the powder layer adheres to the workpiece and is ready for baking. The biggest advantage of electrostatic coating is that over sprayed powder could be recycled and reused. In addition, the final film thickness is less than 100 μm, resulting in a significantly improved coating finishes compared with other application methods.

Nowadays, electrostatic spraying is widely utilized by majority of powder coating industry for decorative purposes, and more than 90% of powder coating is applied to metal finishing [49]. Corona charge spraying and tribo spraying are two commonly used types of electrostatic spraying which are reviewed as follows. Corona discharges are low power electrical discharges that take place at atmospheric pressure. The corona is generated by an electric field and always associated with sharp edges on an electrode or small diameter wires. Generally speaking, corona charging is a process to charge materials using ion sources from corona discharge. Powder coating particles (size larger than 0.5 μm) get charged by contacting with free ions which is called field charging [51, 52].

The particle saturation charge by field charging can be derived from Pauthenier limit and described as [47, 51-53]:

$$Q_{max} = 12\pi\varepsilon_0\varepsilon_r r^2 E/(\varepsilon_r+2) \qquad \text{Eq.2.2}$$

where Q_{max} stands for saturation charge, and ε_r is the particle relative permittivity. Corona current for a certain electric field could affect the particle charging time, so as to reach the saturation charge [27,49,53]:

$$\tau = 4\varepsilon_0 E/J \qquad \text{Eq.2.3}$$

where τ is the time for particle to reach half saturation charge, and J is current density. In addition, charging efficiency is also a significant parameter which is described by charge-to-mass ratio (Q/M) and given by [51,52]:

$$Q_{max}/M=9\varepsilon_0\varepsilon_r E/(\varepsilon_r+2)\, r\rho \qquad \text{Eq.2.4}$$

Where Q_{max}/M is inversely proportional to particle radius, and ρ is the particle's true density.

Corona spray gun is one of the most widely used devices for corona charging applications. Particles are directed by flow from a feeder to the inside of the spraying gun, and then they are imparted by high voltage from electrode(s) to get charged. Corona gun also has a good control of the deposition of powder by adjusting electrostatic voltage setups. Figure

2.12 demonstrates a corona charging process. An external high voltage is connected with one electrode inside of the corona gun (some designed with more than one electrode). Normally a negative charge from -30 kV to -100 kV is applied to electrodes and is discharged at the electrode tip of spray gun nozzle. It ionizes the surrounding air and creates negatively charged free electrons in the vicinity of gun tip, which is known as

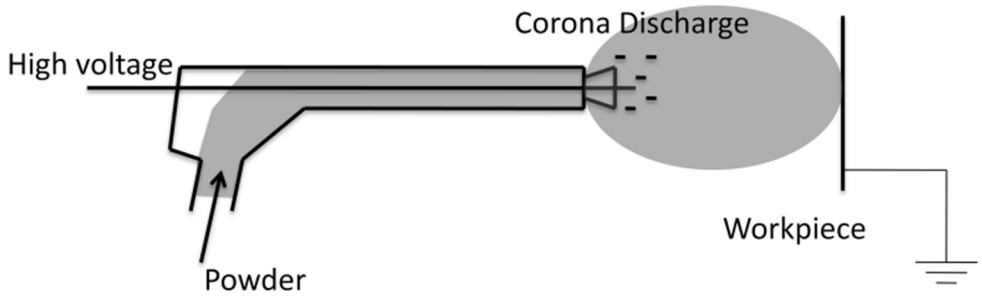

Figure 2.12 A corona charge spraying process

corona discharge. Powder particles obtain negative charges when being sprayed out from the gun and carry free electrons to the coating target. However, not all the moving particles are charged and not all ions are attached onto the particles. It is found that only 0.5% ions are associated with charging particles while 99.5% still exist as free ions in powder cloud [50]. In other words, the powder cloud created by the spray gun consists of charged particles, uncharged particles and negative ions. At the same time, corona discharge also creates a strong electrostatic field between the electrode tip and coating target. As a result, the moving particles are governed by a combination of electrostatic forces and aerodynamic forces [47]. The electrostatic forces become dominant when particles move closer to coating target [56]. Hence, the charged particles attach on the surface of grounded workpiece to form the final film.

Electrostatic spraying has one limit in that it does not cover the recessed area of coating substrate. So it is not favorable for coating targets with complex geometries. Particles tend to cover along edges and corners and this phenomenon is known as Faraday Cage effect. As a result, coatings accumulate on the edge and leave those recessed areas covered with insufficient particles, leading to uneven finishes.

Tribo charging is another significant alternative for powder coating spray. Different from corona charging mechanism, particles get charged mainly by friction. Figure 2.13 shows a tribo spray gun. The basic mechanism of tribo gun is that particles flowing inside of gun chamber touch the wall and baffles, so as to form intensive friction. During this

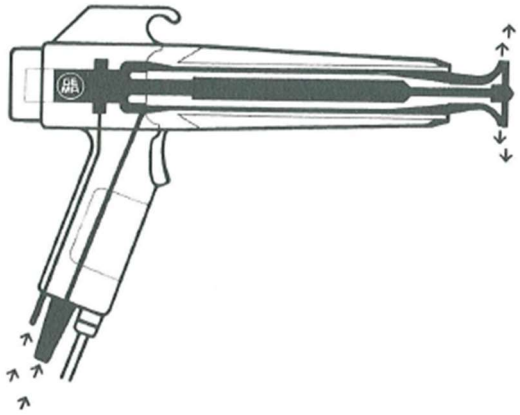

Figure 2.13 Tribo charging gun (source: Ransbwg Gema AG)

process, positive charges are created resulting from the difference of dielectric constants of particle and gun wall surface. It was explained by Davies and Henry that if two insulators are brought into contact, the unipolar charge created by charge transfer remains after their separation [54,55]. In addition, some researchers suggested that the ionic transfer or bulk material transfer should be involved and combined with the friction mechanism to better explain why it is necessary to get sufficient charge transfer [50].

The advantage of the tribo gun is that it eliminates the electrostatic filed between gun tip and coating target, which effectively avoids the Faraday Cage effect. In this way a smoother and uniform film is achieved, even for the coverage on recessed areas. However, the performance of tribo spraying process is sensitive to many factors such as humidity, powder properties and surface condition. Also it has lower charging capability than the corona spray gun, which is considered as a disadvantage in industry with high intensity of production. What is more, the adhesion between the powder layer and coating substrate is weaker due to less particle charge compared with using the corona spraying gun [57-59].

2.5 Trends of Powder Coating Technology

(a) Fine powder coating

Powder coating technology has been fast developing for many years. In recent years, it is widely used in finishing industry in Europe, North America and Asia due to its advantages of no VOC emission and economical consideration [17]. However, powder coating has the main restriction on coating quality so it could not thoroughly replace the liquid paints. The commonly used powder coating has medium particle size from 30 μm to 60 μm, which is known as coarse powder. With current technology, the extensively employed powder coatings cause many aesthetic problems such as thick film thickness (50-100 μm) and coating roughness, reflected by strong orange peel. As a result, powder coating application in most of the finishing industry, especially automotive industries, is only limited to underpart components with lower aesthetic requirement [60]. A potential solution of this problem is using fine powder with particle size less than 30 μm. It has been referred that the film smoothness could be improved and the film thickness is comparable to liquid coating film (25- 50 μm) by using ultrafine powder [61]. In recent years, many automotive industries applied ultrafine powder coatings on car bodies with higher aesthetic requirements. BMW utilizes powder clear coatings on several series of sedans, General Motors also applies powder coating as primer in their 13 plants in North America [62,63]. Since there are fundamental problems in ultrafine powder handling such as dispersion and agglomeration of ultrafine powder coatings, researchers concentrated more on improving the flowability of ultrafine powders. Zhu and Zhang developed an ultrafine powder coating technology with flow additives for enhancing the powder flowability, which successfully realized powder coating application for particles less than 20 μm [64].

(b) Low temperature cure

The curing process of thermosetting powder coating occurs at a temperature from 180 to 200 ℃ for 10 to 20 min, which is not suitable for some heat sensitive substrates. Coating parts like plastic, wood or other temperature sensitive materials are almost impossible to

be powder coated and cured as metal targets. In recent years, the development of low-cure powder coatings has been devoted to formulating powders that could cure at a relatively low temperature (near 100 °C). Low-cure powder coating contains basic resin with curing promoters, where they are functioning as catalysts to accelerate the crosslinking reaction. With this promising technology, more heat sensitive materials made of plastic and wood could be coated and cured without compromising durability or quality [65]. However, it is necessary to pay attention to its transportation and storage stability.

(c) Functional powder coatings

In recent years, powder manufacturers started to offer powder coating product for premium application with higher aesthetic appearance requirements. The utilization of metallic powder is one typical example to provide extra shininess of the final finishes.

In addition, there are also many other new opportunities of functional powder appearing, such as antibacterial and antimicrobial powders, which prevent the spread of bacteria. Furthermore, the finishing on plastics works on improving weatherability, anticorrosion and chemical resistance [66].

(d) Powder coating on insulated substrate

The use of plastic components has been growing steadily due to its lighter weight in reducing overall vehicle weights so as to increase the fuel efficiency. Powder coating on plastics has potential advantages in providing good adhesion, abrasion resistance as well as multitude of color choices. Powder coatings can also be used as a primer in coating plastics to increase the surface conductivity [67].

Reference

[1] Duran, Jacques. Sands, powders, and grains: an introduction to the physics of granular materials. Springer Science & Business Media, 2012.

[2] Lee, Sang Sun, et al. "Gloss reduction in low temperature curable hybrid powder coatings." Progress in organic coatings 46.4 (2003): 266-272.

[3] Yang, Jun, et al. "Dry particle coating for improving the flowability of cohesive powders." Powder Technology 158.1 (2005): 21-33.

[4] Schwedes, Jörg. "Review on testers for measuring flow properties of bulk solids." Granular matter 5.1 (2003): 1-43.

[5] Geldart, Derek. "Types of gas fluidization." Powder technology 7.5 (1973): 285-292.

[6] Taylor, Michael K., et al. "Composite method to quantify powder flow as a screening method in early tablet or capsule formulation development." AAPS PharmSciTech 1.3 (2000): 20-30.

[7] Carr, Ralph L. "Evaluating flow properties of solids." (1965): 163-168.

[8] Jenike, A. W. "Gravity Flow of Bulk Solids. University of Utah Engineering Experiment Station." Bulletin 108 (1961).

[9] Ploof, D. A., and J. W. Carson. "Quality control tester to measure relative flowability of powders." Bulk Solids Handling 14 (1994): 127-127.

[10] Prescott, James K., and Roger A. Barnum. "On powder flowability."Pharmaceutical technology 24.10 (2000): 60-85.

[11] Huang, Qing, Hui Zhang, and Jesse Zhu. "Flow properties of fine powders in powder coating." Particuology 8.1 (2010): 19-27.

[12] Krantz, Matthew, Hui Zhang, and Jesse Zhu. "Characterization of powder flow: Static and dynamic testing." Powder Technology 194.3 (2009): 239-245.

[13] Bailey, Adrian G. "The science and technology of electrostatic powder spraying, transport and coating." Journal of electrostatics 45.2 (1998): 85-120.

[14] Fu, Jing, et al. "Investigation of the recyclability of powder coatings." Powder technology 211.1 (2011): 38-45.

[15] Bocchi, G. Powder coating technology Adv. Mater Process. (1999): 155 23-26.

[16] Richart D., Powder Coating Process, in Kirk-Othmer Encyclopedia of Chemical Technology, John Wiley & Sons, published online, (2001): 7, 35-68.

[17] Bocchi G.J., Join with PCI to improve powder coating community, Products Finishing, (2006): 70(6), 73-74.

[18] Liberto, Nicholas. User's guide to Powder Coating. Society of Manufacturing Engineers, 2003.

[19] Martin, Charlie. "Continuous mixing of solid dosage forms via hot-melt extrusion." Pharmaceutical Technology 32.10 (2008): 76-86.

[20] Misev, Tosko Aleksandar. Powder coatings: chemistry and technology. John Wiley & Sons Inc, 1991.

[21] Wilson, Matthew, et al. "Hot-melt extrusion technology and pharmaceutical application." Therapeutic delivery 3.6 (2012): 787-797.

[22] Particle Sciences, Hot Melt Extrusion, Technical Brief, (2011): 3.

[23] Shapiro, M., and V. Galperin. "Air classification of solid particles: a review."Chemical Engineering and Processing: Process Intensification 44.2 (2005): 279-285.

[24] Schaller, R. E., and C. E. Lapple. "PARTICLE-SIZE CLASSIFICATION OF PLASTIC POWDERS." JOURNAL OF PAINT TECHNOLOGY 44.571 (1972): 86.

[25] Xiang, R. B., and K. W. Lee. "Numerical study of flow field in cyclones of different height." Chemical Engineering and Processing: Process Intensification 44.8 (2005): 877-883.

[26] Su, Yaxin, Anqiao Zheng, and Bingtao Zhao. "Numerical simulation of effect of inlet configuration on square cyclone separator performance." Powder technology 210.3 (2011): 293-303.

[27] Bhasker, C. "Flow simulation in industrial cyclone separator." Advances in Engineering Software 41.2 (2010): 220-228.

[28] Lim, K. S., H. S. Kim, and K. W. Lee. "Characteristics of the collection efficiency for a cyclone with different vortex finder shapes." Journal of Aerosol science 35.6 (2004): 743-754.

[29] Stairmand, C. J_. "The design and performance of cyclone separators."Trans. Inst. Chem. Eng 29 (1951): 356-383.

[30] Lee, Jin W., Hoe J. Yang, and Dong Y. Lee. "Effect of the cylinder shape of a long-coned cyclone on the stable flow-field establishment." Powder technology 165.1 (2006): 30-38.

[31] Hoffmannc, A. C., et al. "Effects of geometry and solid loading on the performance of gas cyclones." Powder Technology 70.1 (1992): 83-91.

[32] Akiyama, T., and T. Marui. "Dust collection efficiency of a straight-through cyclone—effects of duct length, guide vanes and nozzle angle for secondary rotational air flow." Powder technology 58.3 (1989): 181-185.

[33] Tong, Z. B., et al. "Numerical study of the effects of particle size and polydispersity on the agglomerate dispersion in a cyclonic flow." Chemical Engineering Journal 164.2 (2010): 432-441.

[34] Trasi, Pradeep R., and William Licht. "Effect of recycle on cyclone performance." Industrial & Engineering Chemistry Process Design and Development 23.3 (1984): 479-482.

[35] Leith D., In Handbook of Environmental Engineering, (N.C. Pereira and L.K. Wang, eds.). Humana Press, Clifton, N.J., I, (1979): 61.

[36] Qian, Fuping, Jiguang Zhang, and Mingyao Zhang. "Effects of the prolonged vertical tube on the separation performance of a cyclone." Journal of hazardous materials 136.3 (2006): 822-829.

[37] Ray, Madhumita B., et al. "Improving the removal efficiency of industrial-scale cyclones for particles smaller than five micrometre." International journal of mineral processing 53.1 (1998): 39-47.

[38] Ingham, D. B., and L. Ma. "Predicting the performance of air cyclones. "International journal of energy research 26.7 (2002): 633-652.

[39] Ji, Zhongli, et al. "Experimental investigations on a cyclone separator performance at an extremely low particle concentration." Powder Technology191.3 (2009): 254-259.

[40] Swamee, Prabhata K., Nitin Aggarwal, and Kuldeep Bhobhiya. "Optimum design of cyclone separator." AIChE journal 55.9 (2009): 2279-2283.

[41] Rong, R., and T. J. Napier-Munn. "Development of a more efficient classifying cyclone." Coal Preparation 23.4 (2003): 149-165.

[42] Krantz M., Powder Characterization and Powder Application in Automobile Coatings, Master Thesis at The University of Western Ontario, (2009): Charpter 6.

[43] Buren van, M.F, Martin, F. F., Spectrum, Advanced Materials and Chemical Specialties - Products and Technologies. 1988.

[44] Lehmann, R. P. "Optimized powder application of critical objects'." DSM Resins Powder Coating Symposium, Noordwijk. 1988.

[45] De Lange, P. "A History of Powder Coatings." Industrial Paint & Powder 80.2 (2004): 23-27.

[46] Gemmer, Erwin. "Fluidized bed coating process for coating with thermosetting materials." U.S. Patent No. 3,090,696. 21 May 1963.

[47] Bailey, Adrian G. "The science and technology of electrostatic powder spraying, transport and coating." Journal of electrostatics 45.2 (1998): 85-120.

[48] Clements, J. Sidney, and R. H. Bair. "Electrostatic powder coating of insulating surfaces using an alternating polarity internal corona gun." IEEE Transactions on Industry Applications 35.4 (1999): 743-752.

[49] Mazumder, M. K., et al. "Twenty-first century research needs in electrostatic processes applied to industry and medicine." Chemical Engineering Science61.7 (2006): 2192-2211.

[50] Hughes, John Farrell. Electrostatic Powder Coating. SOUTHAMPTON UNIV (UNITED KINGDOM) DEPT OF ELECTRICAL ENGINEERING, 1984.

[51] Wu, Souheng. "Electrostatic charging and deposition of powder coatings."Polymer-Plastics Technology and Engineering 7.2 (1976): 119-220.

[52] White, H. J., Industrial Electrostatic Precipitation (Addison-Wesley Publishing Company, INC.). 1963.

[53] Cross, Jean. Electrostatics, principles, problems and applications. CRC Press, 1987.

[54] Davies, D. K. "The generation and dissipation of static charge on dielectrics in a vacuum." Proceedings of the Conference on Static Electrification, London, pg. 1967.

[55] Institute of Physics (Great Britain). Static Electrification Group. Static electrification, 1971: proceedings of the third conference on static electrification. No. 11. Taylor & Francis, 1971.

[56] Cross, Jean. Electrostatics, principles, problems and applications. CRC Press, 1987.

[57] Mayr, M. B., and S. A. Barringer. "Corona compared with triboelectric charging for electrostatic powder coating." Journal of food science 71.4 (2006): E171-E177.

[58] Kleber, W., and B. Makin. "Triboelectric powder coating: a practical approach for industrial use." Particulate science and technology 16.1 (1998): 43-53.

[59] Trigwell, Steve, et al. "Effects of powder velocity and contact materials on tribocharging of polymer powders for powder coating applications.". Particulate Science and Technology 26.2 (2008): 145-157.

[60] Henson, Bob L. "A derivation of Warburg's law for point to plane coronas.". Journal of Applied Physics 52.6 (1981): 3921-3923.

[61] Giubbilini, Pierluigi. "The current-voltage characteristics of point-to-ring corona." Journal of applied physics 64.7 (1988): 3730-3732.

[62] Gribble P., Development Status of Powder Coatings for OEM Automotive Applications, Finishing Today. 2003.

[63] Biller K., OEM Automotive Powder Coatings, Finishing Today. 2006.

[64] Zhu, Jesse, and Hui Zhang. "Fluidization additives to fine powders." U.S. Patent No. 6,833,185. 21 Dec. 2004.

[65] Palmer, Jeff. "Powder coating expands its reach into industrial finishing."Metal Finishing 103.1 (2005): 9-10.

[66] Kiefer, Steven L. "Powder coating material developments promise new opportunities for finishers." Metal finishing 102.1 (2004): 35-37.

[67] Weigel, K. "A New Technique for the Powder Coating of Plastics."International Polymer Science and Technology 17.5 (1990).

[68] Kaliyaperumal, Souresh, et al. "Fluidization of nano and sub-micron powders using mechanical vibration." Particuology 9.3 (2011): 279-287.

[69] Jiang, Yanbin, et al. "Evaluation of flowability of composite particles and powder mixtures by a vibrating capillary method." Journal of chemical engineering of Japan 39.1 (2006): 14-21.

[70] Yang, Jun, et al. "Dry particle coating for improving the flowability of cohesive powders." Powder Technology 158.1 (2005): 21-33.

[71] Konstance, R. P., C. I. Onwulata, and V. H. Holsinger. "Flow Properties of Spray-Dried Encapsulated Butteroil." Journal of food science 60.4 (1995): 841-844.

[72] Spyrou, Emmanouil. Powder Coatings: Chemistry and Technology. Vincentz Network, 2012.

[73] Fu J., Characterization of fine powders and development of processes for powder coatings, PhD. Theses of UWO. (2013): 54-56.

3 Chapter 3: A novel classifying cyclone for reducing particle size distribution

3.1 Introduction

In the application of the powder coating, the powder flowability is a critical characteristic because it directly affects the final coating quality during the powder handling and spraying. Narrowing down the particle size distribution can improve the flowability so as to achieve a better surface condition [17]. The direct method to reduce the particle size distribution is to remove small particles of the collected particle samples. However, it is very challenging to accomplish since there is a large amount of small particles less than 5 μm generated from the grinding process. In general, utilizing a classifier or other conventional sieving during the collecting process could reduce particle size distribution. Furthermore, some grinding system involves multi-classification processes which could further reduce the finer particle content. Due to the complex operation and relatively high costs, those methods are not widely used in powder manufacturing processes. In this study, a modification of a conventional cyclone was proposed and utilized as a function of classifying cyclone, which would give better classifying performance during the collection of fine powder coatings.

Cyclones are the particle removal devices which collect entrained particles by centrifugal force. It has been established as a low-cost unit operation for removing dust from industrial gas streams in the late 1800s [1,2]. The cyclone efficiency is generally good for particles larger than 5 μm in diameter [3]. As one of the most widely used gas and solid separators, it spins the gas stream without any moving parts. Because of its advantages of simple construction, low capital cost and the applicability to a wide range of operating conditions, cyclones are still widely used today for solid-gas and solid-liquid separations [4].

A typical cyclone contains a cylindrical barrel, a cone and a vortex finder, as shown in Figure 3.1. Due to the suction of the air outlet, particles are guided tangentially into the top of the cyclone barrel during the operation. Then the particles flow mainly near the wall of the inner barrel, driven by the gravitational forces and the centrifugal forces. Most

of the particles flow helically because of the rotating gas flow, while some particles are driven by the exiting air through the vortex finder and then escape from the top after entering the cyclone [5]. Many numerical studies suggest that the air velocity becomes much lower in the lower part of the cyclone, and as a result, the air flow eventually turns around and towards the top of the vortex finder due to the outlet suction. This creates the inner vortex in the middle of the cyclone. Meanwhile, the remaining smaller particles would easily be carried away from the outer vortex. This process is denoted as a horizontal inward drift, and the smaller particles are removed from the introduced powder as they are more subjected to the aerodynamic forces.

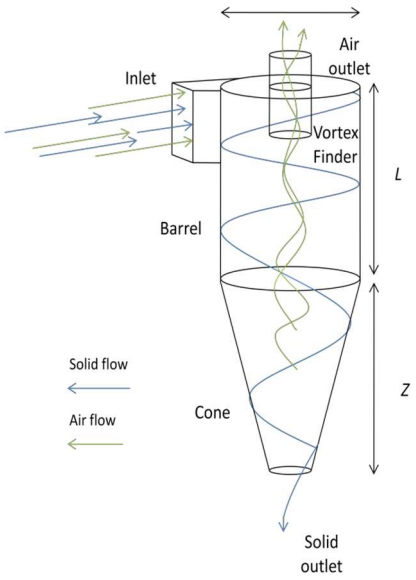

Figure 3.1 The reverse flow cyclone

In recent years, more industrial operations required higher collection efficiency and researchers focused on improving the efficiency of those particles smaller than 5 μm. The collection efficiency and pressure drop are two main criteria for evaluating the performance of the cyclone collection [6]. Many researchers who have devoted to designing cyclones for decades also used these two factors. The main purpose of modifying the cyclone is narrowing down the particle size distribution, which can benefit the powder flowability so as to improve the quality of the powder coating for high-end uses. As previous numerical studies indicated, the particles orbit along the cyclone wall and around the axis on a cross-section of the barrel of the cyclone. At the same time, the

air flow moves upwards in the radial direction and goes through from the vortex finder, resulting in discharge. In this way, the brought up particles are removed from the cyclone [1,5]. Leith stated that the separation of the particles from the air relies on the spinning gas stream, as a result of the existence of centrifugal forces [7]. Both the inward air drag force and centrifugal forces have influence on different particle sizes, as shown in Figure 3.2 [1,8,9,10]. The larger particles are affected more by the centrifugal forces, so the combined force acting on the particle points towards the cyclone wall. If the particle is small and light, the inward drag force is dominant, so the combination of the force points opposite the wall and towards the cyclone axis. Due to this phenomenon, the small particles are easily cleared away, resulting in the reduction of the collection efficiency. However, by utilizing a classifying cyclone, it could help with reducing the particle size distribution of the collected particles in a way that the small particles are retained inside the cyclone and then removed.

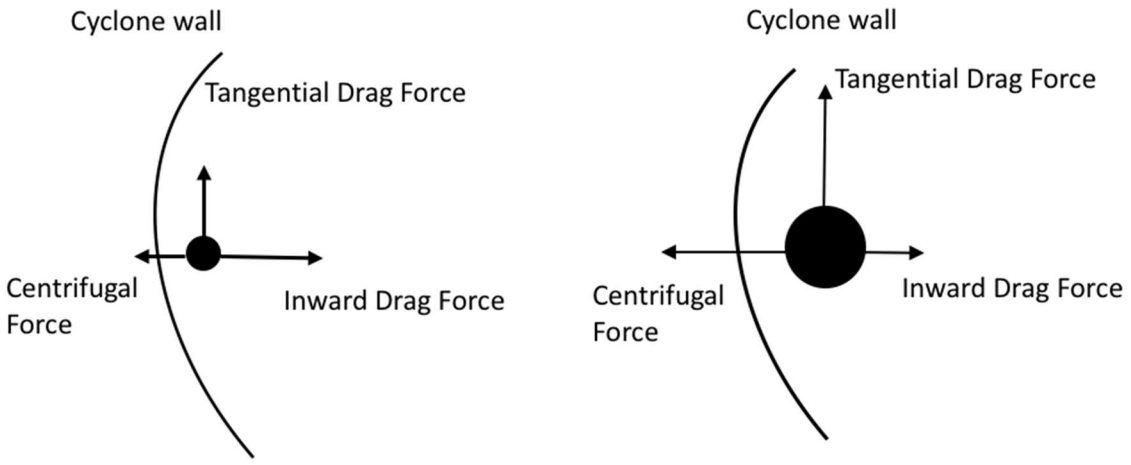

Figure 3.2 Forces on small particles (left) and large particles (right) on a cyclone cross-section [10]

Furthermore, in an ideal situation, a cyclone has a theoretical grade efficiency curve with a certain cut-size shown in Figure 3.3. The particles smaller than the cut size should not be collected in the final samples whereas the collection efficiency could reach 100% for the particles larger than the cut size. However, due to the existence of agglomeration of the smaller particles as well as the difference of forces acting on the particles, the actual collection efficiency curve follows an S-shape, as illustrated in Figure 3.3 in dotted line.

The finer particles get agglomerated and even form into larger and heavier clusters due to the strong inter-particle cohesion, so they are difficult to disperse in the cyclone at low flow rates [11]. When the finer particles agglomerate into larger clusters, they are no longer dominated by the inward force. Instead, the clusters could be retained inside the cyclone. In addition, the smaller particles are likely to attach onto the large particles or the cyclone wall by the inter-particle force during pneumatic transport. In this way, the collection efficiency of the particles below cut-size would not be 0%. In terms of the large particles, the collection efficiency could not reach 100% for the reason that they may also escape through the vortex finder during operation due to the impact of turbulences, bouncing and eddies. In consequence, the actual collection efficiency of the large particles above the cut-size is smaller than 100%.

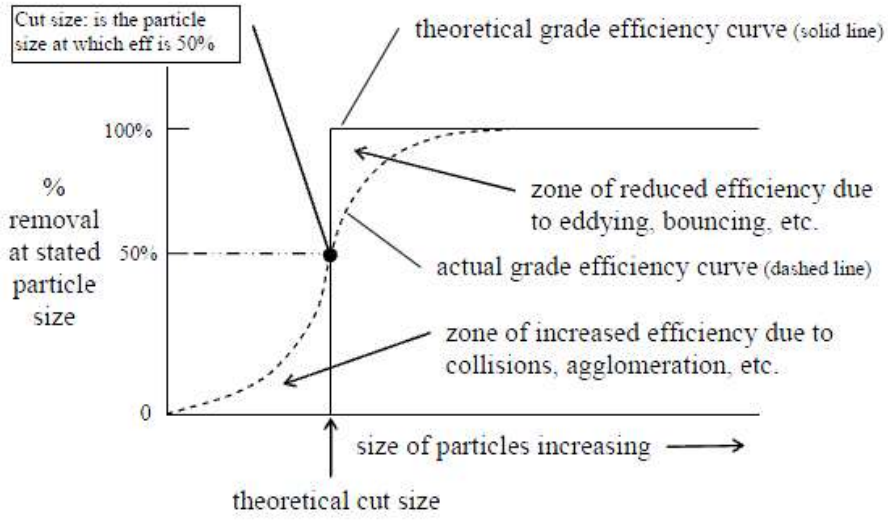

Figure 3.3 Diagram of grade efficiency curve characteristics [10]

Previous researchers indicate that when optimizing the dispersion performance, both effects of flow rate and particle size distribution should be taken into consideration [11]. Some work shows that the principal source of de-agglomeration is drag force, while other believes that the agglomerates would be reduced by the separation force due to mechanical impaction [12,13]. As an inspiration to this study, when removing the small particles, a certain amount of large particles could also escape during the process.

In this study, the proposed classifying cyclone is somehow contradictory to the conventionally used cyclone which focuses more on improving and maximizing the collection efficiency. However, the classifying cyclone of air classifying mill (ACM) in this study is aiming at removing specified particles. In processing the powder samples, after the grinding and classifying system, a large amount of fine particles is generated in the powder sample. When applying the collected powder into a spraying booth, it is more difficult to spray ultrafine powders compared with regular powder coatings, as the fine particles deteriorate the powder flowability, resulting in a poor film quality. In this study, the ACM is utilized in grinding and classifying the particles. Experimental results showed that the D_{10} is less than 6 μm for the fine powder particles and 12 μm for the coarse powder collected by the conventional cyclone. The generated fine particles get agglomerated easily so that the modification of the new cyclone is aiming at removing the smaller particles so as to narrow down the particle size distribution.

3.2 Related Work

The purpose of the cyclone modification and optimization in this study focused on removing particles rather than maximizing the collection efficiency compared with the traditional improvement on the cyclone. Along with the reduction of small particles, the particle distribution could be improved. However, the collection efficiency is affected and becomes lower with the reduction of the amount of smaller particles. In order to optimize the cyclone efficiency, the new cyclone design introduces the secondary air inlet at the bottom of the reverse flow. As shown in Figure 3.4, there is a thin gap opening at the bottom of the cyclone. Given that the gap is relatively smaller than the whole scale of the cyclone, the air is easily induced into the cyclone at a high speed by the vacuum due to the suction from cyclone top. As a result, the upward flow can be enhanced so as to help remove the small particles. Meanwhile, the introduced secondary air also breaks down the particle agglomerates at the bottom of the cyclone. This design does not require any other external power supply, as the secondary air gap was open to the atmosphere.

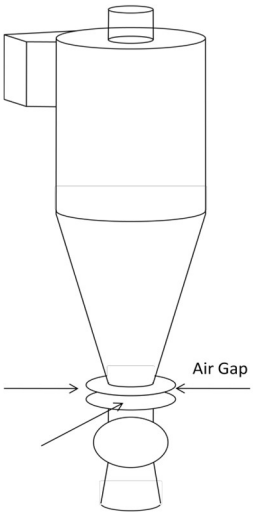

Figure 3.4 The reverse flow cyclone with the secondary air gap

Although a few similar designs and modifications have been mentioned in previous literature, especially for the cyclone application in ACM, some of the study and findings could still provide a guidance for the work today in this study. Darrow invented a cyclone utilizing reverse air to remove the fine particles [14]. As shown in Figure 3.5, the additional classifying air inlet is introduced at the bottom of the cyclone. This was more efficient due to the inner structure which could redirect the fine particles near the wall

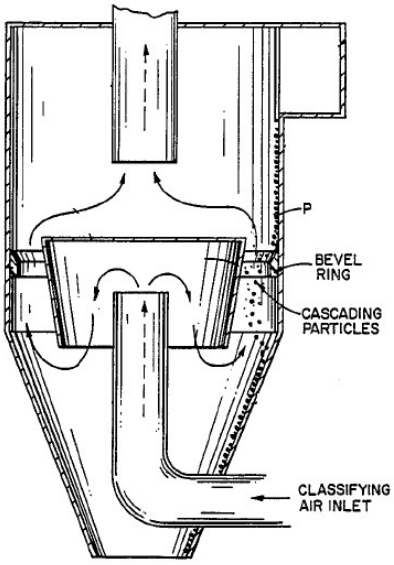

Figure 3.5 The classifying design by Darrow [14]

back to the classifying air. Similarly, Schwamborn et al. proposed a cyclone collector having two secondary air nozzles at bottom which could provide the upward flow, as illustrated in Figure 3.6 [15]. Thus the fine particles nearby can be carried away by the

classifying force and taken back upwards. Ikebuchi's cyclone bottom design has the annular pipes around the lower conical part, as shown in Figure 3.7 [16]. The gas streams are blown through these pipes so as to form a swirling current, thus the particles inside of

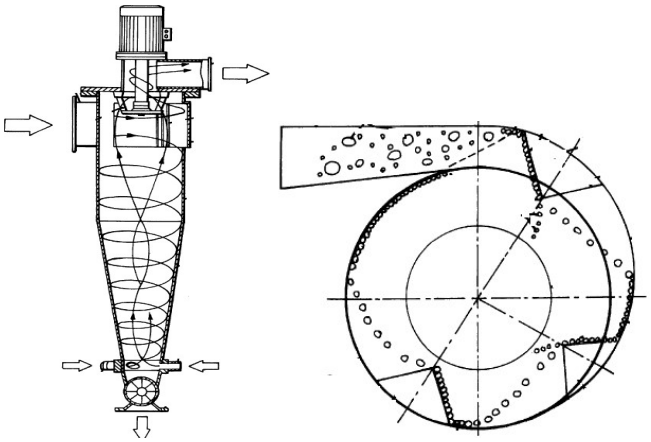

Figure 3.6 The classifier design by Schwamborn et al [15]

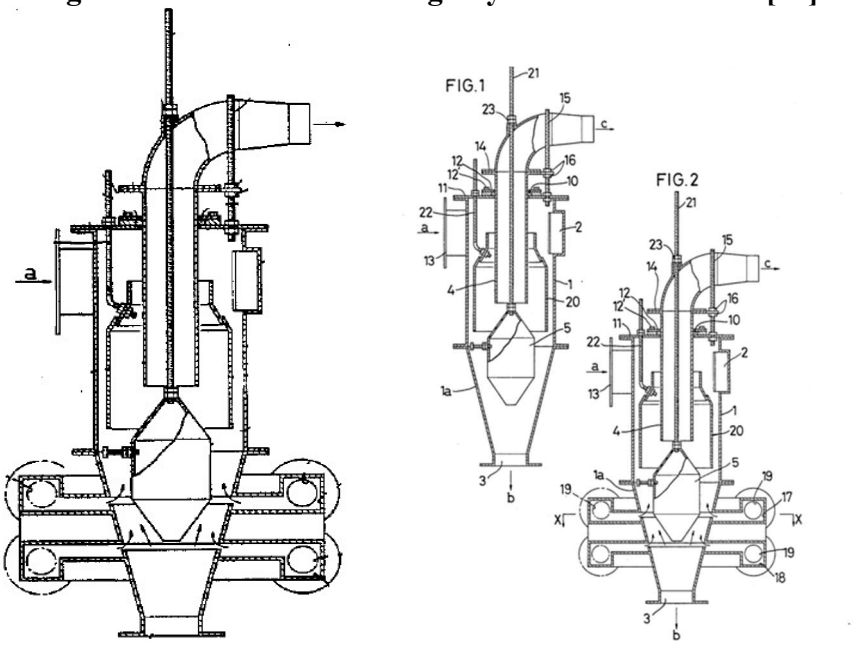

Figure 3.7 Classifier design by Ikebuchi et al [15]

the cyclone would be reclassified. According to the above three patented designs, additional reverse flow are all utilized to get rid of fine particles but this study proposes a different modification method. In the referred invention, removal of small particles can definitely improve the classifying efficiency of the cyclone but it causes the reduction of collection efficiency due to increased entrainment of the larger particles. So the inner structure deflectors are added in the cyclone body in order to minimize the adverse effect

brought by the reverse flow, so as to maintain the collection efficiency [14-16]. However, those designs of the cyclone were too complex and very difficult to adjust and modify during industrial application.

3.3 Materials and Methods

The new modification of cyclone in this study aimed at removing smaller particles as it has the ability to break down the powder agglomerations and guide more particles by the enhanced upper flow. Most importantly, compared with previous designs, fine powder was also investigated in the new cyclone other than only using the coarse powder in the previous patented designs. So it was more challenging in removing the small particles since the agglomeration is more severe for fine particles. In the case of the powder grinding system, since ACM is the most commonly used and integrated machine, it is difficult to change or reassemble any part of it. So the biggest advantage of this new design was that the secondary air inlet at the cyclone bottom can be adjusted easily without changing any structure of the cyclone, also other parts of the ACM can remain unchanged. In addition, the simple design at the bottom of the cyclone provides more convenience for future research and industrial scale-up.

Nevertheless, same as the patented designs, the collection efficiency is still the most significant factor when removing the particles and it may be further reduced by adding the external air inlet. Therefore, the invention of the air guiders was made in order to solve the problem. As shown in Figure 3.8 (a), the air guider is made by cylindrical solid wires of different diameters mounted on a thin plastic shim. Thus the wires can provide the different heights when being installed between the gap. During the experiment process, the shim was inserted with the air guider facing downward, as Figure 3.8 (b) shows. In this way, the air guiders provided the spinning motion in the same direction as the vortex at the bottom of the cyclone. As discussed in previous studies, due to the centrifugal effect, the outer vortex could be enhanced and it helps retain the large particles. As a result, the outer vortex at the bottom part could be strongly enhanced without carrying out the larger particles, so as to maintain the collection efficiency.

(a) The secondary air guider

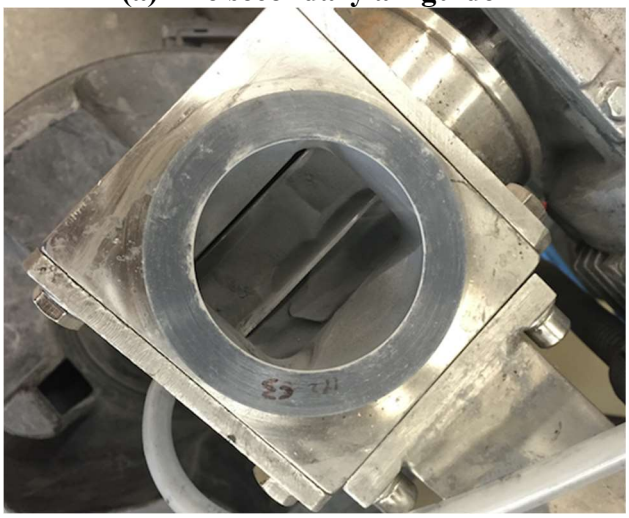

(b) provide spin motion with the same direction of

Figure 3.8 The insert shim with secondary air guider at cyclone bottom

Several series of experiments were conducted in evaluating the real performance of the modified classifying cyclone. The modification was carried on the cyclone connected to an air classifying mill (ACM) (manufactured by Donghui Powder Processing Equipment Co., Ltd., China). As illustrated in Figure 3.9, the original resin chips were fed into the ACM and ground by the center rotating mill into particles. In general, different particle sizes could be obtained by adjusting the rotor grinder and classifier speed. The classifier keeps the larger particles inside the grinding chamber for further grinding while the particles with proper diameter can go through and be collected by the cyclone. When the particles were guided into the cyclone, the classifying effect still existed because of the effect of rotating gas flow. The schematic of the cyclone is shown is Figure 3.10. The

materials of the powder and chip sample were provided by Seibert Powder Coatings (Cleveland, Ohio, USA).

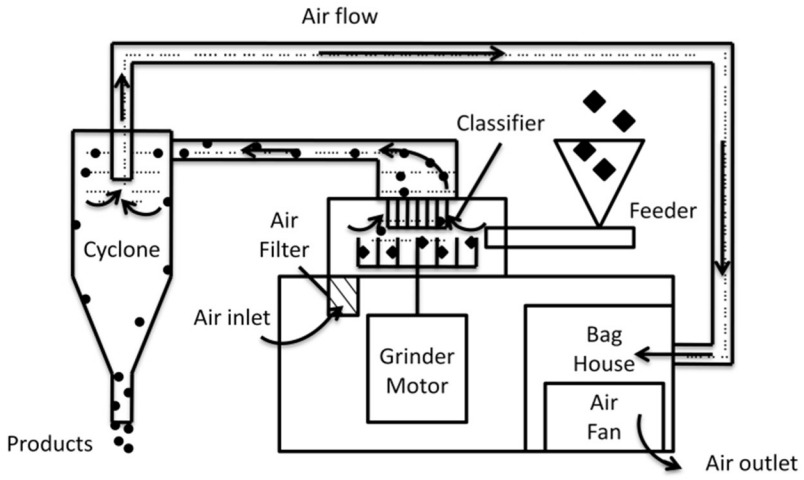

Figure 3.9 Schematic of the laboratory scale ACM [10]

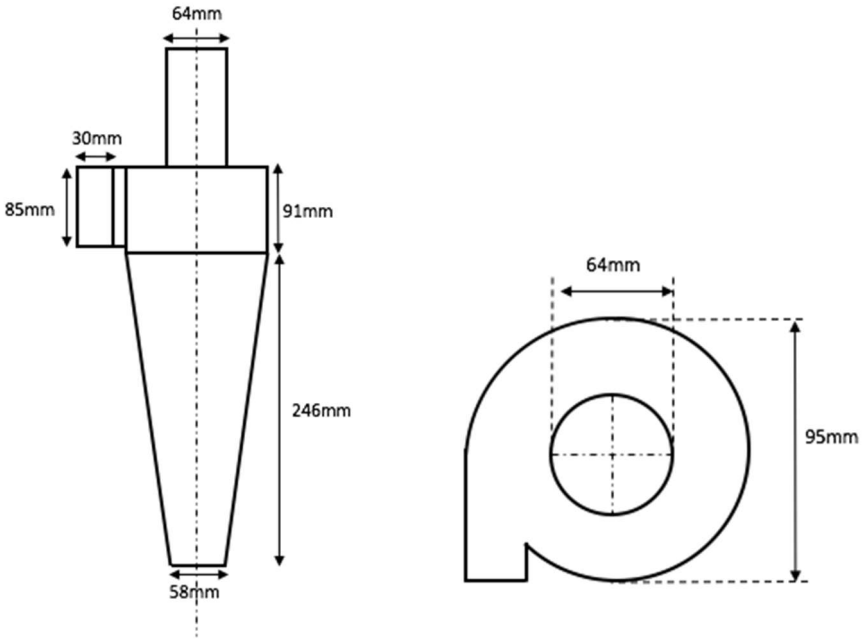

Figure 3.10 Dimensions of the cyclone on the ACM (drawings were not to the scale)

In this experiment, three different configurations of the secondary air guider have been investigated. As shown in Figure 3.11, the secondary air guider consists of a plastic ring shim with an inner circle diameter of 58 mm, the same as the connection part of the cyclone bottom (with outer circle diameter of 80 mm). The shim was attached with the cylindrical solid wire on it for guiding the direction of inlet air. The three shapes of the

air guider are chosen as convex, linear and concave by adjusting the curvature of the wire. Each of the shims have 16 evenly distributed wire guiders at different angles. The actual air guider at 45° angle is illustrated in Figure 3.11 (a) left. The first applied convex shape

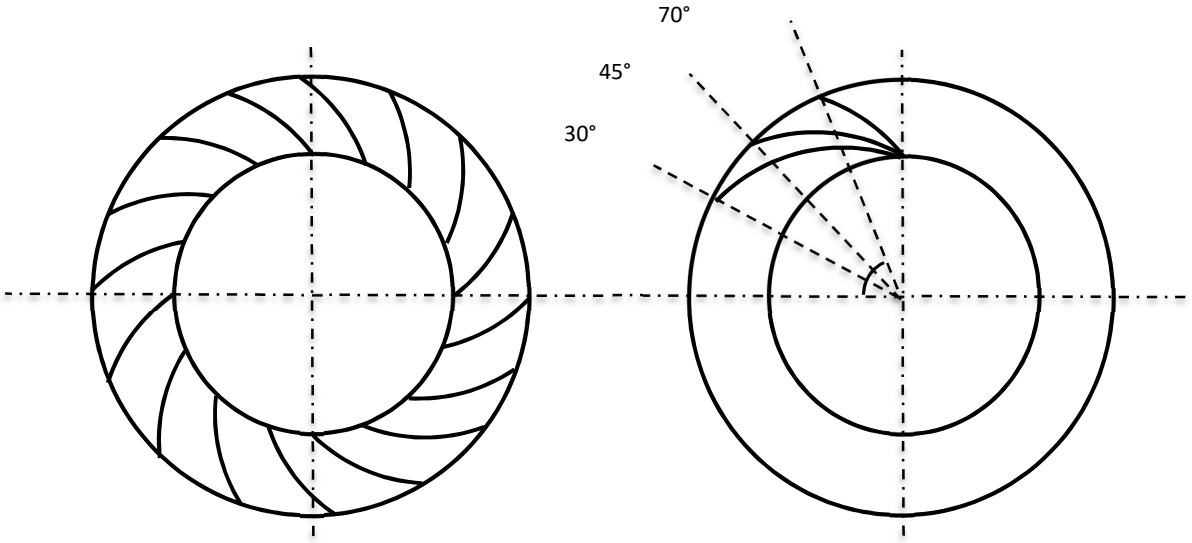

(a) Convex secondary air guider and 70° guider example

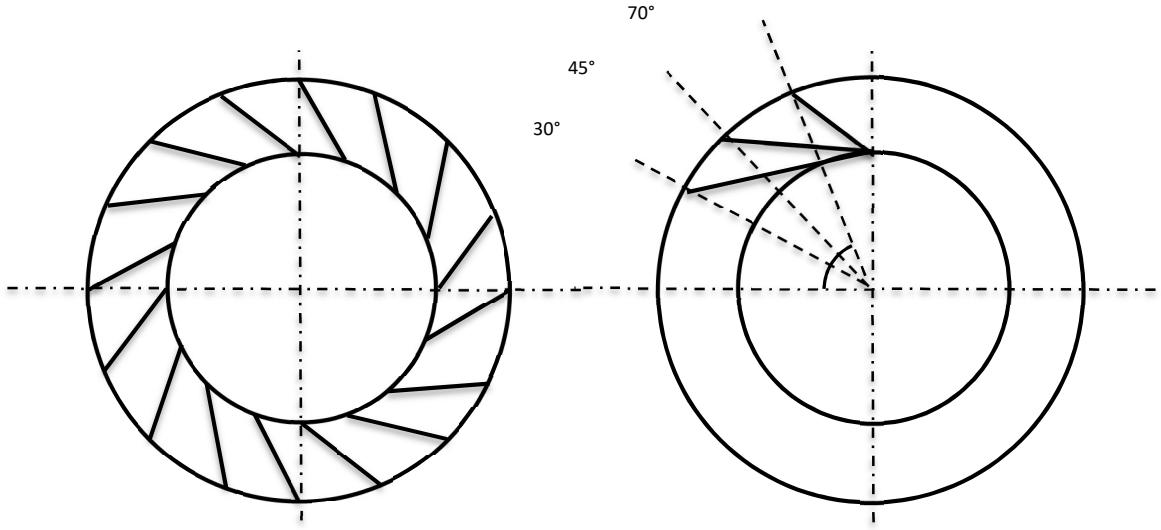

(b) Linear secondary air guider and 70° guider example

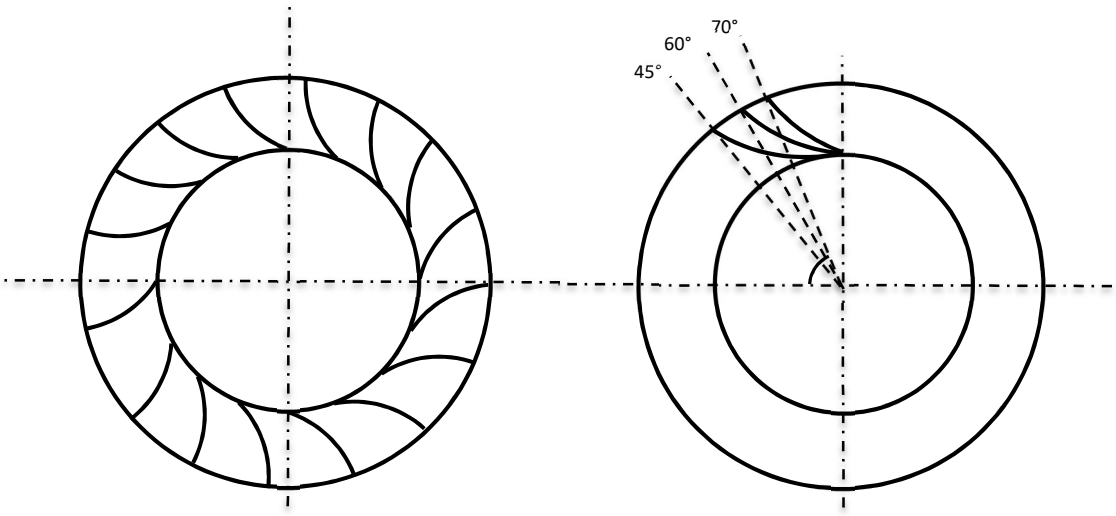

(c) Concave secondary air guider and 70° guider example

Figure 3.11 Schematic of the second air guider with different shapes

air guider started from the inner circle arc to the outer circle arc, decided by the angle from the circle center, as shown in Figure 3.11(a) right. The rest of the air guiders followed the same angle. There are two other angles for each of the air guider shapes: 30˚, 45˚ and 70˚, as shown in Figure 3.11 (b) to (c). Similarly, the manufacturing of linear and concave guiders used the same method. In order to control the accuracy, the curvatures of both convex and concave wire come from the arc of a circle with 50 mm diameter, the three angles were also utilized in each shape. However, for the concave air guider the angle switched to 45˚, 60˚ and 70˚ for better experimental comparison, as shown in Figure 3.11 (c). In general, when the reverse air goes into the air guider, the higher degree of the air guider mainly leads the air velocity through the radial direction while lower degree provides air velocity along a tangential path. The wire shape influences the air velocity into the cyclone so as to create different secondary air spinning motion. In this way the small particles could be driven by the various upward flow conditions. Adjusting the wire with different diameters could change the opening gap of the secondary inlet

when inserting the shim at the cyclone bottom. Three sizes of the secondary inlet opening gap have been investigated: 0.25 mm, 0.56 mm and 1.00 mm, named as Gap1, Gap2 and Gap 3 respectively.

In addition, the materials fed into the ACM were in two groups: coating chips and the ground powder. The experimental study started with grinding powder chips into coarse powder in ACM. Four main parameters of ACM in controlling the final sample were adjusted during the grinding. In order to obtain coarse powder (around 35 μm in D_{50}) from powder chips, the rotor and classifier speeds were relatively lower compared with collecting the fine powder (around 22 μm in D_{50}), also the fan speed which controlled the total air flow was adjusted to the optimal operating range and maintained. At the same time, the feeding speed remained unchanged once other operating conditions were finalized during the whole experiment. As listed in Table 3.1, each of the two types of feeding material was ground into coarse powder and fine powder. The coating chips were the product of the extruder and they had irregular shapes with an equivalent diameter of 5-30 mm. The grinding process started with feeding the chips directly into the ACM rotating feeder. By adjusting the speed of main grinder and classifier, powder samples with selected size distributions were obtained. In this study, both coarse and fine powders were processed and classified through the new modified cyclone. So the powder produced directly from coating chips in the ACM without using secondary air guider was used as a control.

Table 3.1 The list of the material tested in the experiment

Material type	Size distribution	D_{50}(μm)	D_{10}(μm)	D90(μm)
Coating chips (Control group)	Coarse powder	35.83	11.94	73.5
	Fine powder	22.37	7.1	47.24
Ground powder (Control group)	Coarse powder	37.41	12.99	74.34
	Fine powder #1	19.99	6.04	43.49
	Find powder #2	22.67	7.99	44.59

The purpose of using the coating powder as the feeding material was to eliminate the influence brought by the rotor grinder and classifier while investigating the efficiency of the classifying cyclone. If the rotor grinder and classifier were at relatively low speeds, almost no grinding happens in the grinding chamber, thus particles do not have much size reduction when passing through the main grinder. As a result, the dominant classifying

process happens in the cyclone with the air supply from ACM, and so the performance of the modified cyclone with a secondary air guider could be better evaluated without side effects from other components of the ACM. In particular, two kinds of fine powders which differ in D_{10} were tested, as shown in Table 3.1. In industry fine powder is defined as that of median particle size below 30 μm, while ultrafine powder with size smaller than 25μm, the D_{10} of which is around 6 μm. The fine powder #1 is a typical ultrafine powder from the industry. However, the fine powder #2 was pre-treated and with D_{10} around 8 μm, which was used for further examining the ability of the new cyclone in removing smaller particles.

In order to further evaluate the performance of the modified cyclone design, the particle size distribution (PSD) and collection efficiency were the two main factors for the evaluation. The particle sizes of the collected powder sample were measured by a laser particle size analyzer (BT9300S, Bettersize Laser Analyzer, China). The collected particle sample were dispersed in water with the help of detergent, then fed into the analyzer through electromagnetic vibration feeding system. During the process of free falling of particles, shoot particle images which pass the lens randomly. Meanwhile, software quickly recognizes and processes particles using the high light LED array light source and screen displays images. Particle size and particle shape data for each particle in real time. As it adopts high-speed CCD that can reach 100 frame/min, thousands of particles can be shot and processed per minute. In addition, image process software can recognize and extract adhesive particles automatically. These technologies improve the accuracy of particle image greatly. A typical particle size distribution curve is shown in Figure 3.12, where D_{10}, D_{50} and D_{90} are three significant values in evaluating the powder size distribution. Particle size distribution indicates the particle size in percentage of a given sample. For example, D_{10} is the diameter value of 10% volume fraction of the particles with the diameter less or equal to, the same as D_{50} and D_{90}. Normally the D_{50} is named as the median particle size of the powder, and D_{10} and D_{90} represent the amount of small and large particles in the sample. Increasing the D_{10} and decreasing D_{90} without changing D_{50} could lead to a steeper distribution curve. One of the other significant

values of the size distribution curve is the span, which is determined by the equation below:

$$\text{Span} = \frac{D_{90}-D_{10}}{D_{50}} \qquad \text{Eq.3.1}$$

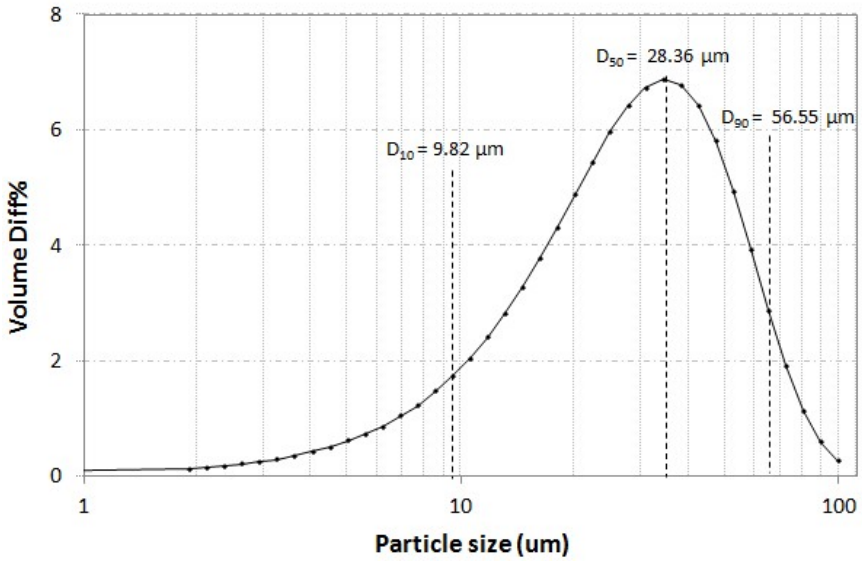

Figure 3.12 An example of particle size distribution

As reflected in Figure 3.12, the span determines the overall shape of the size distribution curve. Narrow PSD curves indicate the reduction of span, which is mainly caused by increasing D_{10} and decreasing D_{90}. It is always desirable to narrow down the size distribution, as when D_{10} and D_{90} are identical to D_{50}, the powder sample has the ideal uniform distribution and every powder particle has the same size. Generally speaking, reducing the span could improve the powder flowability as well as the coating quality.

In addition, the collection efficiency was calculated by:

$$\eta_{Collecting} = \frac{W_{Collecting}}{r_{Feeding} \times t_{Feeding}} \qquad \text{Eq. 3.2}$$

where $\eta_{Collecting}$ was the collection efficiency, $r_{Feeding}$ stood for the feeding rate, $t_{Feeding}$ was the feeding time and $W_{Collecting}$ represented the weight of collected powder sample. The feeding rate remained constant during the experiments. In conclusion, the

classification target was to narrow the span without sacrificing the collection efficiency, and above all, to remove the small particles (to increase D_{10}) from the powder sample.

3.4 Numerical Study

3.4.1 Modelling design

Numerical simulations of the air flow inside the proposed classifying cyclone have been conducted in this study. The models of cyclones were drawn in GAMBIT (version 2.4). As shown in Figure 3.13, in order to prevent the air escaping from the cyclone bottom, the original cyclone was attached with a collecting box, which was similar to the function of an airlock in real cyclone. A total of three models were drawn, namely (a) original cyclone, (b) cyclone with convex air guider, (c) cyclone with linear secondary air guider, (d) cyclone with concave air guider. The simplified model name of Model O, Model Convex, Model Linear and Model Concave were used to denote the original cyclone and three modified cyclones in the following discussion. All the three models of modified cyclone had identical dimensions of all cyclone parts as Model O and had 1.0 mm opening gap. The angle of air guider was 45° in each model. The modeling object is the fluid air under the turbulent flow dispersion model.

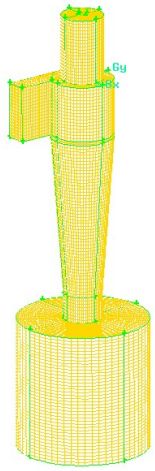

(a) Original model of the original cyclone, Model O;

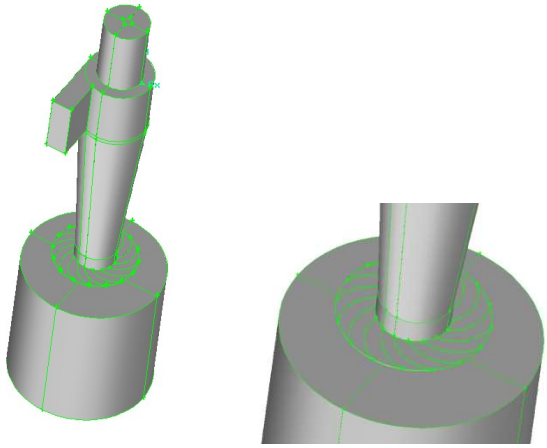

(b) Cyclone model with convex secondary air guider, Model Convex

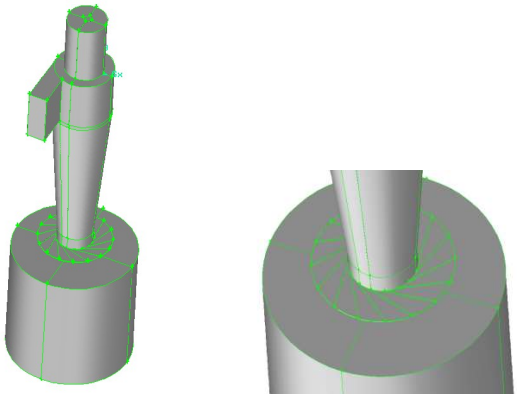

(c) Cyclone model with linear secondary air guider, Model Linear

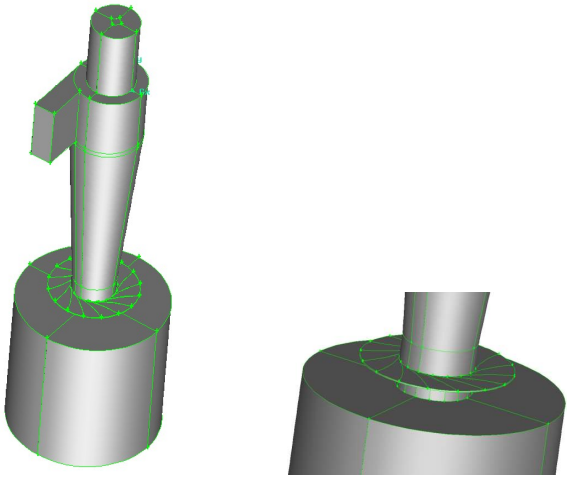

(d) Cyclone model with concave secondary air guider, Model Concave

Figure 3.13 Cyclone model drawn by GAMBIT

The air flow inside the three models was simulated in Fluent (6.3). The model O had one air inlet and one outlet while the other three had two air inlets and one air outlet. The input parameters were measured from the actual cyclone. The injected air velocity is

10.89m/s and the secondary air inlet velocity is 0.5m/s under the Reynolds stress model (RSM).

3.4.2 Results and discussions of the numerical simulations

The axial velocity vector of model O is illustrated in Figure 3.14. The color gradient represents the magnitude of air velocity and the arrows represent the air directions. According to the figure, the air starts to accelerate when it enters the cyclone from the air inlet and when moving to the center vortex finder, the velocity reaches its maximum due to the suction from the cyclone top. As a result, smaller particles are guided out by the escaping air through vortex finder, while some larger particles go downward with

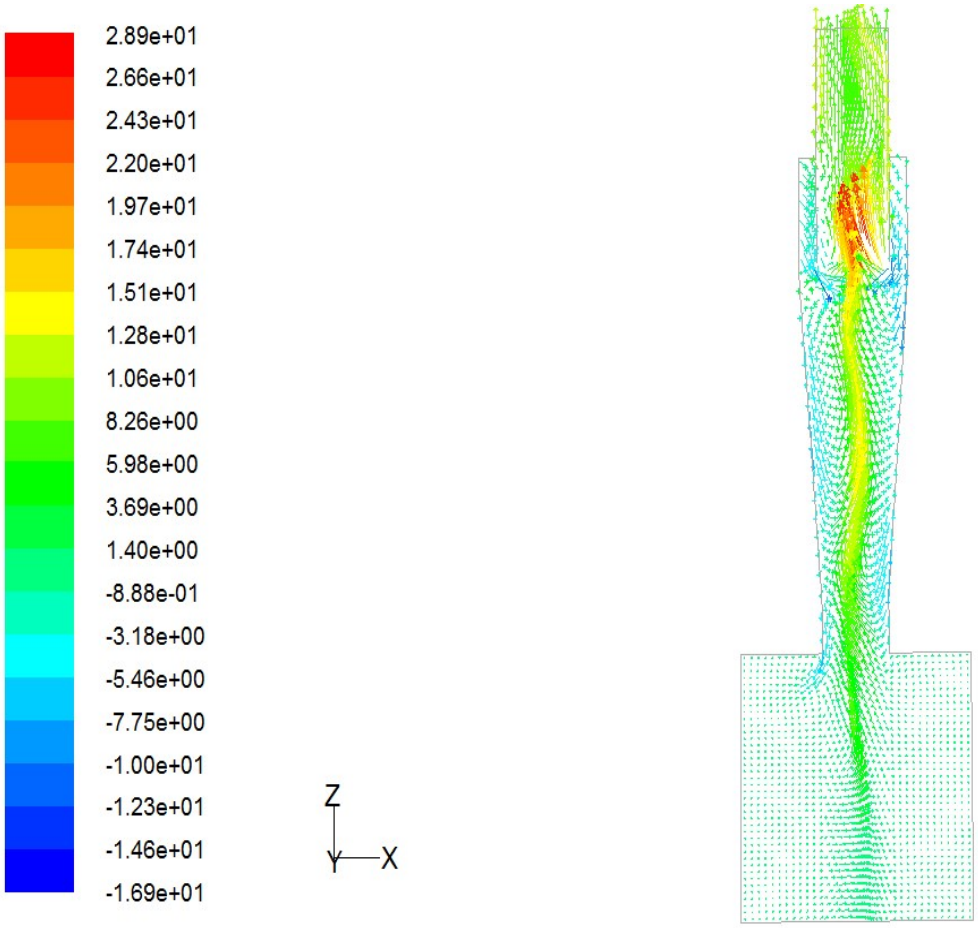

Figure 3.14 Axial air velocity of Model O

swirling air flow. According to the 2D velocity vectors, it is obvious to see an upward flow in the middle of cyclone representing the inner vortex. The velocity vectors close to the cyclone bottom along the wall indicate a downward outer vortex. However, the

velocities decrease when reaching the very bottom part and finally turn upward due to the suction at the air outlet. Meanwhile, the inward drag is induced between inner and outer vortexes, illustrated by the horizontal velocity vectors.

The Model Convex has a secondary air inlet at cyclone bottom to induce the reverse air flow. The convex air guider introduced the inlet air into cyclone to form the air spinning at the same flow direction as the outer vortex. As shown in Figure 3.15, compared with Model O, the downward velocity at the wall region at the cyclone bottom was decreased, indicating the introduced reversed upward air flow. Meanwhile, the smaller particles were dominantly controlled by inward drag force as the decreasing of downward flow. As

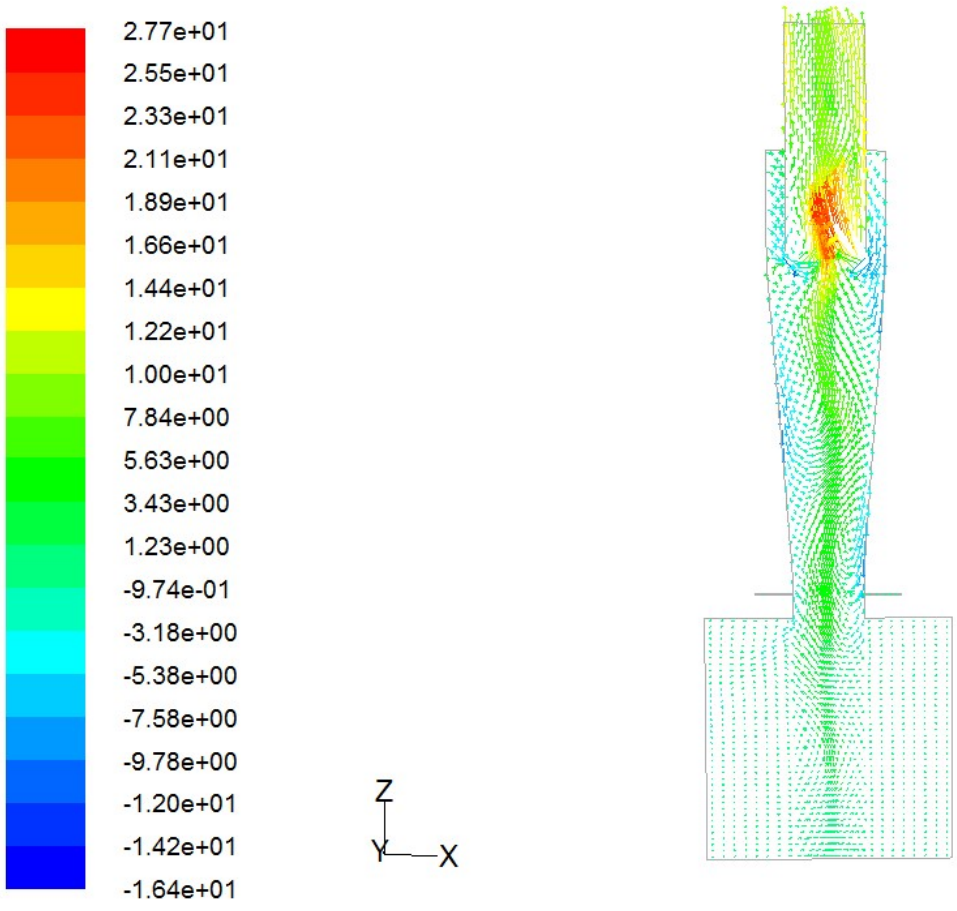

Figure 3.15 Axial air velocity of Model Convex

a result, they were easily driven by air force to the cyclone center and carried away from cyclone top. It has also been observed that the outer vortex region became wider and

extended to the collecting box. The model only simulated the air flow inside of the cyclone, it could still interpret that the strong upward air flow at cyclone center was

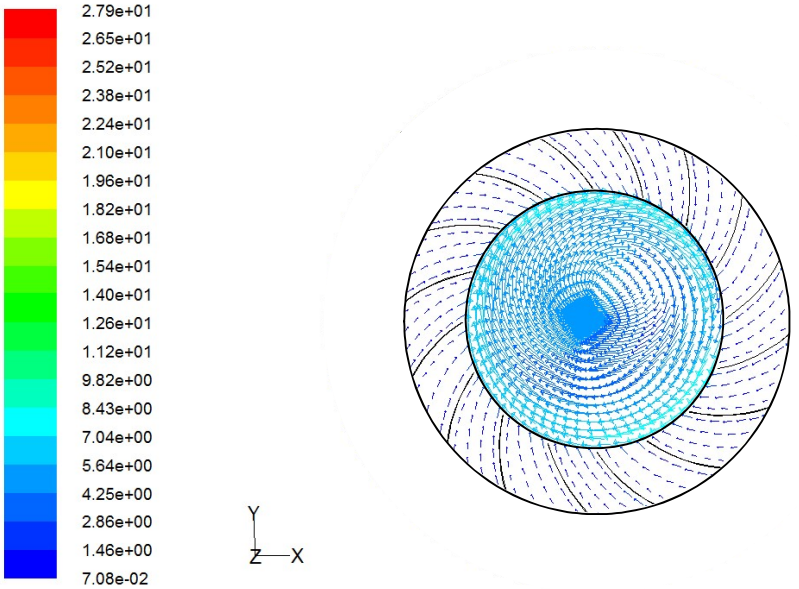

(a) Model Convex

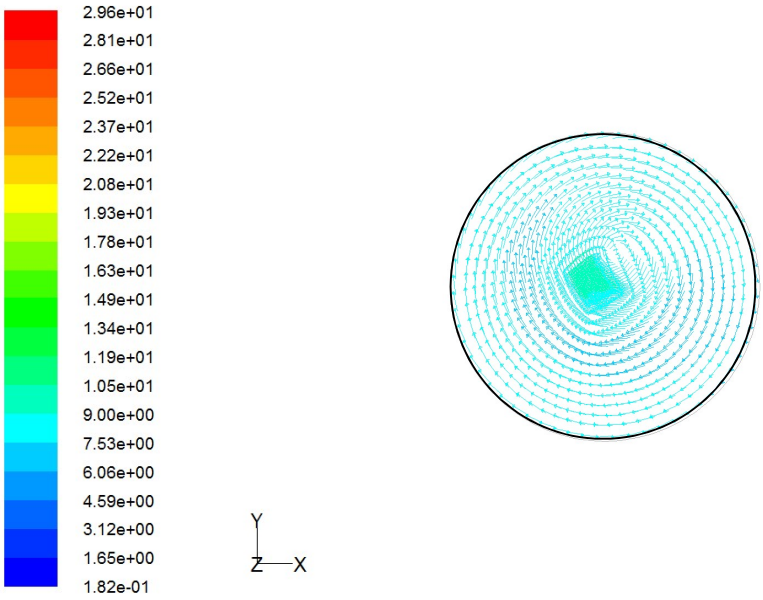

(b) Model O

Figure 3.16 Velocity vectors of cyclone bottom cross section with Model Convex and Model O

diminished so as to prevent a large amount of particles from escaping through the cyclone top. In this way the collection efficiency was maintained.

This phenomenon could also be explained by the velocity vector at the cross section of the cyclone bottom with convex air guider, as shown in Figure 3.16 (a). It is obvious that the secondary air flow enters the cyclone tangentially and accelerated when moving to the cyclone core. The maximum air velocity occurred along the wall region, resulting in a stronger outer vortex. Then the radial velocity became smaller when moving near to the axis, which implies that the air was controlled by the inner vortex and started to flow along the axial direction.

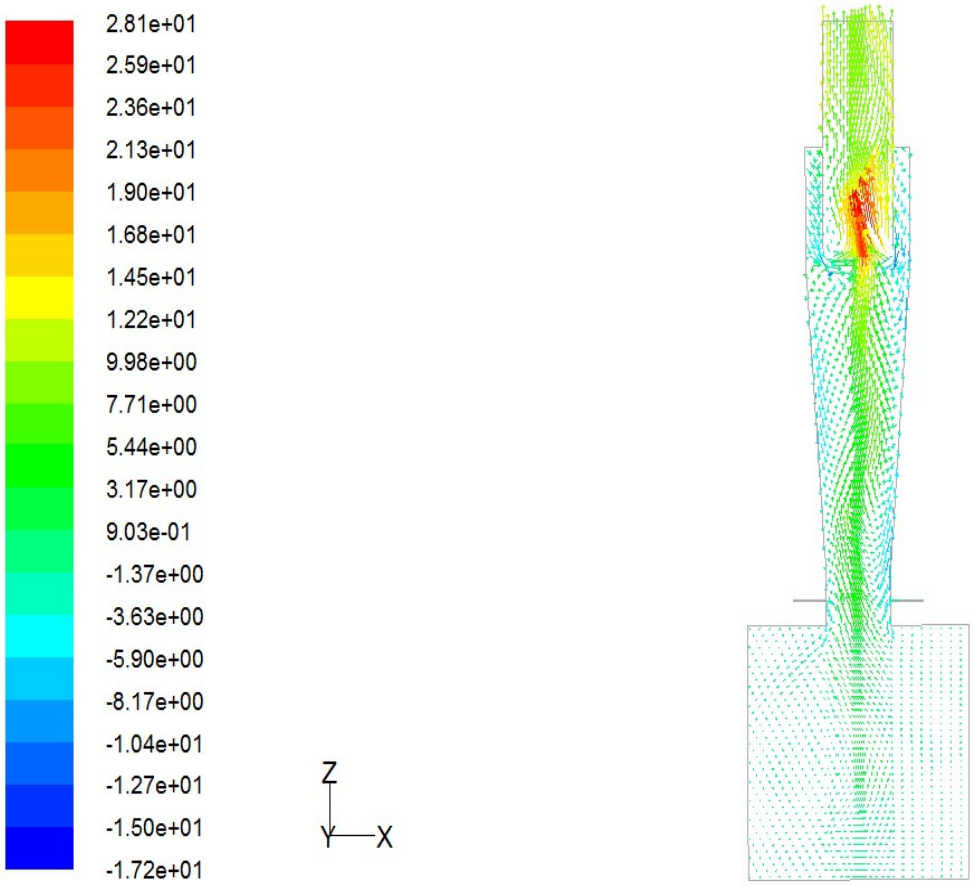

Figure 3.17 Axial air velocity of Model Linear

Compared to the velocity vector at cross section of the Model O, (Figure 3.6 b), the convex air guider could provide an obvious air spin motion with both outer and inner vortexes, so as to further enhance the classifying at the cyclone bottom. Meanwhile, small particles could be further carried away by the drag force induced between the outer and inner vortex. While the Model O without air guider does not provide a secondary

classifying process when particles reach the cyclone bottom. In summary, the secondary air spinning created by the air guider could effectively enhance the outer vortex so as to help further classify particles. During the spinning, small particles attached on larger particles could be blown away due to this enhanced outer vortex, leading to a better particle size distribution of the collected powder. The modeling result obtained from the linear secondary air guider in Figure 3.17 had similar results as Model Convex. There was an obvious reverse flow region at the cyclone bottom wall compared to model O. Similar to Model Convex, the linear air guider results showed a much narrower inner vortex and wider outer vortex, owing to the existence of the secondary air inlet and air guiders. Larger particles could be retained due to the reduction of the inner vortex. The air velocity vectors at the cross section of the air guider is illustrated in Figure 3.18. The tangential air inlet has the maximum velocity near the wall annulus region, greatly

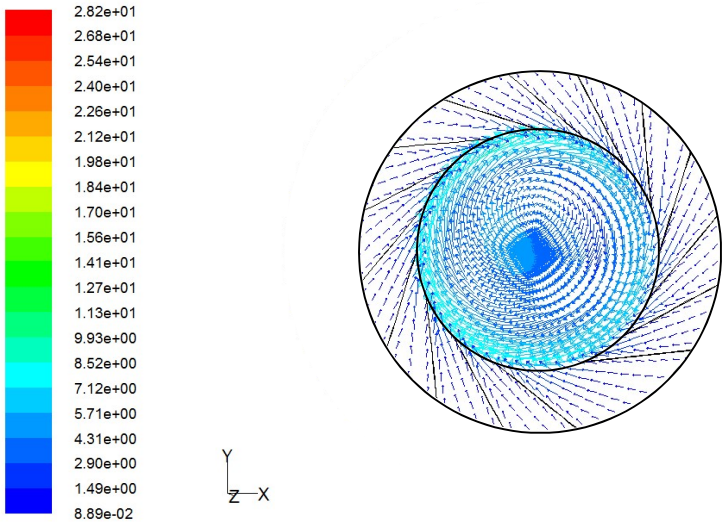

Figure 3.18 Velocity vectors of cyclone bottom cross section with Model Linear

boosting the outer vortex. The secondary classification of small particles happened during this air spinning. Meanwhile, the larger particles were driven by this outer vortex and finally collected in the final powder sample. When the secondary air reached cyclone center, it became much slower. Compared to Model Convex, the secondary air inlet provided by the linear air guider had similar intensity near the cyclone wall, indicated by the color of air velocity.

Figure 3.19 demonstrated the results of axial velocity utilizing concave air guider. The reverse flow had higher intensity when entering the cyclone bottom compared to Model Convex and Model Linear. Furthermore, this phenomenon could be better explained by the air velocity near the air guider, as shown in Figure 3.20. The air velocity in the annulus region became higher in forming the outer vortex, then decreased at the cyclone core. This outer spinning was greater than Model Convex and Model Linear, resulting in the stronger outer vortex so as to remove more small particles during the air spinning. When moving to the cyclone core region, the radial velocity decreased due to the inner vortex.

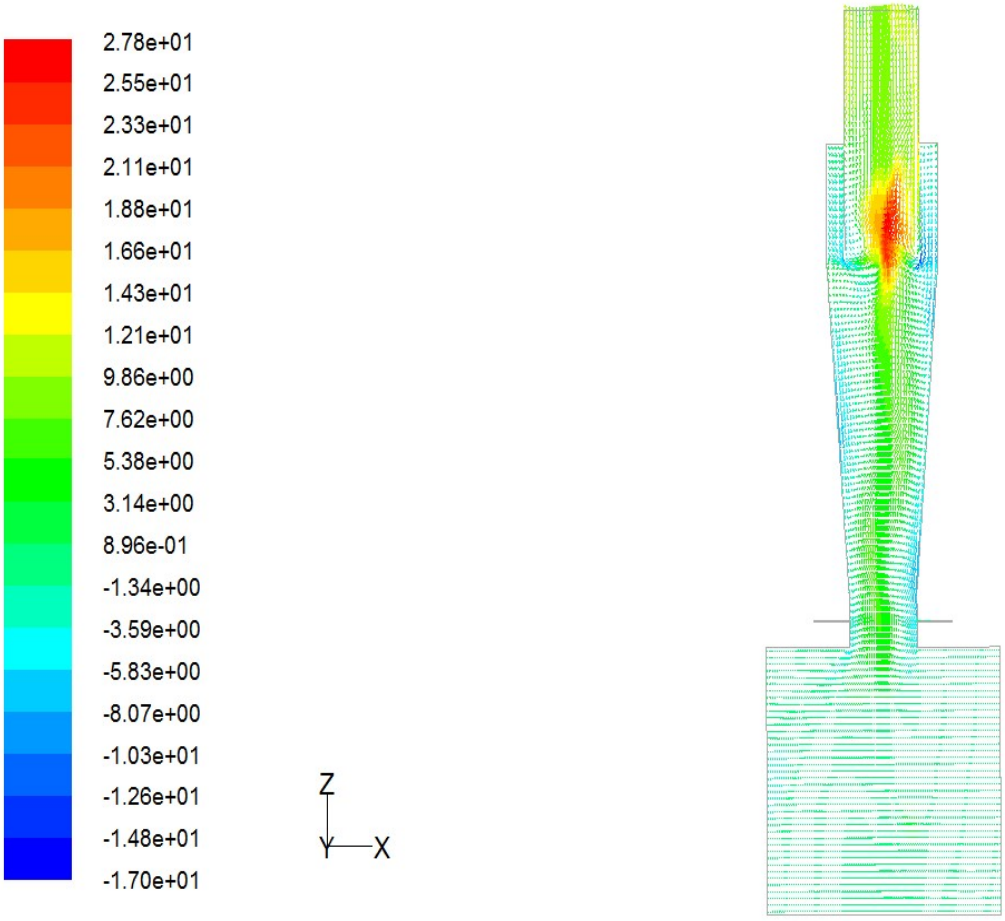

Figure 3.19 Axial air velocity of Model Concave

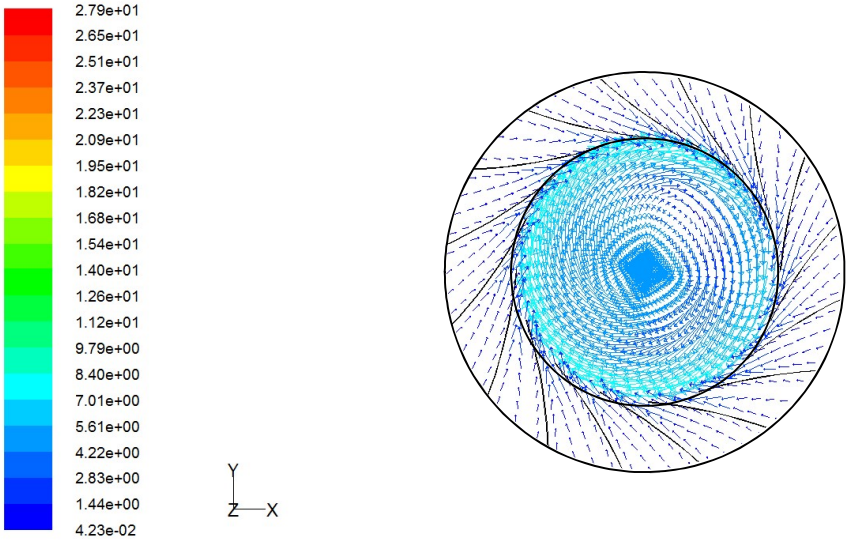

Figure 3.20 Velocity vectors of cyclone bottom cross section with Model Concave

The axial air velocities with respect to the cross-sectional radius of secondary air inlet of all the three models have been studied. As plotted in Figure 3.21, the concave air guider could provide the relatively stronger reversed air flow at the wall region, in line with the downward axial velocity result of Model Convex. Similarly, both the concave and linear air guider showed smaller downward air flow in most of the wall region to enhance the outer vortex compared to the original cyclone. During this time, smaller particles at the wall region could be classified again and carried away from the cyclone top. The secondary classifying was achieved by using the secondary air guider. On the other hand, those downward velocities implied that the downward outer vortex carried large particles to the collecting box, helping with retaining the collection efficiency. In the cyclone center, the inner vortex flow has been greatly reduced in utilizing secondary air guider, which demonstrated that the air flow was less destructive. Hence, less particles would be driven out due to the suction and turbulences. The overall air velocity at the cross section of the cyclone obtained by using secondary air guider was less violent compared to the original cyclone. As a result, the collection efficiency could be maintained during the removal of smaller particles. In addition, the above result only represents the instantaneously axial velocity, due to the inward drift of the outer and inner vortex, the

velocity distribution among different radial position is uneven, reflected by the higher downward velocity at annulus region on the left but slower on the right.

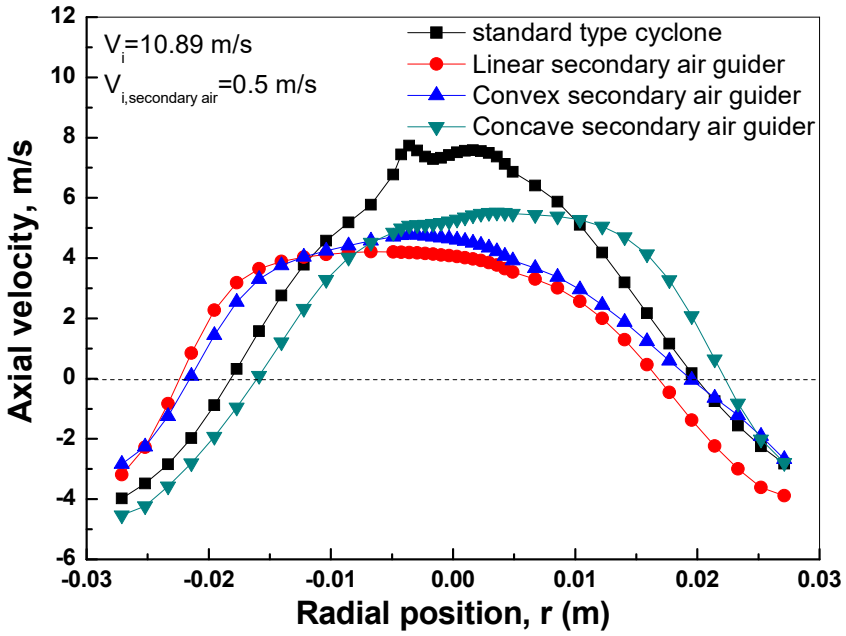

Figure 3.21 Comparison of axial velocity at the cross-section of secondary air inlet in four types of cyclones

All three of these models of the air guider with different shapes and angles indicated that the existence of a secondary air inlet at cyclone bottom could provide the reverse air flow. Due to the existence of the secondary air guider, the better size distribution could be achieved without sacrificing collection efficiency. It is believed that the strength of reverse flow varies with the different opening gaps. Also the angle of the air guider affects the flow pattern and the size distribution of the collected particles. Series of experiments have been conducted so as to find the classifying performance under the influence of different air guider designs.

3.5 Results and Discussion

3.5.1 Characteristic of classifying process with chips feeding

3.5.1.1 Characteristic of classifying process from chips to coarse powder

The experiment started with grinding the chips into coarse powder, by applying the secondary air guider with different shapes, degrees of air guider angles and inlet opening

gaps, the particle size distribution has been influenced with the existence of the secondary air inlet. As shown in Figure 3.22, the samples collected with secondary air guider in gap 3 (widest inlet opening) had relatively smaller span, due to the stronger reverse air flow, especially for the shape of concave in 70˚. The span in gap1 did not change much compared with the span of control group illustrated as solid line. When the inlet opening

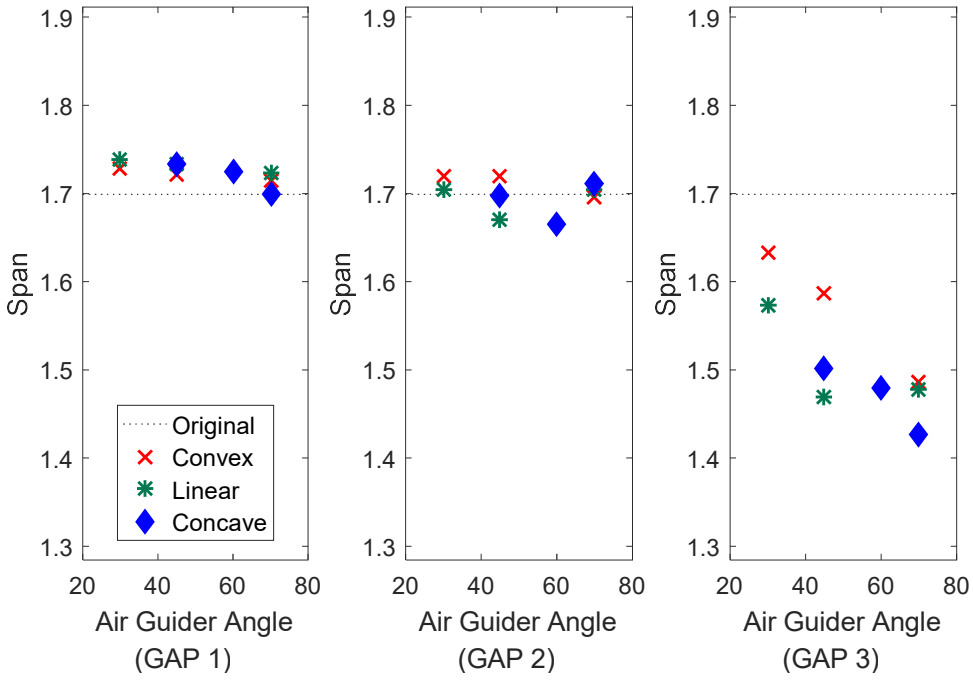

Figure 3.22 Comparison of Span with respect to angle degree in different inlet opening gaps (from chips to coarse powder)

became bigger, using the linear and concave shape air guider could help with the reduction of the span, the convex air guider did not lead to much change in span. It is obvious that providing more reverse flow by increasing the opening gap could effectively remove the small particles, and in this way the span could get narrowed. It is very promising to see that the span could reduce from 1.7 to nearly 1.4 with a decrease of 17.6%. In considering the air guider angle, the span obtained from concave air guider was relative lower than the other two shapes. When observing the effect of air guider angle degree, it was found that higher guider angle degree could lead to smaller span in most cases, which indicated that the reverse air entered from the cyclone bottom on a relatively

radial path to the inside of the cyclone, then the spin motion was formed. So the shape had less influence on span compared with inlet opening gap and air guider degree.

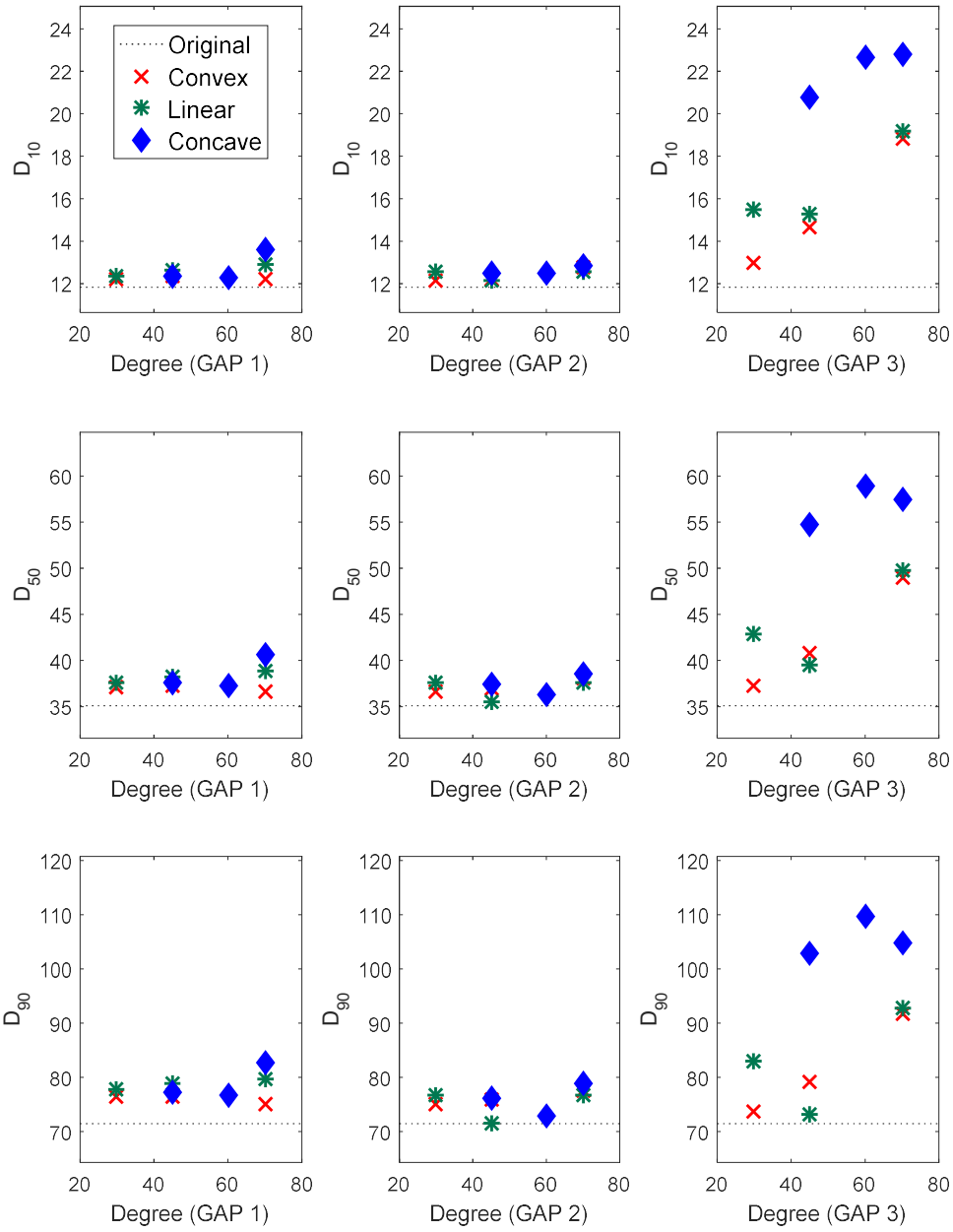

Figure 3.23 D_{10}, D_{50} and D_{90} with respect to angle degree in different inlet opening gaps (from chips to coarse powder)

Figure 3.23 showed featured sizes with respect to angle degree in different inlet opening gaps. It is obvious that the highest opening gap cause the biggest changes of D_{10}, D_{50} and

D_{90}. Compared to convex and linear air guider, concave shape air guider under higher opening gap could provide the largest D_{50}, naturally the D_{10} and D_{90} has greatly increased compared to the original cyclone. This sizes change could be explained by that utilizing concave air guider, the large amount of smaller particles has been moved.

Furthermore, the collection efficiency was another significant parameter of the cyclone evaluation. The final revision of the cyclone design is aiming at removing the small particles without sacrificing the collection efficiency. Figure 3.24 showed the corresponding collection efficiency. It is noticed that the collection efficiency drops because of the removed small particles are not collected in the final sample compared with the control sample. Particularly, it has a quick decrease in Gap 3 compared with Gap 1 and 2, especially for the concave shape air guider and one linear guider at higher angle degree. It implied that more amount of smaller particles has been removed in Gap 3 with inner cyclone flow, and the turbulence could also cause the loss of large particles. The

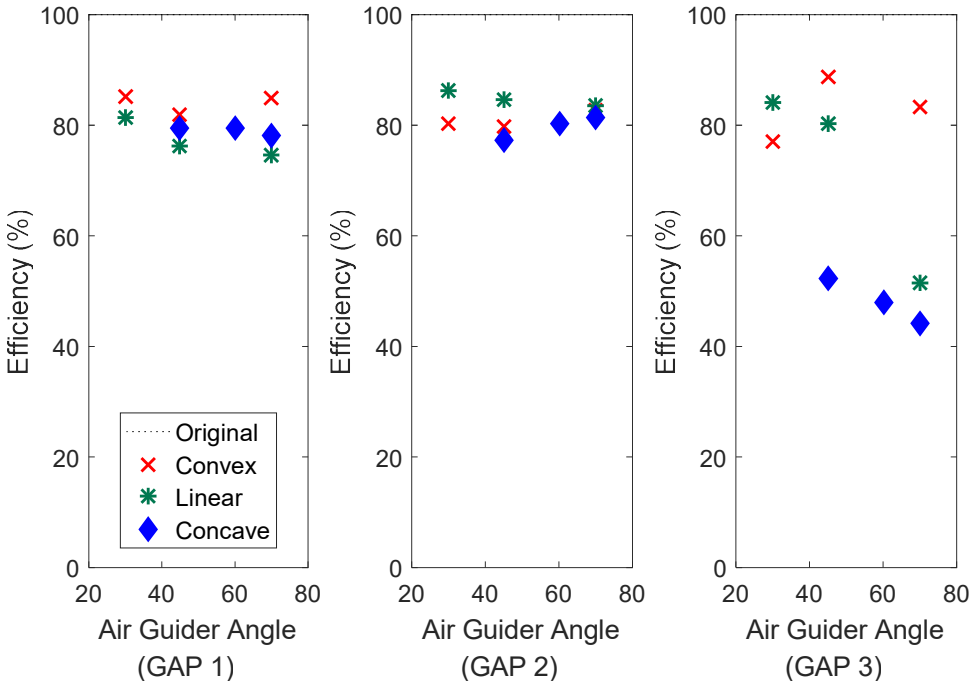

Figure 3.24 Comparison of collection efficiency with respect to angle degree in different inlet opening gaps (from chips to coarse powder)

low efficiency indicates that the cyclone could not retain the large particles when the higher reverse flow intensity. This result is also in accordance with the Figure 5.23 in which concave air guider has the lowest span value. Besides the removal of the small particles, the turbulence of the secondary air flow could also lead to the turbulence of the strong reverse flow exists, and the problem was similar to the previous research in cyclone classifier modification [14-16]. Under the condition of opening gap 1 and gap 2, the angle degree and shape did not affect the efficiency much, in general, the narrow opening gap would not introduce the upper flow air so the large particles could still be collected, resulting in little reduction of the collection efficiency.

However, for the shape of convex air guider, it shows promising results as it has a small span but at the same time no rapid decrease in collection efficiency compared with the control group. The convex air guider could create a similar outer vortex and the inward drag inside in the inner part to the original cyclone. Furthermore, with the air guider, the upward air flow has much less significance to enhance the out vortex and retain the large particles. That could also be the reason why concave air guider provides a different inner vortex and causes the complex turbulence of the inner cyclone, resulting in the large particles removal and drastic collection efficiency drop.

Compared with the effect of degree and shape, both span value and collection efficiency are more sensitive to secondary inlet opening gap. Increasing the gap from 0.25 mm to 0.56 mm does not cause major reduction of span and collection efficiency. However, by changing the gap from 0.56 mm to 1.00 mm, the span reduced quickly and the collection efficiency was sacrificed. According to the objective of modifying the cyclone, the desired span could be even smaller whereas the collection efficiency should still be maintained, for which the secondary air guider is used. In comparing the different air guider designs, the convex shape with smaller angle degree for providing the tangential air inlet is preferable at wider opening gap as it could create a low span value while still have the efficiency over 85%. By checking the industry method of narrowing down the size distribution, it is very complex and time consuming to use conventional sieving process or secondary classifications, which has a low effectiveness in reducing the span.

Figure 3.25 illustrates the size distribution of both control group obtain from the original cyclone compared to the improved size distribution collected in using convex shape air guider at degree of 60° in Gap 3. Due to the removal of smaller particles, the size distribution curve became steeper, indicating the lower span of the improved powder

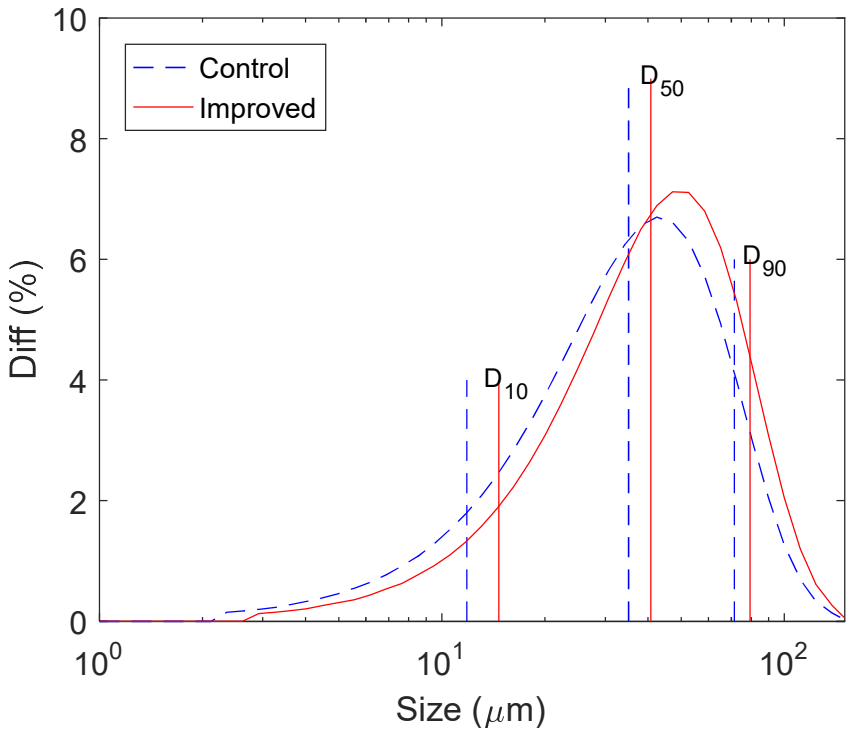

Figure 3.25 The size distribution between control group and improved sample in using secondary air guider (from chips to coarse powder)

sample, without causing much difference in D_{50}. In particular, the D_{10} changed from 11.8 µm to 14.67 µm with an increase of 24.3%. As a result, the method of using secondary air inlet with air guider on the ACM cyclone is an easy and promising way because of its excellent capability in reducing the span while at the same time with an acceptable collection efficiency.

As it is known that using the reverse flow could remove the small particles and perfecting the size distribution, several additional experiments are conducted in changing the total air flow of the ACM for testing classifying cyclone behavior. Figure 3.26 shows the span of the original power compared with the powder collected by the modified cyclone with

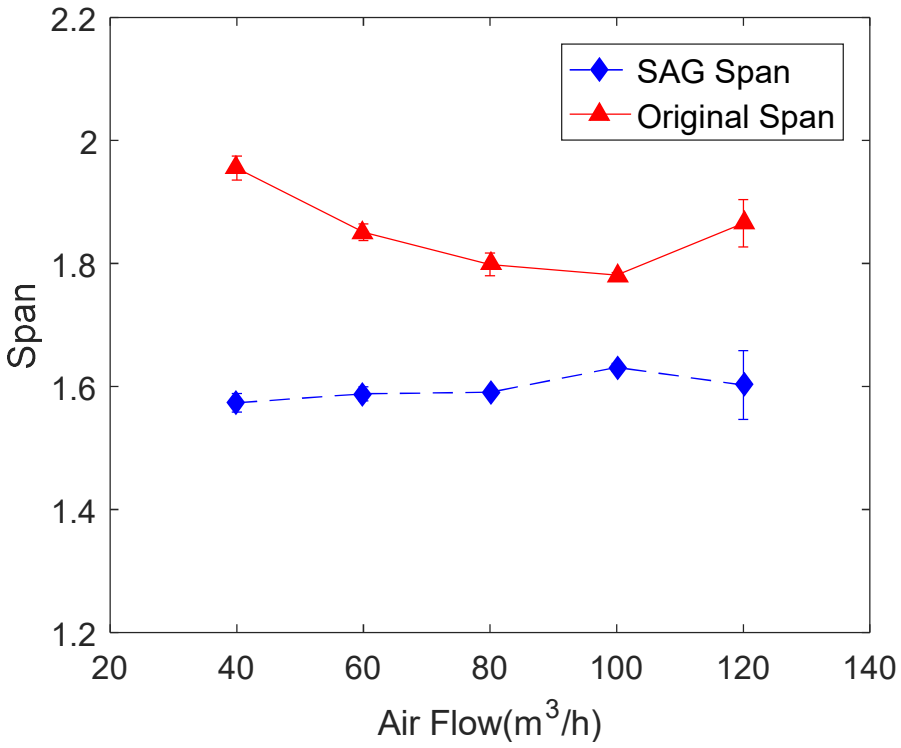

Figure 3.26 Span with respect to air flow of ACM (from chips to coarse powder)

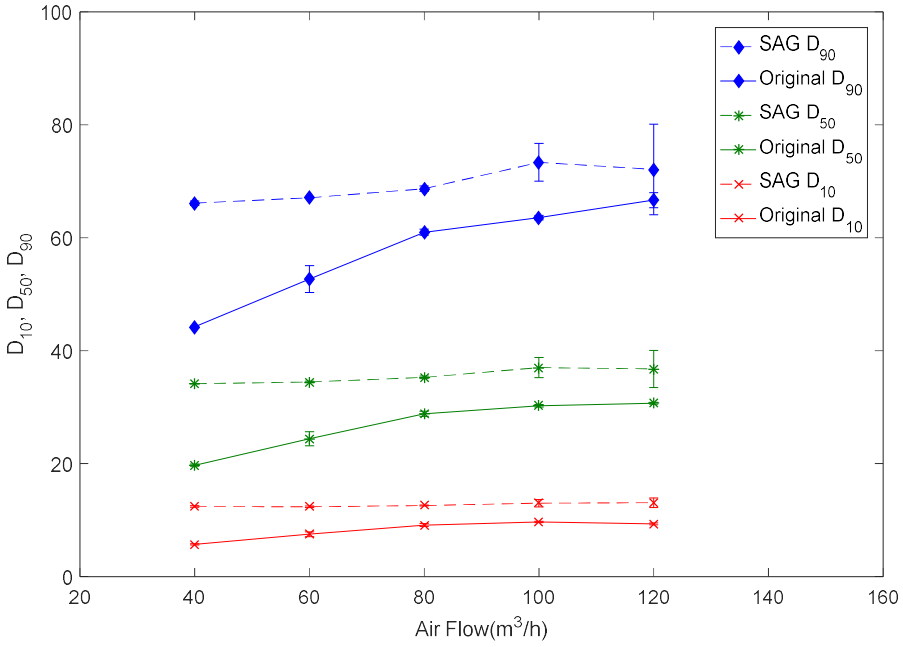

Figure 3.27 Size comparison of D_{10}, D_{50} and D_{90} (from chips to coarse powder)

secondary air guider (SAG)with the coarse powder sample. In general, the high total air set the easier smaller particles to be removed. As illustrated in the figure 3.26, when changing the total flow of the ACM from 40 to 120 m^3/h, all the powder samples collected from the cyclone with air guider are much higher than the original groups, indicating that during the wide range of operating conditions the revised cyclone could

provide the satisfied sample. On the other hand, D_{10}, D_{50} and D_{90} comparison is shown in Figure 3.27. All the featured size of the improved powder sample is higher than the original powder sample. In addition, D_{50} could maintain in relatively steady range compared with the original powder. The air flow less than 60 m^3/h is considered as the critical operating in that the D_{50} has dropped to less than 25 μm. In summary, the size distribution of the collected powder could be improved under regular cyclone operation condition in utilizing the designed secondary air guider.

3.5.1.2 Characteristic of classifying process from chips to fine powder

The experiment continued in grinding the coating chips into the fine powder. The biggest challenge in manufacturing fine powder is that the small particles less than 10 μm are very likely to get agglomerated, causing poor flow properties. So removing the small particles is an urgent need as well as a hard task. In Figure 3.28, the lowest span value is also observed in Gap 3, and the biggest change is from 1.79 of the control group to nearly 1.3, which is a huge reduction of span. However, differing from the coarse powder, all the spans of the collected sample using secondary air guider are lower than the control group, even with the narrowest inlet opening gap. As a result, the introduced reverse upward flow has more influence on the fine powder grinding and classifying. On the other hand, the angle degree of air guider also differs in the flow spin motion. According to the design, the higher degree of the air guider implies that the air velocity goes from the air inlet into the inner part of cyclone, while lower degree guides the air to enter the cyclone tangentially along the edge of secondary air guider. Overall, for all the three shapes, the radial air inlet could provide a smaller span in each inlet opening gap, as the air velocity goes directly into the inner part the cyclone. This secondary air velocity could

enhance the inner vortex and the upward flow greatly, so as to remove the fine particles better.

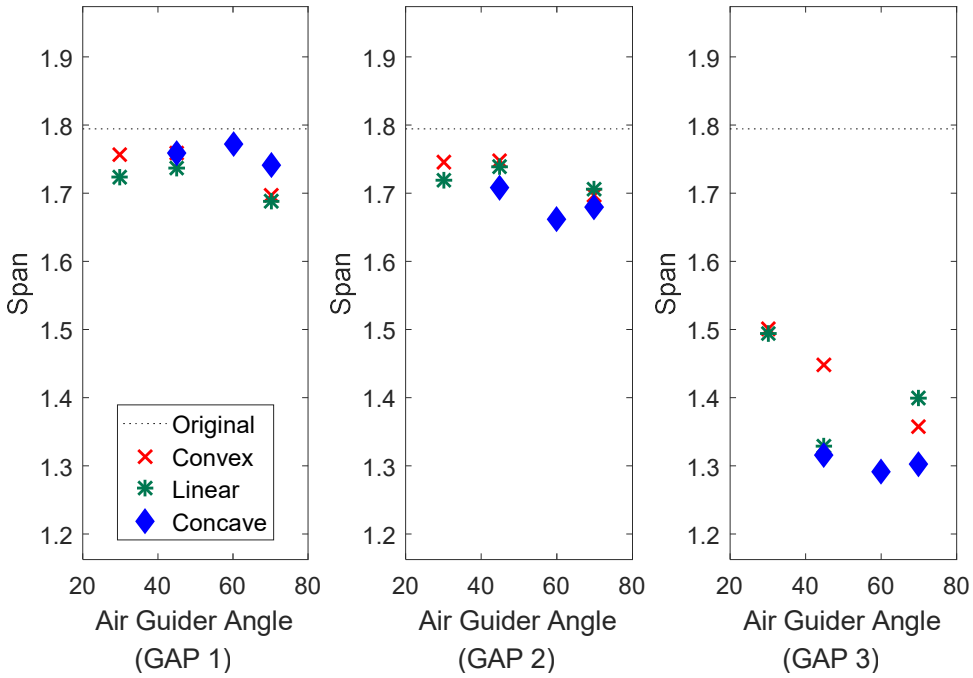

Figure 3.28 Comparison of span with respect to angle degree in different inlet opening gap (from chips to fine powder)

Figure 3.29 shows the particle size changing for the fine powder collected by the modified classifying cyclone. Compared with the coarse powder, D_{10} of the fine particles had a larger increase, especially in Gap 2 and 3. This is very promising since almost all the particles less than 10 μm have been removed when opening gap reaches the highest. Along with the removal of small particles, D_{90} became larger together with the D_{50} value. The smaller D_{90} than the control group in Gap1 and 2 groups is the sign of loss of larger particles. The phenomenon is in agreement with the findings that an increase of upper flow could also cause the loss of large particles. Differing from the coarse powder, the D_{90} of the fine particles in this case is only around 50 μm, and this size could possibly be removed from the cyclone by the reverse air flow. Moreover, as the convex and linear air guider are at 70˚, the D_{50} values are greater than the fine particles range. This is mainly due to that at 70˚ air guider angle, the intense air flow accessing towards the cyclone

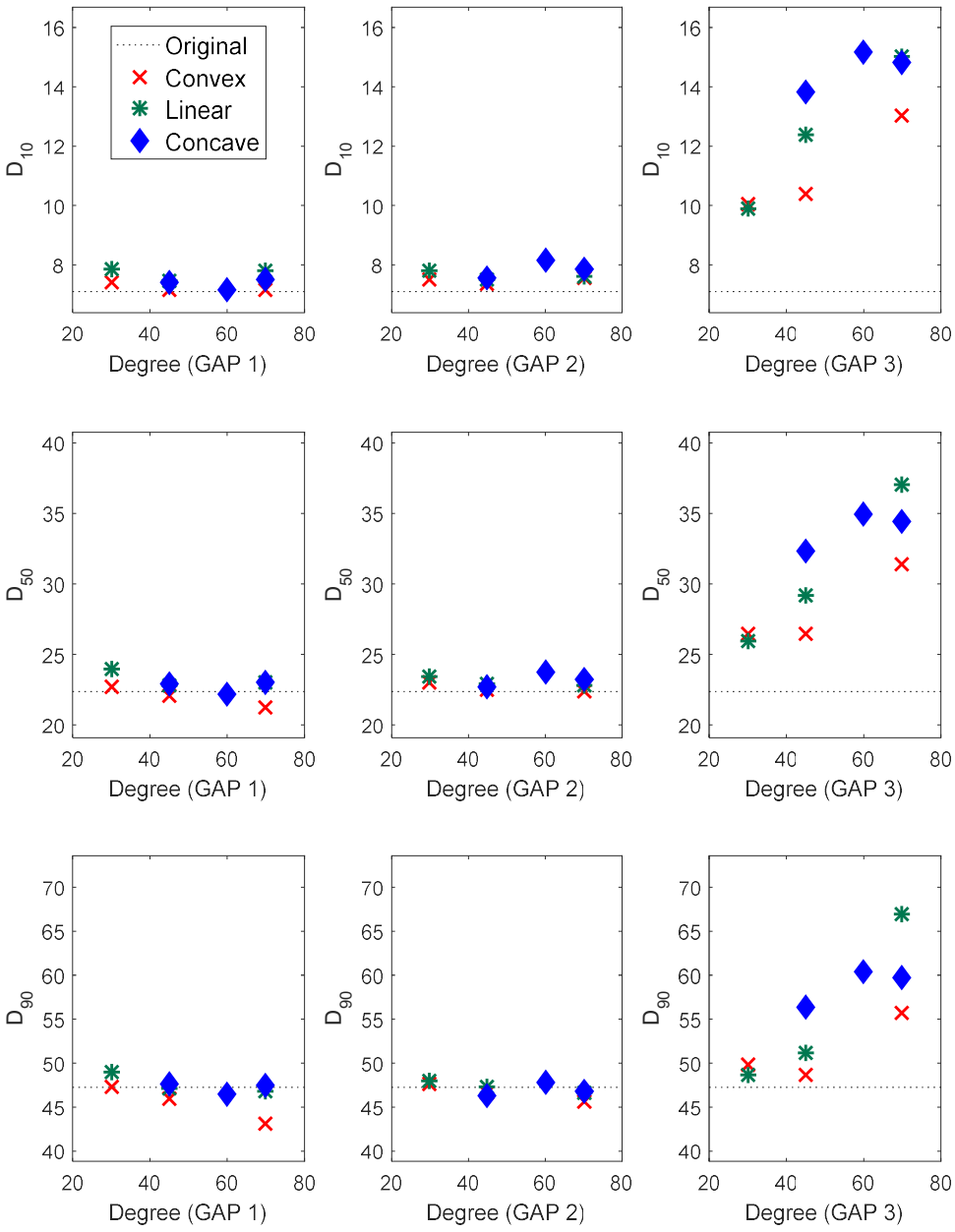

Figure 3.29 D_{10}, D_{50} and D_{90} with respect to angle degree in different inlet opening gaps (from chips to fine powder)

center from the air guider may destroy the original inner spin motion and become dominant in driving most of the particles to the top of the cyclone. Thus a few particles could go downward and be collected. Therefore, the condition of 70˚ air guider could be

considered as a critical point of the inlet angle. It is also noticed that the collected powder samples still belong to fine powder category after classifying. In this case the D_{50} should be similar to the control group (less than 25 μm). According to Figure 16, all the concave shape air guiders in the widest inlet opening are not proper for fine powder classifying, as well as the concave and linear shape air guiders at highest angel degree. It is still mainly due to that the secondary air flow entering in a radial way would strengthen the inner vortex, the smaller and lighter particles are much easier to be removed compared with the coarse particles. By observing Figure 16, it is noted that the convex and linear air guiders with angle degree smaller than 45˚ provide wonderful results in classifying fine particles at the widest inlet opening.

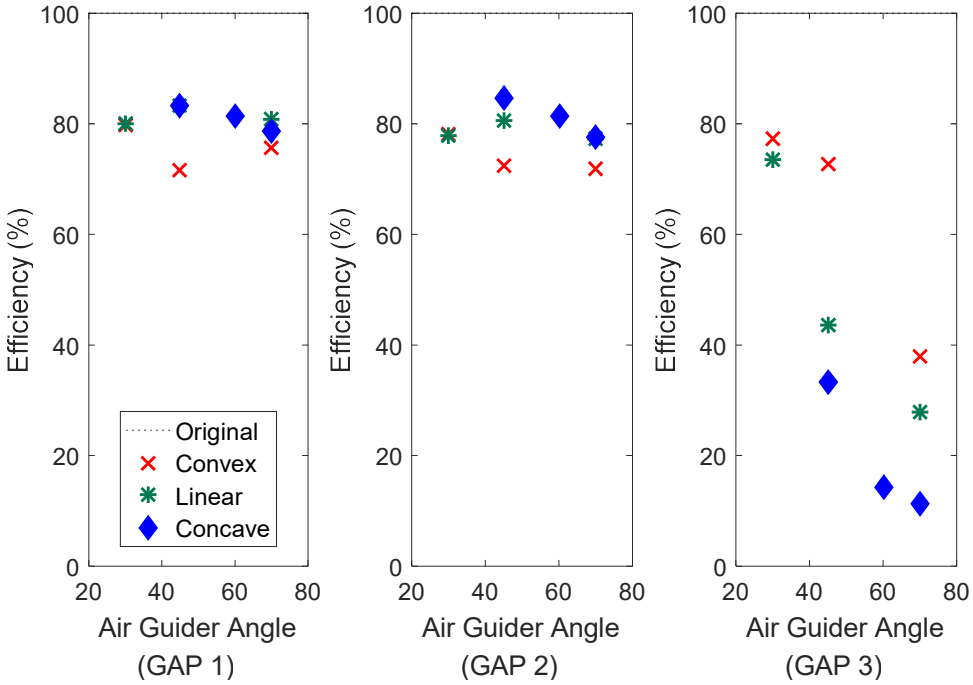

Figure 3.30 Comparison of collection efficiency with respect to angle degree in different inlet opening gaps (from chips to fine powder)

On the other hand, collection efficiency of the fine powder derived from the coating chips is also a crucial factor for classifying fine powder. As shown in Figure 3.30, in similarity, fine powder collection efficiency shows the same trend as the coarse powder. When the opening gap becomes wider, the collection efficiency drops dramatically resulting from

eliminating the small particles. So the dominant and direct factor affecting collection efficiency is the inlet opening gap. The design of air guider angle and shape also have some influence on the collection efficiency. For instance, the convex shape has less colleting ability than the linear and concave shapes with smaller opening gap, but it could retain much more particles in higher opening inlets. In other words, the convex shape guider could create a spinning motion in order to get rid of mall small particles when the inlet air flow is weak. When the upward flow became stronger, the convex air guider could retain the large particles, as illustrated in the figure with efficiency larger than 75%. In general, the tangential inlet air velocity guided by smaller air guider degree has more possibility of retaining the large particles at the bottom of the cyclone than the condition of inlet air entering radially. Also it could be a good explanation why higher degree results in a larger D_{10} and lower span. For the same reason, most of the groups having a lower collection efficiency would not be proper choices for classifying the fine powder in Gap 3. Besides the result caused by reducing the amount of the small particles, the fine particles could get strong agglomerates, and could also cause the poor collection efficiency as the agglomerates are finally guided out through the top of the cyclone. In evaluating the span, D_{50} and collection efficiency comprehensively, the satisfactory design of the secondary air guider for fine powder is the condition of convex shape with a lower guider angle in the widest opening inlet, which is similar to the condition of grinding coarse powder.

Figure 3.31 illustrates the difference between the particle size distribution of control group which shown in solid line, and the improved size distribution utilizing the satisfied secondary air guider (Convex air guider with the 45˚ angle, Gap 3) as shown in dotted line. It is noted that an obvious D_{10} increase from 7.1μm the control group to nearly 10.3 μm of the improved group, with an increase of 45.1%. It is quite a huge improvement since the fine powder with D_{10} is more than 10 μm. In comparison with the classifying coarse powder, narrowing down the fine powder distribution could be much more effective in using the same secondary air guider. During the time of eliminating the small particles, the D_{50} of collected particle sample could still be within a certain range, in guaranteeing the powder sample still belongs to fine powder (<30 μm) almost without changing also the D_{90}. In this case, the improved size distribution curve is narrower and

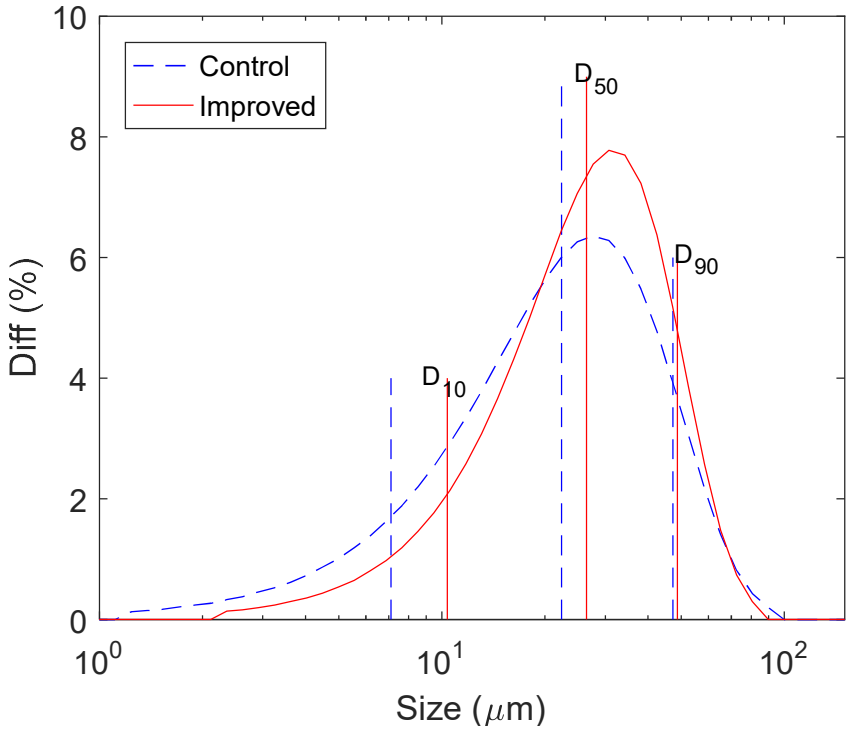

Figure 3.31 The size distribution between control group and improved sample in using secondary air guider (from chips to fine powder)

steeper than the control group, which indicates a lower span. As a result, the modified classifying cyclone with the design of secondary air guider has shown promising results in cleaning the small particles up and narrowing down the span, which is very effective in improving the particle size distribution of fine powders.

In summary, the new design of the revised cyclone with an air inlet at the bottom have the ability in removing smaller particles with the wider secondary inlet opening. When the opening gap reaches 1mm the removal reaches the best, however, collection efficiency is strongly decreased. With the secondary air guider, inside the air inlet, the large particles could also be retained in keeping the large particles not to be driven away by the strong upward flow by the cyclone. What's more, the secondary air guider has made in different shape which could guider the secondary in inlet velocity when getting access to the cyclone bottom. At the same time, each of the guider has manufactured with three different angles in introducing the air velocity goes tangentially or radially to create the enhanced spin motion. Using each shape of the air guider in lower opening inlet could

obtain the particles with lower span than the control group, however in the higher opening gap the concave air guider has big particles loss due to the strong disturbance of the inner vortex. Experimental results indicated that convex shape air guider with a lower degree leading to a tangentially air velocity inlet could effectively create the secondary reverse flow vortex, so as to sweep most of the smaller particles away. As the opening gap became wider, the convex air guider could still have a collection efficiency higher than 80% which could consider as the promising air guider design and provide the promising results for the further studies.

In similar, the fine powder is also investigated in changing the total air flow. As shown in Figure 3.32, within the changing range of the air flow, all the powder collected by revising cyclone has great higher span than the original sample, which indicates the method is also efficient for fine powders. In better explain the comparison of the size

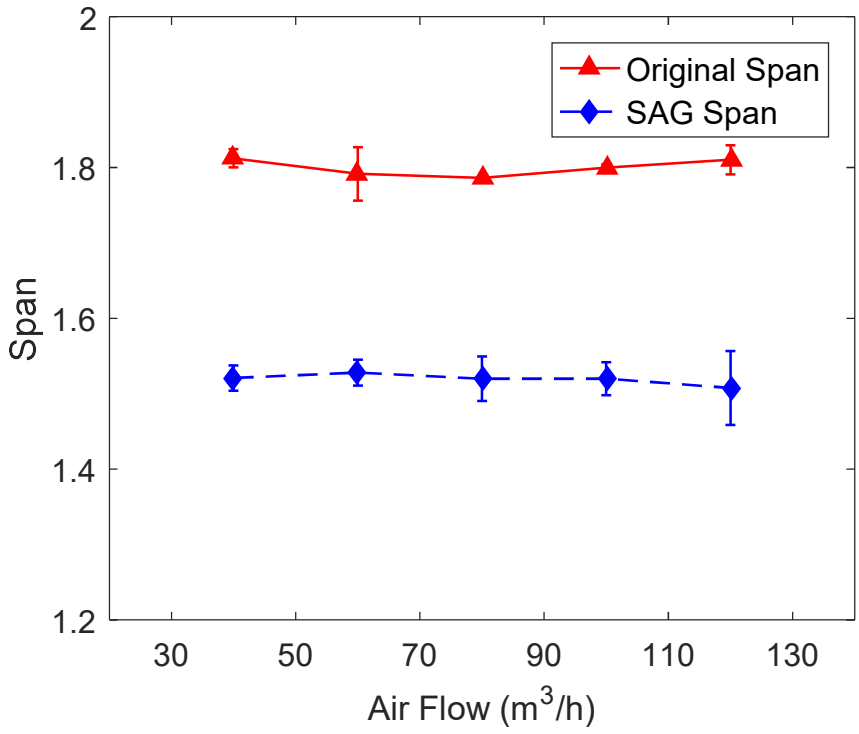

Figure 3.32 Span with respect to air flow of ACM (from chips to fine powder)

distribution, the figure of D_{10}, D_{50} and D_{90} showed in Figure 3.33. A large increase of the D_{10} is seen, as is the main reason of the span reduce. In addition, during the classifying

procedure due to the strong reverse flow, the D_{90} is likely to be guided away as well, resulting in the reduction of D_{90}. On the other hand, D_{50} in all the operating condition could still be preserved between 20 to 25μm. This also shows that the stability of the ACM is very high due to the fact that the modified cyclone has no side effect on the ACM and can perfectly cooperate with it to keep the size accuracy.

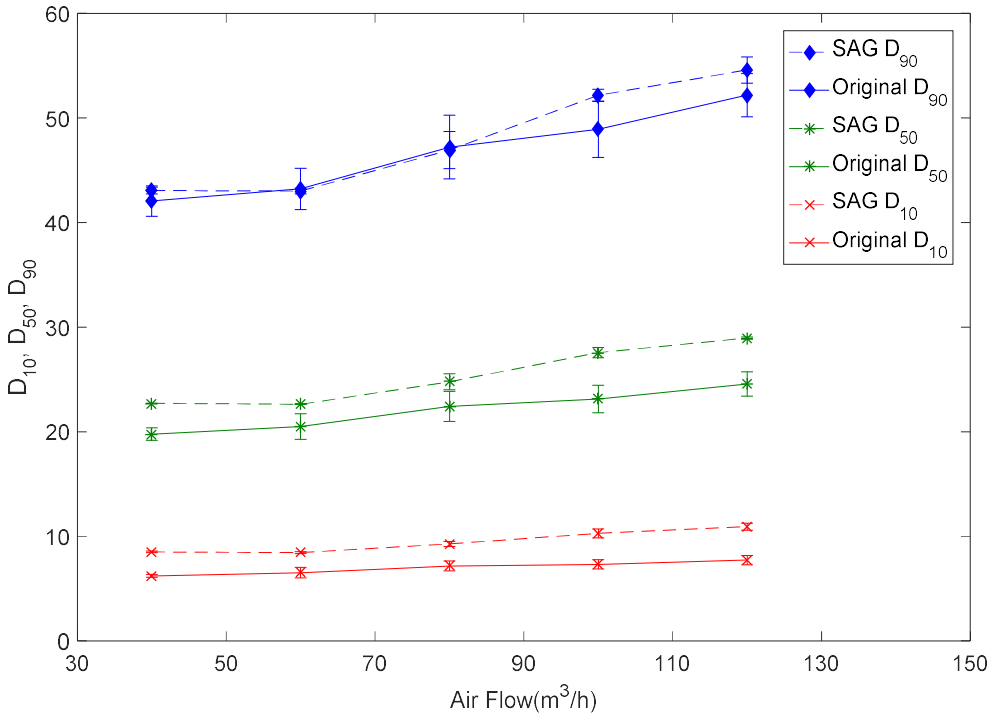

Figure 3.33 Size comparison of D_{10}, D_{50} and D_{90} (from chips to fine powder)

However, the powder with higher D_{50} also own larger D_{10}. It is needed to compared the smaller particle amount of the sample particles with same D_{50}. Figure 3.34 illustrates the particle featured sizes with respect to D_{50} obtained from modified cyclone with SAG (concave shape, 60°) and the original cyclone. The modified cyclone with SAG showed an overall better classifying performance than the original cyclone. The D_{10} get increased and D_{90} is smaller when the particle has the same D_{50}. As a result, the SAG cyclone could be able to produce the powder sample with much smaller span and the better size distribution, shows in Figure 3.35.

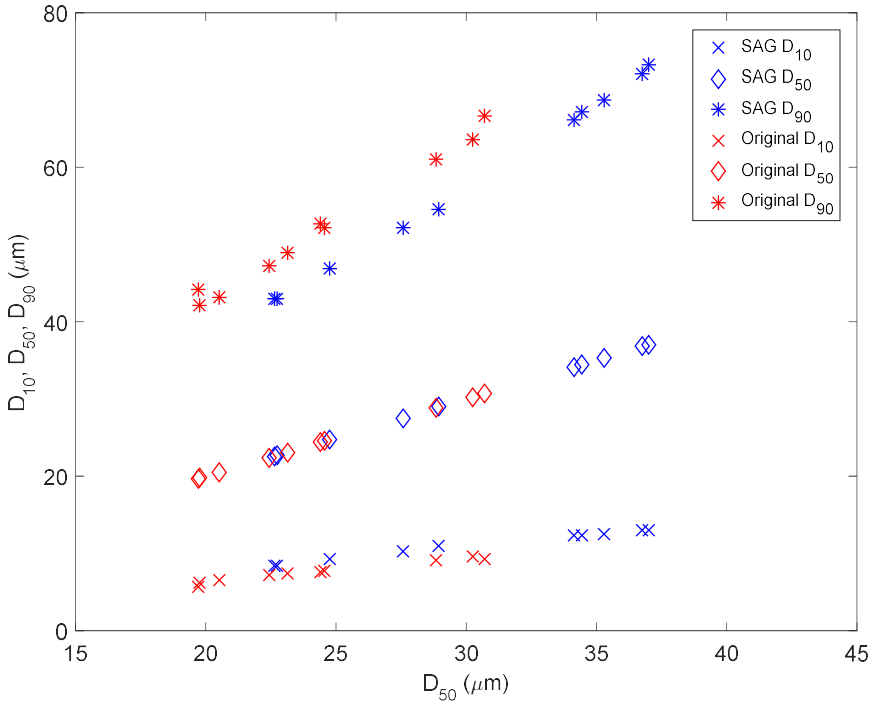

Figure 3.34 Size comparison of D_{10}, D_{50} and D_{90} of SAG sample and original sample with respect to D_{50}

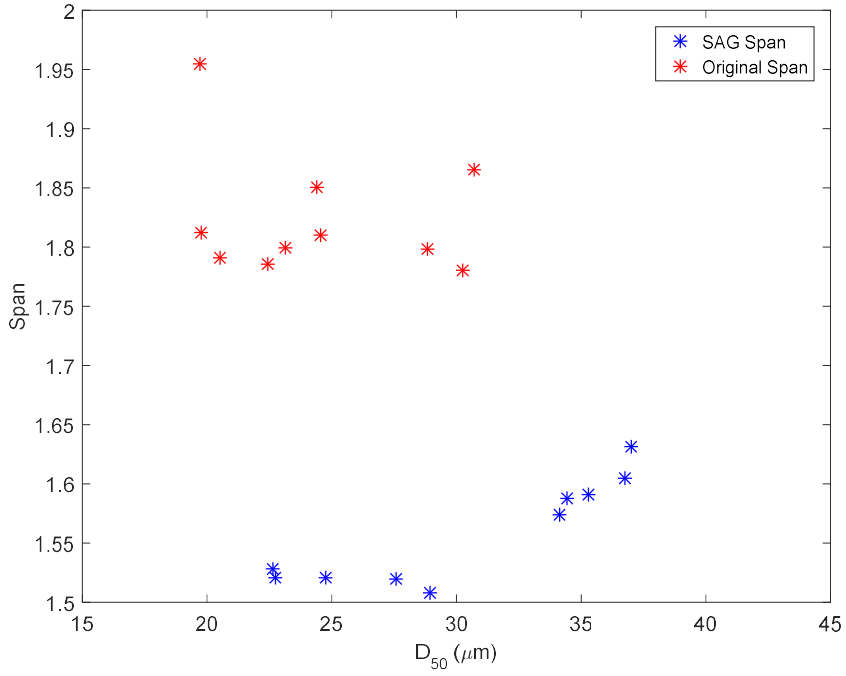

Figure 3.35 Span comparison of SAG sample and original sample of D_{10}, D_{50} and D_{90} with respect to D_{50}

3.5.2 Characteristic of classifying process with powder feeding

3.5.2.1 Characteristic of classifying process with coarse powder

In order to further tested small particles removing capabilities of the modified cyclone with secondary air guider, the powder sample is used as the feeding material of the ACM. During the experiment, the rotor grinder and classifier were adjusted to very low speed without further grinding (for maintaining the original size distribution) the powder sample meanwhile still keeping the normal operating status of the ACM. By this means the particles distribution collected from the cyclone bottom would be mainly separated by the modified classifying cyclone, without the influence from the grinder and classifier of ACM.

Figure 3.36 illustrates the span with respect to the inlet opening gap of the collected powder samples. It is noted that compared with the chips feeding, the span value has less

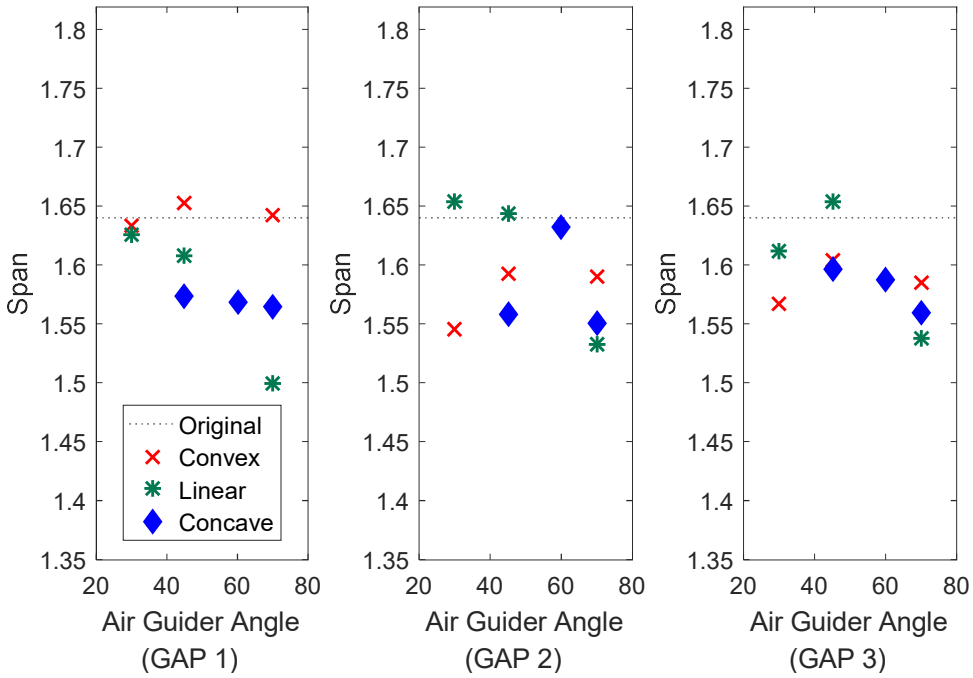

Figure 3.36 Comparison of spans with respect to angle degree in different inlet opening gaps (with coarse powder feeding)

influenced by the opening inlet gap. The highest span reduce is from 1.65 to less than 1.55 happened at high degree of linear and concave shape air guider. Among the three

shape, convex shape air guider could obtain relatively steady span in changing with gap than 40μm in that the distribution with size larger than that may cause poor coating

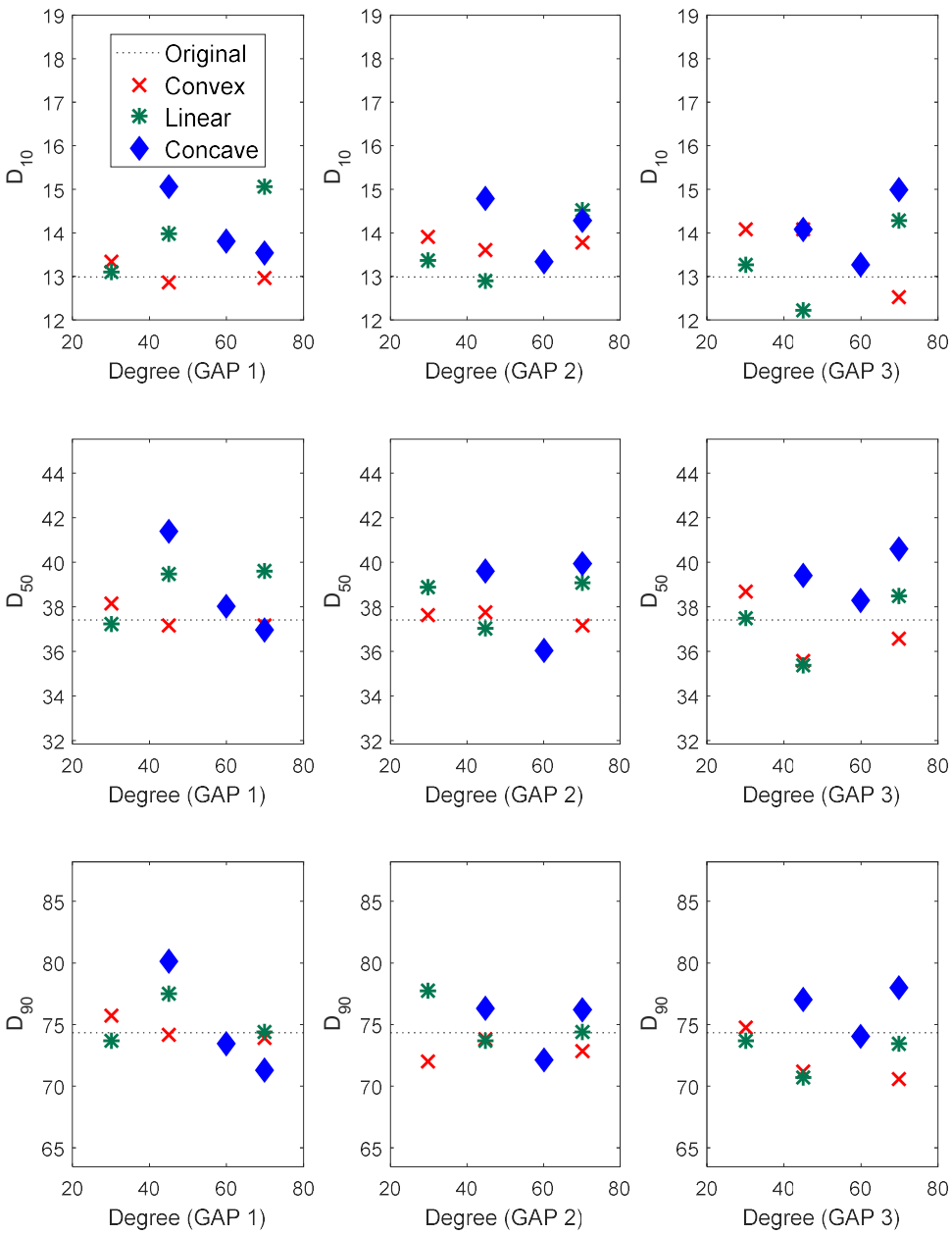

Figure 3.37 D_{10}, D_{50} and D_{90} with respect to angle degree in different inlet opening gap (with coarse powder feeding)

surface results from relatively large particles. In this case, the convex shape would not be a proper choice if the preferred D_{50} powder sample is around 35μm. The reduction of

span could also be better explained according to D_{10} and D_{90} changes, as shown in Figure 3.37. In general, concave air guider performs better in removing small particles, however the obtained D_{50} has big changes and some of them are higher than 40 μm. Based on the span and featured sizes, using the concave shape air guider with high opening gap is a good choice to remove small particles as well as getting a reasonable median sizes.

On the other hand, collection efficiency of the collected powder from powder feeding is a significant factor shouldn't be neglected. Similar as the previous experimental discoveries in our study, opening gap is key factor in effecting the collection efficiency. In figure 3.38, Both linear and convex shape air guider is good enough in preserve almost 90% collection efficiency which is comparable to the original group during the removal of smaller particles. In other word the reverse spin motion only sweeps the small particles away without cause the side effects among large particles.

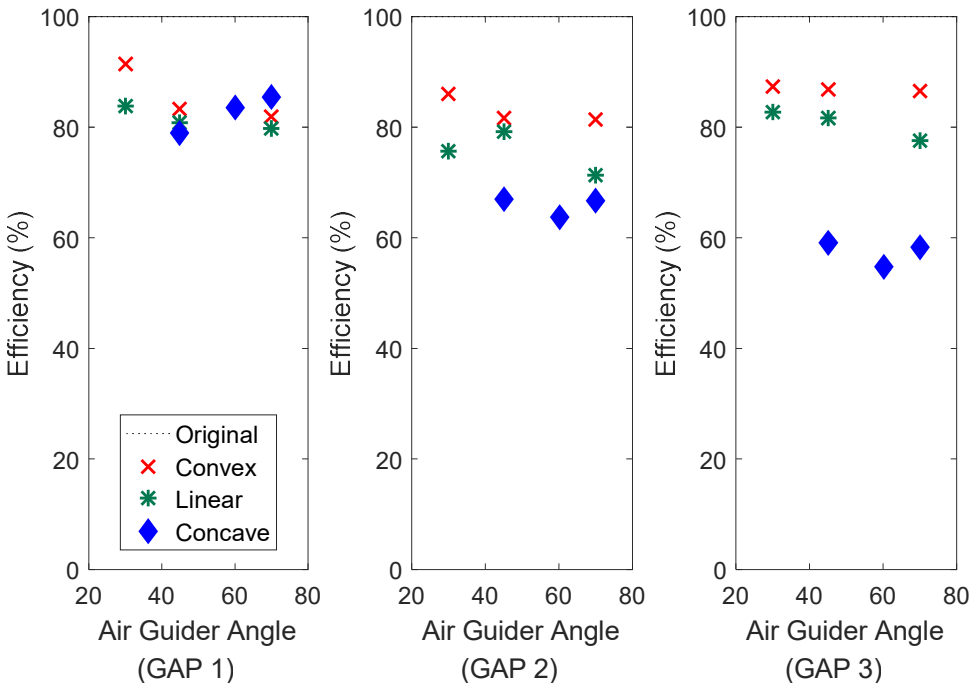

Figure 3.38 Comparison of collection efficiency with respect to angle degree in different inlet opening gap (with coarse powder feeding)

Despite the concave air guider had the best ability in reducing the span, it still couldn't consider as a satisfied option in wider opening inlet in that they sacrificed in collection

efficiency. Also in similar, with the identical shape of the guider, higher guider degree provides a radial air inlet has less efficiency because of larger purging of small particles. In considering the particle size distribution and colleting efficiency, the shape of linear and convex with lower guider angel performed behaved promising results in all the opening inlet gap. Hence if the powder sample product has the need in further treatment could consider using the similar procedure so as to reduce the span.

Figure 3.39 shows the size distribution between the control group of coarse powder and the collected sample using convex shape, 30˚ air guider in Gap3. The D10 changes from 12.9μm to 14.1 μm, which consider as an unease improvement in coarse powder.

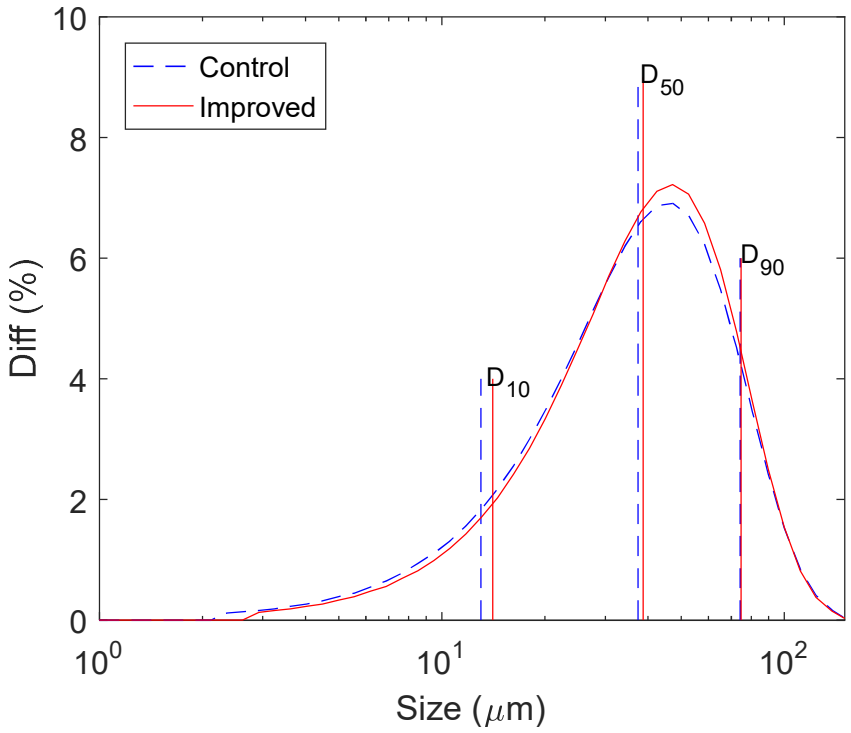

Figure 3.39 The size distribution between control group and improved sample in using secondary air guider (with coarse powder feeding)

The D50 and D90 didn't vary too much indicates the classifying mainly took place inside of the cyclone and there are few influence caused by the slow speed rotor grinder and the classifier from ACM. Thus the span is only perfected by the revised classifying cyclone.

3.5.2.2 Characteristic of classifying process with fine powder feeding

In addition, the fine powder material is also investigate using the same method. It is very difficult in classifying the fine powder coatings due to the agglomeration of the fine particles as the ordinary D_{10} is around 6 µm. Figure 3.40 shows fine powder span with the respect to different secondary air guider. It is obvious that all the span has been preferably improved by the reduction in value compared with the control group of 1.93. The lowest span value in Gap 3 could be lowered to 1.58 with a decrease of 18.1%. Different from the coarse powder, the big reduction of the span in fine powder declared that the fine powder is much easier to be carried away by the reverse air flow from the cyclone bottom than the heavier particles. Also, the results in Gap 1 and 2 showed that

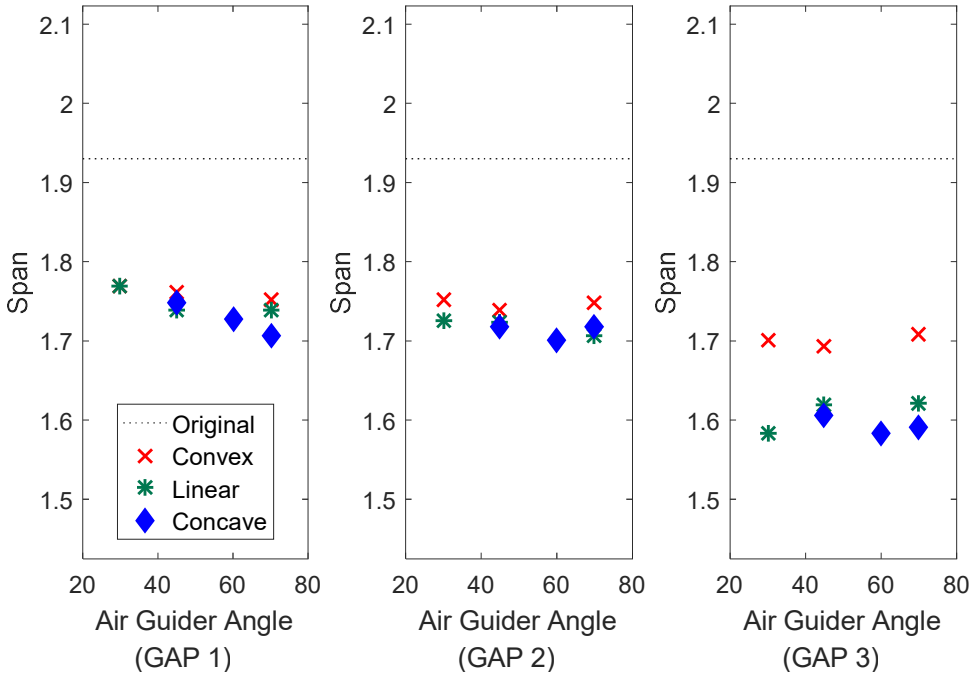

Figure 3.40 Comparison of span with respect to angle degree in different inlet opening gap (with fine powder feeding, D_{10}≈6 µm)

shape of air guider did not have much difference, while in Gap 3 the linear and concave air guider could obtain an even lower span than convex shape. In addition, the guider angle also has minor effect on the span compared with the coarse powder.

In addition, the D_{10}, D_{50} and D_{90} are shown in Figure 3.41. When the opening inlet gap became larger, the D_{10} had more significant increase, especially for the concave and

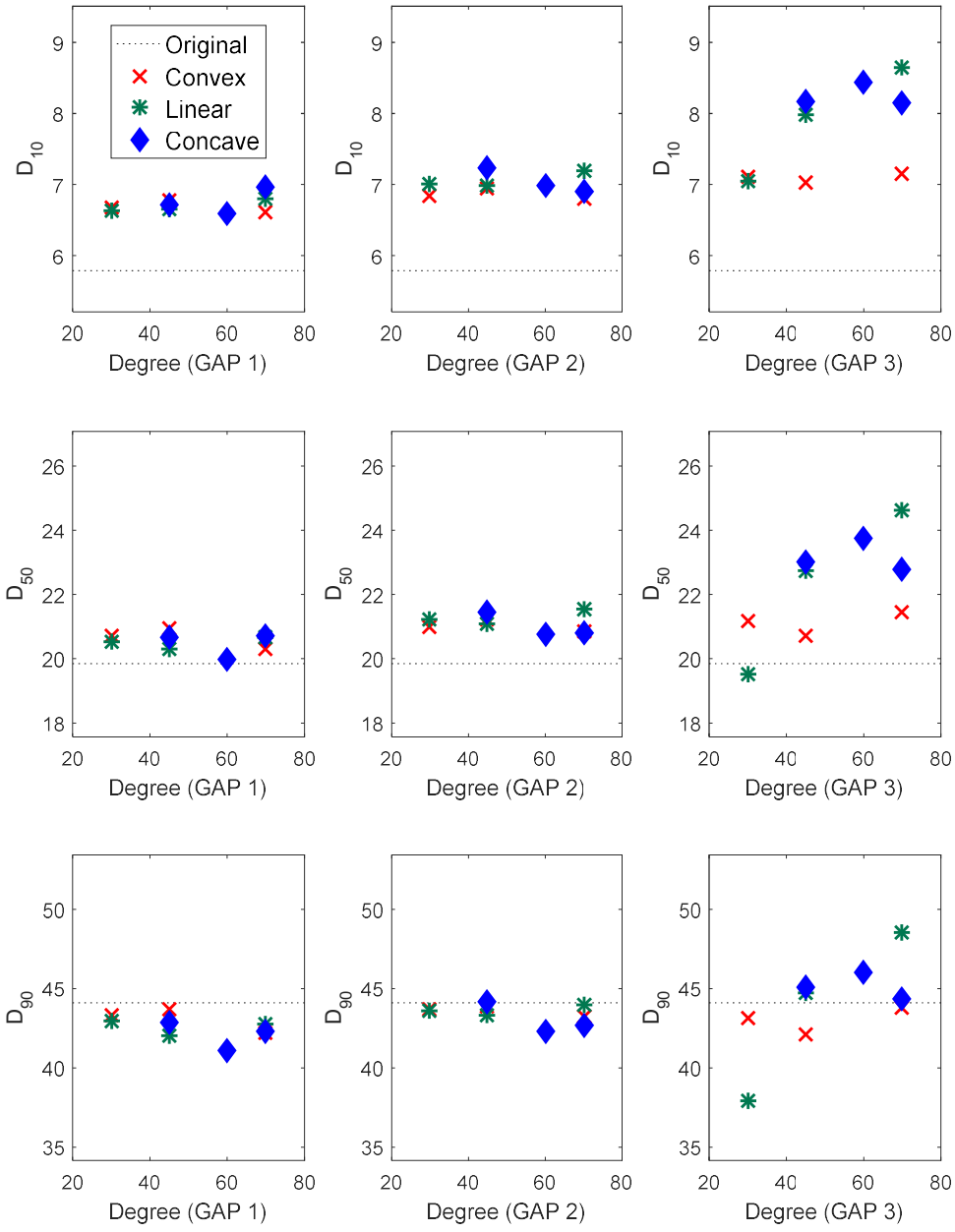

Figure 3.41 D_{10}, D_{50} and D_{90} with respect to angle degree in different inlet opening gap (with fine powder feeding, D_{10}≈6 μm)

linear shape air guider. The D_{90} showed the similar trend for each opening gap as D_{10}. In general, the angle of air guider did not affect the size distribution much on the fine

powder. Above all the D_{50} is even more crucial in handling the fine powder, as if the D_{50} is higher than 30 µm the collected sample could not be considered as fine powder. It is very pleased to see all the improved powder sample has the D_{50} less than 25 µm, and most of them are very close to the original group. Due to the relatively smaller particle size for all the particles with D90 is less than 50 µm, D_{90} is likely to be driven by the combined force of the centrifuge and the enhanced upward drag force and some of them are guided out from the cyclone, which is the main reason causes the D_{90} size reduction. The featured size suggested that all the cyclone with reverse air flow and secondary air guider could effectively improve the particle size distribution of fine powders.

Whether the designs of the secondary air guider are applicable for the fine powder size improvement, there is always a need to see the collection efficiency. As illustrated in Figure 3.42, except for the concave shape air guider in Gap 2 and Gap3 has low

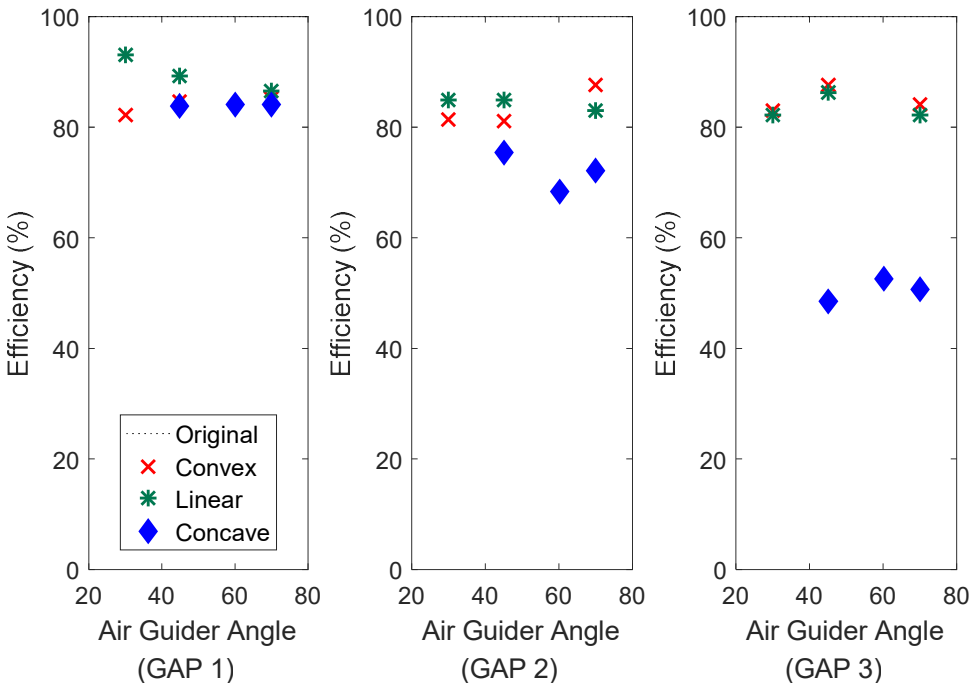

Figure 3.42 Comparison of collection efficiency with respect to angle degree in different inlet opening gap (with fine powder feeding, D_{10}≈6 µm)

collection efficiency, the other design shows good results with the collection efficiency higher than 80%. It is not difficult to explain that the particle span is lowest in using

concave air guider. A larger amount of smaller particles was removed from the cyclone top, and less amount can be collected, sacrificing collection efficiency. The angle of the air guider showed similar results as the coarse powder that both tangential and radial air inlet is slightly lower in collection efficiency due to the better removal ability for smaller particles.

Figure 3.43 indicates the final size distribution of the original sample and the new powder utilizing the convex air guider in 70˚, Gap3. The steeper size distribution curve shows in dotted line in comparison with the control group of original power sample. With the D10 increasing from 6.04 to 8.65, without cause to much reduction in collection efficiency,

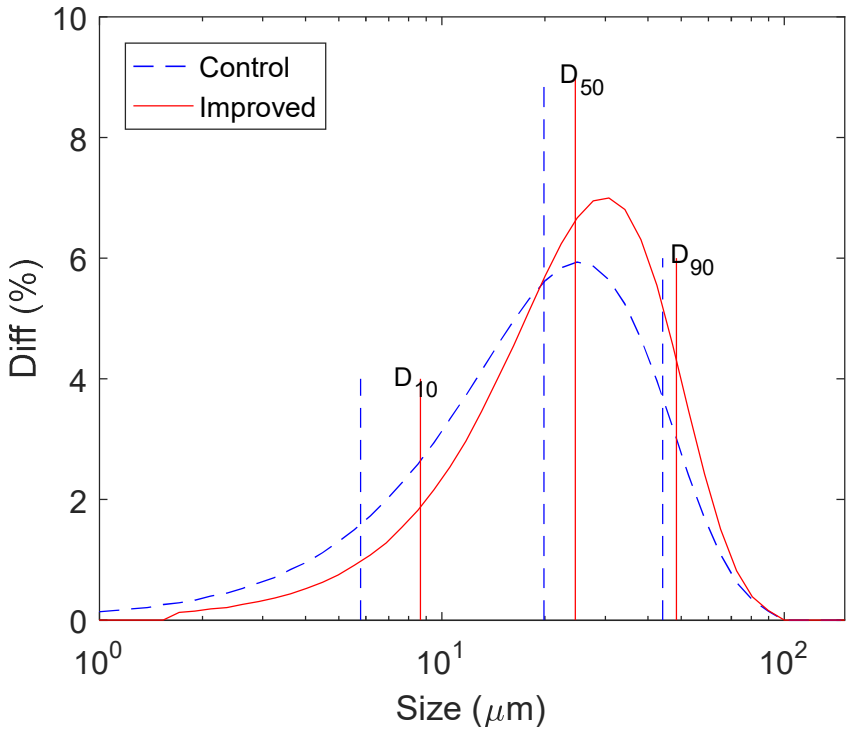

Figure 3.43 The size distribution between control group and improved sample in using secondary air guider (with fine powder feeding, D_{10}≈6 μm)

it is a great result in dealing with the fine powder. Also, the D_{50} and D_{90} is preserved in the proper range. In summary, utilizing the modified classifying cyclone could obtain promising results for the further treatment of the fine powder and even ultrafine powder coating samples. The last but not the least experiment conducted using the fine powder sample as well. However, the difference from the above testament is the fine powder

sample pre-treated and has the D_{10} around 8 μm. Normally the fine powder coatings manufactured by the industry always has a D_{10} around 6 μm, the even finer particles cause huge difficulties in the next spraying processes as a result of the strong agglomeration of the fine particles. The pre-treated powder sample with the D_{10} of 8 μm had already lost part of the smaller particles. Hence the purpose of this experiment is to see how effective the revised classifying cyclone is. If the D_{10} could be further increased with an acceptable collection efficiency, the cyclone modification is considered as a great method of dealing with the span reduction problem.

As shown in Figure 3.44, the span has minor changes compared with any other groups above in that the powder is pretreated and few larger particles could be removed by reducing the span. In Gap 1 and 2, the span is comparable with the original powder indicating that the reverse flow function is not obvious in this powder sample.

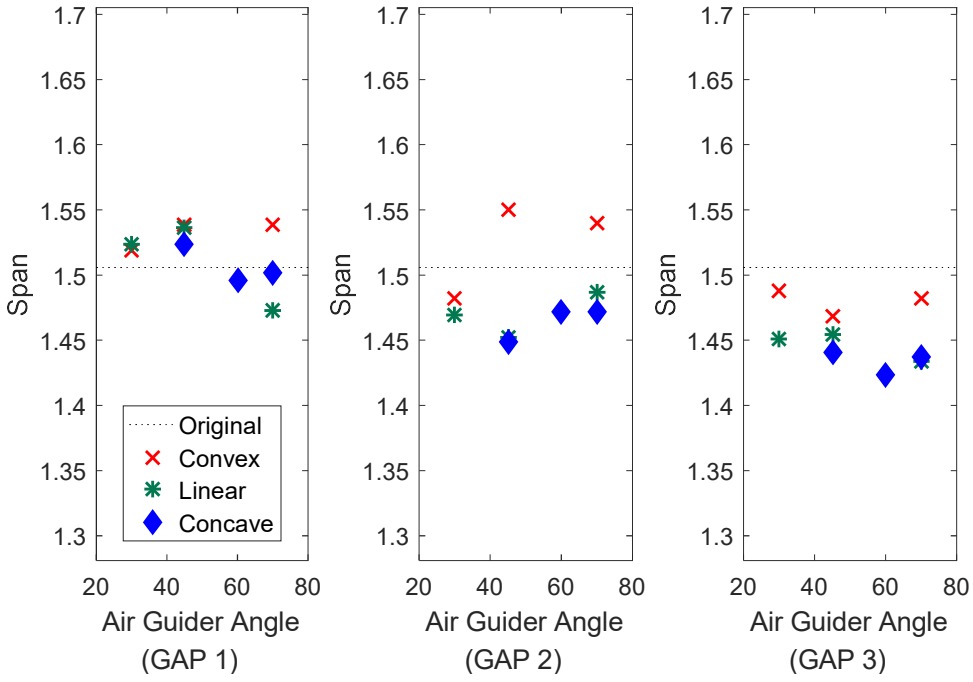

Figure 3.44 Comparison of span with respect to angle degree in different inlet opening gaps (with fine powder feeding, D_{10}≈8 μm)

But it is still μhaving the removal condition when the opening gap opened to widest, showed in Gap 3 all the span is smaller than the control group. It is also observed that the

influence of the shape and degree still followed the similar trend in the group of using fine powder with D_{10} in 6μm. It is always satisfying to see the span reduction in every

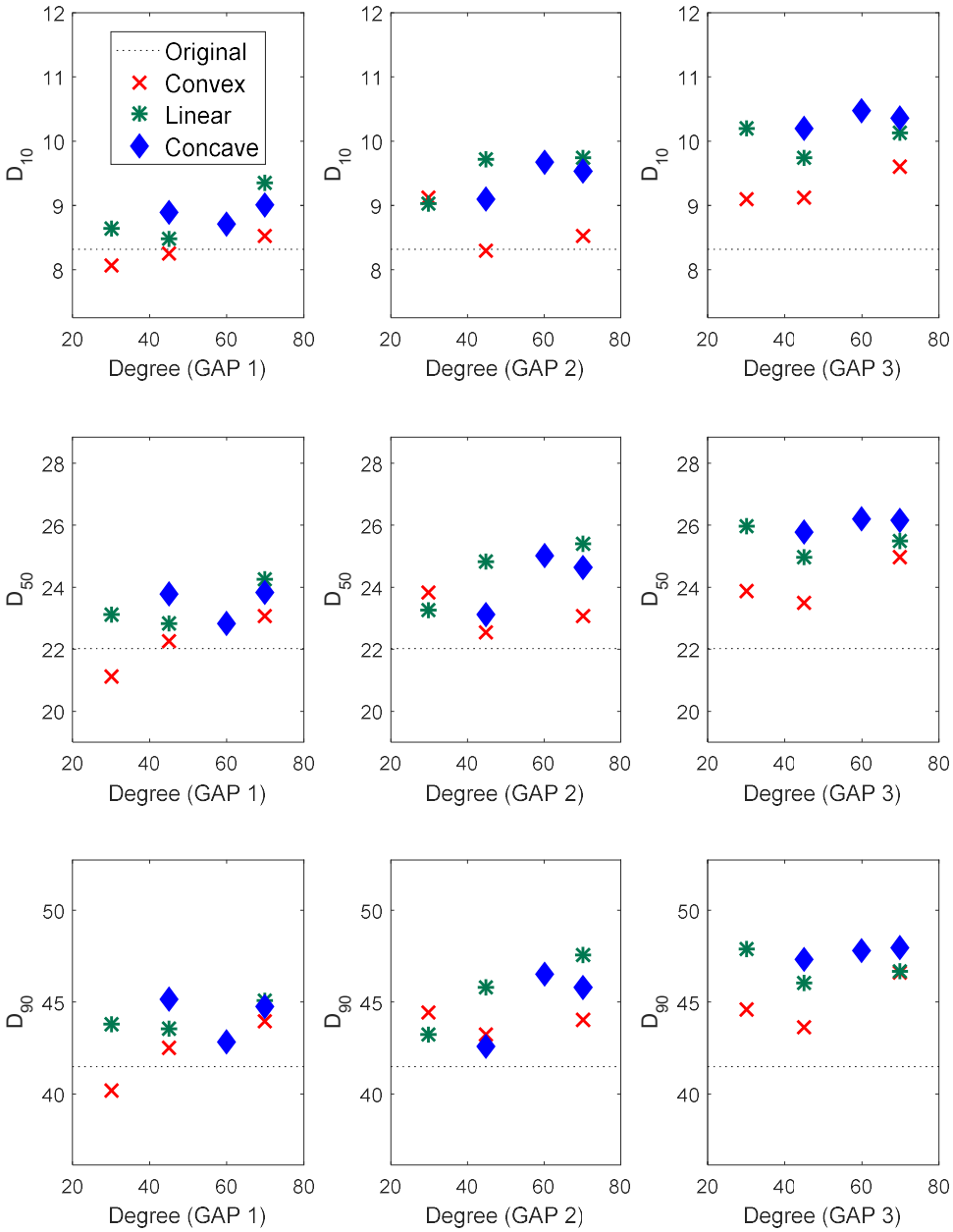

Figure 3.45 D_{10}, D_{50} and D_{90} with respect to angle degree in different inlet opening gaps (with fine powder feeding, D_{10}≈8 μm)

case. In the Figure 3.45, the higher D_{10} than control group is still observed. That is to say, the reverse flow could still sweep a certain amount of the smaller particles away even for the pretreated powder with higher D_{10}. Along with this, the D_{90} has been retained and

also had certain increase and caused the higher D_{50}, but it still belongs to fine powder (less than 30μm). The opening gap width is still dominant in fine powder as usual and concave and linear shape air guiders could still acquire higher D_{10} than the convex guider. In similarity, both low and high degrees of the guider angle lead to the relatively higher D_{10}.

By looking at the collection efficiency charts in Figure 3.46, it can be figured out which air guider is better in retaining the large particles. After all the larger particles are the important content of the collected powder sample. It is very clear that the opening gap of the secondary air guider plays a significant role in controlling the collection efficiency. Under the condition of Gap 3, the concave air guider has the lowest collection efficiency

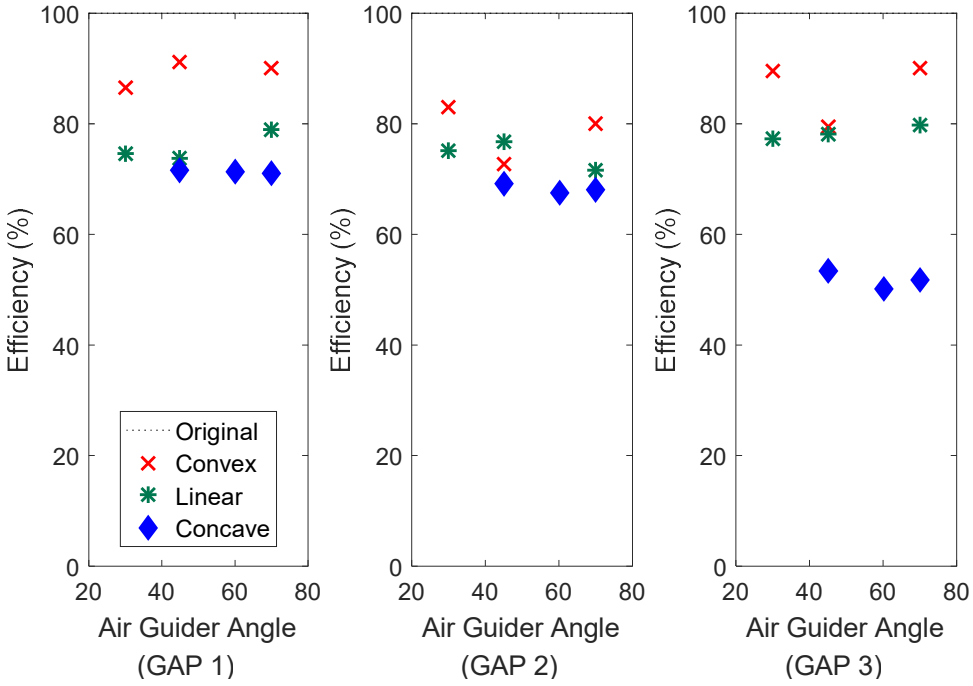

Figure 3.46 Comparison of collection efficiency with respect to angle degree in different inlet opening gaps (with fine powder feeding, D_{10}≈8 μm)

while in lower gap all the three shapes of air guider still having the collection efficiency greater than 70%. On the other hand, the guider angle does not cause too much difference as the spin motion in promoting the upward flow has less influence on the relatively large

particles since there are few smaller particles which could easily be driven by the inner vortex left.

Figure 3.47 shows the original group of the particle size distribution compared with the newly collected sample using revised cyclone and convex air guider in 45˚. This time, the D_{10} value had a little increase, as well as D_{50} and D_{90}, but the span still became smaller, reflected in the steeper and narrower distribution curve. taking the comprehensive factors into consideration, the modified cyclone with secondary air guider is proven be able to further reduce the span of the fine particles with an even higher D_{10}.

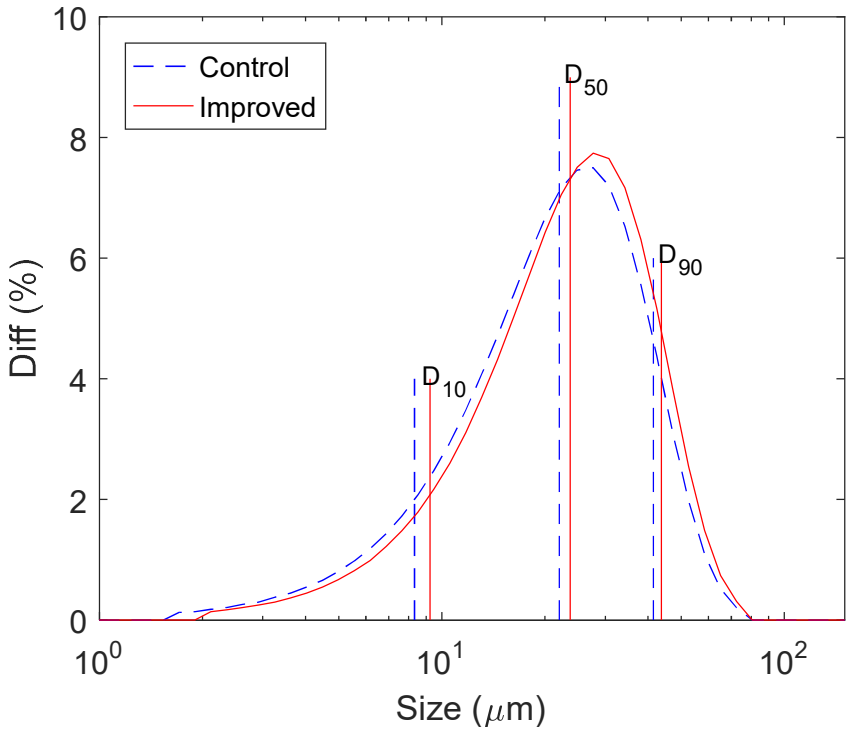

Figure 3.47 The size distribution between control group and improved sample in using secondary air guider (with fine powder feeding, D_{10}≈8 μm)

3.6 Conclusion

A novel classifying cyclone was revised from the conventional cyclone of the air classifying mill. The new development of this revision was to provide the classifying function during the collecting process of the powders by introducing a secondary air inlet at the cyclone bottom. This novel classifying cyclone could remove a large amount of the

smaller particles so as to improve the size distribution. The span has the biggest decrease of 17.6% for coarse powder and the huge reduction of 27.4% for fine powder.

During the operation, if the upward flow is too strong when the opening gap reaches a certain height, larger particles at the cyclone bottom could also be removed and cleared away from the cyclone top causing the huge reduction of collection efficiency. In order to retain the large particles so as to maintain the collection efficiency, an additional revision in adding a secondary air guider with a simple design for the purpose of retaining larger particles from being removed. The air guider is designed in different shapes and angles in accordance with the air spinning direction. In this way, the secondary air inlet gets access to the air guider in a certain direction and creates different spin motion. With the help of the developed secondary air guider, the collecting efficiency could be maintained as more than 80% of the original cyclone's.

Two kinds of powder sample were used to test the performance of the new classifying cyclone. Experimental results showed many promising results in removing the small particles without sacrificing the collection efficiency. According to the analysis of all the results in span, D_{10}, D_{50}, D_{90} and collection efficiency, it showed that when the inlet opening gap became wider, the span has the most reduction as D_{10} strongly increased. Also, the collection efficiency was affected mainly due to the inlet opening gap. On the other hand, using a concave shape air guider could always achieve the lowest span but the lowest collection efficiency, in the reason that the spin motion provided by the concave air guider disturbs the original inner vortex during removal of small particles. It could also remove larger particles during the disturbance. In this case, the linear and convex shape guiders are suitable for further reducing the span without losing much collection efficiency.

In addition, the angle of the air guider in three different degrees has been tested. Experimental results showed both 30˚ and 70˚ (for concave guider is 45˚ and 70˚) is preferable in helping with a better size distribution. It is owing to that air guider at these two angles, leads the air to get access to the cyclone bottom tangentially and radially, which faster creates the upward spin vortex. Furthermore, inlet air with radial velocity

helped with clearing the smaller particles away while tangential velocity is beneficial for retaining large particles. Overall, the obtained particle size distribution in using a novel cyclone had a huge improvement as the span is reduced and the D_{10} is improving. In conclusion, the new revision of the classifying cyclone with a secondary air guider is an effective method for reducing the particle span as well as further improving the particle distribution.

Reference

[1] Dirgo, John, and David Leith. "Cyclone collection efficiency: comparison of experimental results with theoretical predictions." Aerosol Science and Technology 4.4 (1985): 401-415.

[2] Ray, Madhumita B., et al. "Improving the removal efficiency of industrial-scale cyclones for particles smaller than five micrometre." International journal of mineral processing 53.1 (1998): 39-47.

[3] Leith, David, and Dilip Mehta. "Cyclone performance and design."Atmospheric Environment (1967) 7.5 (1973): 527-549.

[4] Swamee, Prabhata K., Nitin Aggarwal, and Kuldeep Bhobhiya. "Optimum design of cyclone separator." AIChE journal 55.9 (2009): 2279-2283.

[5] Su, Yaxin, Anqiao Zheng, and Bingtao Zhao. "Numerical simulation of effect of inlet configuration on square cyclone separator performance." Powder technology 210.3 (2011): 293-303.

[6] Ramachandran, G., et al. "Cyclone optimization based on a new empirical model for pressure drop." Aerosol Science and Technology 15.2 (1991): 135-148.

[7] Leith, D. "Handbook of Environmental Engineering, Vol. I, NC Pereira and LK Wang, eds." (1979): 61.

[8] Xiang, R. B., and K. W. Lee. "Numerical study of flow field in cyclones of different height." Chemical Engineering and Processing: Process Intensification 44.8 (2005): 877-883.

[9] Bhasker, C. "Flow simulation in industrial cyclone separator." Advances in Engineering Software 41.2 (2010): 220-228.

[10] Fu J., Characterization of fine powders and development of processes for powder coatings, PhD. Theses of UWO. (2013): 54-56.

[11] Tong, Z. B., et al. "Numerical study of the effects of particle size and polydispersity on the agglomerate dispersion in a cyclonic flow." Chemical Engineering Journal 164.2 (2010): 432-441.

[12] Dunber, Craig A., Anthony J. Hickey, and Peter Holzner. "Dispersion and characterization of pharmaceutical dry powder aerosols." KONA Powder and Particle Journal 16.0 (1998): 7-45.

[13] Voss, Austin, and Warren H. Finlay. "Deagglomeration of dry powder pharmaceutical aerosols." International journal of pharmaceutics 248.1 (2002): 39-50.

[14] Darrow, David S. "Classifying cyclone." U.S. Patent No. 4,743,363. 10 May 1988.

[15] Schwamborn, Karl-Heinz, and H. J. Smigerski. "Cyclone collector and cyclone classifier." U.S. Patent No. 5,958,094. 28 Sep. 1999.

[16] Ikebuchi, Iwao, et al. "Cyclone classifier." U.S. Patent No. 4,872,973. 10 Oct. 1989.

[17] Huang, Qing, Hui Zhang, and Jesse Zhu. "Flow properties of fine powders in powder coating." Particuology 8.1 (2010): 19-27.

4 Chapter 4: Improvement on the Faraday Cage effect by Modifying Corona Spray Gun

4.1 Introduction

Regarding the spray application of powder coatings, there are two major electrostatic charging methods: corona charging and tribo charging. Corona charging spray gun is more popular in powder coating applications due to its reliable charging performance and good control of powder deposition [1]. Powder coating application by corona charging is achieved by spraying, curing and cooling. During the corona spraying process, the electrode of spray gun generates a strong electrostatic field to charge the particles. Then the charged particles deposit on the grounded coating target, followed by curing process at a high temperature (180 to 200 ˚C). Figure 4.1 illustrates a typical corona charging and spray system. The spraying process starts with the high-voltage charging provided by the generator to the electrode at the tip of the spray gun. With the charge accumulating on the electrode, it generates a strong electric field to charge powder particles between the gun tip and target substrate. The charged particles are driven by air flow and then deposited onto the grounded target [2].

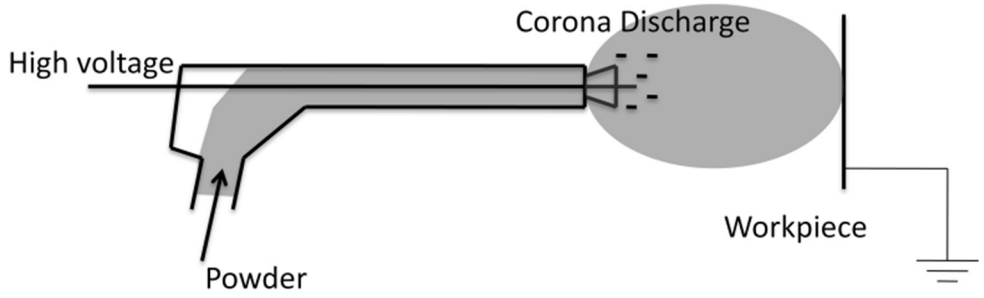

Figure 4.1 A corona charge spraying process (duplicated from Figure 2.11)

There are several major requirements for powder coating spraying application: high first-pass transfer efficiency (FPTE), good surface finish with desirable mechanical, chemical and weather resistance, as well as uniform film thickness of the entire target substrates. Among these factors, higher FPTE is able to be achieved by utilizing the corona spray gun with higher voltage [3]. However, there are some drawbacks of using corona spray gun under a high voltage operating condition due to the fact that copious free electrons

created from the gun electrode tip could break down and ionize the surrounding air. This phenomenon is known as corona discharge. A small percentage of the charged ions attaches to the particles sprayed out of the gun while large amount of these free ions directly deposit onto the target together with the particles [5]. If those free ions are continuously building up on the deposited powder layer, the field intensity exceeds the breakdown tolerance of powder layer. The ions tend to penetrate through the powder layer and cause the dropping of the particles and repellence of further particles deposition. This is known as back ionization, which eventually causes insufficient particle deposition rate and poor film qualities [4].

The presence of the electric field between the gun nozzle and the substrate leads to problems when coating articles with convex geometry by corona spray guns. As a result of electrostatic law, the field lines cannot penetrate to recessed areas of coating target. Charged particles driven by the force always follow the field line pattern and tend to cover the sharp edges when flying close to the target, so powder deposition is reduced in recessed area or holes [6] (Figure 4.2 and Figure 4.3). As the result, the recessed areas or corners have insufficient particle coverage compared with other part of the coating surface. This phenomenon is known as Faraday Cage effect, casing the uneven powder distribution and coverage on the final coating finishes.

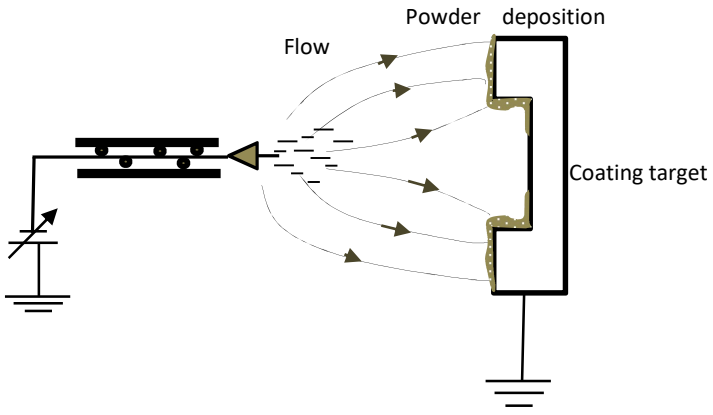

Figure 4.2 Typical flow pattern of corona gun and Faraday Cage effects

Figure 4.3 Coating target with complex configurations

The other significant charging system called tribo or triboelectric charging gun could at least in principle, help eliminate the above problems of the corona discharge as well as preventing the Faraday Cage effect. The mechanism of tribo-charging is to charge particles by intensive friction between particles and the gun internals made of polytetrafluoroethylene (PTPE) as the frictional component. Powders become positively charged when passing through the gun and in contact with the PTFE internals. Subsequently the gun internals are left with a negative charge and must be conducted away afterwards. Unlike the corona gun, the tribo charging gun does not contain an electrode which generates an electric field between the gun tip and target. As a result, the transportation of the charged particles from the gun is entirely realized by the air flow passing through the specially designed spray head [7]. As a result of the charging mechanism of the tribo gun, the electrostatic field between the spray gun and work piece is weaker so as to effectively eliminate the Faraday Cage effect, leading to a good coating film quality [8].

However, the low transfer efficiency of tribo gun is always a problem. On different coating substrates, corona and triboelectric charging differ in the electrostatic powder charging performance and transfer efficiency. Earlier studies indicated that corona gun had relatively higher powder deposition efficiency than a triboelectric gun with coating metal plates, while it had the same efficiency in coating metal tubes [9]. Mayr et al. analyzed the effectiveness of corona and triboelectric charging systems in transfer

efficiency and adhesion using powder of selected sizes. The results showed that corona charging system could provide the highest transfer efficiency as well as better adhesion among all the tested spraying systems [4]. In general, although using tribocharging is one possible solution in avoiding back ionization and Faraday Cage effect, some problems and drawbacks of tribo gun are still remaining to be solved. It is more sensitive and difficult to predict than the corona spray gun due to the fact that the tribo system is easily influenced by many factors during the operating such as humidity, material electrical characteristics and the surface condition of the coating target (roughness and shape) [10]. It is also hard to predict the quality of coating.

In powder coating industry, Faraday Cage effect seriously affects the final product quality such as film thickness and smoothness. Thus additional make-up procedures are needed, causing cost increase and extra waste. In the past few decades, many efforts have been made in mitigating back-ionization and Faraday Cage effect by modifying the spraying devices. One famous idea called internal-corona (IC) modification in the corona spraying system has been developed to solve these problems. In 1988, Kiefer et al. proposed an idea to let the electrostatic charging electrodes charge particles in gun chamber near the nozzle region. Then the grounded substrate is coated with a cloud of all charged alike particles, and then the layer of particles melts and cures to a continuous film [11]. Similarity, Nagasaki et al. invented a plasma electrode pair disposed inside the spray apparatus so as to charge the flowing particles passing through [12]. Usually, the electrode is enclosed by a grounded cylinder in most of the internal corona spray gun design. During the spraying, the electrostatic field and free ions go to the cylinder instead of coating surface, so the induced electric field near target surface space is minimized to overcome the problem of Faraday Cage effect. However, these designs of the spray gun may lead to large amount of the charged particles accumulating inside the cylinder wall and gun tip. Over accumulation of those particles could cause reverse discharge and back ionization. More seriously, sparks from reverse discharge may ignite the surrounding particles. Several solutions aiming at modifying IC guns have been studied since then. Clements [13] et al. investigated an IC gun with an attached cylindrical section to the nozzle to coat the insulated targets with electrostatic powder. The electrode was provided with both alternating polarity and dc voltage supplies. Since the IC gun does not emit

many free ions, it could reduce the charge accumulation on the coating target in order to solve back ionization and Faraday Cage effect problems. However, the TE obtained by this method is very low, also the adhesion between powder coating and insulating target is weak. So the final film does not always meet the requirements.

On the other hand, the biggest challenge of the internal charge gun modification is that the gun electrode is enclosed in limited space. It reduces charging intensity so the free electrons tend to attach on cylinder wall. As a result, the actual charging of the particle is very poor. Therefore, the amount of deposited powder on the target is much less than being adequate. So far, there has been almost no successful method and design of IC spray gun.

4.2 Materials and Methods

In this study, we proposed a new method in modifying corona spray gun to overcome the Faraday Cage effect. The main innovation of the corona gun is to add four additional electrodes with alternating voltage supply. Theoretically, comparing with conventional constant voltage supply systems, the induced electrostatic field of the alternating voltage supply has a low field intensity, avoiding the ions' continuous building up on the powder layer of coating target. As a result, more charged particles have access to the recessed areas for solving the Faraday Cage effect problem. In addition, this modified gun with multi-electrodes could create repellency of the electrostatic field near the gun tip, which allows particles flowing out from the spray gun to interact the electrostatic field with much less intensity compared with a single electrode. The main goal of this study is to comprehensively investigate the performance of the modified spray gun. Series of experiments were conducted to examine the results and it was mainly depicted by measuring of Faraday Cage Resistance (FCR) and FPTE.

The experiments were conducted using a corona spray system (Encore® XT manual powder spray systems, Nordson Corporation, Amherst, Ohio, USA). Conventionally, a corona spray gun includes one single electrode at the gun tip and is supplied with constant high voltage. However, the modified spray gun proposed in this study consists

of four additional electrodes surrounding the center gun tip, as shown in Figure 4.4 (a). Additional electrodes were installed in a plastic plate on the outside circumference of the

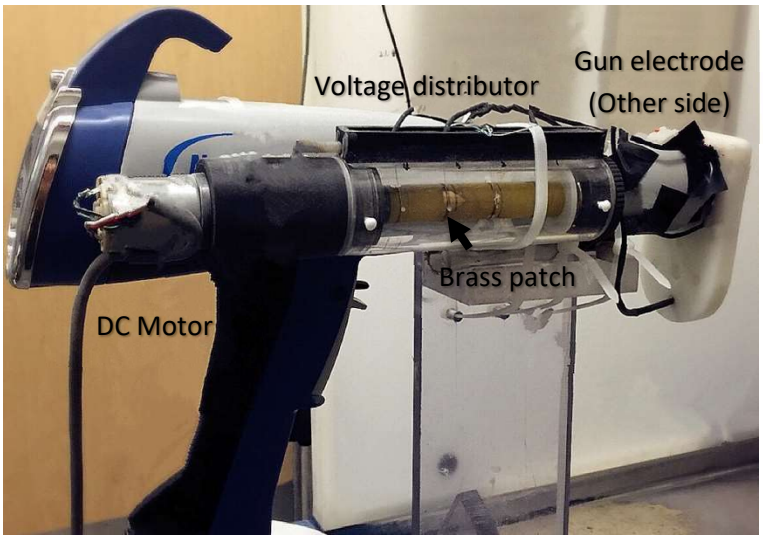

(a) The modified corona spray gun

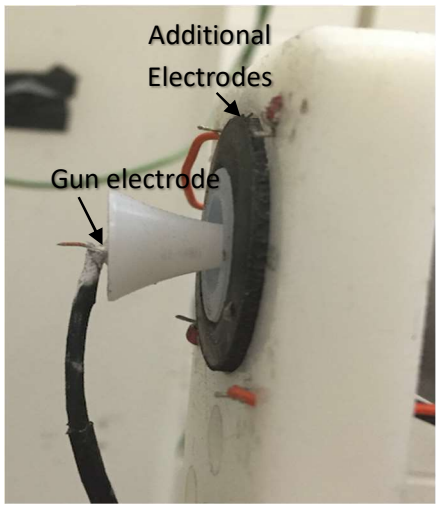

(b) Configuration of four additional electrodes

Figure 4.4 The schematic of the modified corona spray gun

gun nozzle, named as electrode 1,2,3 and 4, as shown in Figure 4.4 (b). For realizing the alternating voltage supply, four electrodes were connected to a specially designed distributor attached to the side of the spray gun, driven by a DC motor, distributing the

high voltage to each of two diagonal electrodes at a time. The main cylinder shaft is made from brass and encapsulated in poly (methyl methacrylate) (PMMA) chamber, as illustrated in Figure 4.5 (a). The main shaft is made from brass with 4 naked triangle patches. Each patch is connected with one electrode through the extension wire crossing on top of the PMMA chamber. Except for the surface of four brass patches, the main shaft is wrapped by ceramic, as illustrated in Figure 4.5(b). During the rotating,

(a) Photo of the distributor

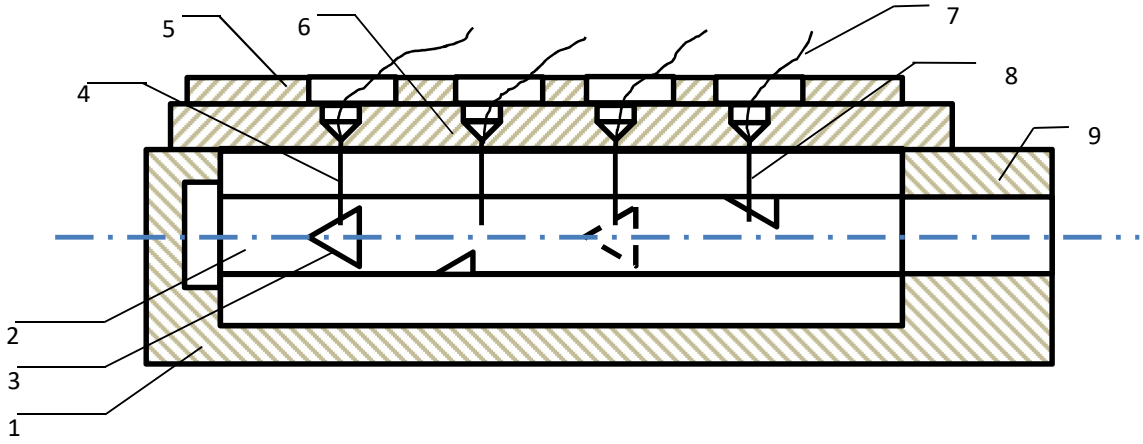

1-shaft cover, 2-main shaft, 3-naked brass contact panel, 4-electrodes, 5- top cover bar, 6-slide bar, 7-extention wire connected with electrodes and brass patch, 8-wire

(b) Design drawing of the distributor

Figure 4.5 The DC motor distributor

electrodes get charged when touched with brass while stop charging when touched with ceramic surface. In this way, the four electrodes can get charged in a certain sequence during the rotation. By connecting electrode 1 with 3, 2 with 4, the DC motors

could distribute the high voltage to each of the two diagonal electrodes simultaneously. Theoretically, this alternating charging pattern could effectively avoid the accumulating of free ions, so the powder cloud produced by this spray gun contains almost no net charge. In this case the Faraday Cage penetration is expected to be avoided due to the reduction of electrostatic field intensity.

The charging programming is demonstrated in Figure 4.6. Each pair of the electrodes in diagonal position have the same charging performance with the empty periods in between two adjacent charging periods. The alternating distribution frequency was adjusted by changing the voltage input of the DC motor. The rotation speed is proportional to the voltage input, so by increasing the charging frequency, both of the charging and empty periods (neutral period) are shorter.

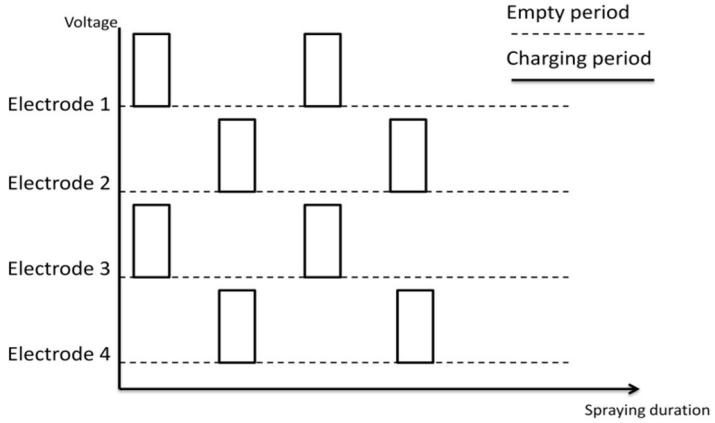

(a) Charging cycles of the pins

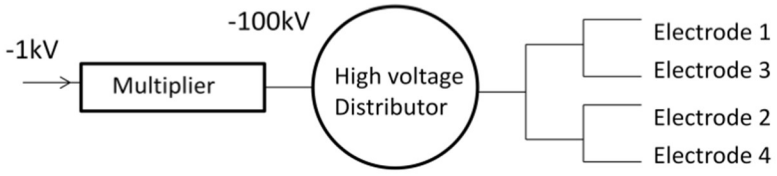

(b) Charging scheme of the gun

Figure 4.6 The charging program of the distributor

The powder samples tested were Avalanche White (PT-3000), provided by Syn-Link, Ontario, Canada. The reason why this powder sample is used in this experiment is that coarse powder is dominant in most of the powder coating applications, and it can represent the most typical powder coatings in the industry for laboratory test and scale-up.

It will benefit in representing the performance of this novel spraying gun, as well as the future scale up researches.

4.3 Experiment Design

In this experiment, the voltage of the DC motor was measured by rotating speed of the main shaft cylinder. The corresponding charging rotation was 400 r/min, 550 r/min, 700r/min, 850 r/min and 1000r/min. In addition, five different voltages of the corona spray gun were set as -30kV, -45kV, -60kV, -75kV and -90kV, where -30kV and -90kV were the lower and upper limits of the normal spray gun, and the normal application voltage setup is in between. In order to optimize the spray gun experiments, the distance between the center gun tip and four additional electrodes was adjusted in both axial and radial directions. The distance of the gun tip to work pieces is 20cm and remains constant throughout the whole experiment.

More importantly, the main parameter in evaluating the spray gun performance is Faraday Cage Resistance (FCR), measured by a U-shape coating panel, as shown in Figure 4.7. There are three aluminum panels, panel A, B and C, being attached to the U-shape aluminum coating panel which was hanging upright during the spraying. Those three small panels have identical dimensions but Panel C was placed in the recessed area with 2.5 cm depth lower than panel A and B. In this way, the Faraday Cage Resistance was calculated by:

$$\mathrm{FCR} = \frac{2 \times W_{Panel\,C}}{W_{Panel\,A} + W_{Panel\,B}} \qquad \text{Eq.4.1}$$

W (g) is the weight of the powder on each panels. The range of the FCR is from 0 to 1, where the higher value of FCR, the better penetration of the powder overcoming the Faraday Cage effect. If the FCR equals to 1, it means that the amount of the powder deposited on panel C is the same as panel A and B, standing for the no Faraday Cage effect. However, if FCR is zero, there is no powder reaching panel C, indicating that Faraday Cage effect is extremely strong.

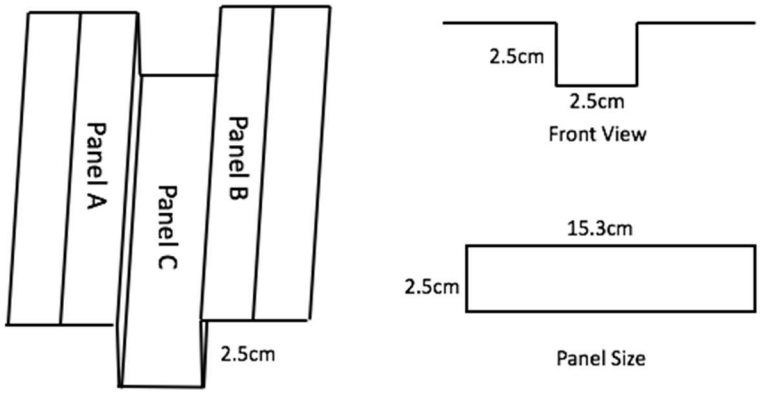

Figure 4.7 The Panel size for Faraday Cage effect measurement

Another significant parameter is the first pass transfer efficiency (FPTE). It was first determined by Chen et al. [14] using a computer-controlled powder coating spray system. The mass of the deposited powder on the target compared with the weight loss from the powder supply is measured using a microbalance. In this way, the measured FPTE was defined as the ratio of the mass of deposited powder to the mass of sprayed powder. According to the weight of powder sprayed onto coating surface, the FPTE could be calculated as:

$$\text{FPTE} = \frac{W_{coated}}{W_{sprayed}} \qquad \text{Eq.4.2}$$

In this experimental study, the powder loading was accomplished by a conveyer belt feeding the powder to a hopper which was connected to the bottom of the spray gun at a loading rate of 3.1g/s, which is comparable to the industry feeding rate. This feeding method is different from the conventional approach utilizing the fluidized air to transport the powder from a powder box through the regulator. In this way, the powder amount is easily controlled and the loading rate could remain constant by maintaining the conveyer speed during the experiments. In this study, the powder loading rate remains 3.1g/s with an amount of 6.3 g for FCR test and 18.6 g powder samples for FPTE test. The results obtained from the original corona spray gun were used as a control. In addition, in order to find the best range of operating conditions of the original corona gun, a series of parameters of the original spray gun were also adjusted: namely gun voltage (-kV),

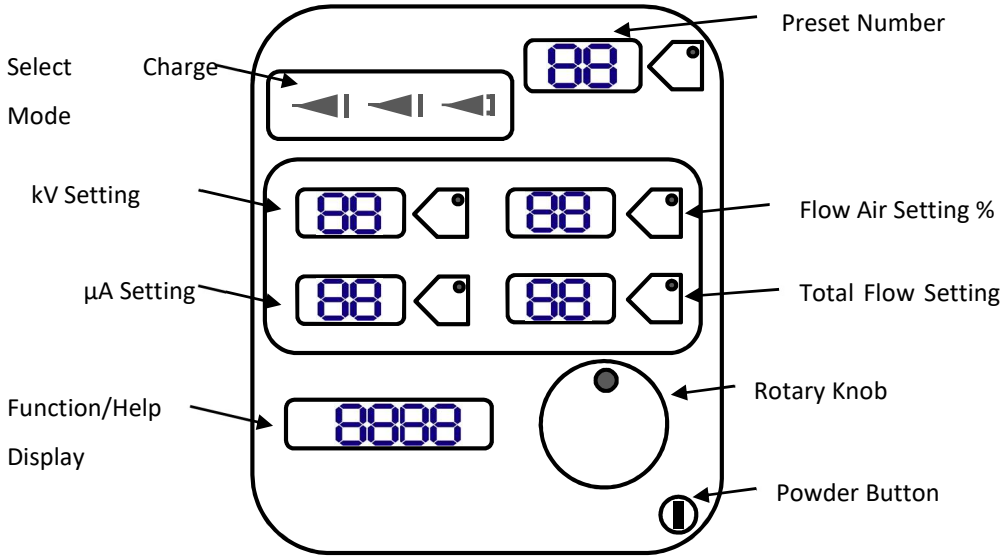

(a) Control board of the spray system

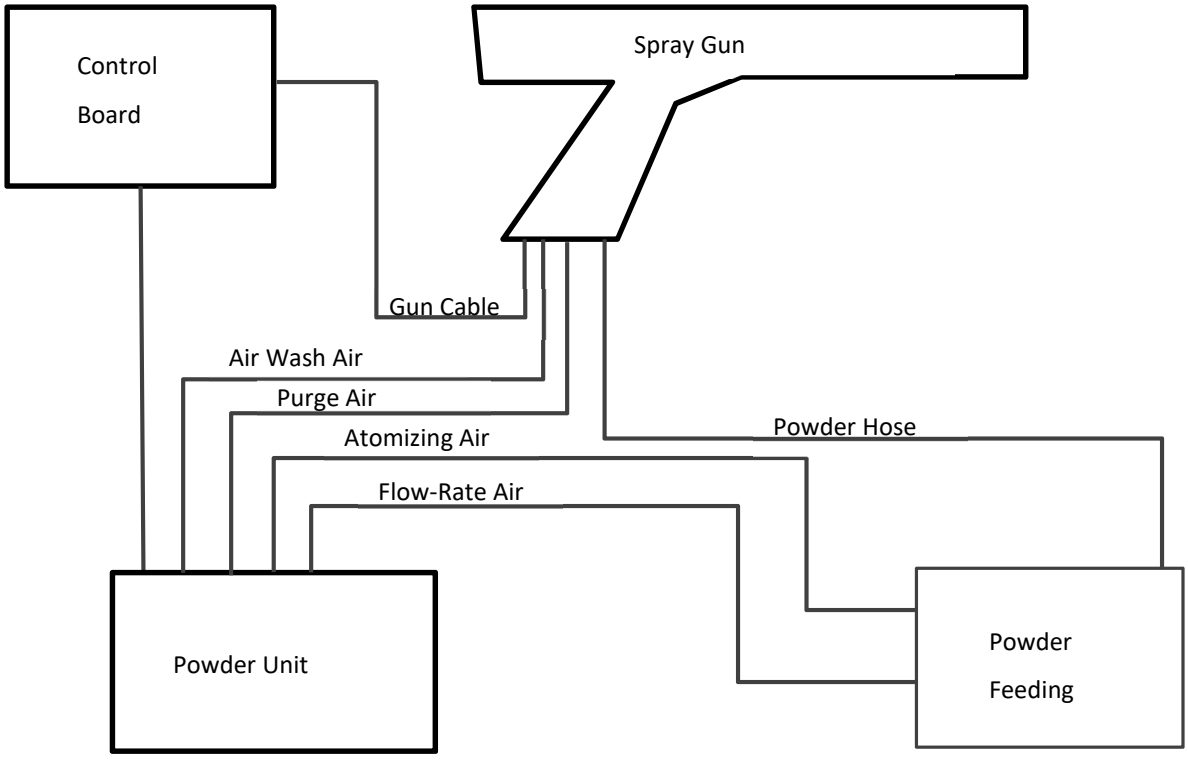

(b) System diagram of the spray system

Figure 4.8 Encore XT Manual Powder System diagram

current (µA), percentage of flow air (%) and total flow (SCFM). The modification experiment was carried out in accordance with those operating conditions. The schematic

of the control board and the system diagram is shown in Figure 4.8. In general, the most commonly used gun voltage range in powder coating industry is from -60kV to -100kV for conductive substrates, and less than -10kV for insulated parts. The tube controlling the total flow is connected to the powder unit with an air supply, controlling the velocity of the powder flow. In this study, the smart flow mode of the spraying system has been used. As controlled by the system, if the flow air % percentage value decreases, the atomizing air pressure increases automatically, so that the powder velocity remains the same. The flow air (%) sets the actual percentage of powder flow rate, depending on the total air amount and the outputs of atomizing air.

During the experiments, several operating conditions have been adjusted and measured for evaluating the performance of this novel spray gun, namely: 1) voltage (-kV); 2) alternating charging frequency (RPM); 3) axial distance of the electrodes to center tip (cm), see Figure 4.8 (a). 4) radial position of the additional electrodes, see Figure 4.9 (b);

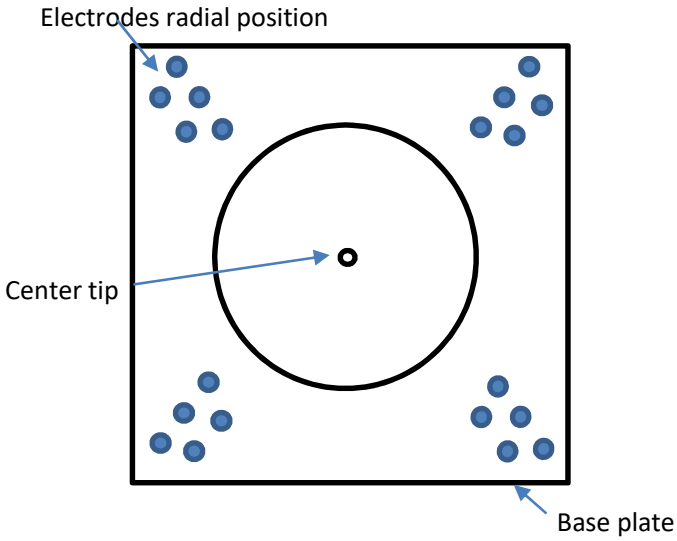

(a) Radial position of additional electrodes to center tip

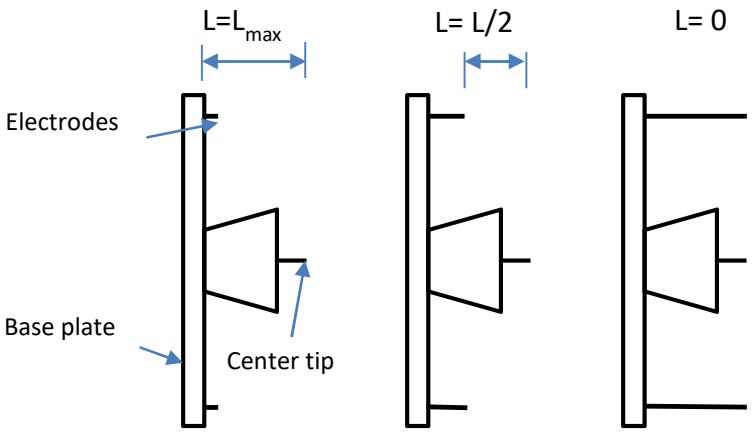

(b) Radial position of the additional electrodes to center tip

Figure 4.9 Axial (a) and radial (b) position of electrodes to the center tip

4.3.1 Finding the baseline of original

The experiment began with the calibration of the Nordson Corona spray gun. The four significant parameters affecting the final spraying performance are gun voltage (-kV), current (μA), percentage of flow air (%) and total flow (SCFM, Standard cubic feet per minute). In order to find the optimized operating condition range of the original spray gun, series of experiments were carried out to determine those factors. They show as follows:

To begin with, total flow was adjusted first in setting the powder velocity to obtain the desired pattern size and penetration. The influence of total flow was tested under 60 μA, 50% flow air and in two ordinary gun voltages. As illustrated in Figure 4.10, within the setting range of total flow (1.5 to 6.0 SCFM), both FCR and FPTE values dropped quickly when the total flow was increased. This is mainly due to the fact that with the constant flow rate but higher total flow, particle velocity is increased by atomizing air, leading to less penetration of the recessed area.

In addition, the effect of particle velocity also could influence the particle charging efficiency, evaluating by charge-to-mass ratio (Q/M). The Q/M increases under relatively low particle speed (1.5-2.5m/s) but decreases soon when the powder flow rate goes up [9]. In our case, according to the size of total flow in the circular duct, Q/M was decreasing

when the total flow was larger than 2.0 SCFM, leading to less powder deposition on all coating panels. As a result, both FCR and FPTE values dropped quickly due to the reduction of the amount of particles.

It is also known that particle velocity is crucial as it affects particles' bouncing behaviors. Higher velocity may help with Faraday Cage penetration if the particle charge is well-controlled. However, particles at a high velocity are likely to cause particle bouncing at the surface of powder layer, resulting in the reduced amount deposited powder [14].

Therefore, the proper total flow should be set to less than 3.0 SCFM. In addition, compared with using voltage of -90kV, the FCR under -75kV was slightly smaller during the total flow region less than 3.0 SCFM, while the FPTE was comparable under the same total flow. The above experimental results indicated that utilizing higher charging voltage and proper particle velocity could help particles reach the recessed area so as to reduce the Faraday Cage effect.

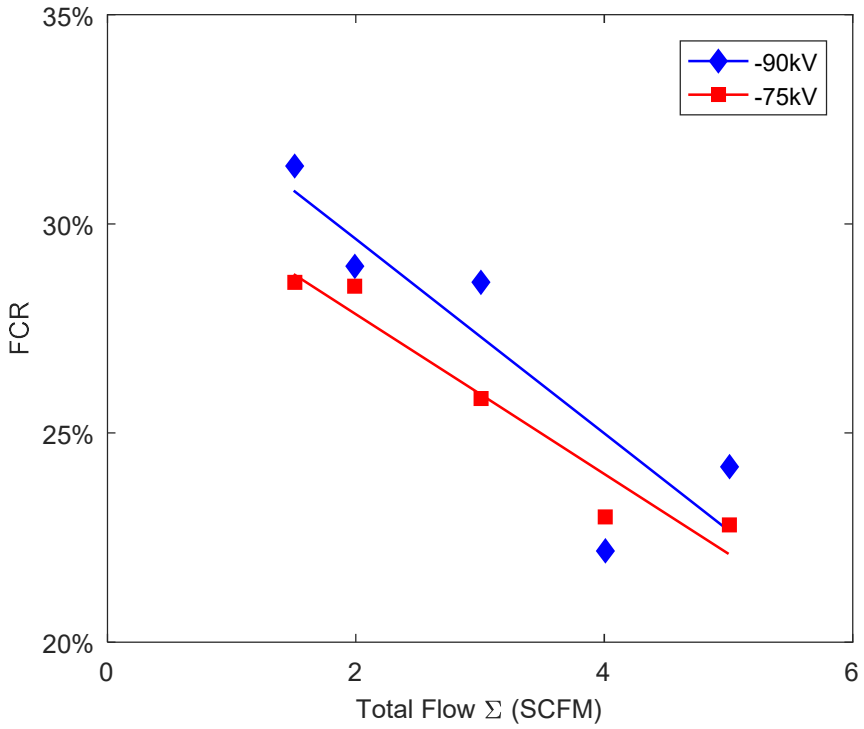

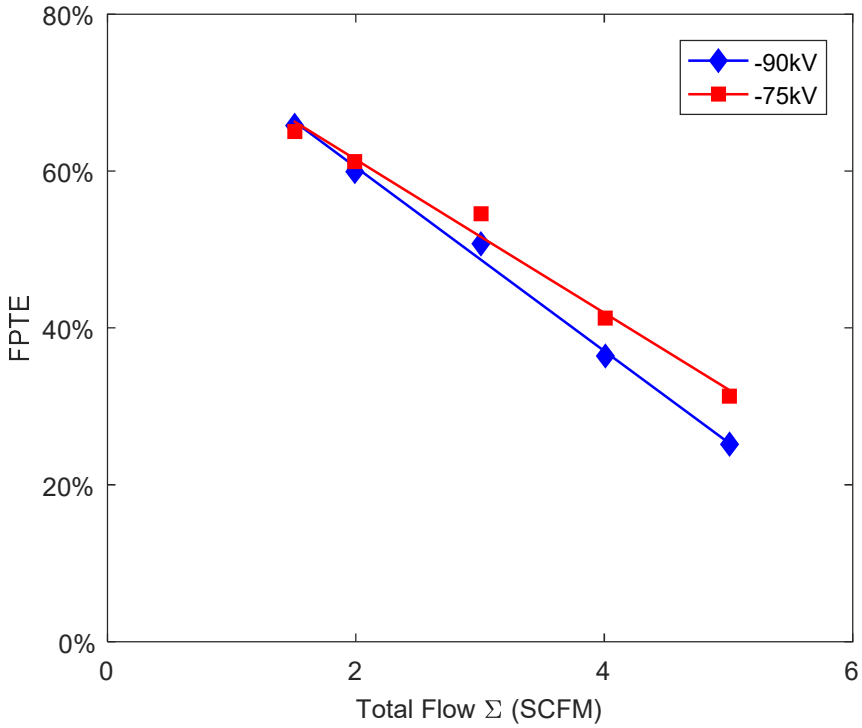

Figure 4.10 Effects of total flow on Faraday Cage and FPTE (50% flow air, 60μA)

After deciding the total flow, it is easy to investigate the influence of flow air (%). As illustrated in Figure 4.11, it showed an increasing trend in the FCR value as the flow air becomes smaller. With a fixed amount of powder feeding from the conveyer, the higher flow air pressure brings higher particle velocity, so that fewer particles get charged leaving the gun. So the Faraday Cage effect is severer under the condition of high flow rate. Meanwhile, FPTE is not sensitive to the change of flow air. However, the flow air could not be set too low so that the extreme setup for flow air (20%) is not favorable for wide range of application conditions and the surface quality.

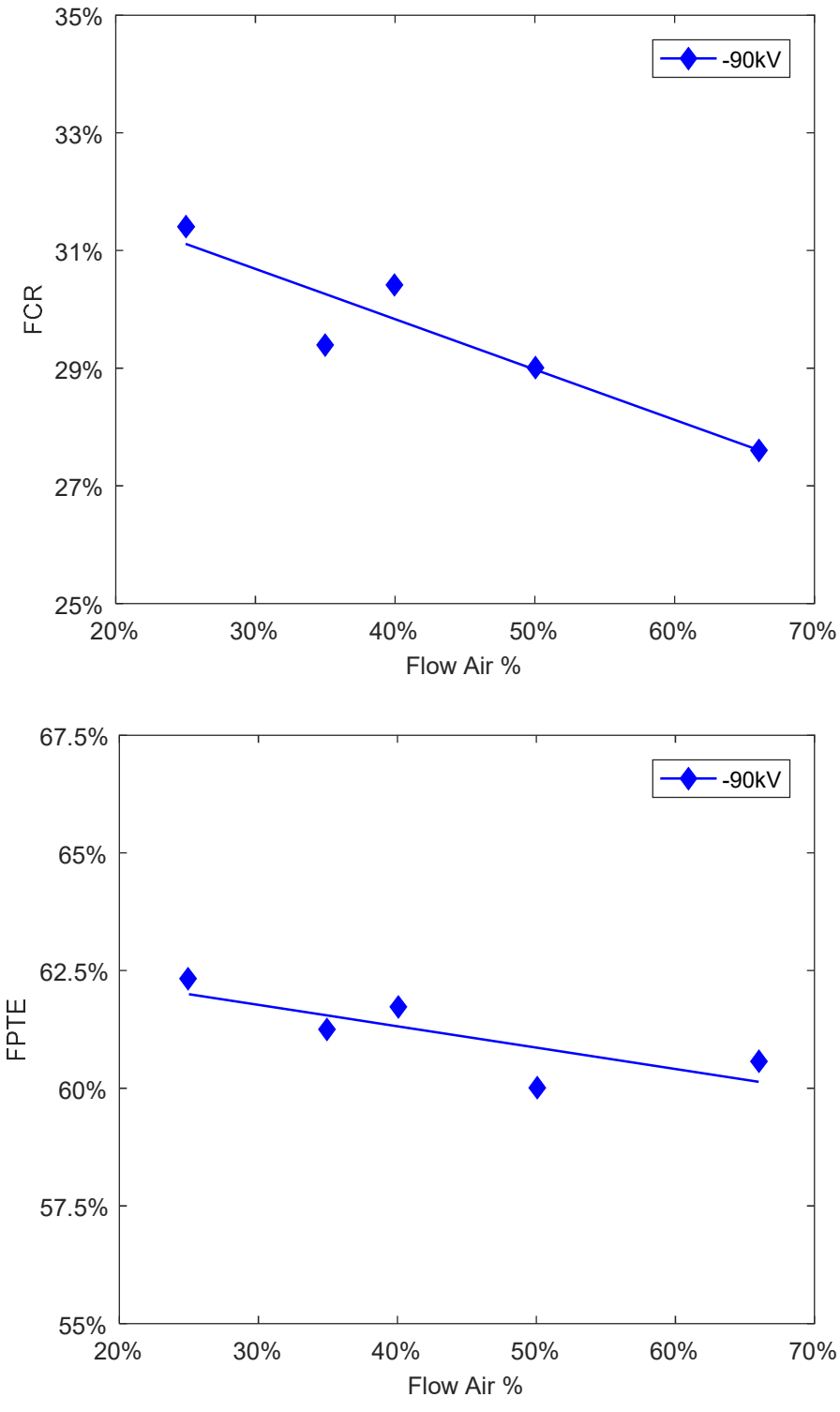

Figure 4.11 The effects of flow air on Faraday Cage and FPTE (2.0 total flow, 60µA)

The corona gun current also controls the charging performance, so it is necessary to find the how the gun current affects the FCR and RPTE. In figure 4.12, both FCR and FPTE

were influenced by adjusting the electrical current of spray gun. In observing the results obtained from changing the current between 20μA and 60μA, it is found that the FCR had an obvious improvement when the spray gun current was low, indicating that the Faraday Cage effect became less serious. At the same time, the FPTE has a minor reduction with the current going higher. This phenomenon is related to the current density of the electrostatic field between the spray gun and coating target.

It happens when free ions keep accumulating near the target surface and particles start to build up. Then it causes the self-limiting in preventing further particles depositing onto the target due to back-ionization, resulting in poor film qualities. Previous researchers determined that the optimal operating conditions to reach a final coating film with few defects is with a high voltage and a low current, meanwhile the FPTE could be maintained [3,15]. In this case, 20 μA is suitable for the future spray gun current setting.

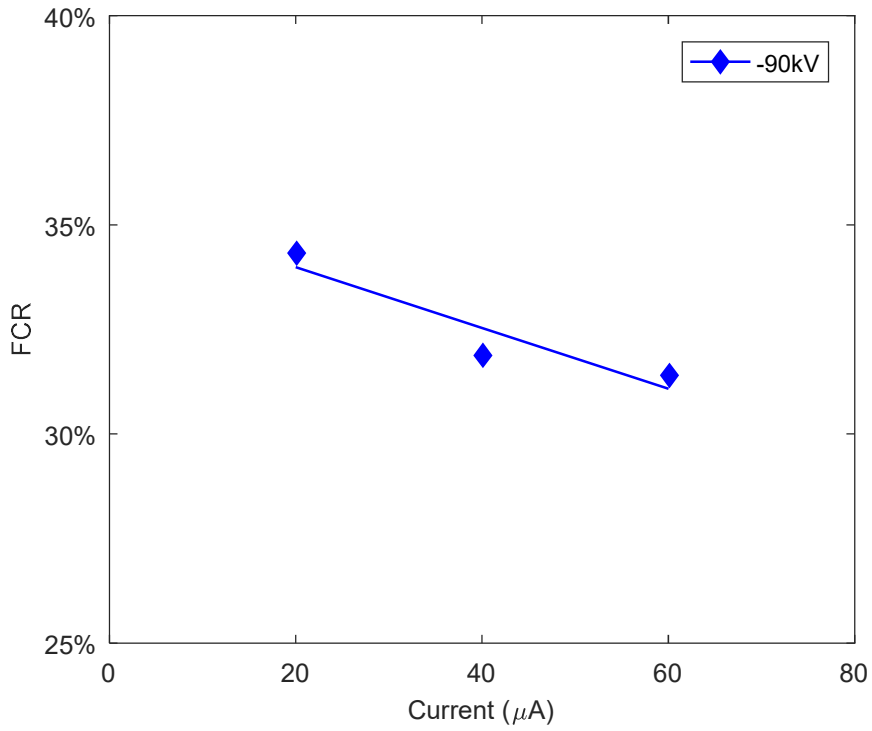

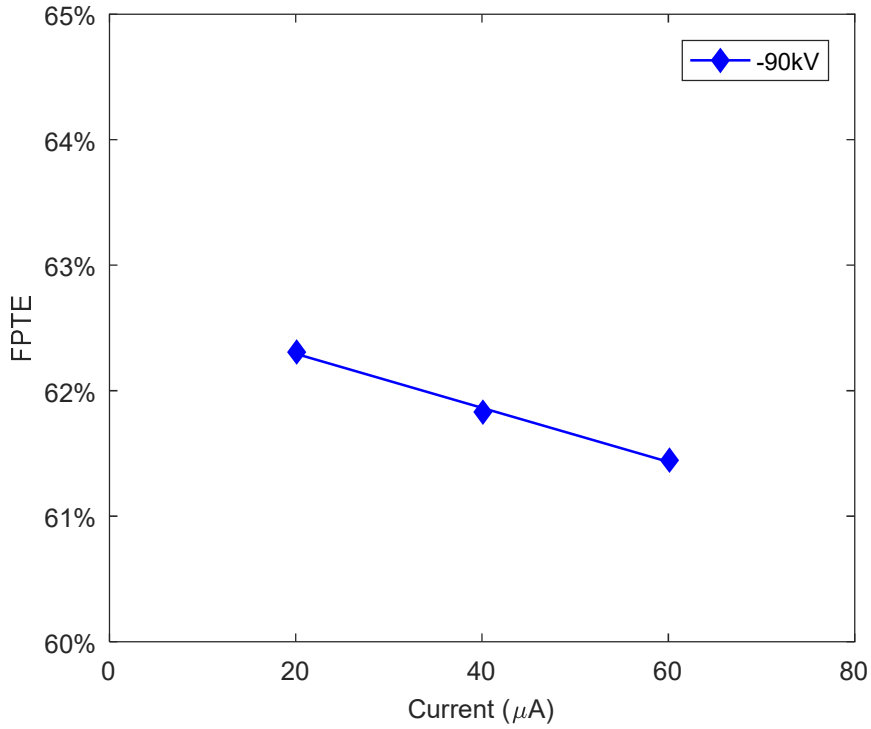

Figure 4.12 Effects of current of spray gun on Faraday Cage and FPTE (2.0 total flow, 25% flow air)

In addition, after determining the settings of main operating parameters, consistent and accurate experiments in evaluating the corona spray gun were conducted by testing FCR in the whole range of gun voltage. As the Figure 4.13 shows, in general, the FCR is within the certain range, which indicates the chosen corona spray gun has a relatively stable operating state. Under the low gun voltage, the average FCR value was slightly higher than that in higher voltage regions. FCR being closed to 1 represents that there is almost no Faraday Cage effect and all the tight corners and recessed areas are covered by a suitable amount of powder coatings. The higher FCR obtained around -30kV can be explained that when operating under a low gun voltage, the total weight loss of particles on panel A and B is greater than that on panel C, this does not stand for the weaker Faraday Cage effect. The further explanation of the weight loss and insufficient coverage can be the poor charge of particles under low gun voltage. During the spraying, the first requirement of the spray gun is to let more particles diffuse from it being highly charged. Only in this way are the particles able to reach the target and adhere on it. But in reality, not all the particles are charged sufficiently due to the inefficient charging process,

especially when using a low gun voltage. Additionally, the corona discharge which is confined to a small vicinity of the spray gun needle where the ion density is sharply decreasing, is also causing less particle charges. Experimental results also found that the corona discharge can shield the spray gun tip, so that no further charging can happen. What's more, as mentioned above, copious free ions in the space between the gun tip and

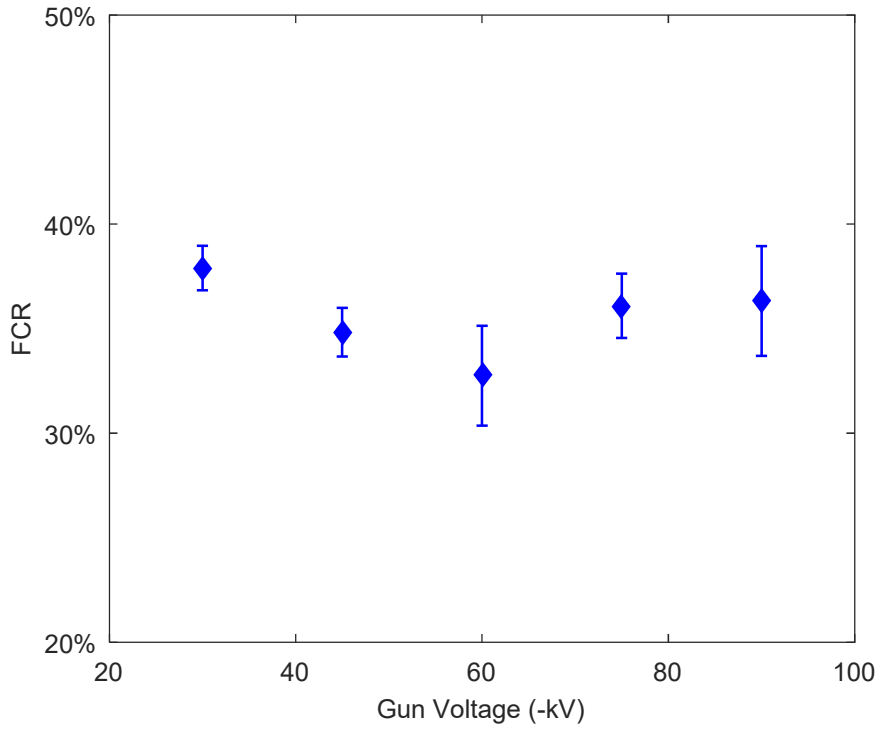

Figure 4.13 FCR of spray gun vs gun voltage (Total flow=2.0, Flow air=20%, Current=20μA)

the work piece repel the further particles adhering onto the coating surface due to self-limiting. It was found that this phenomenon occurs in the particle radius less than 50μm [16]. Also, according to the visual observing of all coated samples, it is obvious that panel C had less powder coverage in the recessed area when coated with a low gun voltage, indicating a more severe Faraday Cage effect. In conclusion, the suggested gun voltage range is between -60kV and -90kV.

4.4 Optimized experiment of the modified corona spray gun

4.4.1 Investigating the length of the additional electrode

According to the previous exploratory research, the condition of the original spray gun was decided with the settings of: total flow=2.0 SCFM; flow air %=25%, current=20μA. The further modification was based on those settings which remaining the same during the whole experiment.

The length of the axial position between the gun tip of the center electrode with additional electrode tips has been investigated as follows. Figure 4.14 shows the condition of largest axial distance between center tip and the additional electrodes tips, denoted as L_{max}. The results obtained from this condition are illustrated in Figure 4.15. In observing the FCR with respect of charging frequency, it is obvious that FCR is getting improved by using the new spray gun, especially under an alternating frequency of 1000 RPM. As the input voltage decreased, the average of FCR became slightly higher. All the FCR values obtained by the revised gun is greater than the control group, indicated that the modified spray gun with additional electrodes with alternating voltage supply was efficient in mitigating the Faraday Cage

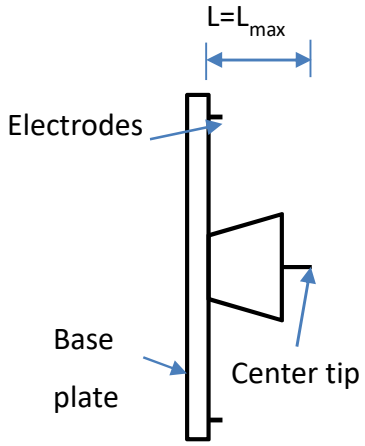

Figure 4.14 Axial position of additional electrodes to center tip (Figure 4.9a left)

resistance, as more particles sprayed out from the gun get charged owing to stronger charging intensity around the gun tip. Meanwhile, other than conventional constant charging, the Alternating charging could effectively avoid ion accumulating so as to help

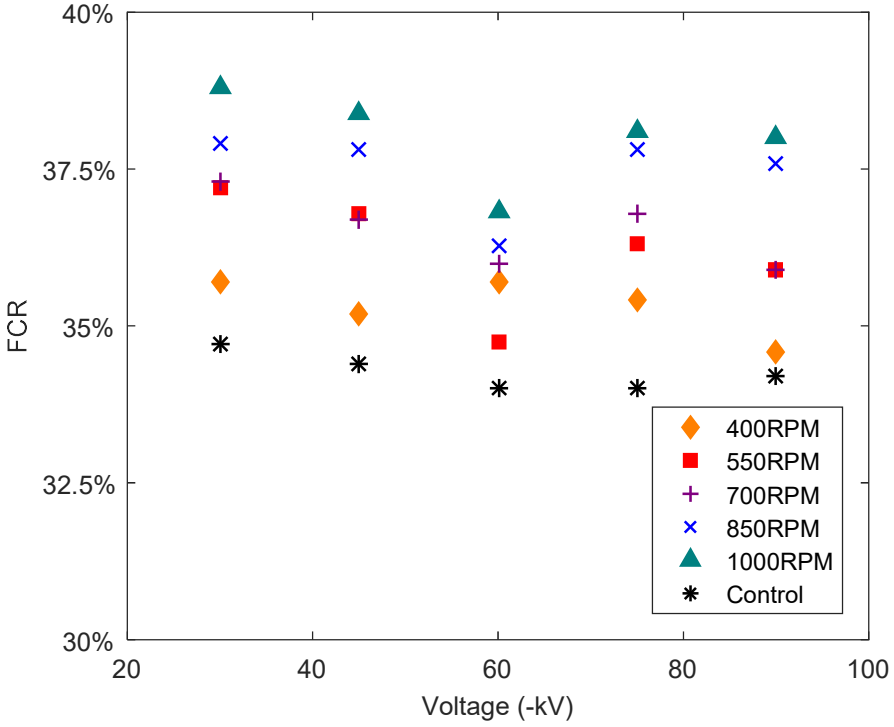

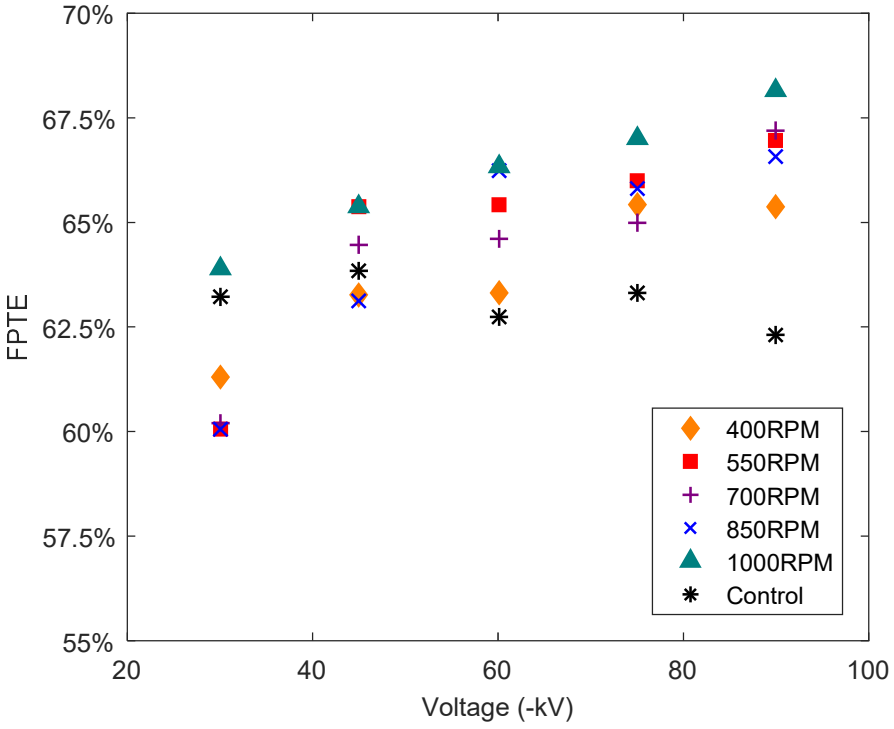

Figure 4.15 The FCR and FPTE for $L=L_{max}$

particle deposition. At the same time, the transfer efficiency has some improvement in higher charging frequency while some of the values are comparable to the control group under the low frequency. Most of the FPTE values were above the control group, demonstrating that the alternating charging by adding the electrodes is capable of improving FPTE under most operating conditions.

Figure 4.16 illustrates the extended additional electrode condition. The axial distance between the additional electrode tips and center tip are L/2. The results obtained from this operating condition is shown in Figure 4.17. It is obvious that by adding higher alternating frequency, the promising FCR values could be obtained, which is also in line with the condition of furthest axial electrodes distance. Compared with the FCR results in Figure 4.13, the peak of the FCR value in most of the alternating frequency is even higher in this testing configuration by extending the length of additional electrodes. On the other hand, the FPTE does not vary much comparing with using shorter electrodes.

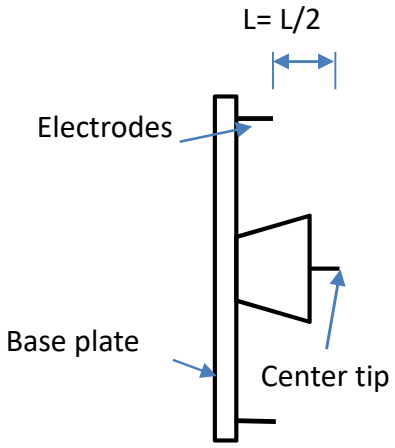

Figure 4.16 Axial position of additional electrodes to center tip (figure 4.9a Middle)

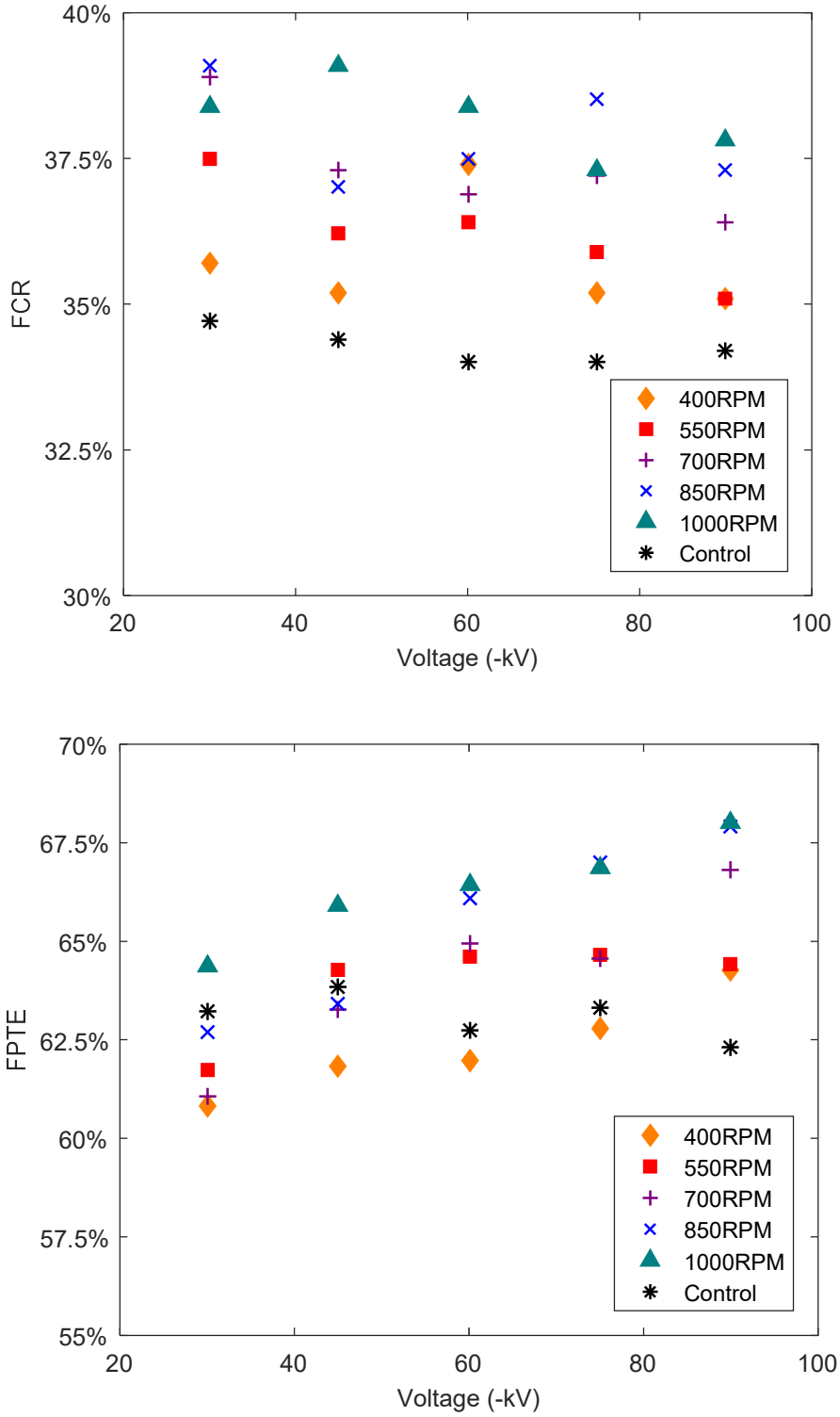

Figure 4.17 The FCR and FPTE for L=L/2

By further extending the length of the additional electrodes, the tip positon of all the electrodes were in the same axial line. Figure 4.18. In other words, the gun tip of all the

five electrodes had the same distance to the spraying target. As the Figure 4.19 indicates, the FCR has an apparent improvement especially under 1000 RPM. Compared with the former two groups, only by adding the minimum alternating frequency with 400 RPM, the average FCR have the larger improvement. Also with the increasing of charge frequency, the even better FCR could be obtained, which indicate the Faraday Cage effect became weaker. The probable average FCR value in 1000RPM roughly had the

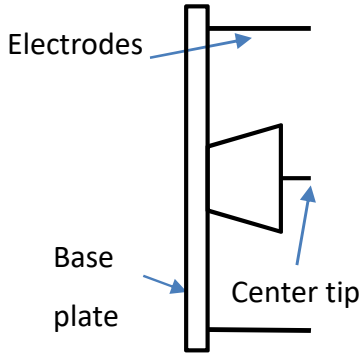

Figure 4.18 Axial position of additional electrodes to center tip (figure 4.9a right)

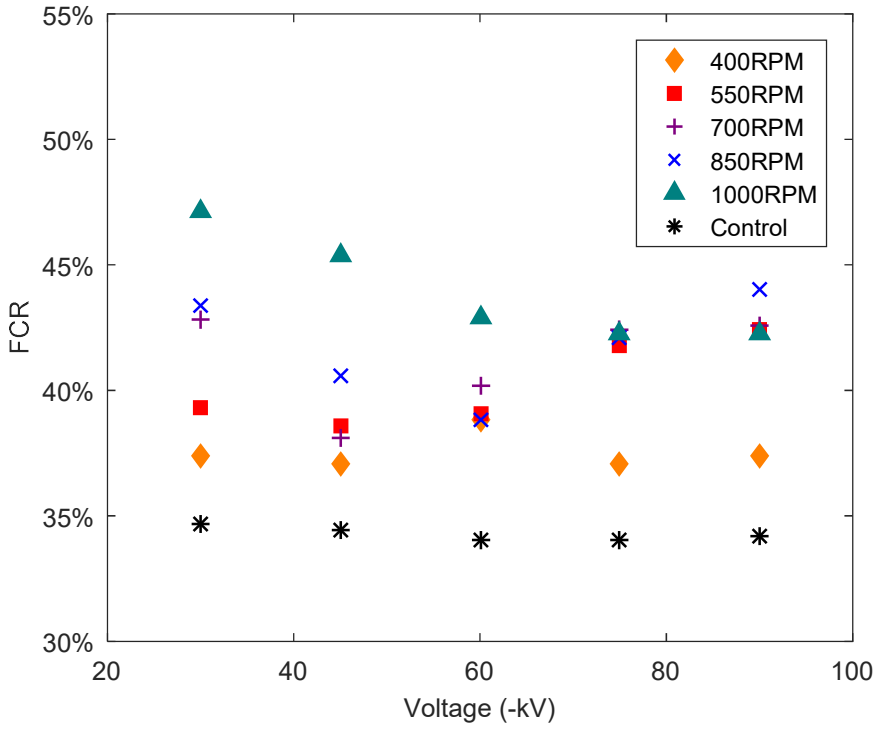

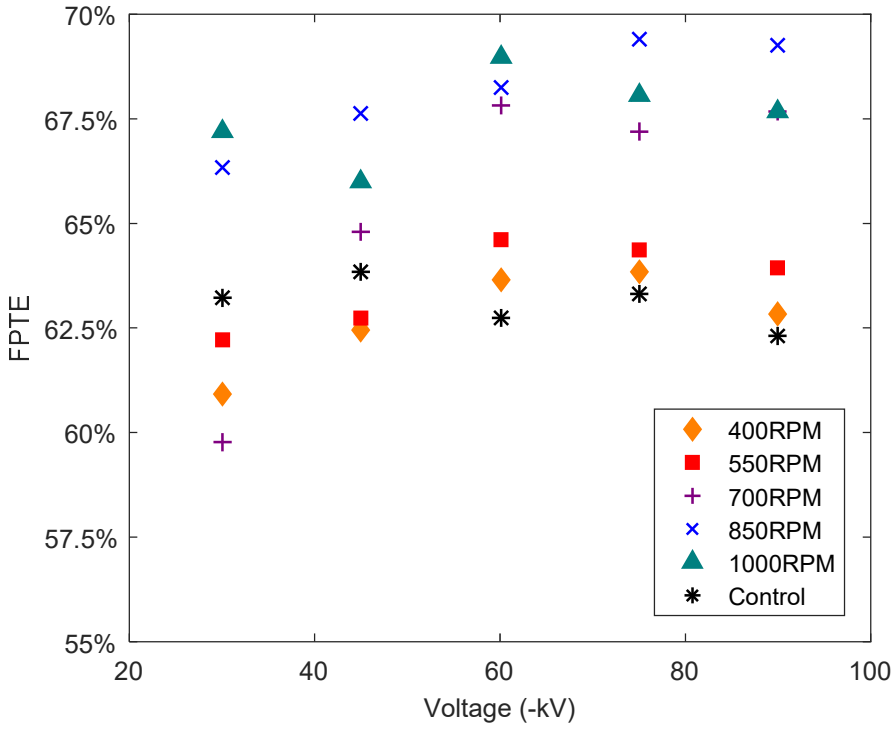

Figure 4.19 The FCR and FPTE for L=0

improvement of 10% than the average control group, which is very promising for the revision of corona spray gun. In addition, the PFTE in this case has slight improvement under higher gun voltage with the charging frequency larger than 850 RPM, although it is still a bit lower than the control group in -30kV and -45kV, similar to the conditions of more additional electrode positions. In general, most of the FPTE of these three groups had relatively lower values under the lower voltage and started increasing with the growth of gun voltage.

In analyzing the FPTE values of Figure 4.15 - 4.19, the transfer efficiency of the original gun and the modified gun was comparable under the low gun voltage and the charging frequency. The difference between control group and improved results became larger when the higher gun voltage and charging frequency were supplied. It implied that the new design of the modified spray gun is desirable due to the fact that it is capable of reducing the corona quenching. Corona quenching was first observed and proposed in the application of electrostatic precipitators. It is the suppression of the corona and influences the deposition of the dust due to the space-charge of the particles [17], which is simply

illustrated in Figure 4.20. Previous researchers [18] summarized that there are two main reasons causing corona quenching: (1) the slow mobility of those charged particles results in the deceleration of the ion movements; (2) the low mobility of charged particles decelerates the movement of ions [20]. The following studies also found that the corona quenching was closely related with the corona onset voltage which could cause the strong current deformation [19]. Meng et al. claimed that the non-uniform current density distribution and the higher corona current is in favor of avoiding the corona quenching [20,21]. In our modification, the charging performance was definitely enhanced by the multiple electric fields. Furthermore, since the alternative charging period is much shorter than the spraying duration, the non-uniform current density distribution is formed near the spray target so that the particle charging could be improved. As a result, the influence from the empty charging periods is compensated by the diagonal alternative charging, in this way the transfer efficiency has no significant reduction and even gets improved under the high gun voltage and rotating frequency conditions.

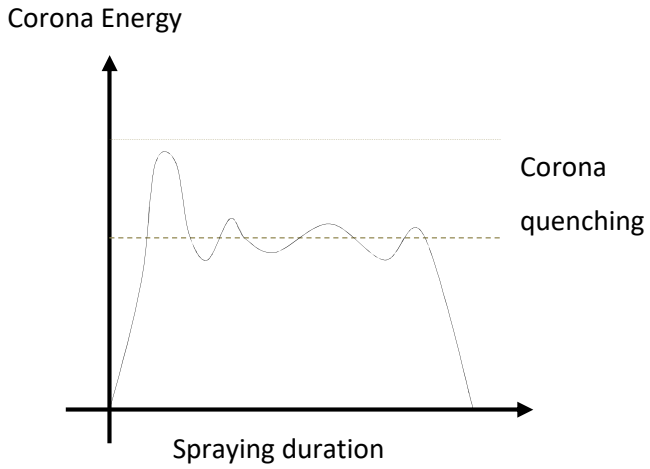

Figure 4.20 Illustration of corona quenching

The other reasonable explanation to the fact that the revised spray gun had much higher transfer efficiency than the original group is due to the reduction of the secondary charging. It was disclosed by Wu [22] that during the coating process, the charging may happen both on the flying powder and deposited powder. The primary charging always occurs near the corona electrode within 50mm of the gun tip due to the high electrostatic

field. While the secondary charging exists when the deposited powders accept additional charges, results from the converging of the electric field on the substrate surface and as a result terminating the further ions on the coating surface [22]. This accumulation of the charges on the coating layer could further generate the powder break down due to the bombardments of the current ions, causing the reduction of powder deposition during the continuous spraying [22,23]. The secondary charging phenomena always occurs with the existence of higher gun voltage. In utilizing the modified new spray gun with the alternating charging pattern, it is able to improve the transfer efficiency by reducing the duration of secondary charging.

After analyzing the above results, the most suitable operating conditions were the chosen as follows: The maximum length of additional electrodes which four electrodes tips had the same axial position as the center gun tip; The suggested alternating frequency is from 800 RPM to 1000RPM; The higher frequency setup was not tested due to the performance of 1000RPM has similar results within -60kV to -90kV during extending the four electrodes.

4.4.2 Investigating the influence of the C/N ratio

As mentioned above, the four electrodes can get charged in a certain sequence during the rotation of the main shaft. Furthermore, the charging period and empty period of each electrode could also be changed by adjusting the connection position of the extension wire on the brass patch. As a result, this alternating charging pattern with both charge and neutral periods influences the FCR and FPTE results. Adjusting the charge-to-neutral ratio (C/N ratio) of the alternator has been studied as well. As mentioned in Figure 4.21, the higher C/N ratio in the same rotating frequency indicates a longer charging period, otherwise a longer empty period. In this experiment, the four different C/N ratios were chosen and calculated according to the design drawing. Experiments of adjusting the C/N ratio were carried out under 1000RPM alternating frequency with L=0. All the results before adjusting the C/N ratio were conducted in the ratio of 2.36, with the maximum charging period. As indicated in Figure 4.21, when reducing the charging period, the average FCR was decreasing gradually, which indicated that the longer charging period is

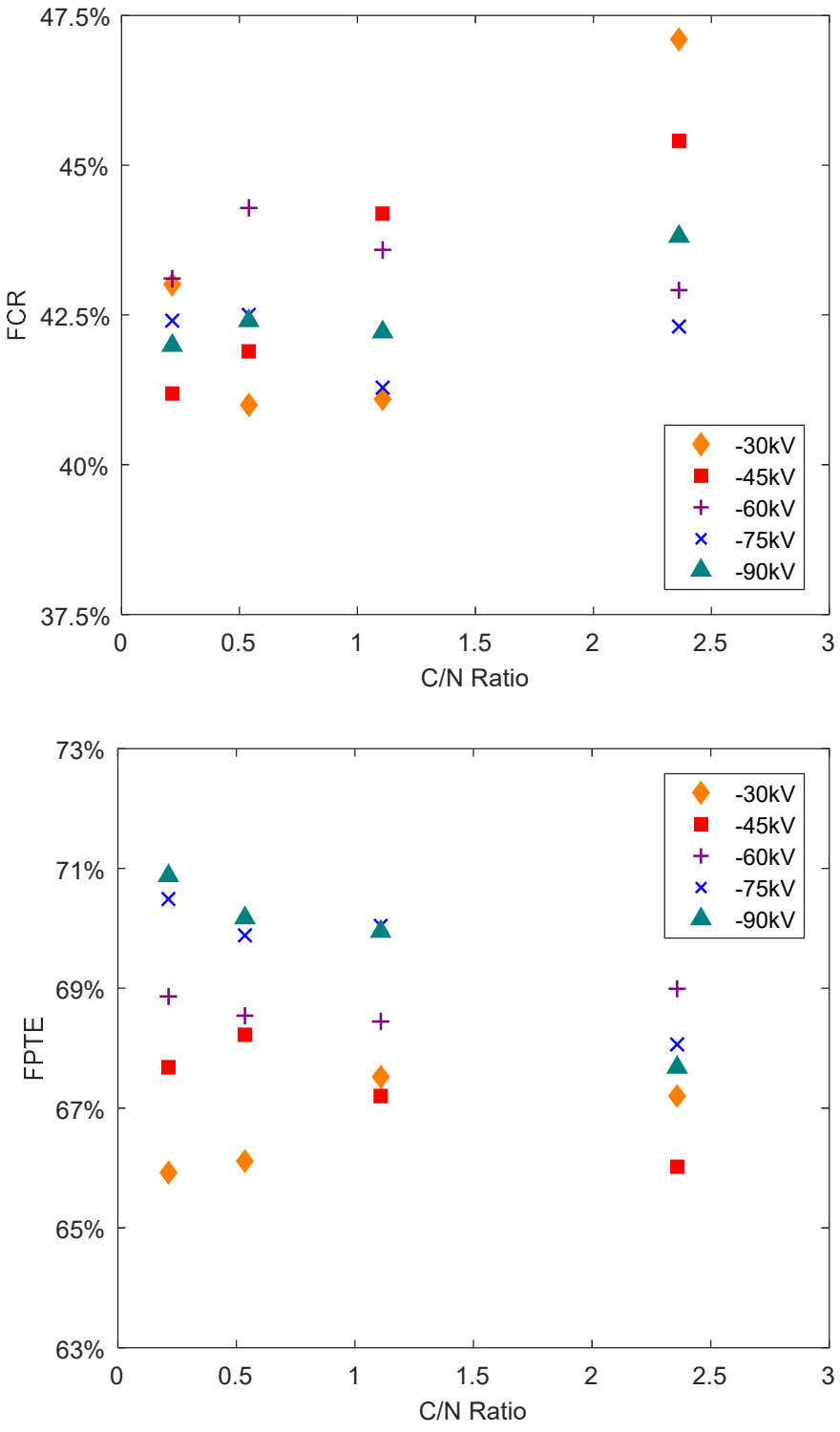

Figure 4.21 The FCR and FPTE for different C/N ratio in L=0, 1000RPM

helpful to overcome the Faraday Cage effect. Similarly, in the low gun voltages the higher FCR value could be obtained when changing the C/N ratio. On the other hand, the

transfer efficiency under every gun voltage is still above the control group (62%) compared with the previous experiment owing to it being supplied with highest alternative charging frequency. However, the transfer efficiency showed reduction when increasing the C/N ratio. This phenomenon could be explained by the fact that by longer period of charging time, the back ionization problem still exists and cause the difficulties in gaining stable results. The transfer efficiency has minor descending but not significant.

It is also necessary to compare the FCR value with the additional rotating voltage in each gun voltage setting with the control group. As illustrated in Figure 4.22, all the testing groups from the revised gun had the higher FCR than the control group. When adjusting the gun voltage to a higher range (-60kV~-90kV), the even higher FCR value was easier to be obtained. That's the reason that the commonly used operating voltage range is from

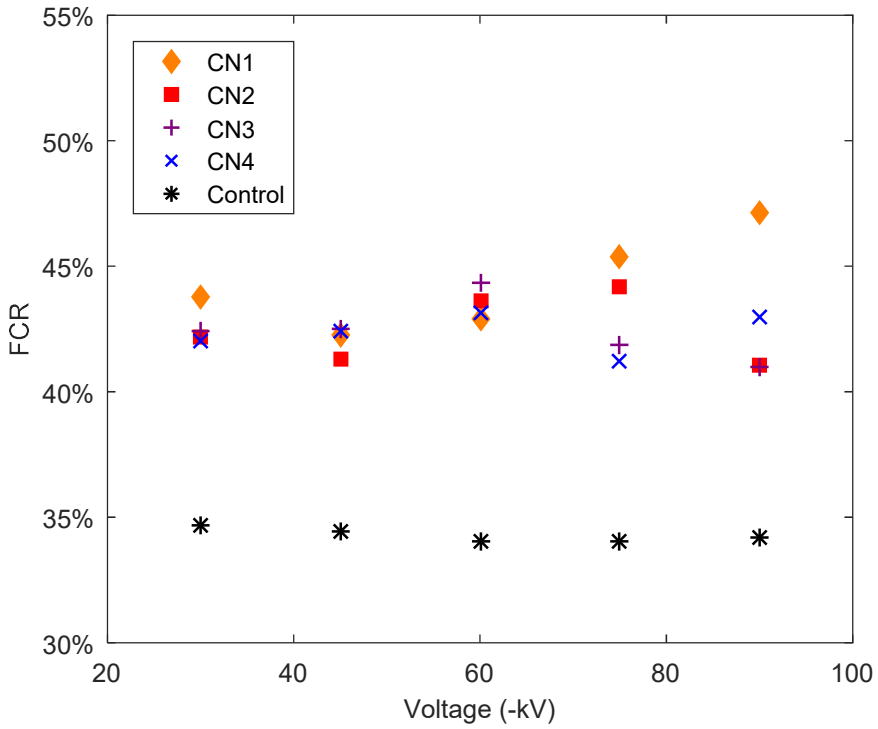

Figure 4.22 The effect of C/N ratio on Faraday Cage resistance in different voltage settings. (L=0, 1000RPM)

-60kV to -90kV other than lower voltage settings, though the voltage lower than -30kV had the minor changes with the changing of C/N ratio. In Figure 4.22, the highest C/N ratio is illustrated by "CN1", which performs better in achieving the better FCR, whereas

“CN4” stands for the shortest charge time, so that the average FCR in each voltage is relatively low. The best performance of the FCR was observed at -90kV by adjusting the additional rotating voltage to reach the maximum C/N ratio. In summary, the revised spray gun with additional voltage supply with C/N ratio larger than 1 is proven to be efficient in improving the Faraday Cage effect within the normal gun voltage operating range.

The researchers in our lab had also investigated some previous works related to the revised corona spray gun proposed in this study. The experiment was conducted by adjusting the C/N ratio in every rotating frequency with a certain gun voltage. As the result, with the higher C/N ratio of the additional voltage supply, the higher FCR value could be obtained, however there was a sacrifice with the minor reduction of the transfer efficiency. It is noted that all the testing groups all had the greater FCR and most of the higher FPTE values compared with the control group with no additional voltage supply [25].

The radial positions of electrodes were also adjusted in investigating the influence of the spraying performance. There are many attempts and arrangements that have been investigated to increase the charging performance of the particles emitted from the corona spray gun. One of the modifications related to our new revising idea was accomplished by Kleber [26] in 1993. He utilized a corona gun with single central point as well as several corona points arranged symmetrically surrounding the gun nozzle at the rim of the gun barrel. The current density patterns of the target were measured and the results showed that due to the mutual effect of the two electrodes, the mutual repelling of the ion clouds emitted from each electrode and creating a dead zone on the target, resulting in the decreasing of the powder deposition, as illustrated in Figure 4.23. A valid arrangement of the position of those multi-electrodes could help with reducing the dead zone. In addition, this kind of multi-electrode design was also beneficial to reduce the free ions if it had a proper electrode arrangement, demonstrated on the right part of Figure. Kleber also disclosed that adjusting the axial position of the additional electrodes have influence on FCR and FPTE. This evidence was also in accordance with the results discussed above: the FCR and transfer efficiency were the highest when the four electrode tips had the

shortest distance from the center corona point. Yanagida et al. proposed that the pin electrode could behaved as a free-ion trap due to the electrodes being maintained at a ground potential [27]. A large amount of the free ions having higher mobility spouted out

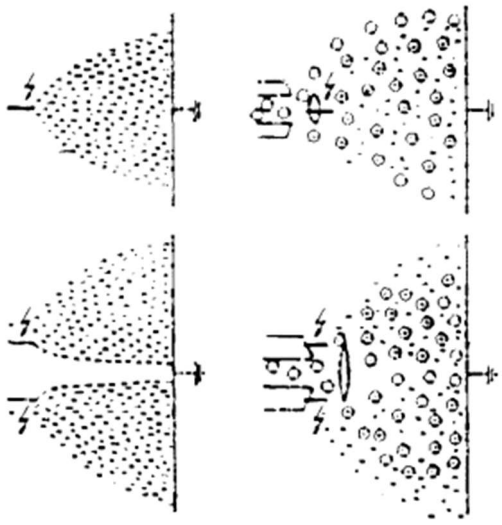

Figure 4.23 Current density pattern with one and two corona points [22]

from the nozzle are likely to get attracted by the gun body and the electrodes. The particles without gaining sufficient charge and having lower Q/M ratios are likely to continue to their path and finally attach on the target instead of turning back to the gun barrel and getting trapped. In this way the free electrons content is decreased in the charged powder clouds so as to avoid the further back ionization problems.

4.4.3 Investigating the radius position of additional electrodes

It is also necessary to investigate the influence brought by adjusting the radial positon of additional electrodes with the center tip. As shown in Figure 4.24, as the additional electrodes move away from the center tip, the charging of the particles became poorer, causing the low FCR and transfer efficiency. However, too small of distance brought a stronger Faraday Cage effect due to the influence of the electrostatic field interaction. The results showed a rather stable FPTE with the changing of the radial position, especially in a high gun voltage where the transfer efficiency could maintain around 69%.

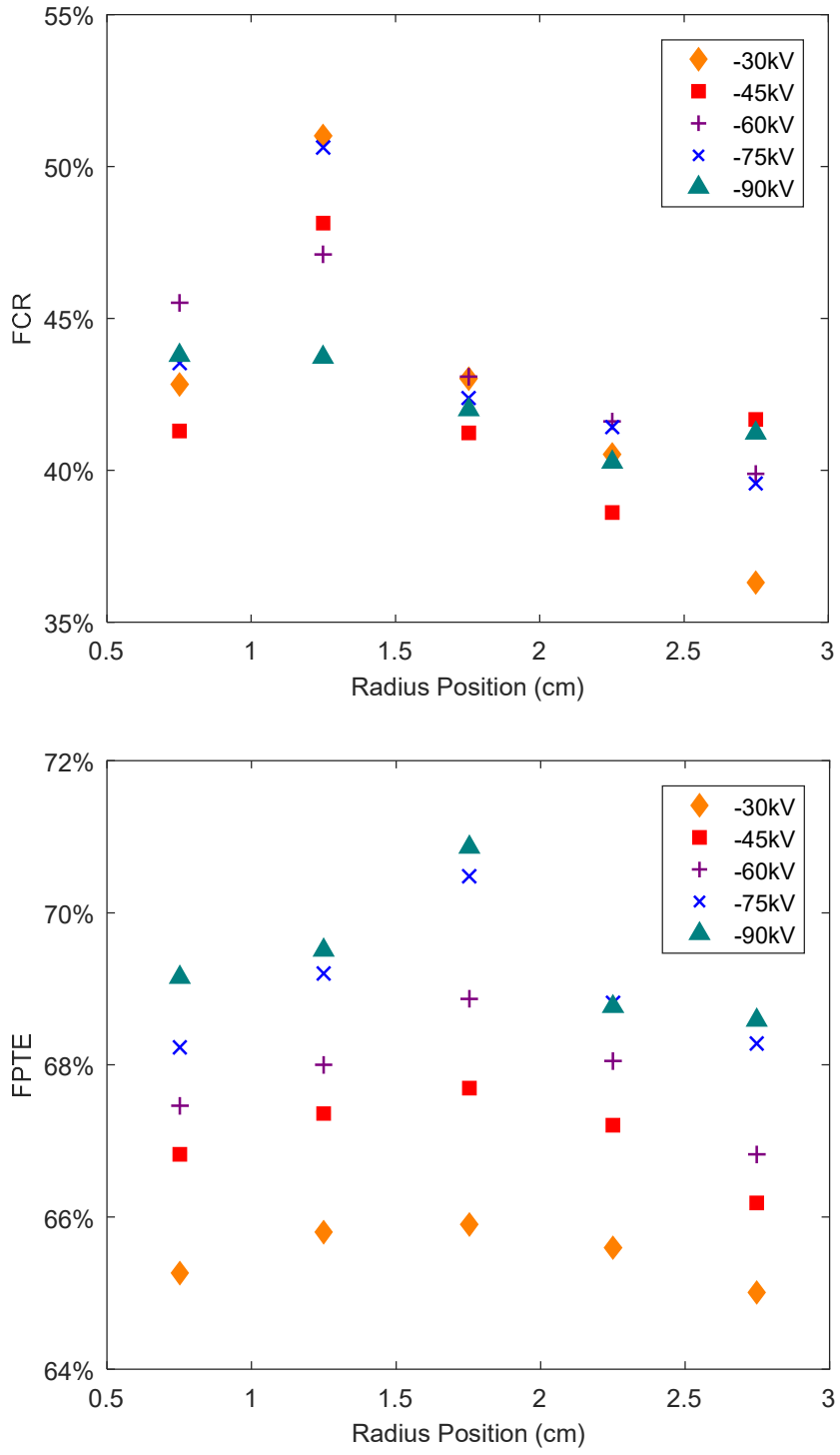

Figure 4.24 Effects of different electrode radial positions, L=0, 1000RPM

In summary, the above results obtained in varieties of operating conditions indicate that the FCR could be effectively improved by utilizing the new spray gun with the additional electrodes during the spraying. Meanwhile the FPTE also improves in most of cases,

although in some conditions it may scarify in a small range. In observing the final results visually in Figure 4.25, the difference of powder distributions is obvious especially on

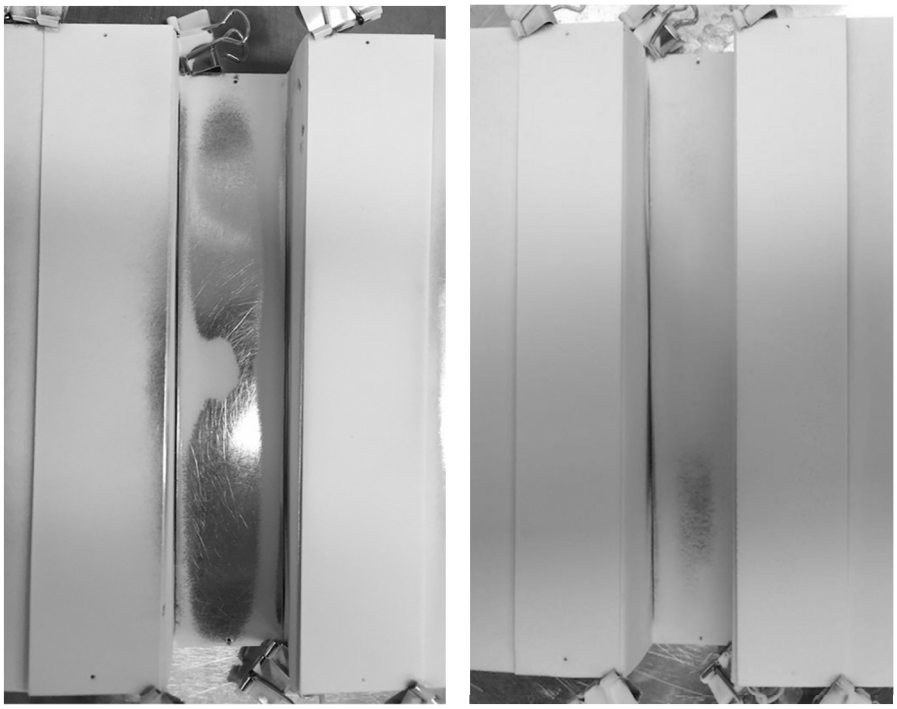

Powders on Panel C obtained using original gun

Powders on Panel C obtained using revised gun

Figure 4.25 The comparison between the original and revised spray gun in -90kV and 1000 RPM, C/N ratio 0.21, additional electrode radius position 1.25

panel C. The powder coverage of the original gun has two uncovered parts on panel C which could be clearly seen as the exposed aluminum color. In contrast, the recessed area had more sufficient powder deposit sprayed by the new spray gun, so that the visual result has strongly proved the effectiveness of the modified spray gun.

Based on the above analysis, the higher rotating frequency is the favorable condition for the alternator, which was decided as 1000 RPM. The most preferable electrodes length is having a same axial gun tip position as the center tip. In accordance with the industry requirement in spraying conductive spray target, the gun voltage is set between -75kV to -90 kV. To reach a more effective and stable operation, the revision of the spray gun and the alternator still needs to be modified to accommodate more research tests in the future work.

4.5 Conclusion

A novel technique in modifying the conventional corona spray gun by introducing the additional multi-electrodes near the tip has been tested. A series of experiments has been conducted and the proposed design was proven to be effective in improving FCR and FPTE under the ordinary operating conditions. The Faraday Cage resistance could be significantly enhanced by increasing the alternative rotating frequency especially under the lower gun voltages and higher charging-to-neutral ratio. Furthermore, the obtained transfer efficiency had significant improvement over the original gun and even got promoted when increasing the gun voltage supply. In addition, experiments in optimizing the electrode position have been conducted to decide the favorable radial and axial position of the additional electrodes tips. By narrowing down the axial tip distance, a stronger charging field formed so that the Faraday Cage effect could be overcome by extending the electrodes length. The optimum radial position of the electrodes is 1.25cm towards the center tip.

Reference

[1] Hughes, John Farrell. Electrostatic Particle Charging-Industrial & Health Care Applications: Ist. Research Studies Press, 1997.

[2] Knobbe, Alan J. "Powder spray guns." Metal Finishing 97.5 (1999): 254-257.

[3] Sims, R. A., et al. "Electrostatic effects on first pass transfer efficiency in the application of powder coatings." IEEE Transactions on Industry Applications 37.6 (2001): 1610-1617.

[4] Mayr, M. B., and S. A. Barringer. "Corona compared with triboelectric charging for electrostatic powder coating." Journal of food science 71.4 (2006): E171-E177.

[5] Kleber, W. "Electrostatic powder gun design." Journal of Electrostatics 30 (1993): 393-402.

[6] Krant M., Powder Characterization and Powder Application in Automotive Coatings, MESc. thesis of UWO. (2009): 8-27.

[7] Kleber, W., and B. Makin. "Triboelectric powder coating: a practical approach for industrial use." Particulate science and technology 16.1 (1998): 43-53.

[8] Hughes, John Farrell. Electrostatic Particle Charging-Industrial & Health Care Applications: Ist. Research Studies Press, 1997.

[9] Barmuta, Piotr, and Kazimierz Cywiński. "Electroseparation and efficiency of deposition during electrostatic powder coating." Journal of Electrostatics 51 (2001): 239-244.

[10] Trigwell, Steve, et al. "Effects of powder velocity and contact materials on tribocharging of polymer powders for powder coating applications."Particulate Science and Technology 26.2 (2008): 145-157.

[11] Kiefer, Steven L., Stephen Hart, and Ronald G. Creech. "Apparatus for electrostatic powder spray coating and resulting coated product." U.S. Patent No. 4,779,564. 25 Oct. 1988.

[12] Nagasaka, Hideo, et al. "Powder charging apparatus and electrostatic powder painting apparatus." U.S. Patent No. 4,805,069. 14 Feb. 1989.

[13] Clements, J. Sidney, and R. H. Bair. "Electrostatic powder coating of insulating surfaces using an alternating polarity internal corona gun." IEEE Transactions on Industry Applications 35.4 (1999): 743-752.

[14] Chen, H., et al. "Powder coating process parameters for a transfer efficiency model." Particulate science and technology 14.3 (1996): 239-254.

[15] Shah, U., et al. "Numerical investigation of coarse powder and air flow in an electrostatic powder coating process." Powder technology 164.1 (2006): 22-32.

[16] Kleber, W. "Electrostatic powder gun design." Journal of Electrostatics 30 (1993): 393-402.

[17] Awad, M., and G. Castle. "Corona quenching in electrostatic precipitators."IEEE Ind. Appl. Soc. Ann. Meet (1974): 945-954.

[18] Awad, M. B., and G. S. P. Castle. "The efficiency of electrostatic precipitators under conditions of corona quenching." Journal of the Air Pollution Control Association 25.2 (1975): 172-176.

[19] Meng, Xiangbo, Jingxu Jesse Zhu, and Hui Zhang. "The characteristics of current density distribution during corona charging processes of different particulates." Journal of Physics D: Applied Physics 41.17 (2008): 172007.

[20] Meng, Xiangbo, Hui Zhang, and Jingxu Jesse Zhu. "The characteristics of particle charging and deposition during powder coating processes with coarse powder." Journal of Physics D: Applied Physics 41.19 (2008): 195207.

[21] Meng, Xiangbo, Hui Zhang, and Jingxu Jesse Zhu. "Characterization of particle size evolution of the deposited layer during electrostatic powder coating processes." Powder Technology 195.3 (2009): 264-270.

[22] Wu, Souheng. "Electrostatic charging and deposition of powder coatings."Polymer-Plastics Technology and Engineering 7.2 (1976): 119-220.

[23] Riebel, Ulrich, Ralf Radtke, and Reinhard Loos. "An experimental investigation on corona quenching." Journal of electrostatics 54.2 (2002): 159-165.

[24] Meng, Xiangbo, Jingxu Jesse Zhu, and Hui Zhang. "The characteristics of particle charging and deposition during powder coating processes with ultrafine powder." Journal of Physics D: Applied Physics 42.6 (2009): 065201.

[25] D. Bao., Anti-Faraday Cage Spray Gun. Report of Particle Technology Research Center of UWO. (2015): 14-19.

[26] Kleber, W. "Electrostatic powder gun design." Journal of Electrostatics 30 (1993): 393-402.

[27] Yanagida, Kenzo, Mitsuyoshi Kumata, and Masashiro Yamamoto. "Application equipment for high quality appearance powder coatings, especially for automotive clear topcoats." JCT, Journal of coatings technology 68.859 (1996).

5 Chapter 5: Cold bonding technique for processing metallic powder coatings

5.1 Introduction

Powder coating is a dry coating technology involving powder material processing. It was introduced in the early 1950s in the United States and fast developed in the metal finishing industries [1]. During the past few decades, powder coating has been gaining popularity steadily and is considered one of the most innovative surface techniques. It is widely used today due to its characteristic of environmentally friendliness [2]. Compared with conventional liquid coating technology, powder coating has obvious advantages that it does not incur any volatile organic compounds (VOCs) emission, as well as its recyclability of over-sprayed materials [3].

The coating finish strongly relies on the powder particle size. Fine and ultrafine powders, with median particle size between 10 μm and 30 μm have been successfully used in many industries and has a remarkable performance in forming a very uniform layer of paint. However, there are not a lot of decorative coating products in the powder coating industry and they have only been used on limited products in the lower end market.

In order to provide a much better aesthetic appearance of powder coatings, some powder manufacturers started to offer new technique of adding metallic color powder to products. In this way, the final coatings get the extra shine and deepness to the color by introducing metallic effect. Processing metallic powders has great difficulties. The cost of the metallic color powders is much higher than commonly used powder coating materials, and also, the manufacturing process is much more complex. Several patents have mentioned some technique related to metallic pigment in powder coating processing. At the beginning, metallic effect coating was realized by spraying multi-layers on the substrate. Researches applied the first base layer with metallic pigments onto the target, then covered it with clear top coating [4-6]. However, it needed preheating of the coated substrate to enhance the cross-linking reaction. Also the time interval of applying the

secondary layer should be controlled based on the curing condition of the base layer. Furthermore, the ratio of powder coating resin to curing agent is strict. Other researchers also devoted in processing metallic pigments with powder coatings. Reisser et al. proposed a synthetic method to produce a resin-coated aluminum pigment. The production of a silicon-organic coating on the aluminum pigment surface was first performed, and then the coating reacted with other compound to form a cross-linked synthetic resin coating [7]. However, this production method was too complex, involving many synthesis steps. Nowadays, the processing technique of metallic pigments with powder coating is mainly utilizing the thermal blending method. Generally speaking, the thermal blending is needed during the process of mixing powder coating with metallic powder coating, where the temperature of the blending is critical in ensuring that the powder coatings are not cured.

In the application process, electrostatic spraying is used in this study. Free electrons generated by a corona charged gun are attached to the particles by collision during spray [8]. Normally the metallic pigments are easy to stay on the panel because of the electrostatic force, whereas the powder coatings are less likely to stay on the panel and can go directly to recycle. Because of the distinctions in shape, size and surface conductivity, the two materials are prone to separate and to have different transfer efficiencies, resulting in the different contents of metallic powder concentration in the recycled powder compared with the original coating. The objective of this research was to improve the bonding between the metallic pigments and the powder coatings, so as to unify the charging performance during the spraying.

In this chapter, a new method in utilizing liquid bonding solution to glue the metallic powder and powder coating is introduced, so as to achieve a better bonding during spraying. This can lead to a more uniform pigment concentration in the reclaimed powder.

5.2 Materials and method

The initial blending method started with mixing the metallic pigments with liquid bonder. At the beginning of this research, the liquid bonder and metallic pigment are mixed in a

high shear blender so that the metallic powder could be well dispersed and encapsulated by the dilute liquid bonder. Before the solvent in the liquid bonder evaporated, the powder coating was added into the mixture. In this way, the powder coating could adhere to the wet metallic pigments. The final product needed an additional drying procedure. In this study, two widely used metallic effect pigments, aluminum flakes (Al) (manufactured by Silberline Manufacturing Co., Inc., USA) and mica flakes (manufactured by Langfabo Manufacturing Co., Inc., China). 10% (by mass) solutions of polyacrylate (PA) and polyvinyl alcohol (PVA, IF14000) were both tested as the liquid bonder.

5.2.1 Mica bonding test

In industry the metallic pigment concentration is normally between 1%~3% to achieve the appearance. Overwhelming dosage of additives other than powder coating may cause surface defects. However, in order to observe and detect the bonding condition between metallic pigments with powder coating, a high concentration of metallic pigments was used in this study. Mica pigments (D_{50}=18 μm) were chosen as metallic powder and the powder coating (manufactured by Langfabo Manufacturing Co., Inc., China) has the

Figure 5.1 High shear blender

median size of 27 μm. First of all, the mica flakes were mixed with the powder coating together in a high shear blender, as shown in Figure 5.1. The ratios are m(mica):m

(powder coating) = 0.2: 1. m(PA):m(mica)=0.06:1, m (D.I. water):m(mica)=0.2:1 [9]. Water was used as solvent for diluting the PA solution and also helped disperse the materials better. Then the samples were air dried for 2 hours until completely dry.

One direct approach of examining the bonding results is by scanning electron microscope (SEM) which could provide a visual analysis of the bonding results. As shown in Figure 5.2, mica flakes stacked severely to each other (B). The powder coatings agglomerated due to the existence of liquid bonder. Although a few well-bonded mica flakes (A) with powder coating could be observed the bonding was still not satisfactory.

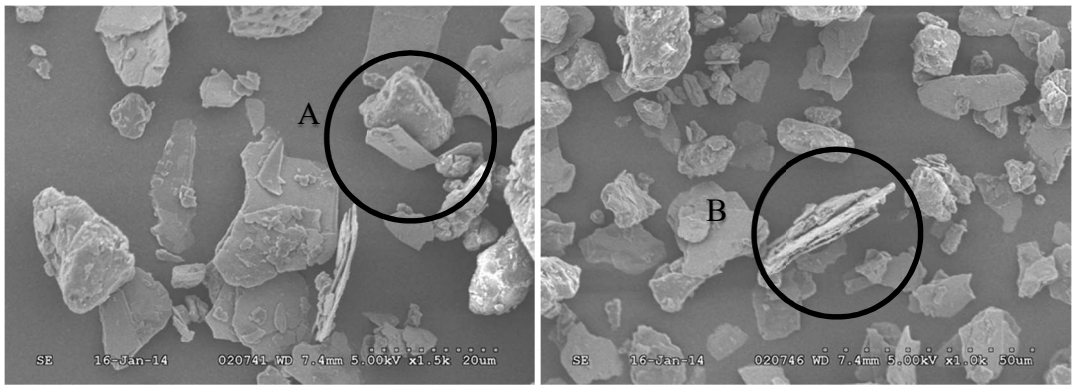

Figure 5.2 Mica bonding with orange powder coating under SEM

Spacer additives

In order to solve the serious stacking problem, a new material with smaller particle size (less than 5 μm) was introduced in this research, working as a "spacer". It could be any material with the stable physical and chemical properties and does not react with other materials used during the process. The main purpose to add this smaller size material was to separate the stacking mica flakes. If the sample is well blended, the space between two neighboring mica is enlarged by the existence of the spacer. As a consequence, the stacked mica flakes would be split during the further blending process with the help of the sheer force.

The appropriate spacer size is around 3-5μm. It is easy to find this kind of size distribution from the recycled powder from the Corona charge spraying bag house.

During the spraying, because of the electrostatic force, part of the powder with the smaller size could not stay on the panel so that it has been directly recycled and stored in the bag house, which couldn't be reused any more. The tested reclaimed bag house powder is polyurethane (PU). The bag house powder (BHP) and mica flakes were blended in the proportion of m(mica):m(BHP) =1:1 in the high shear blender, then the powder coating was added to the mixture then blended a second time. Figure 5.3 shows the result of accomplished bonding sample. The smaller particles with sizes around 5 μm are the bag house powder. However, they are easily agglomerated to form a cluster due to Van der Waals force (B_1). By examining the SEM results, the stacking problem was partly solved by introducing the bag house powder, but this method was still not very effective because it could not separate those completely overlapped flakes (B_2). Meanwhile, the bag house also had a risk to be surrounded by PA solution and then became strongly agglomerated to larger clusters, leading to a new side effect during the blending.

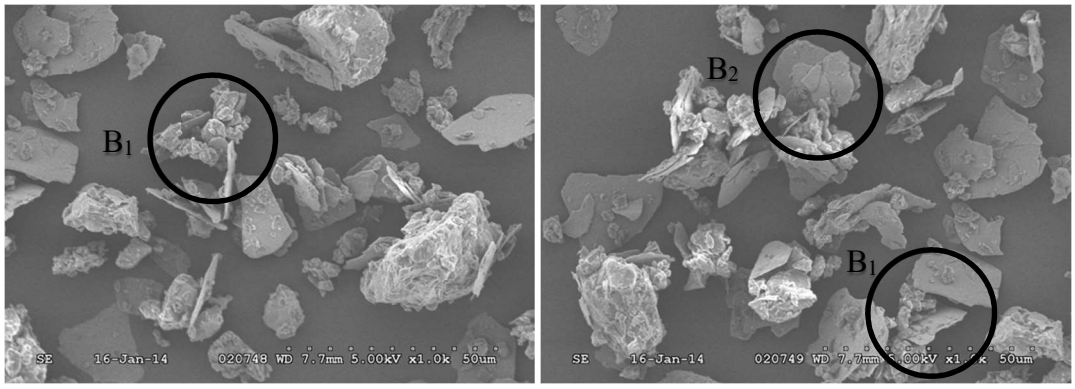

Figure 5.3 SEM images of powder bonding sample with bag house powder

The reclaimed bag house powder has its own drawbacks such as agglomeration and it was not small enough to go into the space between two tightly stacked mica flakes. In this case, an even smaller size material such as nanoparticles, could substitute the bag house powder. The nanoparticles (R287, manufactured by Evonik AG, Germany) was blended at the same dosage as bag house powder with mica flakes into the high shear blender.

The final product with nanoparticles is illustrated in Figure 5.4, showing the dry blend of mica and nanoparticles only. It is obvious that the nanoparticles are highly likely to adhere onto the mica flakes so as to increase the roughness and prevent stacking. However, in Figure 5.4 (b), due to the existence of liquid bonder, nanoparticles were not effective in solving the stacking problem where several mica flakes strongly adhered to each other, even though the nanoparticles were attached onto the mica flakes. Although a large amount of these are attaching onto the mica surface, it still could not prevent stacking mainly due to the relatively small size of nanoparticles.

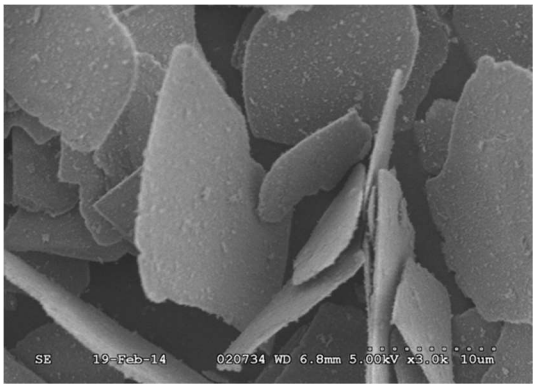

(a) Mica and Nanoparticles

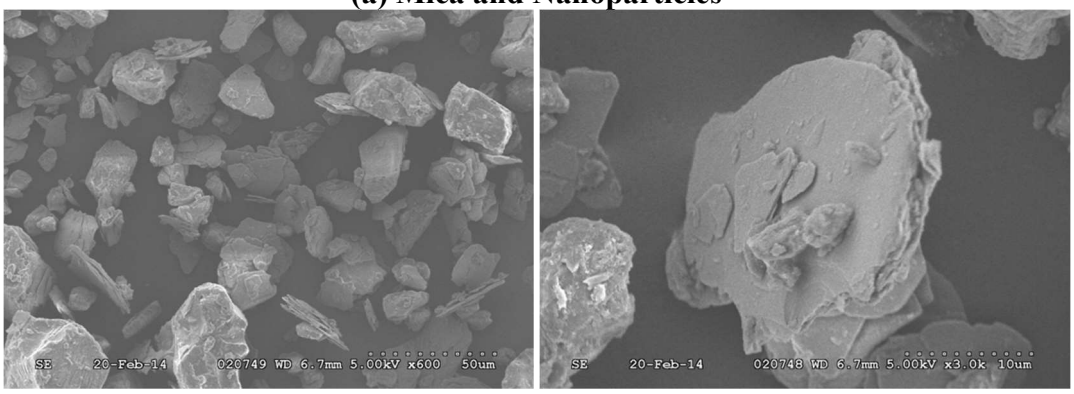

(b) SEM of mica bonding with R972 nanoparticles

Figure 5.4 Images of mica sample bonding with nanoparticles under SEM observation

Another two possible new substances could be chosen as the spacer in this experiment, namely alumina (aluminium oxide, Al_2O_3) and aluminosilicate (zeolite, manufactured by PQ Corporation, USA). The particle sizes are both 2-5 μm and relatively inert in terms of chemical properties. Furthermore, the Al_2O_3 could bring more gloss than nanoparticles

and bag house powder to the final panel. The SEM of Al_2O_3 and zeolite are shown in Figure 5.5.

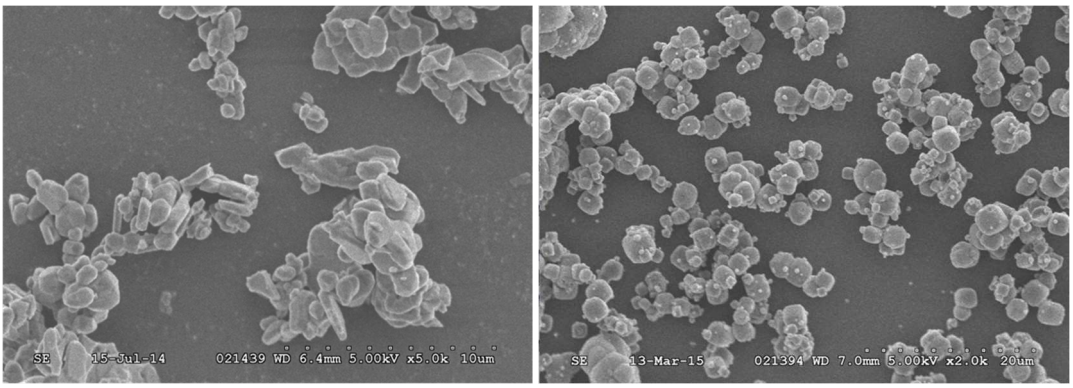

(a) Al_2O_3 **(b) zeolite**

Figure 5.5 Images of Al2O3 and zeolite under SEM

The above two figures demonstrated that compared with Al_2O_3, zeolite has relatively regular shape and a uniform size distribution. Some Al_2O_3 particle sizes are larger than 15 μm, and they would not help in solving the stacking problem. Additionally, because of the porous structure, zeolite has a larger specific surface area than the same amount of Al_2O_3. It could carry more liquid bonder, and have more opportunity in connecting mica and powder coatings.

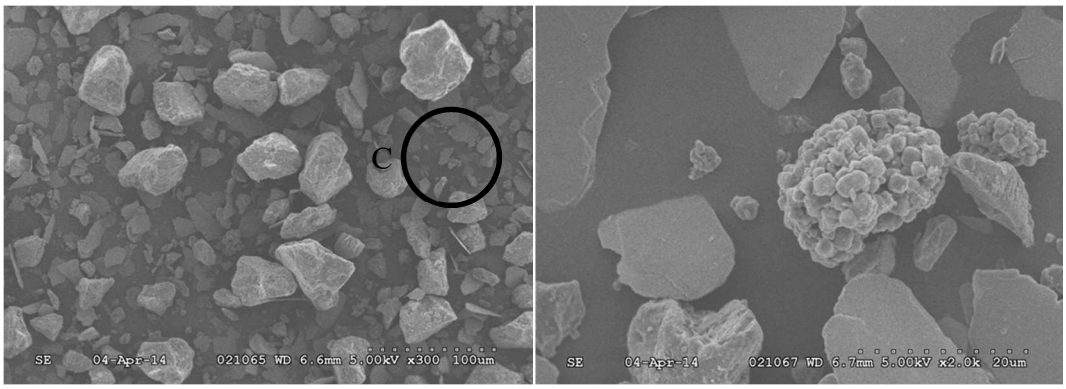

Figure 5.6 SEM image of bonding samples with zeolite

The experiment involving zeolite conducted with the same blending ratio with powder coating and followed the same operating conditions. As the result shown in Figure 5.6, the unbounded flakes are scattered without stacking to each other (C). This demonstrated that during the blending, zeolite did have the function of preventing the stacking of mica.

However, there were quiet large amounts of particle agglomerations observed under smaller magnification. Those were the zeolite aggregates under SEM. In this case, a stronger blending method should be invented to solve the existing problem of mica flakes and the agglomerates of the zeolites.

5.2.2 Modification mechanism

The current blend machine has short and blunt blades. It is easy to predict that by modifying the blade the powder sample could get a better dispersion, so as to solve the mica and zeolite stacking problems. The original flat blade has a flat surface, which provides a weak shear force to the sample powders. An extra blade is added onto the current blade with a sharp terminal made of aluminum plate, as shown in Figure 5.7. It is easy to modify the shape and the weight is light enough not to toss out because of the

Figure 5.7 Modified high shear blender with sharp blade

centrifugal force during the high speed blending. Also the terminal should not get too long to touch the edge of the blender.

It was assumed that the powder sample processed by this new blender is well mixing and has limited numbers of stacking. However, the bonding of powder coatings with mica could not be realized in this new machine as the modified blade was aiming at splitting particles. The extra blender was named bonding machine, inspired by the blade modification of the high shear blender, which was introduced into the experiment, as shown in Figure 5.8. Bonding machine was using the same base as the high shear blender. The only change was that the blade had an extra flat space. The sharp blade could provide

a higher rotation and shear force in breaking those agglomerations. For the same reason, the bonding machine also needs to offer a force for gathering the particles together. To reach this goal, a flat impact surface, which has the same length as the original blade, was added onto the base blades, but in a vertical way. When the blades started rotating at a high speed, the new blade could drive the particle mixture in a certain direction, where the powder samples would collide with each other to realize bonding mainly between powder coatings and mica flakes.

Figure 5.8 Bonding machine

The mixing process could be done by utilizing the above two blending machines. However, the pretreatment of the materials before putting them into blending machine was crucial. Our new bonding process started with wetting the zeolite and PA solutions in a mixing tube with a rubber scraper in it. The function of the rubber scraper was to mix and stir the materials better, as shown in Figure 5.9. Zeolite, water and PA solution were blended in a mixing tube for 1 min, and then the wet zeolite was put into a new high shear blender with the mica flakes for 40 s. This procedure makes the encapsulated zeolite touch the mica flakes evenly. The entire sample was taken out of the new blender, then poured into the bonding machine with the powder coating in it. Now the micas were combined with powder coating. The PA has the function in gluing powders when it is not dry.

Figure 5.9 Mixing tube and stand mixer

Figure 5.10 shows the SEM of the final powder sample obtained from the bonding machine. Well bonded mica flakes with powder coatings could be observed under the SEM (A). The new high shear blender separated the materials completely so there was large amounts of unbound flakes (C). This is due to several reasons: some of the mica flakes did not even get wet by the PA; those micas with PA may get dry quickly during the high shear process so that it could not glue any other particles any more. Those well-bonded parts were split again because of the collision in the bonding machine. It was more likely because of the first reason due to the fact that the PA solution was firstly

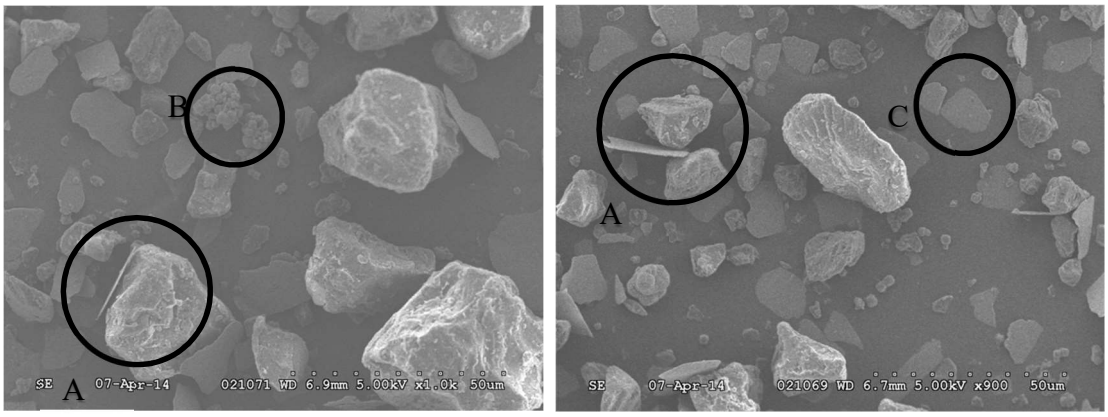

Figure 5.10 The SEM of the final powder sample

absorbed by zeolites, and then mixed with large amount of dry mica flakes. So that only a small amount of PA could touch the mica flakes, not to mention to encapsulate them. That was also why some zeolite agglomerations could be observed (B).

To further prevent the mica stacking and zeolite agglomerations, the first step of material mixing procedures should be improved. On one hand, it is important to make sure that PA solution can soak into the spacer thoroughly. On the other hand, it is also essential not to let the PA glue them too much before proceeding to the next bonding step. The mixing tube performed well in mixing PA solutions with particles. However, the high shear blender could not separate those sticky zeolites according to the SEM results. Therefore, a stronger splitting system was needed to solve this problem.

A jet mill machine is a widely used particle grinding and classification equipment. Size reduction happens in the designed chamber due to the particle collisions between particles. The particles are fed from a vibratory feeder, right upon the injection nozzle which provides the high gas velocity and drives the particles to the chamber. Due to the Venturi effect, the powder passes through the thin nozzle at a high velocity. As a result,

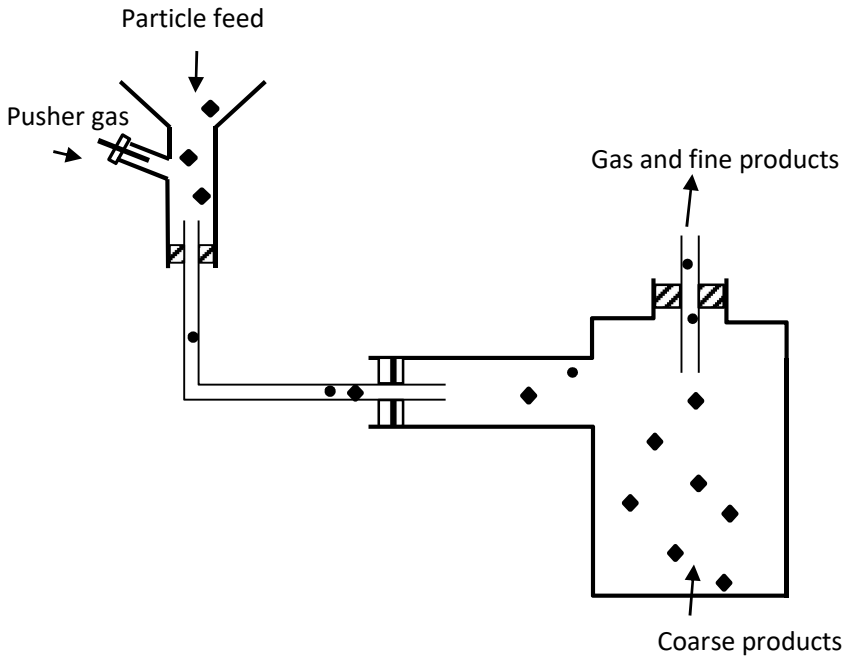

Figure 5.11 Jet-mixing system

the clusters of zeolites or other agglomerations can be segregated. In this research, only the jet mill nozzle was used to separate the powder samples, and no additional jet mill

chamber was used. A rubber tube connected the recycle system and the powder sample was collected by a cyclone-like bin where most of the particles were gathered into it. This approach revised from jet mill machine was named jet-mixing system, as shown in Figure 5.11. The injection pressure was set at 15 psi after some trial and error experiments. Otherwise higher pressure blew those bonding parts apart and accelerated the PA solution drying, while lower pressure was not strong enough to split the stacking part.

The final sample accomplished by jet-mixing system observed by SEM is shown in Figure 2.12. Some obvious bonding of one or more mica flakes attached with one or two powder coatings took place in this sample (A). However, the non-bonded flakes existed, which meant that the bonding between mica flakes and the powder coating was not strong

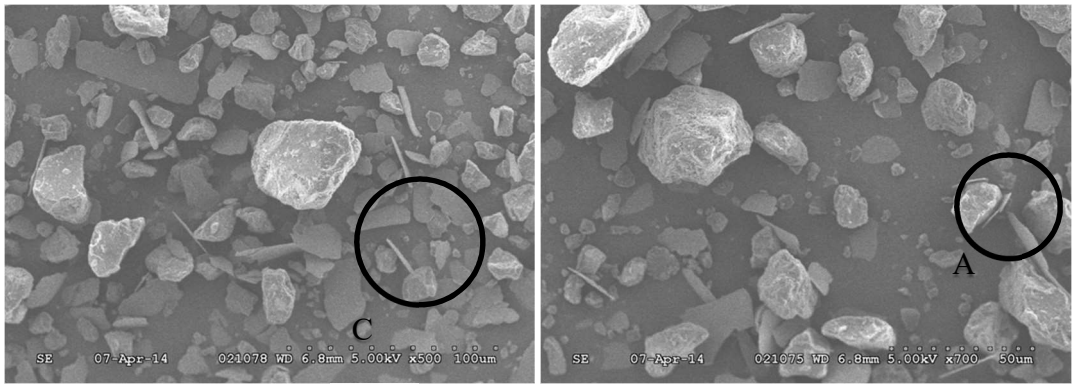

Figure 5.12 SEM of the Jet-mixing sample

enough (C). This problem could be solved by adding more liquid bonder, or switching to a more powerful liquid bonder. In this case, the solution did not get dried easily when passing through the jet mill nozzle.

The other liquid bonder was polyvinyl alcohol (PVA, IF14000 WP21649) which could provide a stronger conjunction between two particles. In addition, adding borax could improve the stickiness significantly (Patent, CN1098430A). To find the appropriate ratio of adding borax, several solutions having different ratios of borax and PVA are listed in Table 5.1.

Table 5.1 Formulas of borax and PVA solution

Borax solution (5%) (%)	0.5	0.8	1.1	1.4	1.7
PVA solution (10%) (%)	10	10	10	10	10
D.I. water (%)	89.5	89.2	88.9	88.6	88.3
Borax/PVA (%)	2.5	4	***5.5***	7	8.5

The experimental results of the bonding test utilizing the jet-mixing system turned out that when borax/PVA=5.5%, the best bonding effect could be reached. Lower ratio of borax/PVA may not provide a stronger adhesion between metallic pigments and powder coating while excessive borax turns the PVA solvent to slime, which could not be diluted or dispersed in the following blending process. Nevertheless, the jet-mixing method could not achieve a steady and satisfactory bonding according to observation under SEM. The non-bonded mica flakes still dominated among all the bonding conditions, and this could not be easily solved by modifying the mechanical parts. Therefore, more liquid bonder had to be used in mixing the mica and zeolites before feeding into the jet-mixing system.

Previously, m(PVA+B):m(mica)=0.06:1. In the following experiment, the amount of PVA and borax solution was increased gradually and the same m(mica):m(zeolite) =1: 0.3 was maintained, then the mixtures went through the jet mixing system. The bonding effect was also examined under SEM. After a series of experiments, m(mica):m(PVA+B) =1:0.42 was chosen as the proper mixing ratio to achieve the best bonded conditions.

5.2.3 Bonding involving jet mixing process

In summarizing the above works, two main approaches have been evaluated to achieve the final bonding, i.e., the bonding machine (renovated from high shear blender) and modified jet mixing system. In further comparison experiments, aluminum flakes (Al) (manufactured by Silberline Manufacturing Co., Inc., USA) were used instead of mica as mica can absorb excessive liquid bonder and solvent. The liquid bonder was chosen as polyvinyl alcohol (PVA) with borax solution, denoted as PVA+B solution.

The key purpose of mixing the metallic pigment with powder coating is to prevent the Al flakes from stacking when contacting the liquid bonder. The jet mixing nozzle offers a

high gas velocity to make sure that the powder goes through and the stacking materials are split the due to the Venturi effect. Then the dispersed materials would recombine and bond to each other due to the cyclone vortex during the collecting.

In order to compare which approach could provide a better bonding, a few experiments have been conducted. All the experiments used the same material formula: m(Al)=1 g, m(zeolite)=0.3 g, m(PVA+B) =1.26g, water=0.162 g, m (clear coat) =15 g. Jet mixing injection pressure P_{in}=15 psi. The first sample was made by mixing the Al pigments with PVA+B solution in the mixing tube, and then dry blended with the epoxy clear coat (dp_{50}=27.13 μm) utilizing the original blender. The collected powder is denoted as control sample. Compared to the control group, the second sample was achieved by the modified high shear blending and bonding machine, named as bonding machine sample. The third group was using the same amount of materials in the mixing tube, but mixed by the jet mixing system, named as jet-mixing sample.

The effectiveness of the above two bonding methods was further examined by a spraying test and ash test. The visual effect of the above two improved samples were sprayed by a corona spray gun (Gema, Switzerland). The process of ash test followed the ASTM D5630-06 [10] from which the exact Al pigment content of the sprayed powder could be obtained and compared to the original Al ratio. In the ash test, final powder samples were burned in crucible at 530 °C in a furnace. This temperature is lower than the boiling point of Al but much higher than the clear coat. In this way, the residues in the crucible would be oxides of Al and zeolite since the clear coat had already burnt off after 2 hours. A term c_{solid} is introduced as the equation:

$$c_{solid} = \frac{W_{residual}}{W_{powder}} \qquad \text{Eq.5.1}$$

where c_{solid} represents the weight percentage of the residuals in the crucible after ash test, which contains Al flakes, zeolite and ash content of the clear coat. $W_{residuals}$ represents the weight of the residual. W_{powder} is the amount of powder sample put into the crucible before the ash test.

In addition, another approach of examining the actual bonding is scanning electron microscope (SEM). The metallic effect of the sprayed panels was under visual examination by the naked eye, since the instruments in measuring the surface gloss is strongly affected by the existence of metallic pigments. The black polyester powder coating (Prism, Model PB-0191-H) with high gloss was used in measuring the metallic effect as well as the coating quality.

5.3 Experiments and evaluations

5.3.1 Ash test examination

The powder samples obtained from the two improved bonding method have to be completely dried. The content of metallic powder in each sample was examined by ash test. There were 6 crucibles prepared for ash test where three of them represents the pre-sprayed sample powders. The other three crucibles contained the powder made from the bonding method, and then sprayed and scraped from the panel without curing process, known as post-sprayed powder. The purpose of dividing one sample into 3 groups was to ensure the accuracy and consistency. In other words, each group consisted of 1 pre-sprayed powder and one post-sprayed powder. Each sample was burnt for 2 hours, then cooled for 2 hours due to the fact that zeolite would absorb the moistures from the air and cause the weight change. The ash test results are shown in Table 5.2. It could be concluded that jet-mixing method performed better in bonding Al flakes with powder coating, indicated by the small solid concentration variation between pre-sprayed and post-sprayed solid concentration. In other words, most of the Al flakes were glued by

Table 5.2 Ash test of control sample and bonded sample

(a) Control sample

Solid % \ Group #	1	2	3
Pre-sprayed C_{Solid}	8.01%	7.95%	8.12%
Post-sprayed C_{Solid}	14.87%	14.94%	15.29%

(b) Bonding machine sample

Solid % \ Group #	1	2	3
Pre-sprayed C_{Solid}	7.54%	7.52%	7.56%
Post-sprayed C_{Solid}	14.00%	13.94%	13.76%

(c) Jet-mixing sample

Solid % \ Group #	1	2	3
Pre-sprayed C_{Solid}	8.64%	8.50%	8.56%
Post-sprayed C_{Solid}	10.25%	10.30%	10.89%

liquid bonder with one or two powder coating particles. As a result, the solid content of the sprayed powder sample on the panel could maintain the same as the recycled powder sample. The sample obtained by jet-mixing method was better than utilizing bonding machine.

Further comparison between the bonding machine sample and jet-mixing sample was performed by SEM images. As shown in Figure 5.13, the jet-mixing sample shows better

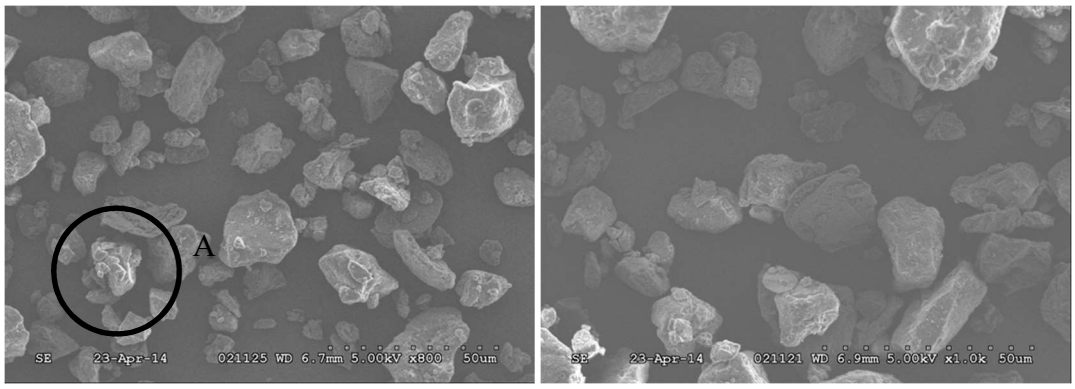

(a) Control sample

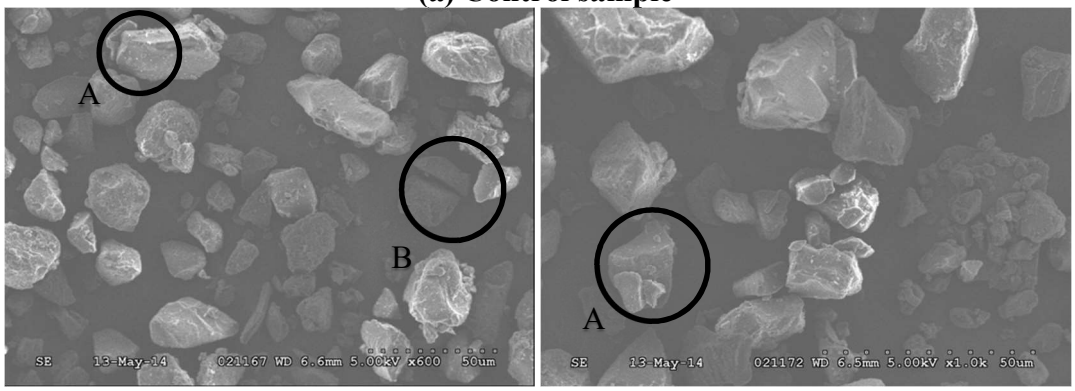

(b) Bonded sample

Figure 5.13 SEM observation of the control sample and bonded sample

bonded conditions than in bonding machine sample, demonstrating by most of the Al flakes are adhered by one or more powder coatings (A). However, some non-bonded

flakes are still commonly seen in jet-mixing sample (B). In this case, future improvement on jet-mixing system should be conducted to achieve better bonding.

Due to the fact that zeolite has relatively small size, it plays an essential role in dividing the neighboring Al flakes so as to prevent them from stacking to each other. However, at the same time, it also brought lots of drawback such as absorbing the water from added PVA and borax solution due to its porous structure and large specific surface area. It was difficult to get the sample completely dry after collecting the products, as may lead to the extra cost during the production. Also the existence of zeolite in the final sprayed panel could absorb the moistures and oil from surrounding environment. To test the zeolite absorbing phenomenon quantitatively, the ash test was carried out containing only PVA+B solution and zeolite. The weight change was measured from taking out from the furnace and till it reached weight equilibrium at room temperature. Experimental results indicated that it took 130 min for the zeolite to finish weight gain during the cooling period. This is the main reason why all the collected samples had to cool and dry for at least 2 hours at room temperature (21 °C) and humidity (35%).

However, the result of c_{solid} in post-sprayed powder was slightly higher than the original blending solid ratio. There could be several reasons: after burning, Al became Al_2O_3, which weighs more than Al; clear coat may contain ash content; the weight of zeolite and PVA +B solution changed after burning. Considering the above influences, a series of experiments were conducted for evaluating the possible effect from all the materials. First of all, in order to test the ash content of the clear coat, the ash test containing clear coat only has been tested; burnt at 530°C in a furnace for 2 hours, cooling for 2 hours and the result is shown in Table 5.3. Results indicated that the amount of ash content was negligible, so the epoxy clear coat had no side effects on the ash test process.

Table 5.3 SEM observation of the control sample and bonded sample

Clear coat ash test #	1	2	3
C_{solid}	0.03%	0.05%	0.08%

Secondly, the effect of Al flakes during the ash test was also studied. In the limited space of the crucible, Al flakes were stacking tightly so that part of the them may not get

oxidized thoroughly during the entire burning process. The different oxidized proportion would bring the Al_2O_3 weight difference. So the amount of Al accumulated in the crucible may affect the results. In this case, the ash test with different amount of Al has been carried out according to the ash test standard. No.1 to 3 crucible had 50 mg Al flakes while No. 4 to 6 with an amount of 120 mg, and No. 7-9 had Al around 230 mg. The average weight gain brought by Al_2O_3 is

$$W_{gain} = \mu_{Al_2O_3\%} - 1 \qquad \text{Eq. 5.2}$$

where $\mu_{Al_2O_3\%}$ is the average weight of the above mentioned Al_2O_3 after the test. Table 5.4 indicated the weight gain of Al with different sample sizes. The result showed that Al amount had negligible influence on the W_{gain} during the ash test process.

Table 5.4 W_{gain} in different Al amount

Al amount (mg)	50	120	233
W_{gain}	4.66%	4.34%	4.38%

The product collected from jet-mixing system was well blended, and the Al flakes was well dispersed into every part. When taking the ash test, Al flakes of this well-bonded sample had more opportunity in getting oxidized as the surrounding clear coat would be burnt off immediately. The exothermic reaction of the combustion of the clear coat may generate the extra heat helping Al oxidation. The Al flakes and clear coat were well mixed with PVA+B solution at the same ratio, and then went through the ash test. The result after drying shows in Table 5.5. It demonstrates that the Al dispersed in the clear coat did not change the oxidizing rate compared with burning only.

Table 5.5 Ash test of Al and powder coating only

Al with Clear coat #	1	2	3
W_{gain}	4.15%	5.12%	3.05%

Zeolite has a crucial role in bonding metallic pigments with powder coating. Because of the characteristic of absorbing moistures from the air, the utilization of zeolite in the final powder may have other side effect on the product. A very tiny amount of zeolite may not

affect the whole panel gloss, so that a reduced amount of zeolite could bring minimal side effect on the final appearance. Meanwhile, the amount should not be too small as it works

Table 5.6 Ash test of bonding sample with reduced amount of zeolite

Solid % \ Group #	1	2	3
Pre-sprayed C_{Solid}	7.98%	8.06%	8.03%
Post-sprayed C_{Solid}	9.90%	9.61%	9.86%

as the spacer. Considering all these factors, a reduced amount of zeolite at the ratio m(Al): m(zeolite)=1:0.2 was conducted utilizing jet-mixing. Figure 5.6 shows the ash test result of the above samples. According to the table, the decrease of zeolite amount could still achieve a good bonding condition, indicating by the little variation before and after spraying.

As the clear coat could not be used as the final coating in the real industry use as it does not contain fillers. In order to examine the final appearance of the bonded sample produced by the new jet-mixing method, a black colored polyester powder coating (supplied by Prism, Model PB-0191-H) was used instead of the clear coat during the manufacturing process. The metallic pigments could also exhibit a distinct color in the background of black gloss.

In order to evaluate the coating performance produced by the new bonding method visually, 5 different powder samples were finished using different processes for comparison. The process details are shown in Table 5.7. No.2 panel is using dry blending (no liquid bonder, by directly mixing and vibrating the powder coating and Al flakes in a

Table 5.7 Different powder formulas for spraying test

Panel #	1	2	3	4	5
Polyester(g)	5.00	5.00	24.01	23.97	10.00
Al (g)		0.10	1.00	1.00	
PVA+borax (g)			1.26	1.26	0.50
Al_2O_3 (g)			0.31		
Zeolite (g)				0.20	0.08
Description		Dry blending	Jet mixing bonding	Jet mixing bonding	Jet mixing bonding

bag). Each sample had the same Al content before spraying. The tested polyester powder coating amount in jet mixing process was scaled up for the future industrial use. Compared with the panel coated only with polyester powder coating, No. 3 and 4 had the perfect effect of metallic effects, while No.2 manufactured by dry blending method presented a significant high of gloss of metallic color, which indicated that the Al concentration was much higher than the concentration in the recycled powder. The photos of the metallic effects of No.1, 2 and 4 are shown in Figure 5.14. No.2 panel

Panel #1 **Panel #2** **Panel #4**

Figure 5.14 Coatings without metallic pigment (Panel #1) compared with coatings obtained from jet mixing bonding (Panel #4) (right) and dry blending (middle)

showed an excessive metallic pigment amount deposited on coating target without using bonding method. When introducing the liquid bonder, No.4 had the smooth shine with the reasonable amount of Al contents.

No.3 and 4 presented similar good visual appearance which was difficult to tell the difference. Figure 5.15 showed the SEM image in further comparing the bonding performance. It could be easily observed the heavy stacking (B) and less bonding in using Al_2O_3 in sample No.3 (C), while zeolite sample No.4 contains more well bonded Al flakes with powder coating (A) and less non-bonded Al flakes. So zeolite could be considered as a proper spacer in jet-mixing bonding method to achieve a better bonding performance.

The purpose of producing No.5 panel was to investigate the gloss influences of PVA+B solution and zeolite. It had no obvious visual difference compared to No.1, demonstrating that PVA+B solution and zeolite would not cause the obvious gloss reduction after curing process. The actual gloss values of those two panels were measured by a triple angle

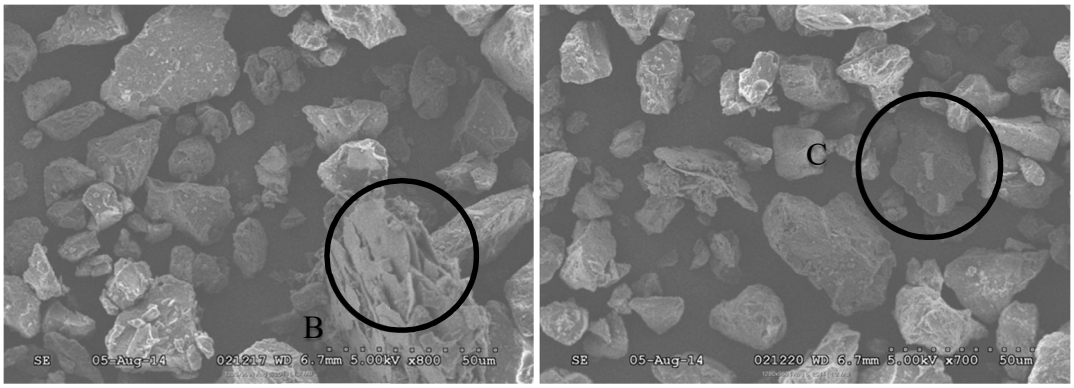

(a) No.3 sample

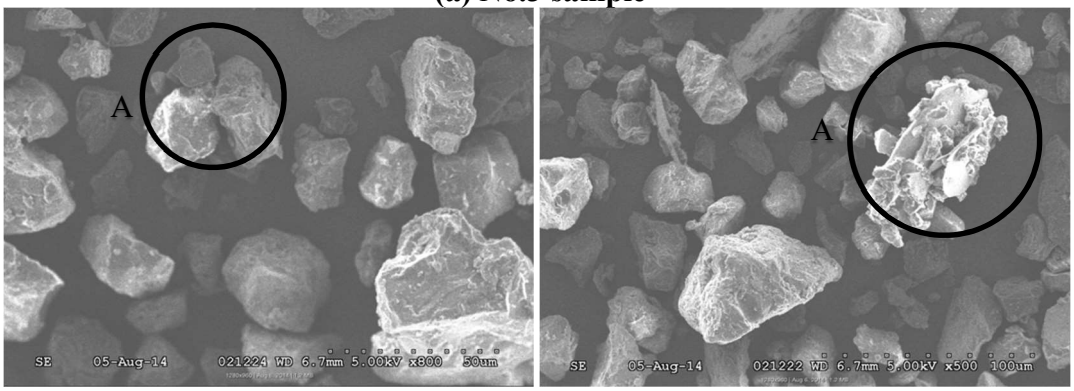

(b) No.4 sample

Figure 5.15 SEM images of the powders

gloss & DOI meter (Manufactured by Elcometer Inc. Michigan, USA), as shown in Table 5.8. There were 9 different measuring points evenly chosen on each panel and detected by the sensor of the gloss meter, as shown in Figure 5.16. The average gloss values were illustrated in Table 5.8. The variation between two average panel gloss could be negligible, indicating little influence of the liquid bonder and zeolite on the coating gloss. It is mainly due to that the amount of zeolite compared to other materials is really small.

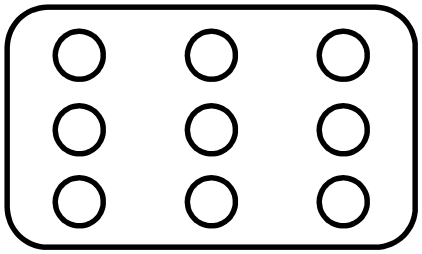

Figure 5.16 Nine measuring points on each panel

Table 5.8 Gloss of panel No.1 and No.5

Panel No.1	Testing point gloss value			Average gloss value
	91.7	92.0	91.6	
	91.5	91.9	91.5	91.14
	91.5	91.8	91.5	
Panel No.5	Testing point gloss value			Average gloss value
	91.7	92.0	91.6	
	91.5	91.9	91.5	91.67
	91.5	91.8	91.5	

In addition, as zeolite has a porous structure and very big specific surface area, it absorbed the solution and reached saturation immediately when blending the liquid bonder. As a result, the property of zeolite is relatively stable and would not absorb anything else in the following procedure of jet mixing and spraying. In conclusion, zeolite is a good choice in bonding the metallic pigments with powder coating.

3.4 The optimization

The most important factor in bonding metallic pigments with powder coating is the amount of the liquid bonder. The changes of the concentration of liquid bonder and the solvent were likely to change the bonding results due to the change of bonding strength and dispersion of the metallic pigments. In this research, 4 different concentrations of PVA+B solution and 4 different combinations with the water amount were prepared for the optimization work. The Al concentration is 3.85% by mass for all the samples.

To find out the proper range of the different concentrations of PVA+B solution, the experiment started with decreasing the water content for getting higher concentration.

The ratio of c(borax)/c(PVA+B) =5.5% remained the same when changing the concentration of the solution. Table 5.9 shows the four different concentrations of liquid bonder. The 96.04% of water is the lowest water content that could be utilized in this experiment.

Table 5.9 Concentrations of PVA + Borax solution

Solvent #	1	2	3	4
Total D.I. water %	92.09%	93.25%	96.84%	96.04%
Description	Irreversible gelation	Irreversible gelation	Irreversible gelation	Clarification Solvent

The ratio of Al and zeolite remained the same. The optimization experiment started with the solution amount with m(zeolite):m(PVA+B) =1:0.42, then the amount of liquid bonder and solvent was increased. 16 different samples tested are listed in Table 5.10,

Table 5.10 Samples of the optimization experiment

D.I. water / PVA+B	-2.9%	0%	+50%	+100%
Zeolite*0.42	Sample 1	Sample 5	Sample 9	Sample 13
*0.63	Sample 2	Sample 6	Sample 10	Sample 14
*0.84	Sample 3	Sample 7	Sample 11	Sample 15
*1.05	Sample 4	Sample 8	Sample 12	Sample 16

where D.I.water represents the additional water content other than the solvent in PVA+B solution. The results obtained from the optimization experiment were evaluated by ash test and the results are listed in Table 5.11. C_{solid} before and after spraying illustrates the final bonding performance, where the final μ_{solid} is calculated by the equation:

$$\mu_{solid} = \frac{\sum C_{solid}}{N} \qquad \text{Eq.5.2}$$

where C_{solid} stands for the solid concentration from the repeating test, and N represents the time of repentance. Table 5.11 shows the optimization results with variations of solid concentration after ash test between pre and post-sprayed powder samples. The variations between the original powder sample and the coated powder are calculated by the following Equation:

$$variation = \frac{Coated\ \mu_{solid} - Original\ \mu_{solid}}{Original\ \mu_{solid}} \quad \text{Eq. 5.3}$$

Table 5.11 Optimization experiment results

Sample #	Pre-sprayed powder (μ_{solid})	Post-sprayed powder (μ_{solid})	Variation (%)	Sample #	Pre-sprayed powder (μ_{solid})	Post-sprayed powder (μ_{solid})	Variation (%)
1	6.42	2.55	-60.28	5	5.03	6.69	33.00
2	N/A			6	4.95	5.88	18.79
3	N/A			7	5.46	5.92	8.42
4	N/A			8	5.59	5.83	4.29
Sample #	Pre-sprayed powder (μ_{solid})	Post-sprayed powder (μ_{solid})	Variation (%)	Sample #	Pre-sprayed powder (μ_{solid})	Post-sprayed powder (μ_{solid})	Variation (%)
9	5.38	6.47	23.46	13	5.11	6.10	19.37
10	4.93	5.58	13.18	14	5.10	5.79	13.53
11	4.93	5.44	10.34	15	4.74	5.36	13.08
12	5.24	5.92	12.98	16	N/A		

The small variations indicate the better bonding of the sample, as the recycled powder had similar composition of the pre-sprayed powder and could be reused.

According to the table above, sample 1 was used as the most concentrated PVA+B solution. The strong agglomeration of powder particles and Al flakes could be observed due to the high concentration of the liquid bonder. It is easy to predict that when increasing the amount using of PVA and borax solution, the condition would get more severe. Hence, the higher amount of PVA+B solution with the same concentration was not necessary to test (sample 2 to 4).

Further analysis shows that when increasing the amount of PVA+B solution, the bonding condition improves significantly illustrated by the variation changes from 33.00% to 4.29% (sample 5 to 8). It is easy to explain that more liquid bonder could provide a stronger force in gluing the materials. Meanwhile, when maintaining the amount of the liquid bonder, the additional D.I. water amount made the bonding effect worse as the dosage increased. That was mainly due to the solvent could dilute the liquid bonder and deteriorate effect of the glue. Also it could explain why the variation of sample 14 and 15 differed little as increasing the amount of solution. This phenomenon elucidates that when the solvent amount is high enough in the manufacture process, it could weaken the function of liquid bonder when connecting the metallic pigment with the powder coating. In this case the water amount should be controlled in a reasonable range.

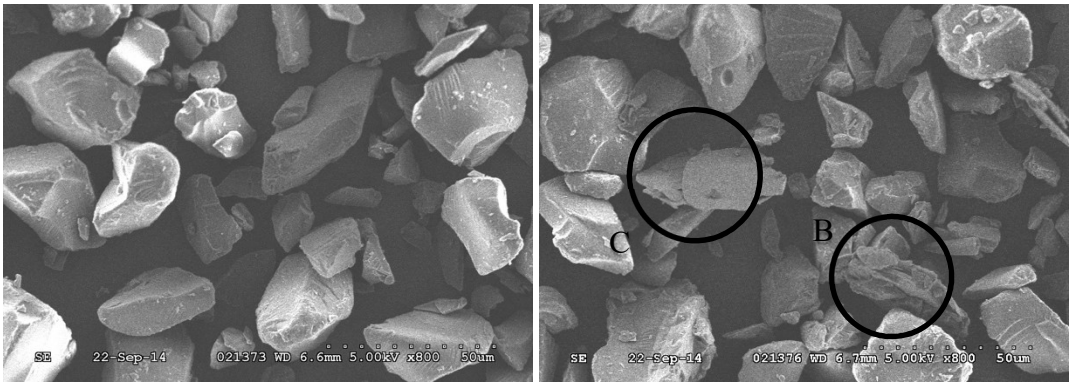

(a) Sample 5

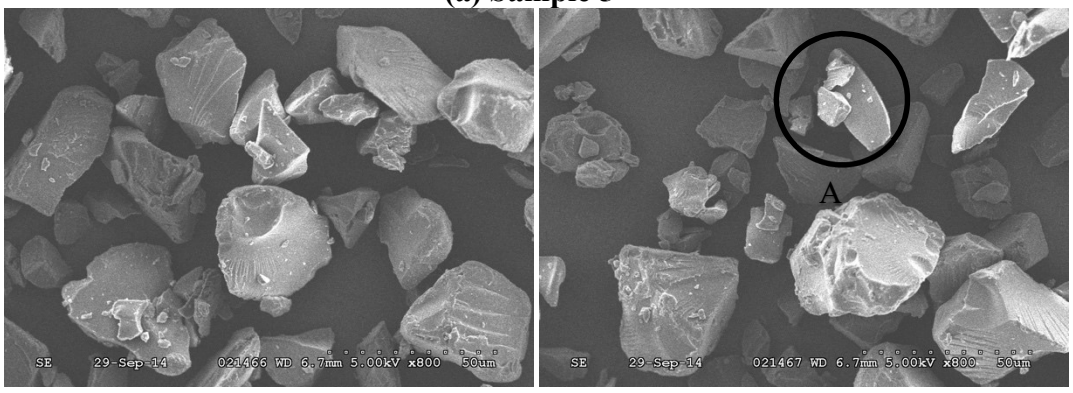

(b) Sample 8

Figure 5.17 SEM images of Sample 5 and Sample 8 (Same D.I. water, increasing PVA+B)

5.3.2 Observations of the bonding effect under SEM

A series of SEM images was conducted for further evaluating the bonding performance. Each SEM picture was taken at the same amplification, and randomly chosen in a certain according to the increase of PVA amount, the non-bonded Al flakes (C) became less, instead of one Al was contacted with more than one powder coating particles in different sizes (A). Meanwhile, a few stacking happened because no additional water was used (B). Sample 5 has relatively more stacking than sample 8 as less amount of solution was used, so that solid pigments did not have a good dispersion in the mixer tube. The similar differences were also observed in sample 9 to 12.

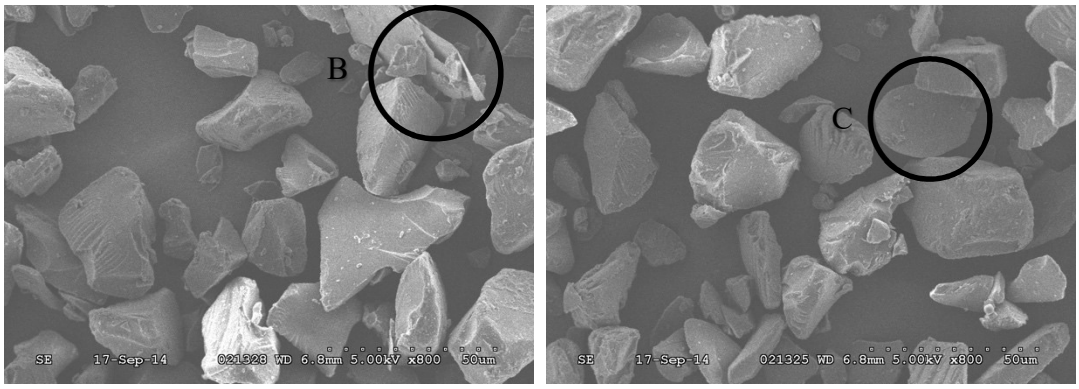

(a) Sample 9

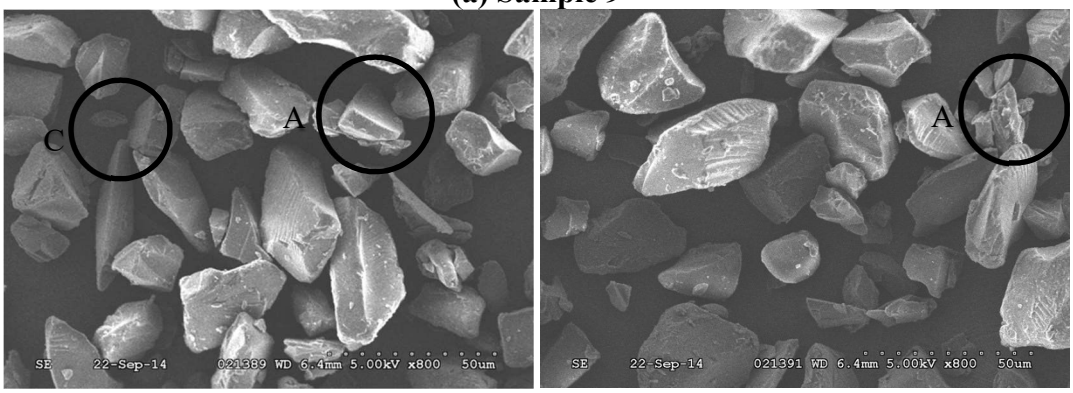

(b) Sample 13

Figure 5.18 SEM images of Sample 9 and Sample 13 (Same PVA+B, increasing D.I. water)

Figure 5.18 shows the result of keeping the PVA+B solution amount and increasing the water amount (Sample 9 and 13). Compared with sample 5 showed above, sample 9

contained 50% more additional solvent in mixing the materials before going through the jet mixing. It shows that sample 9 has more non-bonded metallic pigments in the SEM images (C), but less stacking (B). The liquid bonder was weaker in bonding large amount of dispersed particles with the insufficient amount. More importantly, those powder coatings bonded with Al flakes are very easy to get split when going through the jet mixing nozzle at high speed. However, with smaller amount of liquid bonder, relatively more water could help with the dispersion of the liquid bonder, so as to enhance the bonding. It is reflected by the well bonded parts observed in samples 9 and 13 (A). This phenomenon also explains why compared with the variation between samples 5,9 and 13, sample 13 had the least variation.

Figure 5.19 shows the SEM results of sample 11 and 15. When the PVA+B solution amount became higher, the additional solvent showed less influence on the dispersion and bonding situation. It is due to the fact that liquid bonder had relatively small amount of solute, which was the functional part for gluing powders. When it reached the limit in bonding metallic pigments with powder coatings, it could not promote the bonding. In this case the water content was mainly contributing to disperse the materials and would not help bonding. Increasing amount of solvent resulted in more non-bonded Al flakes. Sample 15 presented a similar condition as sample 11, illustrated by many well-bonding situation (A) in each SEM pictures and less stacking (B), but more non-bonded Al flakes (C). This also explains that the variation became larger when the D.I. water increased while the liquid bonder remained the same.

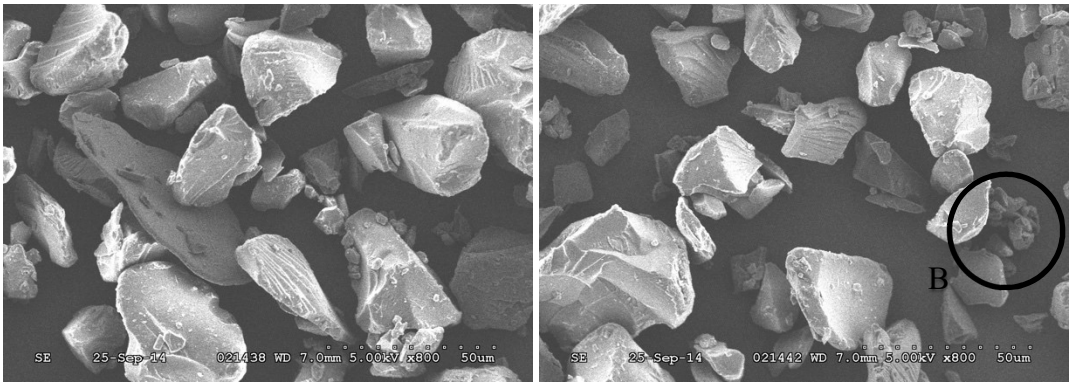

(a) Sample 11

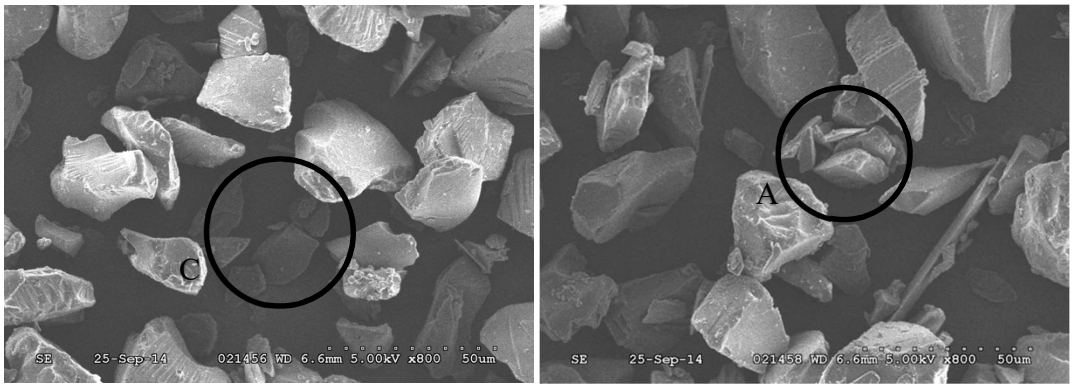

(b) Sample 15

Figure 5.19 SEM images of Sample 5 and Sample 8 (Same D.I. water, increasing PVA+B under larger amount of PVA+B solvent)

As mentioned above, when the dosage of PVA and borax solution is high enough, more added water solvent is not helpful with the bonding. That mainly results from that the liquid bonder contains large amount of water solvent itself. Overdosed solvent surely deteriorates the bonding performance. As the Figure 5.20 indicates, sample 12 has more Al and powder coating stacking (B) as well as detached Al (C) compared with sample 8 with less solvent amount. The overall result was less desirable than sample 8 in both variation and SEM observation because of the added water, so the sample 16 was not further tested.

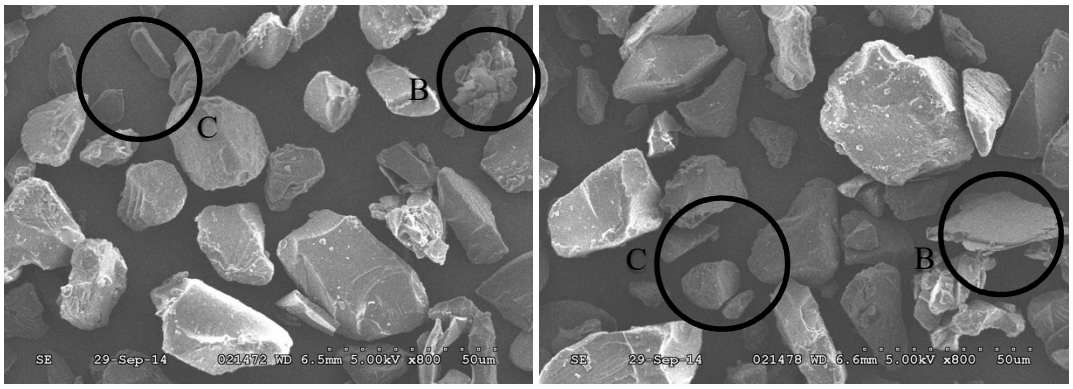

Figure 5.20 SEM of image of Sample 12

5.4 Results and discussion

In order to evaluate the bonding effect in a quantitative way instead of simply observation, a series of work has been done. By observing numerous SEM images, the number of the Al flakes could possibly be counted from each picture. In other words, the number of non-bonded, well bonded, or stacking condition of Al flakes could be recorded statistically. Based on the above analysis, a set of criteria has been proposed in this study in defining the bonding performance of the optimization experiment. Table 5.12 shows the standard of the measurement. The method of counting the number of three different bonding conditions has its drawback due to limitation of the experiment. The observation was based on enough SEM images randomly chosen for each sample.

Table 5.12 Measurement of the bonding conditions

D.I. water PVA+B amount	0% Sample 5-8	+50% Sample 9-12	+100% Sample 13-15
Total Al Well-bonded Stacking Non-bonded	Numbers of the corresponding conditions		

However, the number counted from the captured pictures could vary a lot from each pictures in that some of them had more than 20 Al flakes but some had only less than 5. Each number related to the corresponding conditions was measured from 9 randomly selected photos with identical magnification. The final results of each condition were the average of the all the counts. Only in this way the results could be representative of each sample.

It is illustrated by different amount of PVA+B solution plotted with the different D.I. water content. Figure 5.21 demonstrated the 12 valid data according to the measurement method collected from the all the SEM images. The samples with the lowest content of

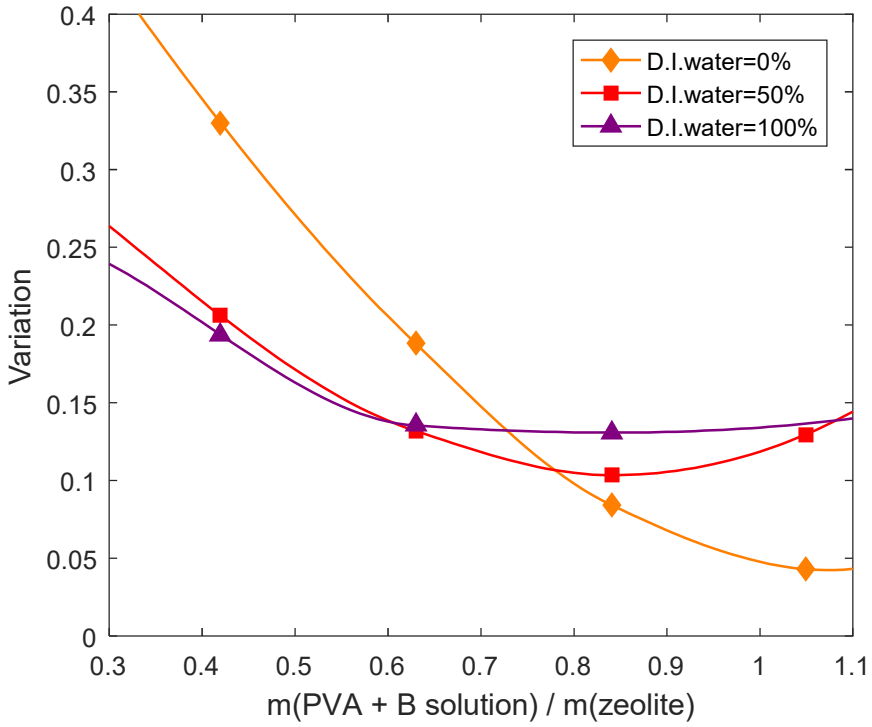

Figure 5.21 Change in the variation between original powder solid% and coated powder solid% with different amount of PVA and borax solution and different D.I. water content

PVA+B solution showed the highest variation, especially the sample 5 (the first sample point of the D.I. water=0%), due to the limited amount of liquid bonder and solvent. Along with the increase of PVA amount, the variation decreases fast.

However, when the PVA+B amount goes higher, too much additional D.I. water was not helpful with reducing the variation. As analyzed above, excessive solvent may hinder the bonding of metallic pigments with powder coatings. It is reflected by the variation trend as the curve is flat or even goes higher. As a result, the samples with the largest amount of PVA+B solution and zero additional solvent could achieve a smaller variation.

Figure 5.22 shows the percentage of 3 bonding conditions within different amount of liquid bonder. The percentage of well-bonded condition is calculated by its count divided by the total count of Al flakes. Apparently, by increasing the amount of PVA+B, more

metallic pigments and powder coatings attended to each other, demonstrated by the well-bonded percentage increases. When m(PVA+B)/m(zeolite)>0.84, all bonding condition

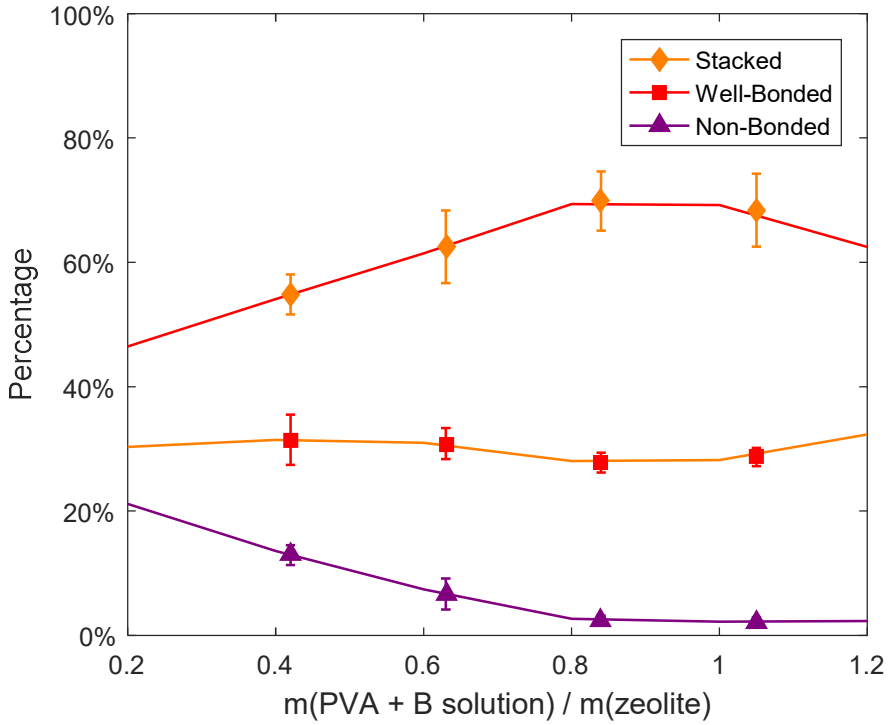

Figure 5.22 Bonding condition percentage with different PVA and borax solution amount (with no additional water solvent)

barely changed, suggesting the maximum PVA and borax amount. As for non-bonded metallic pigments, they tend to decrease as the existence of increasing amount of liquid bonder, but stacking percentage had minor decrease.

The bonding condition shows different distribution when adding 50% additional D.I. water. as shown in Figure 5.23. the well-bonded percentage increasing initially, but over the point of m(PVA+B)/m(zeolite)>0.84, it was dramatically reduced. The stack percentage both had smooth decreases while the non-bonded flakes percentage does not

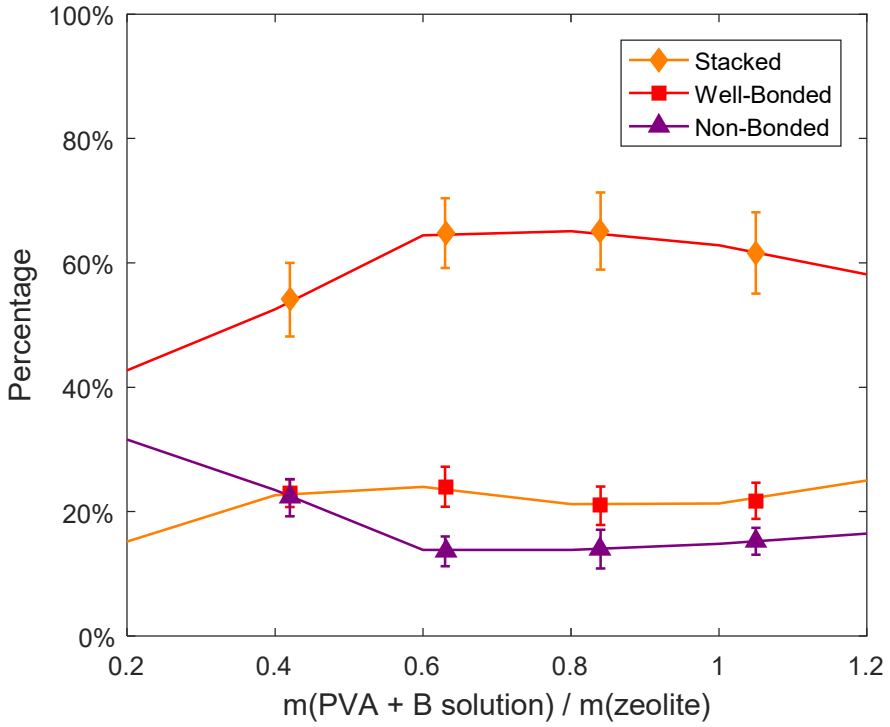

Figure 5.23 Bonding condition percentage with different PVA and borax solution amount (with 50% additional water solvent)

change much along with the solution increases. This phenomenon also suggests that the maximum amount of liquid bonder usage is around m(PVA+B)/m(zeolite)=0.84. In conclusion, with the higher PVA and borax solution in the blending process, more solvent amount could cause even worse bonding condition.

Figure 5.24 illustrated the condition of 100% additional water dosage. Compared to the 50% additional solvent condition, those three bonding percentage did not have much changes. The latter had relatively steady status by increasing the PVA+B amount. In general, the extra water diluted the solution and helped particle dispersion, resulting in that the non-bonded flakes percentage goes higher.

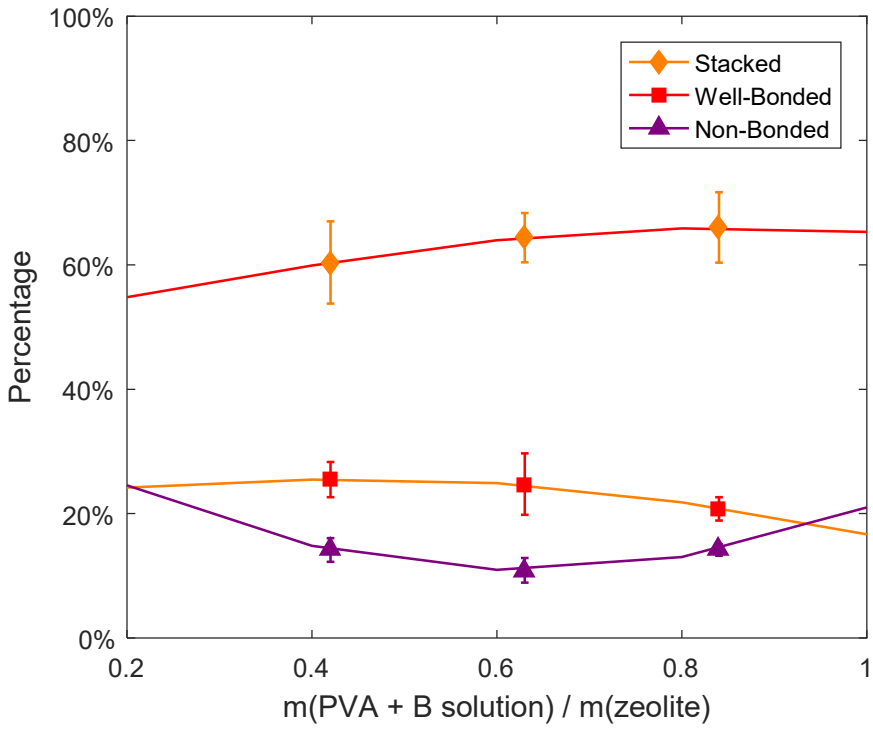

Figure 5.24 Bonding condition percentage with different PVA and borax solution amount (with 100% additional water solvent)

Based on the above analysis, larger amount of the liquid bonder could provide a better bonding between Al and powder coatings, unless no additional solvent is added during the process. The increase of the water was helpful to powder dispersion, resulting in less stacking. However, it hinders the bonding between Al and powder coatings. The water from the PVA+B solution was enough for dispersing and separating the agglomerations during the jet mixing process.

5.5 Conclusion

In this study, a new processing technique of the metallic pigments with powder coating was proposed. The most important part of this method is to ensure the bonding between metallic pigments with powder coatings due to the difference of transfer efficiency of these two materials during spraying. A liquid bonder was introduced to blend with materials instead of conventional thermal blending method. Also, a new important additive called spacer was utilized to prevent the metallic pigments from stacking.

This research started with evaluation of the material which are considered as spacer. Experimental results indicated that aluminosilicate (zeolite) was capable to separate metallic flakes without bringing other drawbacks. In addition, several mechanical processes in obtaining bonding between metallic pigments and powder coatings were tested. Jet-mixing system was the satisfactory operating system to finalize the powder sample before spraying. Similar concentrations of metallic pigments are found in pre-sprayed powder and in post-sprayed powder samples, indicating that the recycled powder could be reused.

In addition, final coating films with metallic effect were examined by both spraying test and the observation of SEM images. Results demonstrated that the bonding situation could be greatly improved by increasing the amount of liquid bonder. At the same time, increased D.I. water amount could help the dispersion of materials for the accuracy of experiment operation. The proper amounts of liquid bonder and water have to be considered in for actual industrial use. Overall, the proposed bonding technology could solve the powder recyclability problem.

In this study, limited kinds of metallic pigments were studied. For the future works of this research, other metallic pigment differing in sizes and shape from the flakes are also worth evaluating in utilizing this proposed cold bonding technique. On the other hand, although jet mixing is able to provide very good bonding and dispersion of the mixed powder, it is still complex for the scale-up operating procedures. A more flexible and simple technique to get the same bonding performance will have to be investigated in the future.

Reference

[1] Bailey, Adrian G. "The science and technology of electrostatic powder spraying, transport and coating." Journal of electrostatics 45.2 (1998): 85-120.

[2] Zhu, Jing-xu, and Hui Zhang. "Ultrafine powder coatings: an innovation."Powder Coat 16 (2005): 39-47.

[3] Fu, Jing. Characterization of Fine Powders and Development of Processes for Powder Coatings. Diss. The University of Western Ontario, 2014.

[4] Drexler, Hermann-Josef, and Ulrich Poth. "Two-layer metal-effect coating and a process for its production." U.S. Patent No. 4,413,036. 1 Nov. 1983.

[5] Drexler, Hermann-Josef, et al. "Water-dilutable coating agent for preparing the base layer of a multilayer coating." U.S. Patent No. 4,489,135. 18 Dec. 1984.

[6] Camelon, Melville J., and Arend WD Vos. "Thermosetting paint binders, curing, amines, metal pigments." U.S. Patent No. 3,953,644. 27 Apr. 1976.

[7] Reisser, Wolfgang, and Guenter Sommer. "Synthetic resin-coated metal pigment, process for the production thereof and use thereof." U.S. Patent No. 5,332,767. 26 Jul. 1994.

[8] Meng, Xiangbo, Jingxu Jesse Zhu, and Hui Zhang. "The characteristics of particle charging and deposition during powder coating processes with ultrafine powder." Journal of Physics D: Applied Physics 42.6 (2009): 065201.

[9] ASTM Standard D5630-06, Standard Test Method for Ash Content in Plastics.

[10] Fu, Jing. Characterization of Fine Powders and Development of Processes for Powder Coatings. Diss. The University of Western Ontario, 2014.

6 Chapter 6: Development of the electrostatic powder coating of insulating surface using the pre-heating method

6.1 Introduction

Powder coating technology was first invented in USA in the early 1960s. The painting with dry powder began to attract attentions from American industry due to its environmentally friendly characteristic. Powder coating has been widely used in the metal painting industry for several decades. Since the early 1970s, powder coating technologies were used for automotive components in North America. Initially the powder coating applications were mainly with underhood metal components, so it has been a basic requirement for the substrate to be conductive. The coating principle is to charge powder particles in an intense electric field known as a corona zone generated by high voltages [1]. During the process, particles receive a charge from the spray gun, forming a cloud across the coating area. With the increasing demand for lighter weight parts to reduce overall vehicle weights with the goal of increasing the fuel efficiency, plastic material components have seen a remarkable growth in automotive consumer industries [2]. Therefore, powder coating plastic components is becoming a real need. The thermoplastic is a typical example due to the fact that it has the polymer compounds.

The purpose of painted plastics is not only for color-matching but also for obtaining the chemical and/or impact protection [3]. There are several advantages for powder coated plastics such as having good resistance of the abrasion or corrosion. However, powder coating has not been successful with plastic substrates using the standard electrostatic coating techniques. Since high temperature of the curing process is needed, the plastic substrate gets warped or distorted along with the elevated temperature. Furthermore, different types of plastic with various properties may affect the painting method, which increases the difficulties in the design of industrial processing. Also plastic substrates tend to absorb moisture from the air during storage. At the high temperature of the curing process, the trapped air and absorbed moisture and/or other volatile materials vaporize out from the plastic substrate and form pinholes in the coating film. This is known as

"popping" problem which is another big difficulty in obtaining smooth finishes on plastic substrate.

The biggest difficulty in electrostatic spraying on plastic targets is that a plastic surface becomes charged quickly when the charged particles and free electrons from the electrostatic spray gun attach on the plastic surface. Because plastics are good insulators, longer charge relaxation times are needed than conductive substrates [4-6]. In this case, there are no opposite polarity electrons flow up through the grounded wire to neutralize the surface charge. The accumulation of free electrons could rapidly form a repelling field. As a result, this field prevents further particle deposition from attaching onto the surface, which finally causes the insufficient and uneven deposit of the particles. This is known as back-ionization, as illustrated Figure 6.1(a). The surface defects could also present the "patchy" finishes owing to the non-uniform deposition as shown in Figure 6.1 (b) [4].

(a)Back ionization **(b) Insufficient particle coverage**

Figure 6.1 Surface defects of the powder coating on plastic substrate

The objective of this study was to find a simple and effective coating process involving the pre-heating method so as to produce high quality surface finishes on thermoplastic targets. In this study, three different commonly used powder coatings were tested on these thermoplastic panels by pre-heating the substrate. The surfaces were evaluated in film thickness, adhesion, gloss, distinctness of image (DOI) and haze.

The other goal was to minimize the curing temperature to far below the conventional curing temperature of thermosetting powder in order to minimize the deformation of the material. Therefore, low-cure powder coatings have been tested in this study as well. Low-cure curing promoters were incorporated into the fine powder coatings, which the promoters function as catalysts accelerating the cross-linking reaction process between the resin and the curing agents. Lower curing temperatures were achieved. To further reduce the curing temperature, an infrared (IR) was utilized for fast heating up the target surface.

6.2 Related work

Previous researches have come up with several solutions to the above mentioned problems in coating plastics. It has been a challenge to apply the powder coatings directly on the plastic surface so that the pre-treatment of the target is necessary. In order to ensure better adhesion of the coatings plastic surfaces, both physical and/or chemical pre-treatment have been widely adopted, such as flame treatment, plasma treatment or chemical oxidation. Applying the primers on plastic surfaces before electrostatic spraying is another type of chemical treatment which could promote the surface adhesion to powder coatings [7]. One of the commonly used practices is utilizing the conductive primers to apply on the plastic surface before spraying powder coatings [4, 8]. Takahashi et al invented a primer with component including conductive materials such as conductive zinc, titanium and other surface active agent, which enhanced the coating efficiency [8]. For automotive industry, these researches preferred to directly add conductive materials to the plastic substrates such as carbon fibers, during the molding process rather than applying primers. Some researchers used conductive backings to the plastic substrate during the electrostatic spraying [9, 10]. However, this method was restricted by the configurations of the plastic parts. Other researchers investigated the method of spraying charged water cloud on the back of a plastic target, while the front side was sprayed with an electrostatic gun [11]. In addition, some attempts had also been investigated on the spray guns for coating plastic targets. Clements et al developed an internal charge spray gun with the alternating polarity without using conductive primers for improving the powder deposition on the surface [3]. However, the powder deposition

was still much less than satisfactory. The researches also suggested that internal charge spray gun could only have better performance on those insulating targets with good powder deposition, such as the preheated targets [3].

Some of the patents related to this field could be valuable to this study. Smith invented a method to powder coat cellulose phenolic composite articles by preheating the targets to degas the volatile compounds for powder spraying [12]. Similarly, Fredericksen also investigated the methods of coating pre-heated plastic articles [12]. After heating the plastic to the temperature below the melting temperature of the plastic, the coating step was carried out without grounding the target. In the furniture industry, the combination of steam and heat between 70 °C and 140 °C was tested for coating medium density fiber (MDF) boards [13]. Those studies proved that the powder deposition was enhanced by preheating the non-conductive target. Nevertheless, some of the inventions needed extra assisting procedures, which complicated the process. More importantly, the coating substrates they used were not the long-fiber reinforced thermoplastic that is discussed herein.

In this study, a method for powder coating fiber reinforced thermoplastic substrates is studied utilizing the pre-heating method. There are two main reasons for preheating the thermoplastics target. On one hand, the moisture and other vaporizable contents could be eliminated through pre-heating to prevent the popping problem of the final finishes. On the other hand, the heat from the plastic substrate melts the powder coating so that the powder could stay on the substrate surface.

6.3 Experimental materials and procedures

6.3.1 Powder coating materials

The substrate panels are made of polyamide laminate co-moulded with 30%wt of glass fibers (Ultramid 8202 HS, JM886 Fraunhofer Institute for Chemical Technology ICT) with identical size (5 cm×7 cm). The three different types of commonly used powder coating materials were supplied by PPG Industries Inc, Ohio, USA (Hybrid: Model PCF-90127; Polyester: Model PCT99101) and Prism (Epoxy: Model SCE830). The characteristics of these powders are illustrated in Table 6.1.

Table 6.1 Powder coating properties and applications

Powder Coating type	Advantages	Applications
Hybrid (Epoxy & Polyester)	Good chemical and corrosion resistance Excellent decorative appearance	Mainly for indoor parts
Polyester	Excellent weathering characteristics Fair corrosion resistance High gloss finishes	For indoor and outdoor parts
Epoxy	Excellent chemical and corrosion resistance Smooth finishes	For indoor parts

6.3.2 Coating procedures

A plastic panel was firstly pre-heated for 15 minutes to the set temperature (the same as the curing temperature) in a convection oven. Then it was quickly removed from the oven to the lab scale manual spray both (Nordson, USA) and sprayed using Gema OptiFlex manual spray gun (Gema, Switzerland). The powder sprayed onto the panel surface got fused on due to the heat from the panel surface. The sprayed panel was returned to the oven for curing at the set curing temperature for 15 minutes (the curing duration time is suggested by the powder coating suppliers).

According to the previous researches, the pre-heating temperature was suggested to be higher than the melting temperature of powder coating but should be below the melting point of the plastic. In this study, the distortion rate vs. temperature was firstly investigated to ensure that the pre-heating and curing did not cause unacceptable deformation of the substrate. In consideration of all the factors, including complete curing of powder coating while maintaining acceptable curing times and substrate distortions, 160 °C was determined as the upper limit for both pre-heating and curing. Because the low-cure powder coatings helped lowering curing temperature, 130 °C and below were chosen as the temperature range for low-cure powders.

6.3.3 Evaluation of coating films

The film thickness of the coating film was measured by a digital micrometer. For each panel, four measurements were taken at four set locations as shown in Figure 6.2. The

coating film thickness was obtained by the overall thickness difference before and after coating.

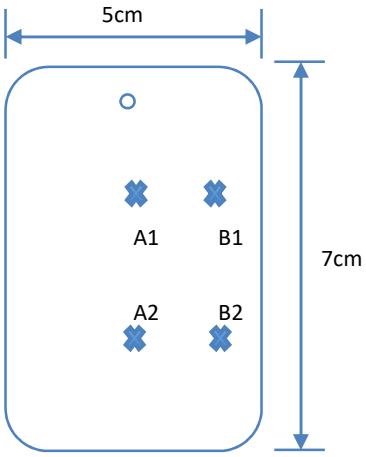

Figure 6.2 Schematic of the measuring points for film thickness

The curing performance of the final coating film was examined by MEK (methyl ethyl ketone) rubbing test (ASTM standard D4752) with 50 double rubs. The adhesion of the film was examined by the cross hatch cutter (Manufactured by Elcometer Inc. Michigan, USA) following ASTM Test Method D3359 (ranges from 0B to 5B, where 5B represents perfect adhesion and 0B stands for the poor adhesion). The gloss of the film was measured by a triple angle gloss & DOI meter (Manufactured by Elcometer Inc. Michigan, USA). The DOI and haze were also measured with the same device according to ASTM standard D523. Table 6.2 illustrates the definitions and explanations of each of the measured parameters. Besides the above measureable parameters, normally the defects of the coating surface can only be evaluated by naked eye observations. In order to provide an overall evaluation for each coating film, the results of visual inspections and instrumental measurements were combined into a grade between 0 and 5 in this study.

Table 6.2 Definitions of measured parameters

Name	Definition	Value
Gloss (GU)	Measurement proportional to the amount of light reflected from a surface; Determining how shiny a surface appears; 60° gloss value >70 considered as high gloss finishes.	0~100
Distinctness of Image (DOI)	Sharpness of a reflected image in a coating surface; Poor coating appearance known as “orange peel”; A perfect surface returns a value of 100.	0~100
Haze (HU)	High quality glossy surfaces have a clear, brilliant finish (HU=0); Haze causes a loss of reflected contrast.	0~100

6.4 Results and Discussion

6.4.1 Film thickness

A thicker coating film could lead to a smoother final surface due to the faster leveling of the coating compared with a thinner coating layer [14]. For non-conductive substrates, the films are required to be thicker than those for the metal substrate to obtain a better coverage of defects from the substrate surfaces, i.e. more than 100 μm is the common acceptable film thickness [12,13]. In this study, the film thicknesses for hybrid and polyester powder coatings were between 100 and 130 μm. For epoxy coatings, the thicknesses had to be around 250 μm for good surface smoothness.

6.4.2 Surface evaluation

6.4.2.1 Hybrid (epoxy and polyester) coating

Epoxy-polyester hybrid powder coatings are known as having a good resistance in gloss and color changes, and have been used for where excellent decorative appearance and good chemical resistance are needed. They combine the advantages of both polyester and epoxy while diminishing the drawbacks. Also the coatings are with competitive prices compared to pure epoxy. In this study the gloss, DOI and haze of those samples were measured and found to change with the curing temperature, as shown in Figure 6.3.

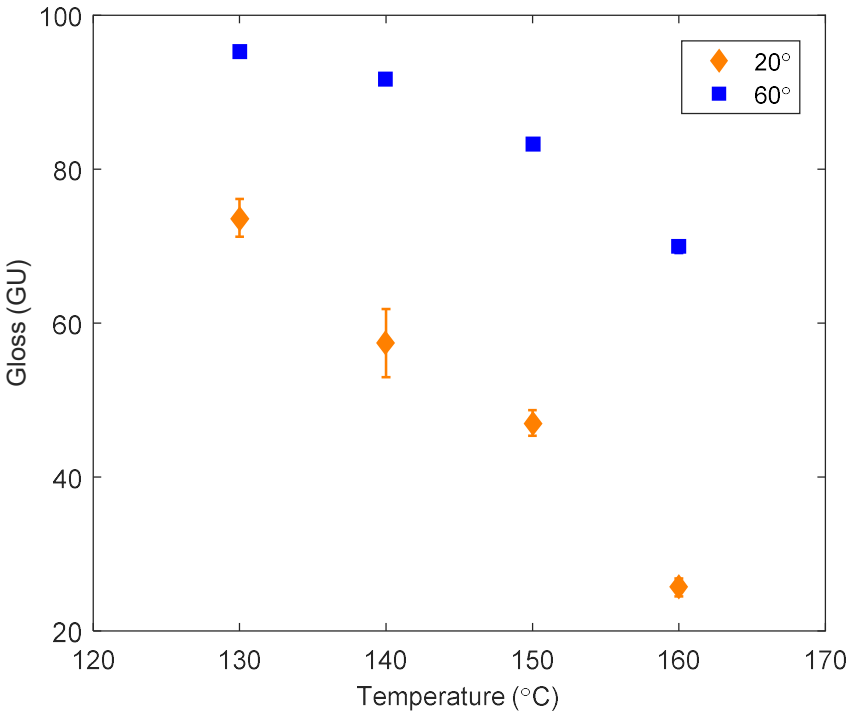
100
80
60
40
20
Gloss (GU)
120
130
140
150
160
170
Temperature (°C)
20°
60°

(a)

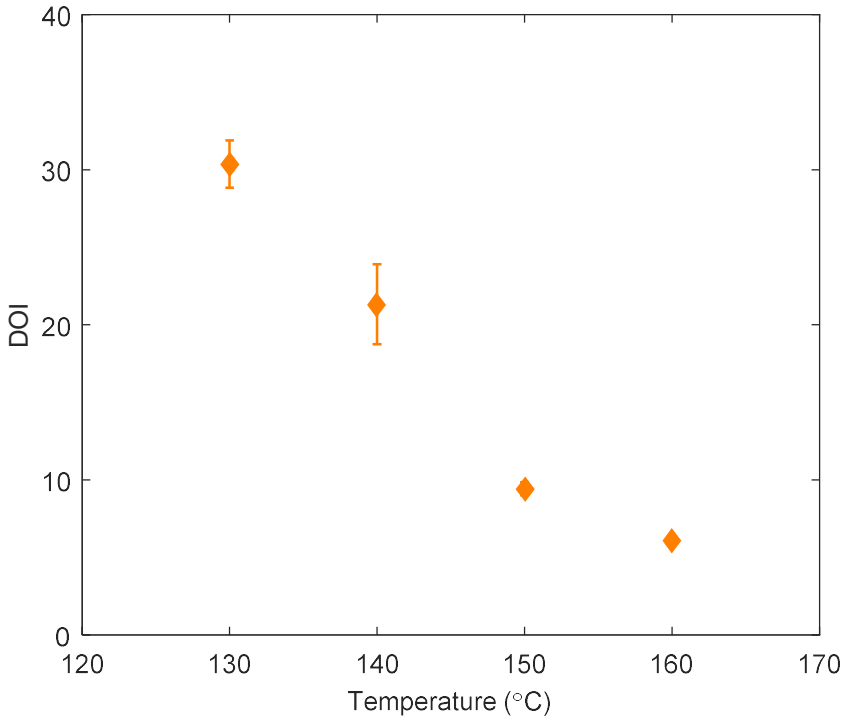
40
30
20
10
0
DOI
120
130
140
150
160
170
Temperature (°C)

(b)

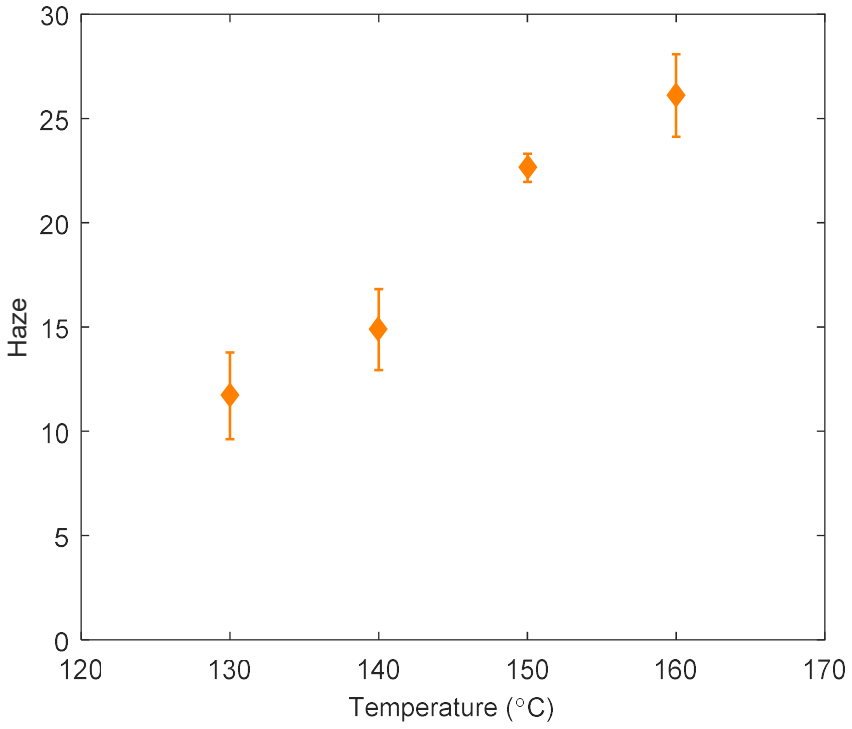

(c)

Figure 6.3 Gloss (a), distinctness of image (DOI) (b) and haze (c) values of the coating surfaces vs. curing temperatures

Figure 6.3 (a) illustrates the effect of curing temperature on the coating gloss. Almost all the surfaces after curing at temperatures from 130 to 160 °C belong to high gloss (60° gloss >70). The gloss values reduce with the elevation of curing temperature. It seems that if there is a requirement for higher gloss, a lower curing temperature is preferred. The DOI value represents the sharpness of the reflect image of the surface. A higher DOI indicates smoother surface. As shown in Figure 6.3 (b), lowering the curing temperature also helps improve the DOI of the surface. On the other hand, a higher haze represents a milky and unclear finish. It was also observed in Figure 6.3 (c) that reducing the curing temperature could effectively lead to an even clearer surface (lower haze value). It is clear that reducing the curing temperature is beneficial for reaching a higher gloss, DOI as well as a lower haze.

The completeness of curing is another important parameter to look after. When the melted coating reaches the minimum curing temperature, it starts to react and eventually

form a higher molecular weight structure which is much stronger and more stable. This process is known as cross-linking which requires a certain temperature and time to accomplish. If the temperature is not high enough or the curing time is not adequate, the coatings would not be fully cured. The completeness of coating was examined by MEK rubbing test, and the results are rated as good, fair and poor. Table 6.3 lists the results of the curing performance vs. curing temperature.

Table 6.3 The influences of curing temperature towards the curing performance of hybrid

Temperature (°C) /Time(min)	MEK Resistance	Cross Hatch Resistance
160/15	Good	5B
150/15	Good	4B
140/15	Good	3B
130/15	Poor	2B
130/25	Good	4B

The adhesion of coatings with the plastic substrate is evaluated by cross-hatch testing. This test is conducted by applying and removing pressure-sensitive tape on the film with a cross-cut area. According to the extent of flaking of the cross-cut area, the results are rated as good, fair and poor, also shown in Table 6.3. It is obvious that the curing has not been completed at 130 °C. A better curing could be achieved by extending the curing time to 25 min at the same temperature. Based on the above analysis the 140 °C /15min are the preferred curing conditions in processing the hybrid coatings in this research。

6.4.2.2 Polyester coating

Polyester powder coatings are known as having a good weathering characteristics for exterior surfaces. The polyester coating film resists chalking and flaking caused by UV exposure, and therefore it is widely used as the outdoor protective finishes. In this study the surface conditions obtained by different curing temperatures are shown in Figure 6.4.

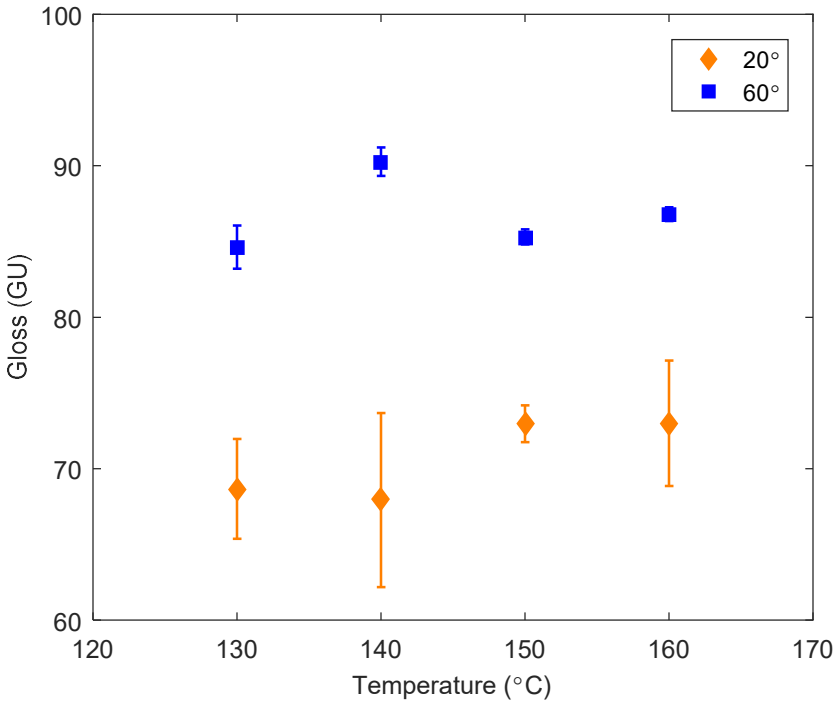
100
90
80
70
60
120
130
140
150
160
170
Gloss (GU)
Temperature (°C)
20°
60°

(a)

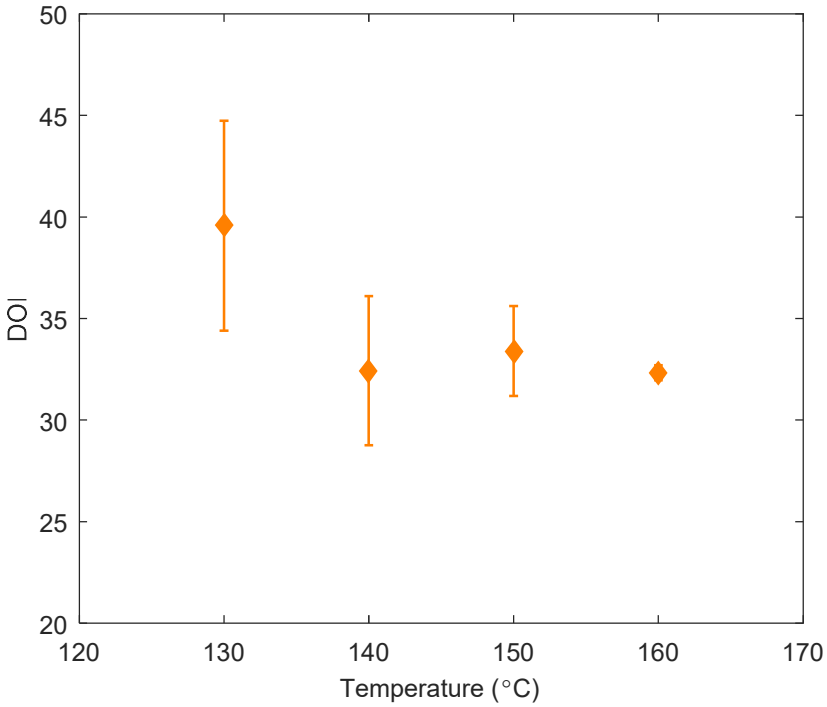
50
45
40
35
30
25
20
120
130
140
150
160
170
DOI
Temperature (°C)

(b)

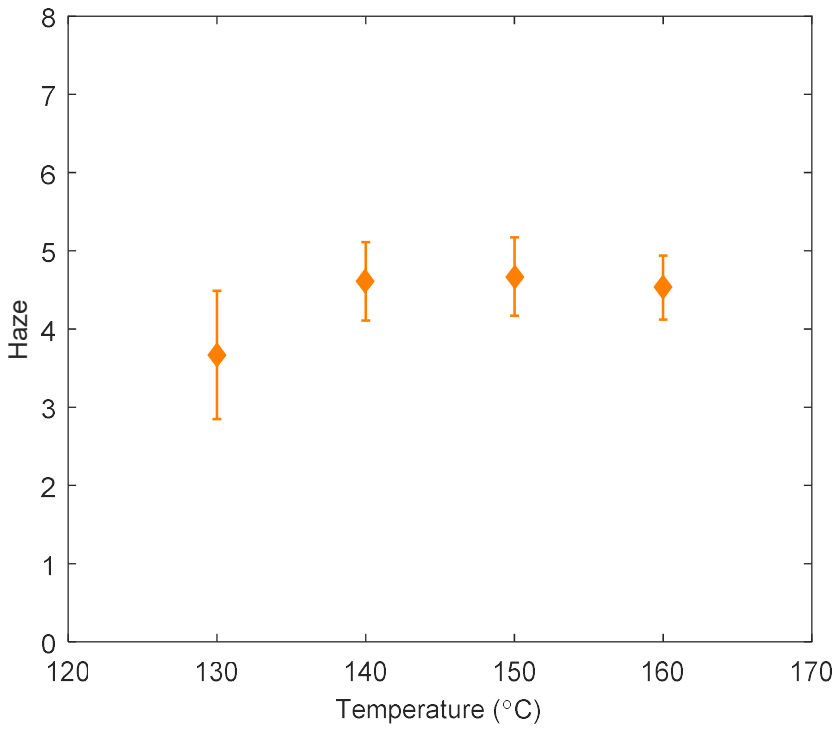

(c)

Figure 6.4 Gloss (a), distinctness of image (DOI) (b) and haze (c) values of the coating surfaces vs. curing temperatures

Unlike hybrid coatings, the curing temperature has less influence on the gloss. When increasing the curing temperature from 130 °C to 160 °C, no significant changes are seen. By observing the DOI and haze tendency with respect to curing temperature, the higher DOI and lower haze value representing a better surface condition happened at 130 to 140 °C. Similarly, the DOI and haze do not vary significantly with different curing temperatures. Table 6.4 lists the MEK and cross-hatch test results in evaluating the curing completeness and the coating adhesion respectively. As the table shows, a temperature lower than 140 °C cannot achieve a perfect curing. The inadequate film curing at low temperature could be solved by extending the curing time to 25 min.

In addition, there is another main difference compared with hybrid coatings related to the surface film. The hybrid coating finishes at each curing temperature showed a smooth surface observed by naked eyes while the polyester coating films had more orange peel, especially when decreasing the curing the temperature and became severe when dropped

to 130 °C. In summary the suggested curing temperature is higher than 140 °C for the polyester coating.

Table 6.4 Influences of curing temperature towards the curing performance of polyester coating

Temperature (°C) /Time(min)	MEK Resistance	Cross Hatch Resistance
160/15	Good	5B
150/15	Good	5B
140/15	Good	4B
130/15	Poor	2B
130/25	Good	4B

6.4.2.3 Epoxy coating

Epoxy powder coatings could provide excellent toughness and corrosion resistance. Due to the major limitation of epoxy powder coatings that they chalk under UV radiation, they are only used on indoor parts. In this study, the surface conditions of the epoxy coating films on plastic panels, at different curing temperatures, were characterized. The gloss, DOI and haze values are illustrated in Figure 6.5.

Different from the hybrid and polyester powder coatings, the gloss of epoxy powder coating film increases with higher temperature. By observing the coating films, it is clear that the orange peel became worse when the curing temperature is lower than 140 °C. These phenomena are also reflected by the DOI and haze values in Figure 6.5 (b) and (c). The lower DOI value represents that orange peel is more obvious. The existence of orange peels may not affect the gloss but the increased haze at lower curing temperatures directly causes the gloss reduction. The epoxy coatings have lower cure-ability compared

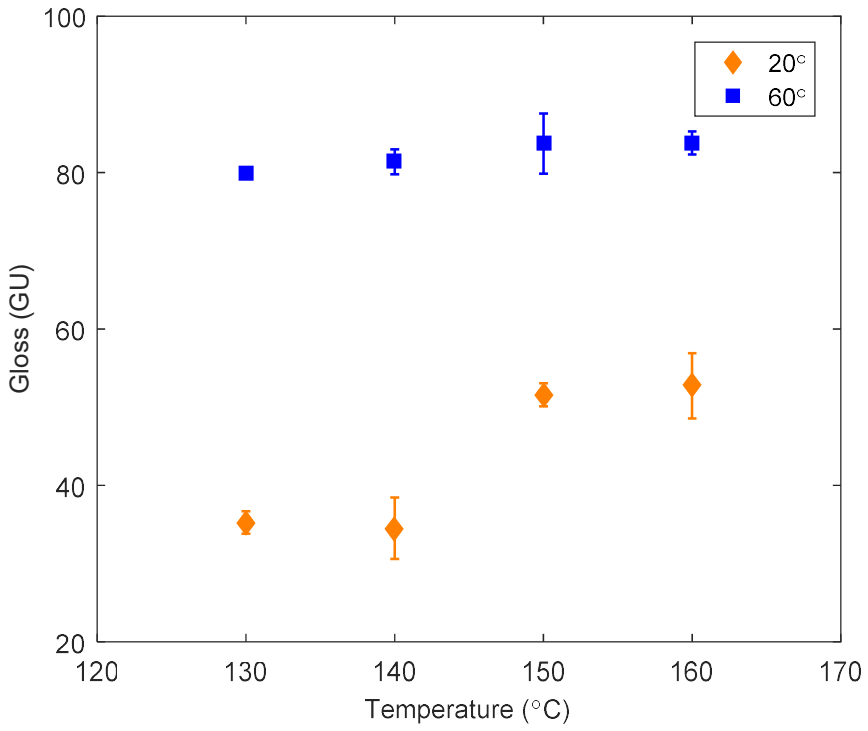
100
80
60
40
20
Gloss (GU)
120
130
140
150
160
170
Temperature (°C)
20°
60°

(a)

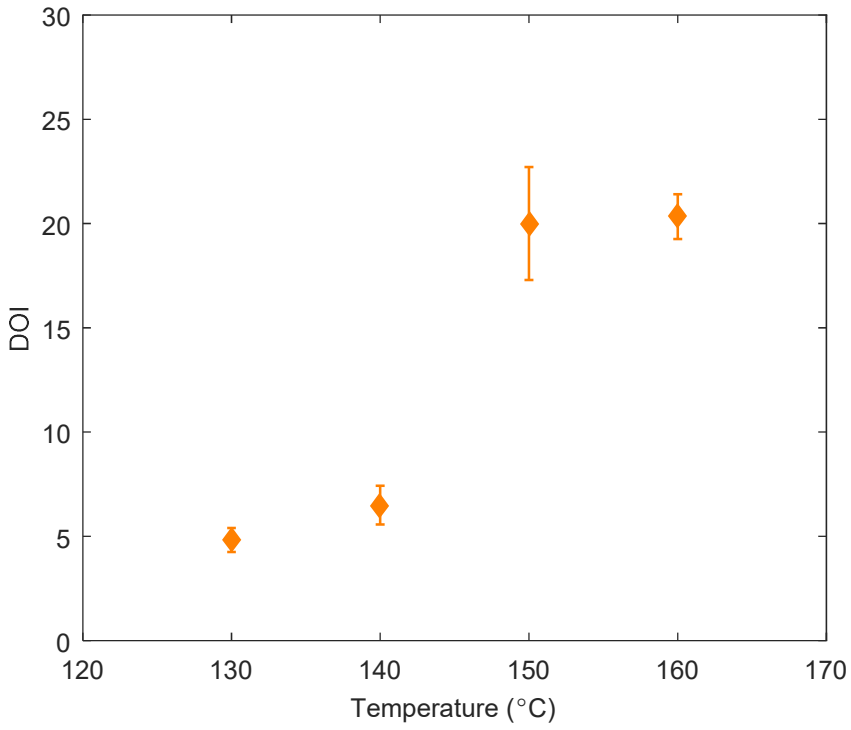
30
25
20
15
10
5
0
DOI
120
130
140
150
160
170
Temperature (°C)

(b)

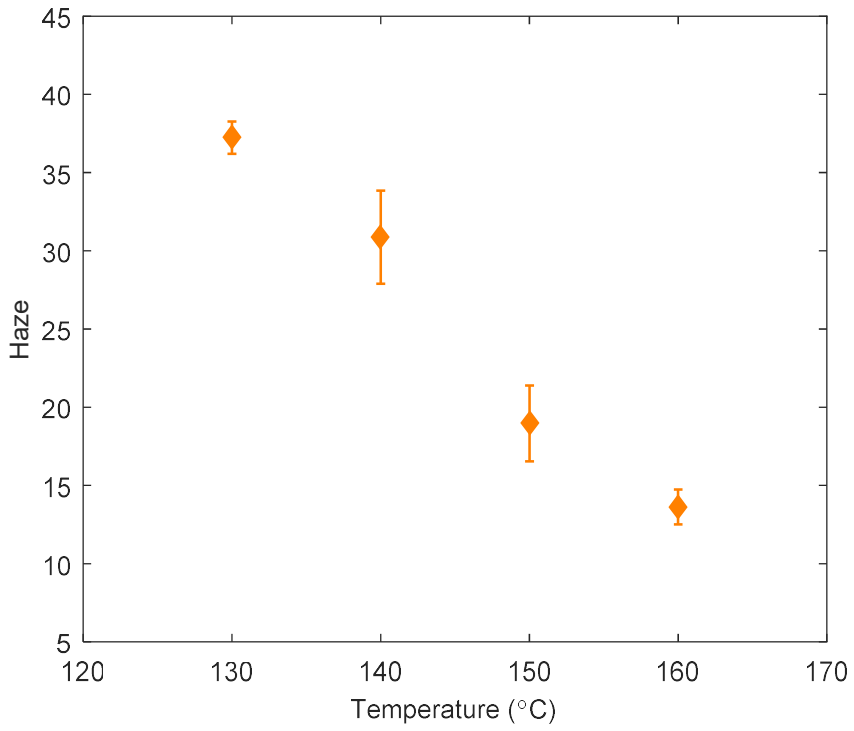

(c)

Figure 6.5 Gloss (a), distinctness of image (DOI) (b) and haze (c) value of the coating surface with respect of curing temperature

with the other two types of coatings within the chosen temperature range. Also the adhesion with the plastic substrate is weaker. Based on the overall evaluation, 150 °C/15 min is the recommended curing temperature in applying the epoxy coating on the thermoplastic target.

Table 6.5 Influences of the curing temperature towards the curing performance of epoxy

Temperature (°C) /Time(min)	MEK Resistance	Cross Hatch Resistance
160/15	Good	5B
150/15	Good	4B
140/15	Fair	2B
140/25	Good	3B
130/15	Poor	2B

6.4.2.4 Low-cure technologies

In order to further explore the curing conditions of powder coatings on the plastic substrates aiming at further decreasing the curing temperatures, low-cure powder coatings were also investigated in this study. The low-cure technique could better protect the plastic substrates from distortion at lower temperatures, while saving energy and the baking and cooling times in the industrial processes. The conventional low-cure powder coatings are produced by adding curing catalyst(s) into the raw materials and thus the catalyst could cause pre-curing during the extrusion process as well as the transportation and storage. Different from those of the conventional low-cure coatings, the UWO curing catalyst is a post-blend-type additive which is incorporated into the ground powder coatings and therefore effectively avoids the pre-curing problem.

In this study, employing the UWO curing catalyst, three types of low-cure powders (polyester, epoxy and hybrid) were produced by converting the regular powders into their low-cure versions. Firstly, the samples of regular powder coatings were grounded down to finer sizes (median size < 30μm). Then they were mixed with the UWO low-cure catalyst with a high-shear mixer. 0.5 wt% of catalyst has been determined as the optimal amount without causing any side effects on the coating quality. A commercial low-cure epoxy (PPG Model: PM90133L) has also been acquired and tested in comparison with the UWO low-cure epoxy.

The experiment started with pre-heating the plastic substrate from 130 °C downwards, due to the regular powder had already got promising results at 140 °C. During the first 3 min of curing period, infrared (IR) was also utilized to aid the melting and film leveling.

(a) Low-cure hybrid (polyester and epoxy) coating

As illustrated in Figure 6.6 (a), both the trend and value of gloss are similar to those of the regular hybrid powder (Figure 6.3 (a)), although the curing temperatures are significantly lowered. Again, the direct reason of the gloss reduction at higher temperatures is the growing value of haze, as shown in Figure 6.6 (c). Both the DOI and haze values fall into their normal range, indicating that no obvious changes in orange peel and haziness occurred when converting regular hybrid to its low-cure version. Similar to

the regular hybrid powder, a lower curing temperature results in higher gloss and DOI, as well as lower haze.

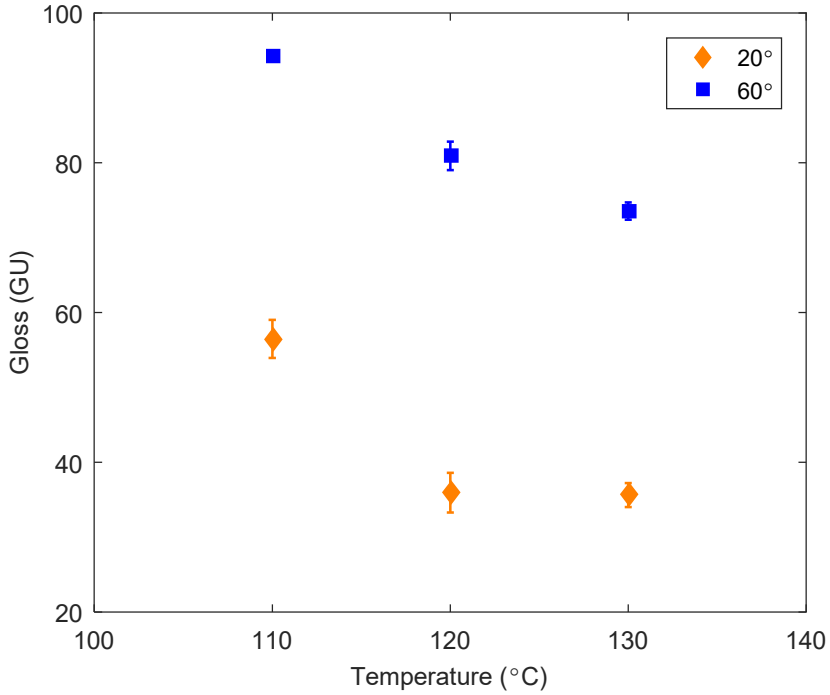

(a)

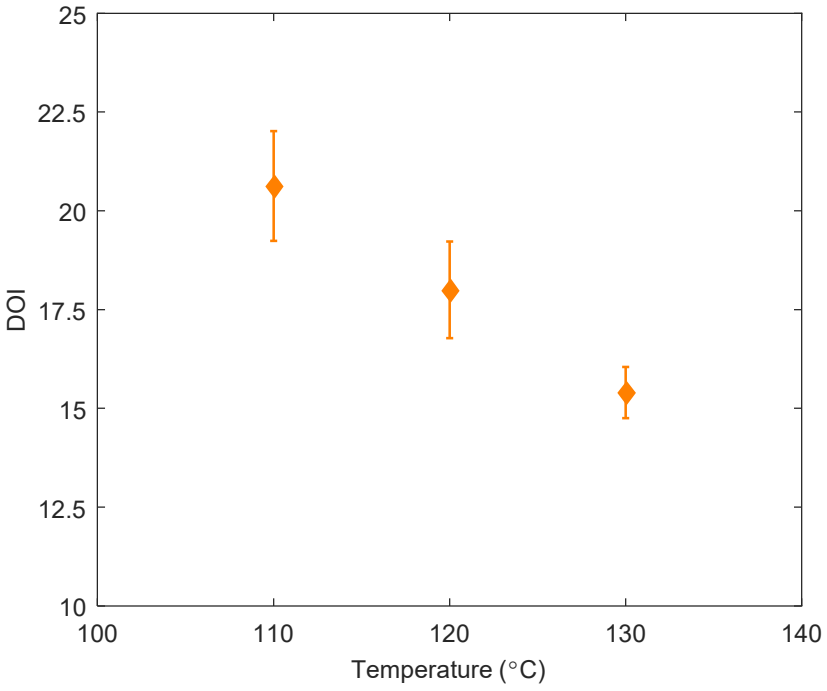

(b)

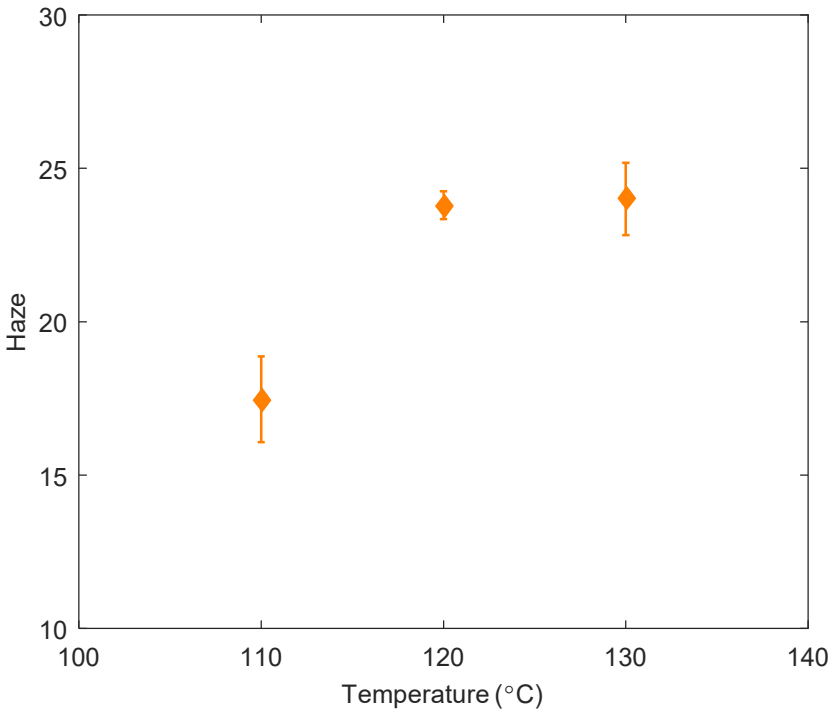

(c)

Figure 6.6 Gloss (a), distinctness of image (DOI) (b) and haze (c) values of the coating surfaces vs. curing temperature

According to the previous definitions, these three types of surface condition values obtained under 110 and 120 °C were satisfactory in realizing the purpose of further reducing the curing temperature. As an important coating film characterizing parameter, curing properties should also be taken into consideration. As Table 6.6 lists, the MEK resistance became worse at 110 °C, at which the curing was incomplete and the film got softened easily by MEK rubbing. However, it could be solved by lengthening the curing time to 25 minutes. Hence, the 120 °C/15 min is a preferred curing condition for the hybrid coating on plastic substrate.

The comparison of the appearance of the regular hybrid and that of the low-cure version is shown in Figure 6.7. Similar glossy appearance can be seen for both versions. The low-cure coating even shows less haze. This indicates that the UWO low-cure technology could obtain good cosmetic effect and high physical properties for hybrid powder coating on plastic substrate.

Table 6.6 Influences of the curing temperature towards the curing performance of hybrid coating

Temperature (°C) /Time(min)	MEK Resistance	Cross Hatch Resistance
130/15	Good	5B
120/15	Good	4B
110/15	Poor	2B
110/25	Fair	4B

120 °C (low cure) 160 °C (without catalyst)

Figure 6.7 Comparison between the process under 120 °C UWO low cure (left)160 °C without catalyst (right)

(b) Low-cure polyester coating

The gloss, DOI and haze with different curing temperatures are illustrated in Figure 6.8. The gloss does not vary significantly with curing temperature. It is also noted that the 20° gloss is slightly higher than the regular powder finishes. The DOI value remains the same as regular powder, and it is less influenced by temperature. The haze reduces with the decreasing of the temperature, leading to slightly higher gloss. As lists in Table 6.7, the MEK resistance is getting worse with the descending of curing temperature. The coating was not fully cured at 110 °C, but can be improved by using a longer curing time of 25

minutes. Hence, the optimal operating condition could be setup as 120 °C/15 min for low-cure polyester.

Table 6.7 Influences of the curing temperature towards the curing performance of polyester coating

Temperature (°C) /Time(min)	MEK Resistance	Cross Hatch Resistance
130/15	Good	4B
120/15	Fair	4B
110/15	Poor	2B
110/25	Fair	4B

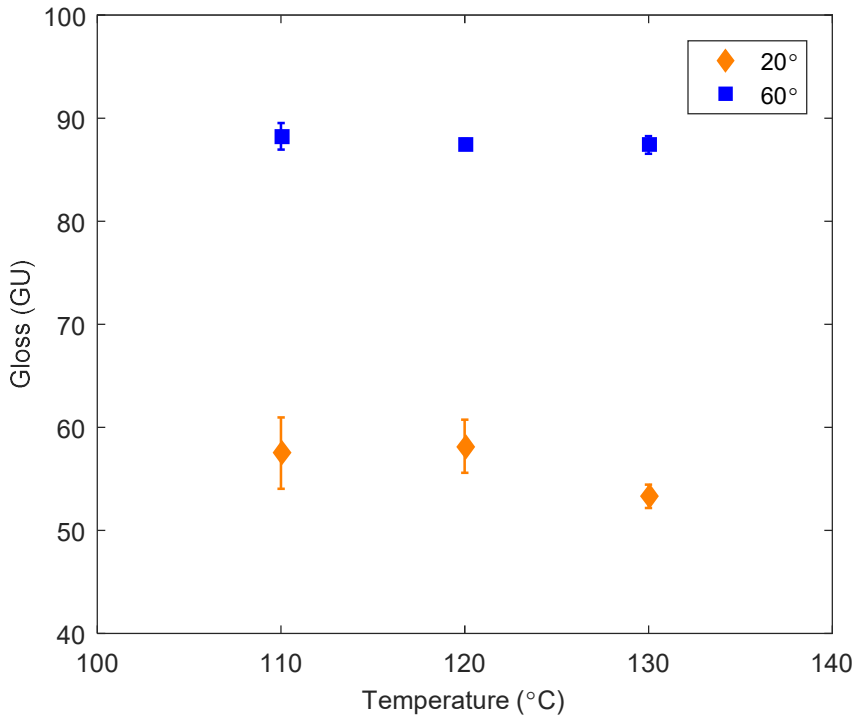

(a)

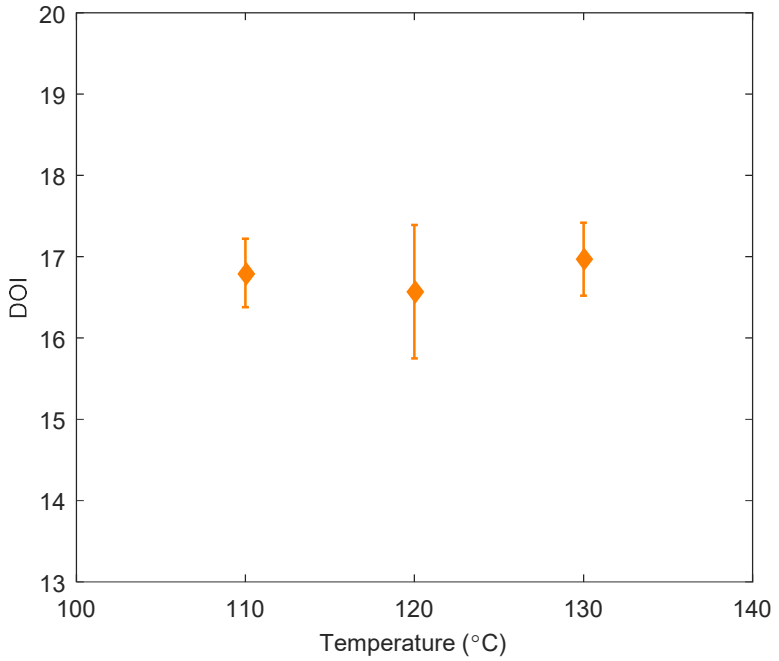

(b)

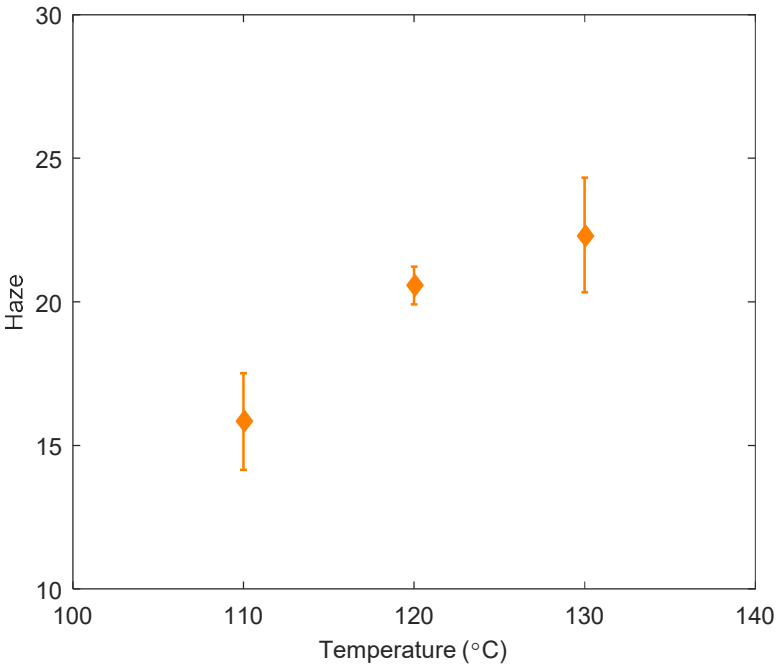

(c)

Figure 6.8 Gloss (a), distinctness of image (DOI) (b) and haze (c) value of the coating surface with respect of curing temperature

Figure 6.9 shows a comparison of the final appearances between the regular polyester (without catalyst) and the UWO low-cure version. It is noted that almost the same appearance and glossy surface were obtained, which indicates applying low-cure polyester coating with UWO low-cure method at a low temperature could achieve satisfactory results.

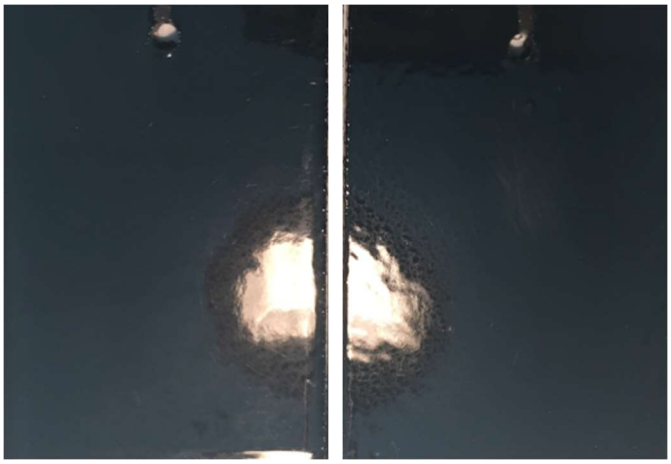

120 °C (low cure) 150 °C (without catalyst)

Figure 6.9 Comparison between the process under 120 °C UWO low cure (left)160 °C without catalyst (right)

(c) Low-cure epoxy coating

As shown in Figure 6.10 (a), the gloss is not obviously affected by curing temperature. The small gloss reduction at 110 °C is again due to the higher haze. The DOI shows a decreasing trend when reducing the curing temperature, standing for more orange peel at lower curing temperature. The results of using commercial low-cure powder coatings with exactly the same curing process are also shown in Figure 6.10. The glosses of both of the low-cure epoxy coatings are similar at 20° and 60°. Also the DOI and haze values of the two low-cure coatings have the similar value range and follow the same trend while the UWO low-cure is slightly better than commercial low-cure powder. By visual inspection, the film of commercial low-cure epoxy coating gets more obvious and severe orange peel when decreasing the curing temperature. Whereas the UWO low-cure epoxy has smooth finishes at all curing temperatures.

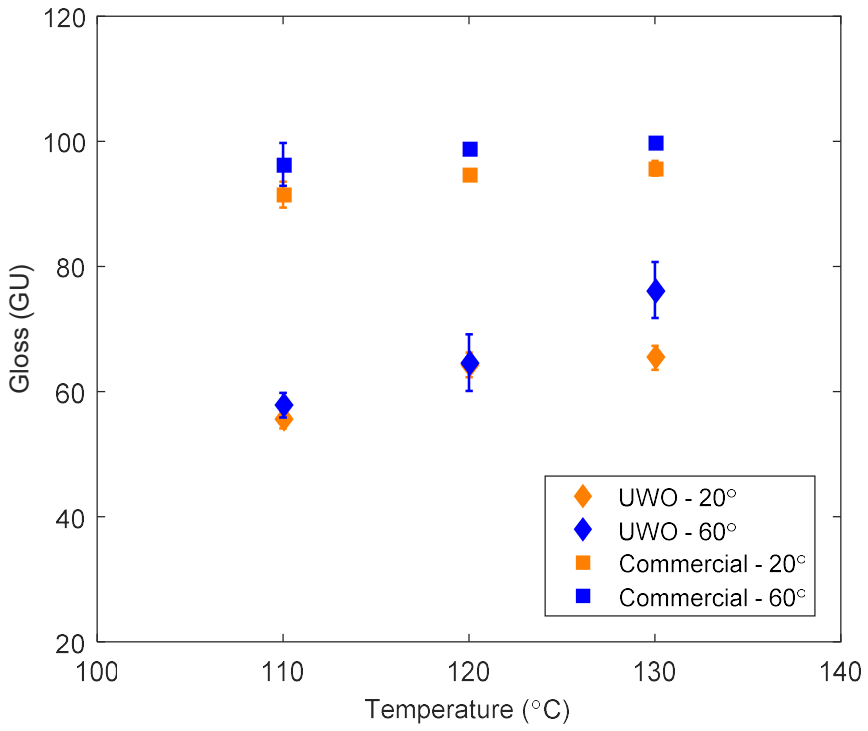
120
100
80
60
40
20
Gloss (GU)
100
110
120
130
140
Temperature (°C)
UWO - 20°
UWO - 60°
Commercial - 20°
Commercial - 60°

(a)

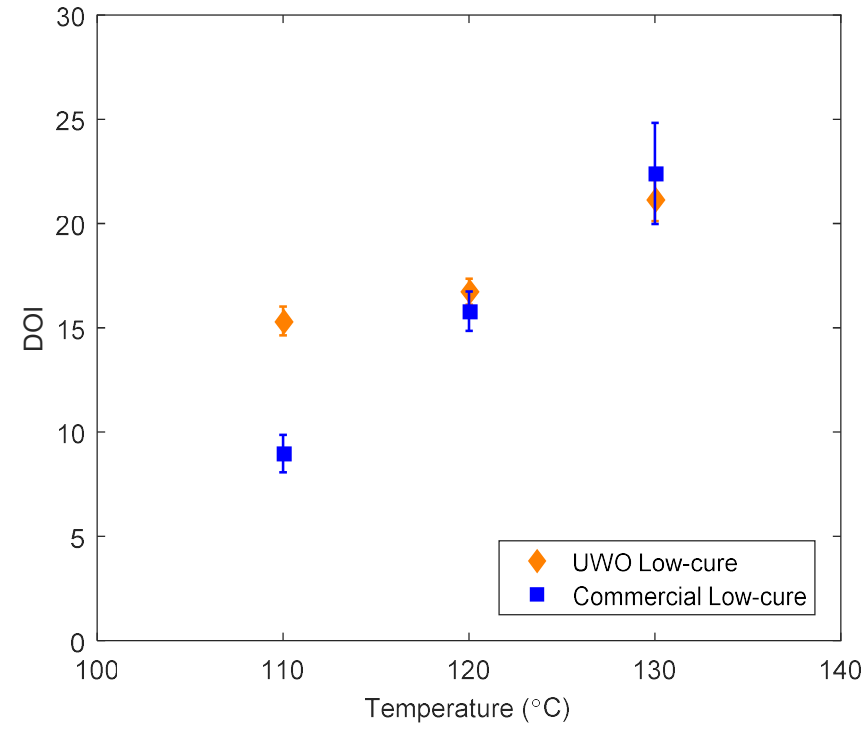
30
25
20
15
10
5
0
DOI
100
110
120
130
140
Temperature (°C)
UWO Low-cure
Commercial Low-cure

(b)

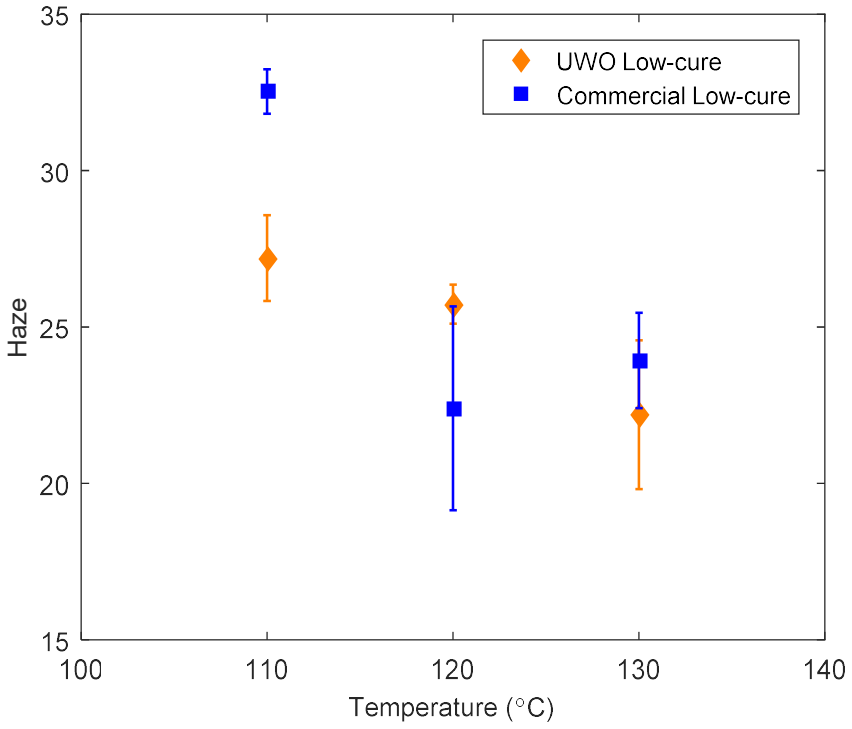

(c)

Figure 6.10 Gloss (a), distinctness of images (DOI) (b) and haze (c) values of the coating surfaces vs. curing temperature using UWO low-cure and commercial low-cure powder coatings

Table 6.8 Influences of the curing temperature towards the curing performance of polyester coating

Temperature (°C) /Time(min)	MEK Resistance	Cross Hatch Resistance
130/15	Good	5B
120/15	Fair	4B
110/15	Poor	2B
110/25	Fair	3B

Table 6.8 reveals that the low-cure epoxy coating could not be completely cured under lower temperature and shorter curing time 120 °C and up to 15 min is recommended for epoxy low-cure coating process. Figure 6.11 indicates the visual comparison of the

coating appearance between the UWO low-cure epoxy and the regular epoxy. By direct visual inspection, the two surfaces show similar smoothness. The UWO low-cure epoxy demonstrates an even higher gloss.

120 °C (low cure) 150 °C (without catalyst)

Figure 6.11 Comparison between the process under 120 °C UWO low cure (left)160 °C without catalyst (right)

In addition, the sample sprayed using commercial low-cure epoxy at 130 °C is shown in Figure 6.12. It is obvious that the orange peel and defects occur on the surface.

Figure 6.12 Commercial low-cure epoxy coatings finish under 130 °C/15min

6.5 Discussion

The gloss change of hybrid coating with curing temperature is obvious. Previous researchers also found this phenomenon that higher gloss was obtained at lower curing temperature but weakened physical properties such as curing completeness also presented.

However, curing temperature has less influence on the gloss of polyester and epoxy. Furthermore, utilizing the low-cure technology could reach a better finish when reducing the curing temperature.

The adhesion between powder coating film and plastic substrate is also crucial. The basic mechanism of the adhesion is chemical bonds. The metal target has many free bonds available to combine with the functional groups of the powder coating. However, the available functional groups such as hydroxyl of the plastic surface in this study could only be provided by the glass fiber or the filler of the thermoplastics. It is shown that epoxy has worse adhesion with thermoplastic substrate compared with the other two powder coating systems.

According to the above comprehensive analysis of tested powder coatings, an overall grade is given to each of them, as shown in Table 6.9. The evaluation is based on the visual inspections, instrument measurements (gloss, DOI and haze), curing temperature and time, and the physical properties. The powder coatings are rated in grades 0-5 where

Table 6.9 Overall grade of the final coated substrate

Coating material	Temperature (°C) /Time(min)	Hybrid	Polyester	Epoxy	Commercial low-cure epoxy
Regular powder (Coarse powder)	160/15	5	5	5	N/A
	150/15	5	5	4	
	140/15	5	4	4	
	130/15	2	2	1	
	130/25	4	3	4	
UWO low-cure (Fine powder)	130/15	5	5	5	4
	120/15	5	4	4	3
	110/15	3	2	2	0
	110/25	4	4	4	2

0 stands for poor appearance and 5 represents the good coating surface that is worth being further examined or researched for industry use. According to the overall grade list, it is clear that using the regular powders at 140 - 160 °C/15 min could produce good coating films. For the low-cure catalyst, 120 °C or higher is the best choice in avoiding insufficient cure. For applications that require even lower curing temperatures, a longer curing time is recommended. Compared with the commercial low-cure epoxy, the UWO low-cure powder could effectively eliminate the pre-curing problem and provide a smoother finish. It is necessary to emphasize that 120 °C is a fairly low curing temperature compared with most of the curing processes and this opens up a lot of opportunities for powder coatings to be applied onto plastic parts.

For all the three chosen powder coatings, the recommended curing temperature is 140 °C~ 160 °C for regular powders, and 120 °C~130 °C for UWO low-cure powder coatings, which is much lower than the conventional curing temperature which is between 180 and 200 °C. Therefore, coating on plastics using pre-heating is proved to be successful in both regular coatings and low-cure coatings.

6.6 Conclusion

It is a challenge to apply powder coatings on non-conductive substrates. In this research, application of three popular powder coatings on thermoplastic substrates have been examined. A pre-heating method was utilized before spraying which effectively helps the deposition of powder coatings to plastic substrates. For the purpose of protecting the thermoplastic substrate from deformation during the curing process while ensuring complete curing and acceptable surface quality, different curing temperatures were investigated and the coating surfaces were examined by different methods.

In order to further reduce the curing temperature, the UWO low-cure method was applied to these three coatings. One commercial low-cure powder coating (epoxy) was also tested against the UWO low-cure epoxy.

In addition to visual inspections, the gloss, DOI and haze were measured and analyzed for the overall evaluation. The results revealed that for regular powder coatings, 140-

160 °C is the proper curing temperature range, while for low-cure powders, 120 °C to 130 °C is good for all the three types of coatings. The most significant achievement of this study is that much lower curing temperatures than conventional curing temperature (190-200 °C) was reached. Compared with the commercial low-cure epoxy, UWO low-cure epoxy performs better in a few aspects.

The pre-heating method is an effective way for applying powder coating on non-conductive substrate such as thermoplastics. The low-cure formulation also provides an opportunity in curing powder coatings at a considerably low temperature.

References

[1] Bailey, Adrian G. "The science and technology of electrostatic powder spraying, transport and coating." Journal of electrostatics 45.2 (1998): 85-120.

[2] Lovano, Sal. "Automotive applications for powder coating." Metal finishing94.9 (1996): 20-24.

[3] Clements, J. Sidney, and R. H. Bair. "Electrostatic powder coating of insulating surfaces using an alternating polarity internal corona gun." IEEE Transactions on Industry Applications 35.4 (1999): 743-752.

[4] Garner, David P., and Alaa A. Elmoursi. "Electrostatic painting of plastics. I: Electrical properties of plastics and primers." JCT, Journal of coatings technology 63.803 (1991): 33-37.

[5] Tepper, Richard M., James E. Sickles, and Themos C. Anestos. "Surface charge buildup during electrostatic spraying." IEEE Transactions on Industry Applications 2 (1977): 177-183.

[6] Migda, F. M. "New methods for evaluating electrostatic paintability of plastics." ASM/ESD Advanced Coatings Conference, Chicago, IL. 1992.

[7] Kloeckner, Harald, et al. "Method for painting plastic substrates." U.S. Patent Application No. 10/634,330.

[8] Takahashi, Katsuhiko, Yoshiharu Suzuki, and Haruyasu Ito. "Conductive primer for plastics or conductive primer surfacer paint and coated plastics molded products." U.S. Patent No. 4,971,727. 20 Nov. 1990.

[9] Castle, G. S. P., and Ion I. Inculet. "The electrostatic fields and discharge hazards of insulating sheets close to a conductor: a review." IEEE Transactions on Industry Applications 33.1 (1997): 274-278.

[10] Elmoursi, Alaa A., and David P. Garner. "Electrostatic painting of plastics using metal backing." IEEE transactions on industry applications 29.6 (1993): 1053-1057.

[11] Inculet, Ion I., and Richard G. Klein. "Electrostatic painting of nonconductive surfaces with water-base paints." IEEE Transactions on Industry Applications 32.1 (1996): 90-92.

[12] Smith, Dwight E. "Process for producing powder coated plastic product." U.S. Patent No. 5,565,240. 15 Oct. 1996.

[13] Holliday, Martin L., Craig Wilson, and Colin G. Piearce. "Process for the application of powder coatings to non-metallic substrates." U.S. Patent No. 6,458,250. 1 Oct. 2002.

[14] Biris, A. S., et al. "Gloss and texture control of powder coated films." Particulate science and technology 19.3 (2001): 199-217.

[15] Schmidhauser, John. "The Role of Catalysts in Low-Gloss Epoxy/Polyester Hybrid Powder Coatings." International Waterborne, High Solids, and Powder Coatings Symposium, New Orleans, LA. 2001.

7 Chapter 7 General Discussion

Powder coating is a dry finishing process in which pulverized particles are electrostatically charged and sprayed onto grounded targets. It first appeared in the coating industry in the 1950s in the USA. Due to one of its outstanding advantages of eliminating the use of Volatile Organic Compounds (VOCs), powder coating became a new trend in the finishing markets. As a result of the overwhelming advantages of powder coating such as saving energy and cost, the satisfactory coating properties and high efficiency of the recycled materials, it had been outpacing the growth of the conventional liquid coating in the past decades.

However, as a relatively young and newly developed technology, power coating is met with many challenges and has not gained a comparable market share with liquid coating in nearly half a century. The main problems include the excessive thickness and relatively poor and rough appearance of the coating film. It is a complex challenge for improving the coating finish. Previous researchers discovered that rough and poor coating film could be solved by reducing powder particle sizes. Yet, the applications of fine powder coatings encountered many obstacles due to the strong cohesion between particles. First of all, fine powders produced by grinding system have more flowability issues compared with coarse powder. What is more, the particle size distribution of fine powder is always wider, and smaller particles are more likely to get agglomerated causing further processing problems. During spraying operations, fine powder experienced lower coating efficiency and a stronger Faraday Cage effect than regular powder coatings.

In this thesis, the experimental study resolved several key problems of machinery modification of powder production and powder handling in a comprehensive way. It started with modifying the manufacturing processes on the air classifying mill to narrow down the produced particle size distribution. Then it was followed by modifying the spray gun so as to improve the charging and spraying performance. A newly developed corona spray gun with a multi-electrode configuration was studied in overcoming the Faraday Cage effect. Furthermore, a new method in processing specialty powder coatings was explored in this study. In addition, a method in powder coating application on plastic

has also been investigated in the last part of this work. The low-cure technology which offers a wider operating window in application of powder coating on plastics was applied.

To begin with, a manufacturing process was improved for narrowing the particle size distributions on the cyclone of air classifying mill (ACM). It has been discovered that utilizing a reverse air flow at the cyclone bottom could effectively remove small particle during the collecting process. In this way, the particle size distribution could get improved due to the smaller amount of small particles collected. Inspired by previous similar designs, this modification had an opening gap at the cyclone bottom through which the reversed air could be introduced directly. Compared to previous complicated classifying cyclone designs, this modification is easily setup and operated. The main contribution is that the obtained particle sample has a narrower size distribution after classification using the new cyclone design. This noticeable improvement applies with both fine and coarse powder, which more obvious achievement could be seen in fine powders. However, the cyclone collection efficiency was highly reduced due to the removal of small particle by strong reverse flow at cyclone bottom. In order to retain larger particles so as to maintain cyclone colleting efficiency, a special designed shim with secondary air guider was invented incorporating into the opening gap. According to the computer simulation, the secondary air guider could enhance the outer vortex air spin and remove smaller particles, it also helped retain larger particles by centrifugal forces. In this way the collection efficiency was expected to be retained and became comparable to an ordinary cyclone. Furthermore, the modified cyclone with reversed air and secondary air guider has a very simple design and does need extra powder supply. Hence, it can be easily utilized into scale-up device and implemented in real productions.

A novel spray gun design in modifying corona spray gun was invented in this study to mitigate the resistance of the Faraday Cage effect. Experimental study started with finding the baseline of the original corona spray gun in a wide range of operating conditions. The novel spray gun design had 4 additional electrode configurations connected with an alternating charging pattern. Instead of a traditional corona spray gun with a single electrode, multi-electrodes could improve the particle charging performance. In addition, supplied by alternating high voltage, the modified gun provided an empty

charging period to eliminate the accumulation of free electrons, as they created a repellence of electrostatic fields of the sprayed powder cloud. The Faraday Cage resistance could be effectively reduced during the corona spraying. Experimental results of the new spray gun were evaluated by Faraday Cage resistance (FCR) and first-pass transfer efficiency (FPTE). The optimization experiment of new electrodes configuration with different axial and radial length has been done. The results indicated that when four additional electrodes were set up with the same axial position as center gun tip, they could provide the satisfactory charging performance of particles as well as better Faraday Cage resistance. Besides Faraday Cage resistance, the transfer efficiency of modified corona spray gun was also studied. Results indicated that overall transfer efficiency obtained from the new gun was higher than the original one. This significant improvement of transfer efficiency was mainly due to the reduction of the duration of secondary charging, which was in agreement with the theory.

Another development of this research was the new processing techniques for specialty powder coatings. The study of manufacturing processes of metallic color powder incorporated with regular powder coatings has been done. The metallic powder could provide an aesthetic appearance with extra shine to the coating surface when blended with powder coatings at certain dosages. However, this technique faced many difficulties not only due to the higher cost of metallic powder, but also the more challenging coating process. The new technique of bonding metallic powder with powder coating was developed to solve those problems.

Conventional techniques utilized thermal blending method for metallic powder processing. It operates in a blender where powder coatings get softened due to the heat generated. Under the high shear the metallic pigments could attach onto the powder particle surface. However, the drawback of this process is that the proper operating temperature is hard to control. Lower speed is not able to achieve bonding of the two materials, while higher speed causes the cure of powder coatings because of the generated heat. In addition, the bonding between powder coating and metallic powder is not strong enough from traditional blending technique. During spraying process, the two

materials separate and vary in charging performance. As a result, the mixing ratio of metallic pigment in recycled powder changes and the collected powder is not reusable.

In this study, a solution for the above problem started with utilizing a liquid bonder to create a better adherence of metallic pigment and powder coatings. After mixing and drying, powder samples with uniform dispersion of the two materials were ready to spray. According to experimental results, the concentration of metallic pigments sprayed on to the work piece could remain the same as the original blend before spraying, as indicated that recycled powder had similar aluminum content. Spraying tests showed that the new technique was efficient in bonding metallic pigments with powder coatings, so that solved the recyclability problem. Another difficulty in bonding process is the strong stacking of metallic pigments. Observed by SEM, besides attaching on particles, flat-shaped metallic pigments tend to overlap each other due to the existence of liquid bonder, which deteriorates the metallic effect in final coating. Therefore, bonding agent was added during blending process for solving the stacking problem, followed by the jet-mixing and drying processes. Bonding agent, which is made of smaller particles (2-3 μm), works as "spacer" aiming at separating the neighboring metallic pigment to avoid stacking. The effectiveness of introducing spacer was also confirmed by SEM. An optimization experiment of adjusting the amount of liquid bonder and spacer has been done in order to maximize the bonding performance. Further results indicated that an increased amount of liquid bonder could achieve stronger bonding, while an overwhelming amount causes stacking problems. The optimal amount of liquid bonder and spacer has been decided after a series of experiments. What is more, other kinds of metallic powder are worth trying with this new technique.

The last but not the least, a method for coating fiber-reinforced thermoplastic substrate was studied utilizing the pre-heating method. In coating industry, over 90% of powder coating is applied to metal substrates. The biggest challenge in electrostatically spraying plastic substrate is that there is insufficient powder deposited and weak powder adhesion on plastics compared to metal target. As plastics are good insulator, there is no counter electrons to neutralize the surface charge. As a result, the accumulated free electrons repel further particles from attaching onto surface. The new technique in this study was a

simple way to produce high quality surface on plastic targets. Three commonly used powder coating were applied on pre-heated thermoplastic, and then examined by a series of surface evaluation parameters such as gloss, DOI and haze. Both visual inspections and instrumental measurements indicated that the good coating appearance and adhesion of powder coating with thermoplastic could be obtained by the new processing technique.

In order to better protect plastic substrate from high temperature during curing process, a UWO low-cure technology was utilized and it successfully lowered the curing temperature. The low-cure technique could prevent the distortion of substrate, save energy and shorten the baking and cooling times in the industrial processes. Low-cure additives were blended with fine powder (< 30 μm) for better dispersion instead of mixing with coarse powder, followed by the same spraying process on a pre-heated thermoplastic target. A much lower curing temperature than conventional curing temperature was achieved using UWO low-cure technology.

In conclusion, this thesis study was composed of many solutions for challenges and difficulties in powder coating manufacturing and application processes. In addition, several original methods were proposed for meeting the challenges. Comprehensive experimental study and analysis have been confirmed and supported the methods. Overall, it was believed that this study is of great help in advancing powder coating technologies and providing a better guidance of powder coating development.

8 Chapter 8 General Conclusions

In this thesis, a comprehensively study on improving manufacturing and application processes of powder coatings has been accomplished. A series of experimental studies was conducted to improve the existing methods and overcome current technical difficulties. General conclusions of this research were stated as follows:

- A new design of the cyclone of air classifying mill (ACM) has been developed for improving particle size distribution. The idea of a secondary opening gap at the cyclone bottom provides a reverse flow which effectively removes small particles. In addition, in order to maintain the cyclone collection efficiency, a secondary air guider was added to help retain the larger particles. A series of experiments were conducted under different air guider configurations, so as to investigate the effect on particle size distributions of the collected coarse and fine powder. Experimental results indicated that the new design of classifying cyclone could effectively remove small particles and achieve a narrower particle size distribution. Additionally, the proposed cyclone design could also provide comparable collection efficiencies compared to that of conventional cyclones, owing to the design of the air guider.

- Another modification was developed for the corona spray gun with the multi-electrode configuration design. The new spray gun was supplied with an alternating charging pattern and it was able to overcome the Faraday Cage effect during the corona spraying process. This modified corona spray gun showed a significant improvement on Faraday Cage resistance and, at the same time, with higher transfer efficiency under ordinary operating conditions compared to conventional corona gun. Furthermore, the relative position of four additional electrodes could affect spray gun performances. An optimized experiment with different electrode arrangements was conducted. Results suggested the best configuration of additional electrodes, and preferred operating condition of this new corona gun has been figured out.

- Furthermore, this study developed a new processing technique for metallic pigment in powder coatings. This new bonding technique involving liquid bonder was aiming at providing a strong adhesion between metallic pigments with powder coating particles. Therefore, the two materials would not separate during spraying and they can have a uniform charge performance. As a result, the content of metallic pigments remains the same in the recycled powder as pre-sprayed powder. More importantly, this new technique eliminates the pre-curing problem of conventional thermal blending methods. A comprehensive experiment has been conducted in optimizing the blending formulation. Results showed an increased amount of liquid bonder and reduced content of liquid bonder solvent could achieve a stronger bonding. The stacking problem with the metallic powder can be resolved by introducing "spacer" made of smaller particles during the blending process.

- In the end, a technique of powder coating on thermoplastics using the pre-heating method has been studied in this thesis. After heating the plastic to the temperature below the melting temperature of the plastic, the spraying step was carried out without grounding the target. The proposed new technique could provide a smooth and acceptable surface condition, as well as strong adhesion between the powder coatings and thermoplastic substrates. Furthermore, a UWO low-cure additive was blended with fine powder coatings, aiming at lowering the curing temperature so as to better protect the thermoplastic substrate from deformation at high curing temperatures. It was found that there is effective reduction of curing temperature by utilizing the UWO low-cure catalyst. The final coating surfaces were evaluated by both visual inspection and instrumental measurement, and the results were promising. So the pre-heating method is a simple and successful strategy for powder coating on thermoplastics, and this method can be a good guideline to powder coating on other non-conductive substrates.

The discoveries of this thesis are of great help to the powder coating manufacturing and application process. Nevertheless, some of the remaining issues related to the proposed

technique are still worthy of further investigation. The future research recommendations are listed below:

- The new design of the cyclone in this study was tested at a small scale. A full scale testing with extended operating durations needs to be conducted. Powder accumulation problems can occur in scale-up testing, so the design of this proposed new cyclone may need to be further optimized.

- A more reliable mechanism for the alternating charging gun needs to be developed. The current charging distributor is not suitable for continuous operations required by industrial applications due to the possibility of erosion. However, in most of the automatic spraying systems, several spray guns are utilized together to coat larger components. Therefore, testing of the interference on a multi-gun setup with a new gun design is also needed.

- The blending and drying of metallic powder processing technique could be simplified. Instead of a jet-mixing machine, a fluidization bed could be a proper alternative device to achieve bonding and could deal with larger amounts of powder sample.

- For powder coating on non-conductive substrates, the current technique is only suitable for those substrates with simple configurations. A more sophisticated spray method for complex shaped substrates is preferred to overcome the Faraday Cage effect.

CURRICULUM VITAE

Name: **Shan Gao**

Education:

PhD, Chemical and Biochemical Engineering,
Western University, London, ON, Canada
2013-2016

MESc (PhD directly),
Western University, London, ON, Canada
2012-2013

Bachelor of Engineering, Chemical Engineering,
China University of Petroleum-Beijing, Beijing, China
2007-2011

Working Experience:

Graduate Research & Teaching Assistant
Western University, 2012-2016

Engineering Intern
Sinopec Beijing Yanshan Company, 2011

Publication:

Gao S, Zhu X-P, Zhang H and Zhu J-X, "Powder Coating of Underhood Plastic Components", Automotive Composites Conference & Exhibition (ACCE), Novi, MI, September 7-9, 2016

Zhao, L., Xu, C., **Gao, S.**, & Shen, B, "Effects of concentration on the alkali-treatment of ZSM-5 zeolite: a study on dividing points", Journal of materials science, 45(19), 5406-5411, 2010

Zhao, L., Wu, Y. K., **Gao, S.**, Zhang, F. L., & Chen, Y, "Quantum chemistry research on the relationship between Si/Al ratios and catalysis activities of ZSM-5 zeolites", Journal of Molecular Science, 2, 004, 2010